Multi Heavy Metal Cyclic Adsorption-Desorption Characteristics of Commercial Resins and Chitosan Derivatives

Thesis submitted in partial fulfillment of the

requirements for the degree of

DOCTOR OF PHILOSOPHY

by

Prabhat Kumar Patel

Centre for the Environment

Indian Institute of Technology Guwahati

Guwahati–781039, India

Multi Heavy Metal Cyclic Adsorption-Desorption Characteristics of Commercial Resins and Chitosan Derivatives

Prabhat Kumar Patel

Multi Heavy Metal Cyclic Adsorption-Desorption Characteristics of Commercial Resins and Chitosan Derivatives

Thesis submitted in partial

fulfillment of the requirements for the degree of

DOCTOR OF PHILOSOPHY

by

Prabhat Kumar Patel
Roll No.: 186152004

Centre for the Environment

Indian Institute of Technology Guwahati

Guwahati – 781039, India

October 2023

Dedicated

to

my family

Centre for the Environment
Indian Institute of Technology Guwahati
Guwahati – 781039, Assam, India

CERTIFICATE

It is certified that the work contained in this thesis entitled **"Multi Heavy Metal Cyclic Adsorption-Desorption Characteristics of Commercial Resins and Chitosan Derivatives"** submitted by **Mr. Prabhat Kumar Patel** for the award of the degree of Doctor of Philosophy has been carried out in the Centre for Environment, Indian Institute of Technology Guwahati under our supervision. To the best of our knowledge, this work is not submitted elsewhere for the award of any other degree or diploma.

(Prof. Ramagopal V. S. Uppaluri)
Department of Chemical Engineering
IIT Guwahati, Guwahati - 781039

(Dr. Lalit Mohan Pandey)
Department of Biosciences and Bio Engineering
IIT Guwahati, Guwahati - 781039

Centre for the Environment
Indian Institute of Technology Guwahati
Guwahati – 781039, Assam, India

DISCLAIMER

The experimental, modelling and characterization related data presented in this Ph.D. thesis was carried out by me and is reported after due verification. To the best of my knowledge, the work summarized in this Ph.D. thesis is not submitted elsewhere for the award for any other degree or diploma.

(Mr. Prabhat Kumar Patel)
Centre for the Environment
IIT Guwahati, Guwahati - 781039

Acknowledgement

Firstly, I would like to express my sincere gratitude to my advisors **Prof. Ramgopal V.S. Uppaluri** and **Dr. Lalit Mohan Pandey** for their continuous support, patience, motivation and immense knowledge-sharing discussions during my Ph.D. tenure at IIT Guwahati. Their guidance profoundly assisted my academic and research needs in the entire tenure of my research and thesis writing. With such gracious support, I do not think that I would have even better mentors for my Ph.D thesis dissertation work.

Besides my advisors, I would like to thank the honourable doctoral committee members of my thesis namely **Prof. Chandan Das**, **Prof. Saswati Chakraborty**, and **Prof. Lal Mohan Kundu** for their highly relevant insights, comments and thought-provoking questions that served as very useful incentives to widen the scope and domain of my research.

My sincere thanks are also due to the scientific officers of Chemical Engineering Department, Centre for the Environment, The Northeast Centre for Biological Sciences and Healthcare Engineering (NECBH) and Central Instruments Facility (CIF) for providing me with all the necessary support in terms of the research facilities. Without their precious support, the thesis would not have had a subjective edge in terms of findings of the surface characterization.

Next, I wish to thank my labmates, seniors and juniors for their friendly support and timely assistance and help. Special thanks to **Dr. Srinu Nagireddi** for his assistance and co-operation towards material synthesis and motivation. My heartfelt thanks are also to my other friends namely Dr. Deepa, Dr. Aritra, Dr. Sushma, Dr. Preeti, Dharitri, Abhishek, Aquib, Ankush, Langtuk, Anweshan, Pulakeshwar, Sudeshna, Udaratta, Prangan, Neha, Kamal, Paushali, Nurruzzaman, Debolina, Sumona for their amicable support and timely assistance during my PhD thesis work tenure. In particular, **Janaki** has been always my strength during my difficult times. I am very

much thankful for her for the constant support, mental boosts, affection, the laughter, the trips and food that we shared.

A special thanks to my family. Words cannot express how grateful I am to my mother, father, brothers, sisters and uncle for all the sacrifices they made for me to reach this destination in my life. Your prayers and continuous support sustained me this far and I am indebted to all of you for such positive and friendly environment at this crucial juncture of my education.

I would like to express my sincere gratitude to the staff members of the Centre for the Environment, namely, Partha Da, Deepmoni ma'am, Rajiv Da, Kaustav Da, Mridul Da and Supriyo Da; security guards, especially, Bipul Da, Sanjib Da and Dipen Da for their sustained help and support throughout my PhD work.

Finally, I also thank all my previous teachers and people whom I am not able to name in this section. However, they have contributed immensely to my life in diverse ways. This PhD thesis wouldn't have been possible without the contribution of every one of them for their sparkling touch in my life with charged vigor and enthusiasm during my tenure.

Prabhat Kumar Patel

pprabhat1991@gmail.com

Abstract

Considering the lacunae in the field of commercial resin and chitosan derivatives based multi-heavy metal sorptive removal from complex adsorbate systems, the PhD thesis involved the realization of five major objectives. These are as follows:

a) Efficacy of commercial resins (Amberlite IR 120H and Lewatit TP260) for multi-heavy metal removal and resin regeneration from Cu and Zn dominant complex adsorbate systems.
b) Synthesis, characterization, batch adsorption and desorption studies of polyvinyl grafted chitosan variant derivatives (low CSPVA, medium CSPVA and high CSPVA) for multi-heavy metal removal and resin regeneration from Cu and Zn dominant complex adsorbate systems.
c) Synthesis, characterization, batch adsorption and desorption studies of citric acid grafted glutaraldehyde crosslinked chitosan variant derivatives (low Cit-CS, medium Cit-CS and high Cit-CS) for multi-heavy metal removal and resin regeneration from Cu and Zn dominant complex adsorbate systems.
d) Synthesis, characterization, batch adsorption and desorption studies of carboxymethyl grafted glutaraldehyde crosslinked chitosan variant derivatives (low CMCS, medium CMCS and high CMCS) for multi-heavy metal removal and resin regeneration from Cu and Zn dominant complex adsorbate systems.
e) Conceptual cost analysis for the multi-heavy metal ion removal from complex adsorbate systems.

For commercial and synthesized chitosan-based derivatives, surface characterization studies such as FTIR, BET, XRD, TGA and FESEM-EDX analyses were conducted. For the adsorption-

desorption characteristics evaluation, the adopted overall methodology is as follows. Based on available prior art, speciation analysis inferred that Pb, Cu and Zn) ions were mostly available in the respective Pb^{+2}, Cu^{+2} and Zn^{+2} forms in the acidic pH range (1-6 pH). For raw chitosan case, the solubility resistance analysis confirmed that the chitosan is soluble from 0.5 – 5 pH. Hence, suitable modification of chitosan structure with relevant functional groups was achieved by conducting relevant displacement and elimination reaction schemes from the perspective of modified chitosan's sustainability in acidic aqueous media. For all adsorbents (Amberlite IR 120H, Lewatit TP 260, CSPVA, Cit-CS, and CMCS) and for complex adsorbate system (Cu, Pb, Fe, Zn, Mg, Na, K and Al in Cu dominant adsorbate system and Zn, Pb, Fe, Cu, Mg, Na, K and Al in Zn dominant adsorbate system), batch adsorption studies were carried for a variation in batch adsorption process parameters as 0.2-2.0 g L^{-1} adsorbent dosage, 5-720 min contact time and initial solution concentration (187.7-563.1 mg L^{-1} for Cu, 61.85-185.55 mg L^{-1} for Fe, and 5.2-15.6 mg L^{-1} for Pb in Cu dominant solution and 194.9-584.7 mg L^{-1} for Zn, 104.8-314.4 mg L^{-1} for Fe, and 2.65-7.95 mg L^{-1} for Pb in Zn dominant solution). For comparative assessment, the adsorptive and desorptive performance of all resins was evaluated for Cu and Zn dominant adsorbate systems at corresponding optimized batch process parameter values.

For the considered resin-adsorbate system combinations, experimentally determined batch equilibrium and kinetics data (Cu, Fe and Pb adsorption data in Cu dominant solution and Zn, Fe and Pb adsorption data in Zn dominant solution) were evaluated for their fitness with suitable equilibrium (Langmuir and Freundlich models) and kinetic (Pseudo-first-order, and Pseudo-second-order models) models. The desorption efficiencies of all adsorbents were carried out with simple and cheaper eluents (acid or base dilute solutions in the concentration range of 0.1 - 2M) and spent adsorbents realized with the initial solution concentration of 375.5 mg L^{-1} Cu, 123.7 mg L^{-1} Fe and 10.4 mg L^{-1} Pb in Cu dominant solution and 389.8 mg L^{-1} Zn, 209.6 mg L^{-1} Fe and 5.3

mg L^{-1} Pb in Zn dominant solution. Finally, the cost effectiveness of all adsorbents was targeted through the evaluation of conceptual synthesized resin fabrication cost (based on retail cost of chemicals deployed for resin synthesis) and retail cost of commercial resins. Further, conceptual processing cost of synthesized and commercial resins was also evaluated for a pilot-scale adsorption-desorption system (3000 m^3 annual capacity of treatment plant with 10000 L h^{-1} flow rate).

From the thesis findings, the following have been achieved. Firstly, the comparative and best efficiency of the derivatives (CSPVA, Cit-CS and CMCS) based on the alternate molecular weight of the chitosan have been affirmed for the simulated complex wastewater adsorbate systems (Cu and Zn dominant solutions). Accordingly, the optimal combinations of various adsorption parameters were identified. Secondly, the morphological, thermal and functional characteristics of chitosan-based derivatives were determined to quantify upon the suitable modifications. Thirdly, the efficacy of chitosan derivatives in terms of cyclic adsorption and desorption characteristics were assessed. Fourthly, the possible scope for cost reduction of chitosan derivatives in terms of resin synthesis cost in both lab and industrial scale have been assessed.

Among all commercial resins and from cost efficacy perspective, compared to the Lewatit TP260 resin, Amberlite IR 120H is the most inexpensive resin with marginally lower adsorption and desorption efficiencies. Among all laboratory fabricated chitosan derivatives, medium CMCS derivative resin provided better adsorptive performance but provided marginally lower desorptive efficiencies as compared to medium Cit-CS derivative resin. From conceptual resin cost perspective, Lewatit TP 260 resin was 4.8 times and chitosan carboxymethyl resin was 14.09 times expensive than the Amberlite IR 120H. Similarly, from conceptual processing cost perspective, Lewatit TP260 resin was 3.3 times and chitosan carboxymethyl resin was 2.5 times expensive than the Amberlite IR 120H.

Among all adsorbents, commercial Amberlite IR 120H resin and medium CMCS synthesized derivative can be inferred to have excellent performance characteristics from adsorption, desorption and cost perspectives. Besides these, the carried out investigations enabled useful insights into the irrelevance of HSAB theory as a generalized rule of thumb to screen and scope potential adsorbents for multi-heavy metal removal and resin regeneration. The mentioned findings of the thesis ascertain technical and economic benchmarks for the realization of low-cost chitosan derivatives based cyclic desorption technology for multi-heavy metal complex adsorbate systems. Accordingly, sustainable technologies for real world situations can commissioned for multi-heavy metal removal from adsorbate systems.

Novelty Statement

The Ph.D. thesis involved the realization of five major objectives. Among these, the first objective refer to multi-heavy metal ion removal from simulated complex industrial wastewater adsorbate systems (Cu and Zn dominant solution) utilizing commercial resins (Amberlite IR 120H and Lewatit TP 260). The next three objectives involved multi-heavy metal ion removal from simulated complex industrial wastewater adsorbate systems (Cu and Zn dominant solution) utilizing alternate molecular weight (low, medium and high) based chitosan derivatives (poly vinyl alcohol grafted chitosan (CSPVA), citric acid grafted chitosan (Cit-CS) and carboxymethyl grafted chitosan (CMCS)). Finally, the fifth objective targeted the comparative assessment of the conceptual chitosan derivative fabrication cost with respect to the retail cost of the commercial resin and processing cost of all synthesized chitosan derivatives and commercial resins. Accordingly, the best performing resin has been identified for the multi-heavy metal removal from two complex adsorbate systems that have close resemblance with industrial heavy waste water systems. Specific novelties of the thesis have been briefly presented in the following paragraphs.

The first four objectives involved the following novelties: (a) criticality of complex adsorbate systems that have closer resemblance with industrial wastewater effluents (was not addressed in the prior art) (b) insights based on cyclic adsorption and desorption capabilities of commercial resins and chitosan derivatives (c) effect of molecular weight of chitosan on the synthesis and cyclic adsorption-desorption behavior for multiple heavy metals (d) efficacy of simple acid (HNO_3, H_2SO_4 and HCl) and base (NaOH and KOH) eluents for the cyclic regeneration of exhausted commercial and chitosan derivatives. Among these, the findings from cyclic

performance studies can provide useful guidelines for the treatment of real world industrial wastewater effluents.

The fifth and final objective involved the following novelties: (a) insights based on conceptual resin fabrication cost (for 10 g of resin) and conceptual processing cost (for 1 L wastewater treatment) (b) comparative assessment of the conceptual resin cost for lab and industrial scale production.

Contents

List of Tables

List of Figures

Nomenclature

Abbreviation

HSAB	Hard and Soft Acid Base
CS	Raw Chitosan
CMCS	Carboxymethyl Chitosan
Cit-CS	Citric Acid Grafted Chitosan
CSPVA	Poly Vinyl Alcohol Grafted Chitosan
FTIR	Scanning Electronic Microscope
BET	Brunauer-Emmett-Teller
AAS	Atomic Absorption Spectrometer
EDX	Energy Dispersive X-ray spectrometer
FESEM	Field Scanning Electronic Microscope
TGA	Thermo Gravimetric Analyser
XRD	X-ray Powder Diffractometer

Notations

C_o	Initial Metal Ion concentration, mg L^{-1}
C_e	Equilibrium Metal Ion concentration, mgL^{-1}
W	mass of adsorbent, g
V	volume of solution, mL
Q_e	Equilibrium Metal Ion adsorption capacity, mg g^{-1}
Q_o	Maximum adsorption capacity, mg g^{-1}
b	Langmuir adsorption constant
R_L	Dimensionless equilibrium parameter
K_f	Freundlich isotherm coefficient
n	Amount of adsorbent taken per l L of aqueous solution, mg L^{-1}
t	Agitation time, min
K_1	Psuedo First order rate constant, min^{-1}
K_2	Pseudo second order rate constant, g mg^{-1} min^{-1}
Q_t	Mass of solute adsorbed per mass of adsorbent at 't' min, mg g^{-1}
C_f	Final Metal Ion concentration subjected to adsorption study, mg L^{-1}
A	Initial Metal Ion concentration on adsorbent subjected to desorption study, mg L^{-1}
B	Initial amount of Metal Ion on adsorbent
V_{sol}	Volume of adsorbate solution, mL
$W_{adsorbent}$	Weight of adsorbent, mg
C	Final concentration of heavy metal ion in eluent, mg L^{-1}
V_{eluent}	Volume of eluent solution, mL

Chapter 1:

Introduction and Literature Review

Introduction and Literature Review

In this chapter, section 1.1 presents a brief overview of the mandatory need for heavy metal removal from waste streams, various competent technologies for the removal of heavy metals, prominence of adsorptive ion-exchange technologies, various multi-heavy metal adsorbate systems and promising adsorbents for multi-heavy metal removal and targeted research perspectives. Thereafter, section 1.2 addresses the available prior art for various adsorptive and ion exchange resins to foster competitive multi-heavy metal adsorption from aqueous and synthetic solutions. In the following section (section 1.3), the scope for further research has been elucidated along with an emphasis towards multi-heavy metal adsorptive removal from complex adsorbate systems. Finally, section 1.4 summarizes the broad objectives of the PhD thesis followed by the overall thesis organization details in section 1.5.

1.1 Background

1.1.1 Heavy metal pollutants in wastewater

Heavy metals are among one of the most detrimental environmental contaminants. This is due to their persistent non-biodegradable characteristics. Both natural and human factors contribute towards their entry into various aqueous systems that are often explored by humankind for their subsistence. They have been proven to be toxic to organisms even at lower aqueous concentrations (ppm or mg L^{-1}). Heavy metals such as chromium, cadmium, arsenic, iron, and nickel do occur naturally in the earth's crust. Due to continued and enhanced industrialization and urbanization, an imbalanced accumulation of these heavy metals occurred in the ecosystem. Thereby, industrial

wastewater streams are the primary sources of their persistent release into the environment (LeVan, 1998; Das et al., 2008).

Often, heavy metal pollutants also enter irrigation water bodies due to their existence in the contaminating effluents that emerge from various industries (Singh, 1994; Fazeli et al., 1998). Table 1.1 provides a brief account of such typical industrial sources for heavy metal-contaminated wastewater effluents and their harmful effects.

Table 1.1: An overview of the several sources emanating from heavy metal wastewater systems and their harmful effects (Singh, 1994; Fazeli et al., 1998).

Metal	Prominent sources	Harmful effects
Chromium	Tanneries, pulp and paper industries, petroleum refineries, chrome plating industries, electroplating industries.	Respiratory problems
Lead	Mobile batteries, petroleum-based industries, and pesticides.	Cognitive and developmental issues in children
Copper	Plating and metal refining industries, plastic industries.	Gastrointestinal issues and liver damage.
Zinc	Dyes, paints and rubber industries, ointments, and wood preservatives.	Gastrointestinal disturbances and essential mineral absorption.
Cadmium	Phosphate fertilizers, pesticides, paint pigments, galvanized pipes, copper, petroleum, and polyvinyl refineries, batteries, and plating industries.	kidney damage, osteoporosis, and lung cancer.
Iron	Engine parts and Metal refineries, mining.	Iron overload disease (Hemochromatosis)
Aluminium	Aluminium phosphate industries, pesticides, wiring products, automobile parts, and ceramics.	Neurotoxicity
Arsenic	Automotive exhaust, dyes, and wood conservatives.	Skin problems, cardiovascular diseases, and cancer.
Mercury	Bulb, tanning, and leather industries, paints and adhesives, and thermometers.	Neurological problems in children, cardiovascular issues.

Alternatively, it can be noted that as minor constituents, several heavy metals such as zinc, lead, and copper do have a synergistic and positive influence on sustainable human metabolism and

health. Nonetheless, at increased contamination levels, they are detrimental and hazardous and can even lead to poisoning of the human biological system due to drinking water contamination. On the other hand, higher pollutant levels of heavy metals in the air are often relevant at emission sites. Also, heavy metal pollution is caused due to their accumulation in the sediments. Thus, the slower accumulation of heavy metals in the human body is caused due to the combined effect of drinking water contamination, air pollution, and sediment accumulation. Eventually, such slower accumulation translates into a lethal case for the entire humankind and demands effective mitigation strategies.

1.1.2 Necessity for Heavy Metal Removal from Wastewater Systems

The continued release of industrial, household, and farm wastes into eco-water systems is detrimental to the subsistence of humankind. Thus, heavy metals are public health jeopardizing contaminants after their entry into the human body through the food chain. Unlike most organic pollutants, heavy metals cannot be mitigated through biological decay. The ecologically non-biodegradable characteristics of the heavy metals in conjunction with their toxic effects on living beings together necessitate upon their efficacious removal from the eco-system for sustained human health protection (Parmar & Thakur, 2013). Also, ever-increasing demand for contaminant-free water also prompts upon the development of affordable methods and technologies to eradicate such contaminants from mining and industrial effluents. Thereby, the cleansed effluents that meet the strict environmental legislations can be appropriately discharged into the water bodies. Through such eco-friendly support systems, the heavy metal constitution would reduce substantially in the industrial and municipal effluents. Thereby, the effluent systems can be handled comfortably for their greater integration into the healthy water bodies. Any further delay

in the affirming of such industry-specific technological innovations would foster an enhanced contamination of heavy metals in the water bodies and will accumulate in the living entities such as fish that sustain on the contaminated flora and fauna of the water bodies. Hence, for sustained human health, technological interventions are the need of the hour in the field of heavy metal removal from waste streams.

1.1.3 Technologies for Heavy Metal Removal from Industrial Effluents

The removal of heavy pollutants such as copper, zinc, lead, and iron from discarded liquid systems is an interesting as well as challenging problem. In the precise field that targets the removal of toxic heavy metals from spent supplies, several processes such as membrane separation (F. Ma et al., 2017), ion exchange resins (Chakrabarty et al., 2011), electrochemical reduction (Y. Niu et al., 2015), nanomaterials (Choi et al., 2020), adsorption process (Gupta et al., 2021), chemical precipitation (Boamah et al., 2015), coagulation and flocculation (Pang et al., 2011), sedimentation filtration (Fu & Wang, 2011), reverse osmosis (Ali et al., 2017), flotation (Smolinski et al., 2017), electrodialysis (Gherasim et al., 2014), solvent extraction (Lertlapwasin et al., 2010), bio removal (G. Wu et al., 2010), photocatalysis (Pathania et al., 2017), phyto remediation (Y. Ma et al., 2016), and ultrafiltration (B. Ma et al., 2018) have been reported for their efficacious performance. In addition, the issue of sustainable and economically viable technology for heavy metal removal is one of the most challenging problems for adequate resolution. This is due to pertinent issues such as environmental friendliness, affordability, permanence, quicker and easier research-ensuring platforms (Nagireddi et al., 2017). Further, as per adopted technologies, heavy metal-contaminated wastewater treatment technologies can be primarily divided into three categories. These are (a) chemical precipitation, electrochemical reduction, and electrolysis that involve chemical reactions

for metal removal; (b) biomass adsorption, metal extraction, ion exchange resins, reverse osmosis, evaporation, enrichment, and procedures that target heavy metal removal through a phase change and through the principle of sorption, and (c) biosorption, bio flocculation, artificial wetlands, and other biological processes that involve biological system based adsorption and enrichment mechanisms for heavy metal removal (Wang & Chen, 2014).

1.1.4 Adsorption and Ion-exchange Technologies

Ion exchange and chelating resin-based physisorption/chemisorption have been proven to be very efficient in extracting heavy metals such as chromium, copper, zinc, iron, and lead. These materials also exhibited very good recovery of heavy metals from aqueous systems being even characterized with extremely low solution concentrations. Thereby, they have been inferred to be among the few competent technologies that cater towards sustainable research commercialization. In addition, compared to synthetic cheating resins, biopolymers such as chitosan, fruit, and vegetable wastes have been proposed to be competitive due to their ease of preparation, cheaper cost, and excellent separation capabilities ((Anwar et al., 2010; Nasernejad et al., 2005)). Chemisorption utilizing chelating resins has been more promising than physisorption. This is due to the physisorption functionality based on adsorbate attraction through Vander Waal's attraction forces, and chemical adsorption functionality based on the chemical bonding between dominating metal ions present in the adsorbate and various chelating functional groups in the resins. As a result, chemisorption enhances heavy metal removal and reuse of regenerated spent adsorbent. Thereby, the technology minimizes waste production and improves metal desorption-based recovery through the deployment of a suitable low-cost eluent system to enable the extraction of heavy metals from the spent chelated resin. Also, other modified physisorbents, such as Na Alginate composite, have

been proven to be inefficient for the mentioned purpose. This is due to their weak desorption characteristics that render them to be non-promising even in the cases involving excellent adsorptive attributes of the adsorbents (Cao et al., 2010).

1.1.5 An Overview of Heavy Metal Adsorbate Systems

Numerous laboratory studies have been addressed till date for heavy metals removal from nitrate (Ahmadi et al., 2011; Anbazhagan et al., 2021; Dev et al., 2020; Guo et al., 2013; Liang et al., 2011; Ling et al., 2010; Liu et al., 2015; Mnasri-Ghnimi & Frini-Srasra, 2019; Ren et al., 2013; Tsai et al., 2016; Zawierucha et al., 2014), sulphate (Huacai Ge and Shiying Huang, 2010; Kavitha et al., 2020; Morcali et al., 2014; F. C. Wu et al., 2010) and chloride (Liu et al., 2013; Pavlović et al., 2007) precursor containing solutions. Few of these articles also addressed the influence of speciation on the adsorption properties. In these studies, it was opined that heavy metals such as zinc, lead, and copper do exist predominantly in the +2 state in the acidic environment (pH in the range 1-6) (Benavente et al., 2011). Therefore, pH-driven speciation alterations have been inferred to be prominently influencing heavy metal adsorptive attributes in the investigated chelating resins.

1.1.6 Competent Adsorbents for Heavy Metal Removal

Till date, for heavy metal removal, several alternate chelating compounds have been reported such as magnetic EDTA-modified chitosan (Ren et al., 2013), chitosan, pristine chitosan (Benavente et al., 2011), EDTA-modified crosslinked chitosan (F. C. Wu et al., 2010), chitosan mercaptanes (Huacai Ge, 2010), chitosan-glutaraldehyde beads (Cárdenas et al., 2001), zwitterion-chitosan (Dev et al., 2020), carboxymethyl chitosan (Kavitha et al., 2020), EDTA-modified chitosan–silica hybrid (Repo et al., 2011), chitosan-coated bentonite (Tsai et al., 2016). From the functional group

analysis, among several reported materials, the resins with oxygen-containing functional groups have been indicated to be the most efficacious for heavy metal adsorption. Notable reported materials with such functionalization refer to the existence of carboxylic, hydroxyl, phenolic, ether, carbonyl, phosphoryl, iminodiacetic acid, and sulfonic acid groups in resins such as Lewatit SP 112, Lewatit TP 260 and Lewatit TP 207 (Hubicki et al., 2011), Dowex HCR S/S (Alyüz & Veli, 2009), GMA/DVB magnetic resin (Atia et al., 2008), Purolite C100 (Abo-Farha et al., 2009), Lewatit TP 208 (Nekouei et al., 2019), Amberjet 1200 H and Amberlite IRN97H (Rengaraj et al., 2004), Dowex Marathon C (Taha, 2021), Lewatit CNP80 (Vergili et al., 2017), modified quebracho tannin resin (Yurtsever & Şengil, 2009), zwitterion-chitosan (Dev et al., 2020), carboxymethyl chitosan (Kavitha et al., 2020). Also, nitrogen functional groups bounded nitrogen in the resident amine groups in several other chelating resins such as SI-ATRP (L. Niu et al., 2010), chitosan-glutaraldehyde beads (Cárdenas et al., 2001) and chitosan-coated bentonite adsorbents (Tsai et al., 2016).

Needless to convey, to target heavy metal extraction from industrial waste systems, the literature emphasizes on the development of functional chelating resins using bio-based resources. Such resources have been regarded to be promising in terms of their non-toxicity, biocompatibility, hydrophilicity, biodegradability, and antibacterial attributes. Among these, chitosan, a partially acetylated glucosamine biopolymer, can serve as a potential bio-polymer for respective functional group modification. In this regard, it shall be noted that the molecular structure of chitosan affirms metal adsorption due to favorable hydroxyl and nitrogen functional groups. However, due to its lower corrosion resistance to the acidic environment, the chitosan bio-polymer needs modification through appropriate grafting methods and crosslinking agents. Further insights into the aforementioned literature reveal that there has been a lack of knowledge in the

cation-exchange resins from the perspective of the resin recovery and reuse from multi-heavy metal containing complex adsorbate systems. Thus, despite providing abundant information with respect to resin chemistry, the literature has been scanty on the efficacy of notable prominent resins from the recycling and reuse perspective and for multi-heavy metal-containing complex adsorbate systems.

1.1.7 Targeted Perspectives in the PhD thesis

The thesis primarily aims to provide newer knowledge on the efficacy of commercial and prominent chitosan derivative resins for the adsorption-based heavy metals removal from multiple heavy metals constituting complex adsorbate systems. Accordingly, for all targeted resins, the following perspectives were targeted:

a) Analyze upon the interaction of functional groups in terms of their adsorptive and desorptive efficacy. Thereby, prompt upon a super-efficient and best-performing resin with relevant functional groups for maximal multi-heavy metal removal and resin reusage.
b) Gain useful insights into the cyclic adsorption and desorption characteristics of commercially available resins and chitosan derivatives.
c) Visualize upon chitosan characteristics and functional group loading on the desorptive efficacy-based performance characteristics of chitosan derivatives.

For the successful multi-heavy metal removal and resin reutilization with effluents being characterized by challenging and complex interactions of chemical constituents, the targeted perspectives aim to broaden the know-how of complex functional and adsorption chemistry for the sustained application of commercial resins and chitosan derivatives for heavy metal removal.

1.2 Prior art

A further deliberation on the summarized research perspectives in section 1.1.7 of the Ph.D. thesis prompts to identify relevant prior art in the following major research themes:

a) Adsorption and desorption efficacy of conventional ion-exchange resins.

b) Adsorption and desorption efficacy of chitosan and other chelating resins.

c) Adsorption investigations of other chelating resins.

In the following sub-sections, a brief overview of the critical findings of the literature has been addressed.

1.2.1 Functional groups interaction with Heavy Metal Species

The abundance and relevance of functional groups critically influence heavy metal adsorption onto commercial resins and chitosan derivatives. Constituent functional group species may donate oxygen, nitrogen, or sulphur to foster the easier and more effective adsorption of heavy metals. This was outlined in the introductory section of the thesis. Further details with respect to functional group chemistry and associated chelation have been delineated in this section for the prior cited adsorbents with O, N, and S donor groups.

The available prior art primarily focused on the pertinent adsorption mechanism of heavy metals onto commercial resins and chitosan derivatives. Only a few literature reported the desorption mechanism of the adsorbents. For heavy metal adsorption, two different kinds of interactions have been suggested. In these, the first refers to the ionic association between heavy metal and ionic functional groups, and the second involves coordination or chelation. Thus, the adsorption of heavy metals may occur through either of these two mechanisms or their combination. The following chemical equations summarize these mechanisms (Benavente et al., 2011; Dev et al.,

2020; Hossain et al., 2014; Hubicki et al., 2011; Liang et al., 2011; Ling et al., 2010; L. Niu et al., 2010):

Ionic interaction:

$$R - SO_3H + M^{n+} \rightarrow (R - SO_3)^- M^{n+} + H^+$$

Chelation:

$$R - NH_2 + M^{n+} \rightarrow R - NH_2 - M^{n+}$$

or

$$-NH_2 + M^{n+} \rightarrow -NH_2 - M^{n+} - NH_2 -$$

In the above equations, it shall be noted that the ionic interaction has been suggested to involve a larger release of the protons. This is due to the groups dominating the acidic pH range in the aforementioned equation. Chelation, on the other hand, is preferred at higher pH. As a result, ionic contact is often and preferentially sought by adjusting the pH of the solution. This principle is often explored for resin regeneration through desorption.

For the Lewatit TP 207 resin and for solution pH about 2 or lower value, both carboxylic groups and nitrogen atoms exist in protonated form. Under these circumstances, the hydrogen ions get engaged in fierce competition with the ions of heavy metals and in the context of occupying available adsorption sites through chemisorption. Both carboxylic groups do get deprotonated at a higher pH of 12. Thereby, the system functions as a conventional cation exchange system. However, at moderate pH levels, the resin exhibits typical characteristics of an amphoteric material. Under these circumstances, the dissociation of at least one carboxyl group and protonation of the nitrogen atoms occurs (Hubicki et al., 2011). According to the authors, Fig. 1.1 provides a summary of the hypothesized mechanism for the TP 207 resin and for any heavy metal cation M^+:

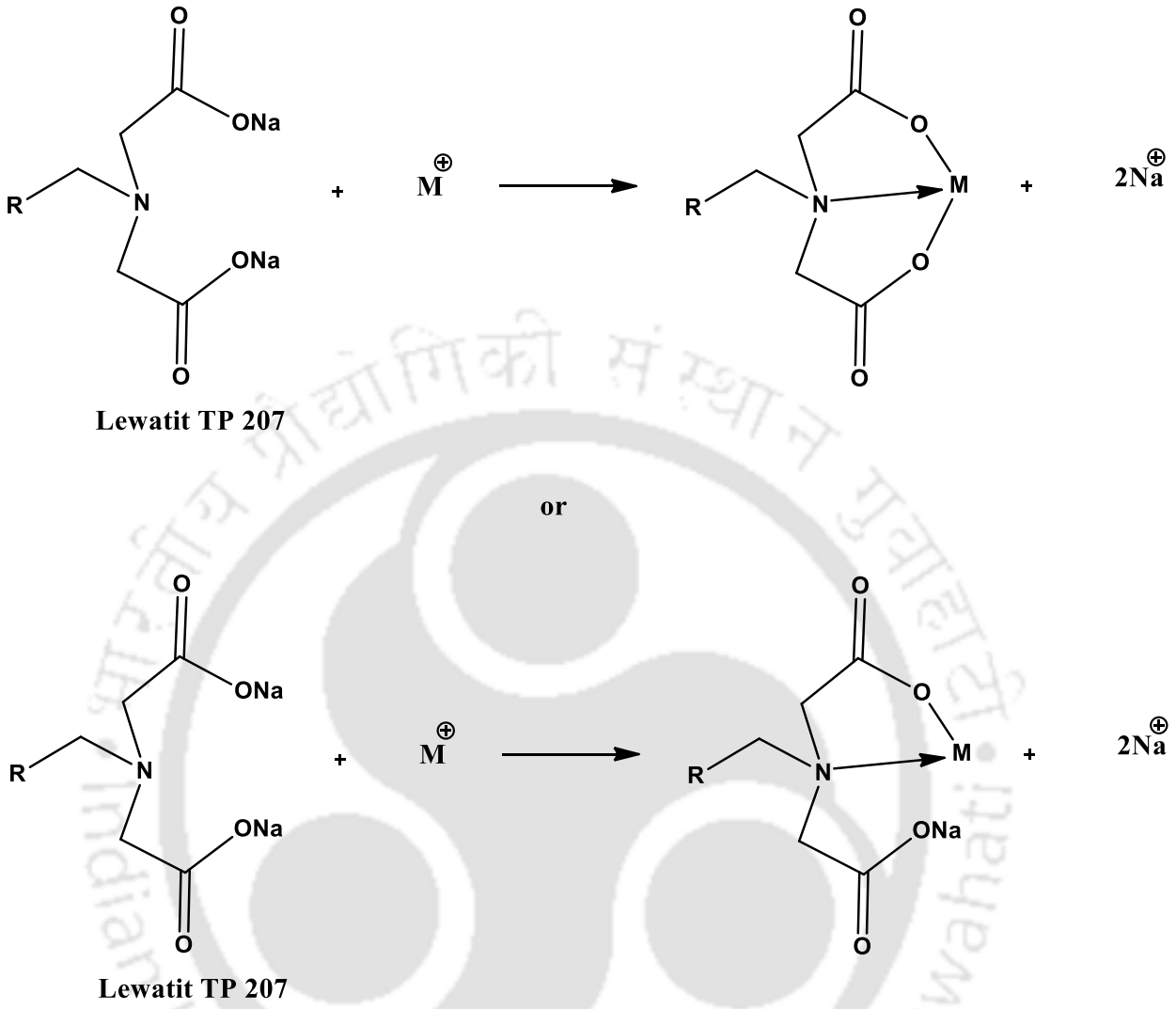

Fig. 1.1. Proposed heavy metal adsorption mechanism for Lewatit TP 207 (Hubicki et al., 2011).

A conjugate adsorbent was developed by grafting polyacrylonitrile onto the surface of chloro-methylated PS beads by surface-initiated atom transfer radical polymerization (SI-ATRP) of acrylonitrile on chloromethylated crosslinked styrene–divinylbenzene resin (Chen et al., 2014). The copper adsorption mechanism in the presence of lead and chromium ions has been reported to follow the hypothesized mechanism being illustrated in Fig.1.2.

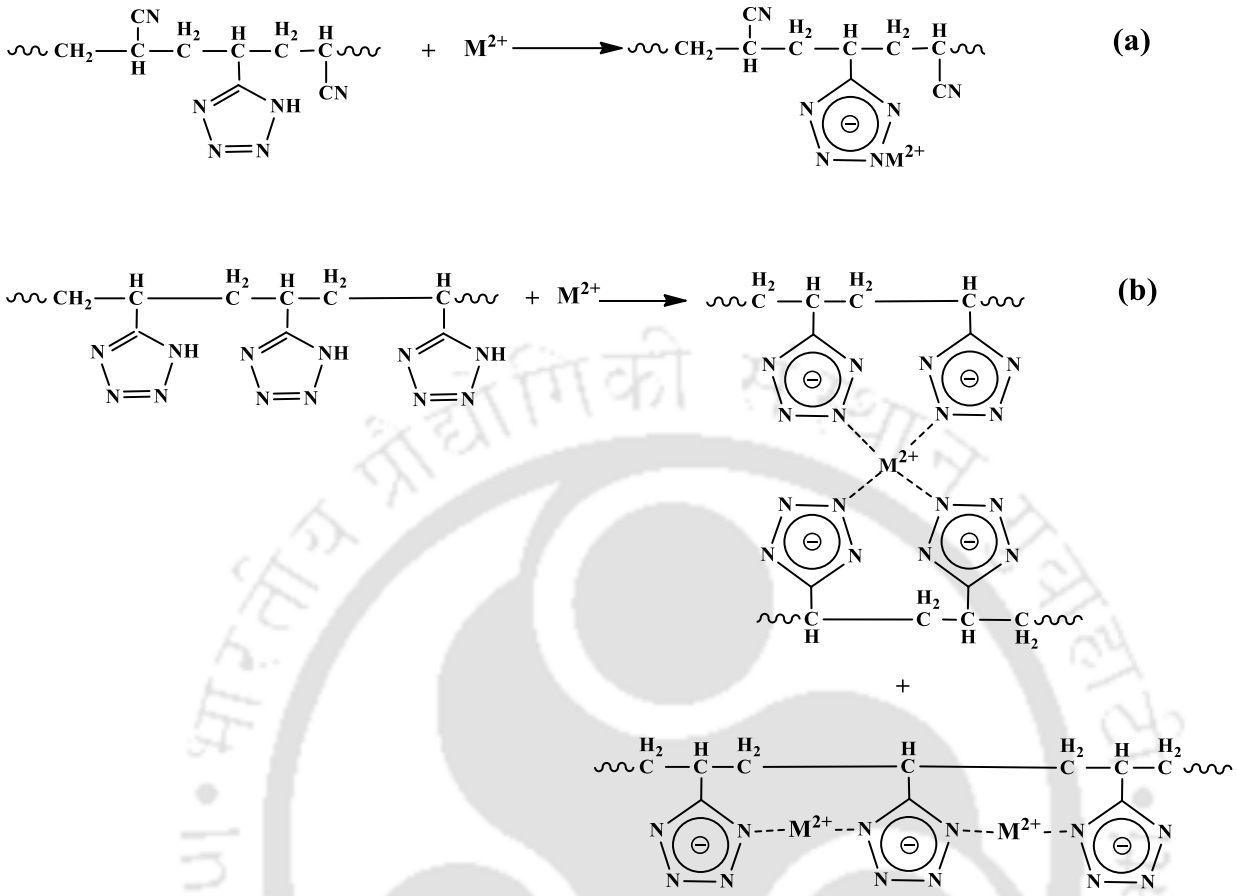

Fig. 1.2. Proposed heavy metal interaction onto PVT-g-PS synthesized resins (Chen et al., 2014).

For the mentioned adsorbent, maximum adsorption efficiencies of 26.3 % for Pb (II), 39.8 % for Cu (II), and 83.2 % for Cr (III) were achieved in the multi-metal solution. Minor reduction in the adsorption capacity was observed after every cycle and after the 10th cycle, the adsorption capacity was only reduced by 2.38 % for Cr (III), 6.11 % for Cu (II), and 4.61 % for Pb (II) (Chen et al., 2014).

Similarly, another research group fabricated carboxylate functionalized chitosan derivative by deploying methacrylic acid (MAA) monomer and glycidyl methacrylate (GMA) cross-linking agents (Dev et al., 2020). For the chosen multi-metal solution system, adsorption capacities of the

mentioned adsorbent were reported as 24.2 mg g^{-1} for Zn (II), 23.83 mg g^{-1} for Cd (II), 41.63 mg g^{-1} for Pb (II) and 34.3 mg g^{-1} for Cu (II).

1.2.2 Adsorption Characteristics of Commercial Resins

In this section, a brief overview of several adsorption studies has been delineated in several articles. These articles addressed multi-heavy metal removal and resin regeneration perspectives of both commercial and chitosan-based resins.

A research group (Rengaraj et al., 2004), analyzed the adsorptive characteristics of Cu(II) using Amberjet 1200H and Amberlite IRN97H (with sulfonic acid functional group) resins. The authors found that the Amberlite IRN97H resin possessed higher metal uptake characteristics (43.29 mg g^{-1}). Another research group (Demirbas et al., 2005), reported maximum adsorption capacity of 50.9, 765.1, 19.6 mmol g^{-1} for Cu (II), Zn (II), and Pb (II) adsorption using Amberlite IR 120 (with the sulfonic acid functional group). Also, another research group (Pehlivan & Altun, 2006) reported maximum adsorption capacities of Cu (II), Zn (II), Pb (II), Ni (II), and Cd (II) (4.7, 4.7, 4.1, 4.7 and 4.8 meq g^{-1}, respectively) at an optimal pH of 8 for the Dowex 50W commercial resin. Another research group (Atia et al., 2008) targeted the recovery of Pb (II) and Zn (II) along with some other metal ions using GMA/DVB magnetic resin (with iminodiacetic acid functional group). The authors inferred maximum adsorption capacities of 2.68 and 2.00 mmol g^{-1} respectively.

For the Purolite C100 (with sulfonic acid functional group), maximum removal of 80.38 and 75.47 % has been reported for Fe (III) and Pb (II), respectively (Abo-Farha et al., 2009). Also, for the Dowex HCR S/S resin (with the sulfonic acid functional group), the maximum adsorption-based metal uptake of 156.25 and 222.22 mg g^{-1} for Ni (II) and Zn (II) adsorption respectively have been reported (Alyüz & Veli, 2009). Another group of researchers investigated Pb(II) adsorption using

modified quebracho tannin resin (with the phenolic functional group) and reported maximum adsorption capacity of 86.20 mg g^{-1} at optimum pH 5 (Yurtsever & Şengil, 2009). For the iminodiacetic acid functionalized amberlite IRC748 resin, maximum adsorption capacities of 2.82, 1.21, and 0.86 mmol g^{-1} for Cu (II), Pb (II), Cd (II), respectively were achieved at an optimal pH of 5 (Ling et al., 2010). The Cu (II), Pb (II), Cr (VI), and As (V) adsorption on aminated resin via SI-ATRP (with amine functional group) has been reported at a pH of 5 (L. Niu et al., 2010). The authors reported a maximum adsorption capacity of 2.6, 0.97, 3.0, and 2.2 mmol g^{-1} for Cu (II), Pb (II), Cr (VI), and As (V) respectively. Other researchers targeted lead adsorption from aqueous nitrate solution and inferred a maximum adsorption capacity of 62.5 mmol g^{-1} at an optimum pH of 7.0 (Ahmadi et al., 2011).

Another group focused on the salvage of Cu (II) and Zn (II) from aqueous solutions using Lewatit TP 260 (with the (aminomethyl) phosphoric acid functional group), Lewatit TP 207 (with Iminodiacetic acid functional group) and Lewatit SP 112 (with Sulfonic acid functional group) (Hubicki et al., 2011). For the chosen resins, Lewatit SP 112 exhibited the highest metal uptake for Zn(II), and Lewatit TP 260 exhibited the highest metal uptake for Cu (II). Yet another team of researchers targeted Cr (VI), Ni (II), Pb (II), and Cd (II) adsorption onto iminodiacetic acid functionalized Styrene–DVB copolymer (Misra et al., 2011). The authors reported 99.7, 65, 59, and 28 % adsorptive removal respectively at 3.5 pH. Also, the desorption efficiency for Cr (VI), Ni (II), and Pb (II) were found to be 65, 70, and 45 % respectively.

The adsorptive behavior of Pb (II) from nitrate solution was examined for the 732-CR resin (Guo et al., 2013). The optimal adsorption capacity of 732-CR resin for Pb (II) was inferred to be 396.8 mg of Pb per g of resin. However, desorption data with appropriate eluents have not been reported in the mentioned literature. Adsorption characteristics of Cu (II) and Ni (II) were examined for the

L-Methionine-modified Dowex-50 resin (Kumar et al., 2013). The literature reported the maximum adsorption capacity of Ni (II) (65.375 mg g^{-1}) and 89.25 mg g^{-1} for Cu (II) in the concentration range of 50-200 mg L^{-1}. Adsorption characteristics of Cu (II), Pb (II), and Cr (VI) were examined with an aqueous solution and for synthesized Polyvinyltetrazole grafted PS resins having Tetrazolyl functional group (Chen et al., 2014). The authors reported that at an optimal pH of 5, the corresponding adsorption capacities were 2.65, 1.52, and 3.36 mmol g^{-1} respectively. Also, after the 10^{th} cycle, 94 % desorption was reported.

To assess upon the Cu (II) and Zn (II) adsorption attributes from industrial wastewater, commercially available anion exchange resins (such as Lewatit 207) were investigated (Morcali et al., 2014). The resin classification was based on the pertinent functional groups i.e., nitrogen and carboxyl groups. For the resin, it was observed that the equilibrium adsorption capacity enhanced from 1-68.5 mg g^{-1} for Cu (II) and from 1-73.0 mg g^{-1} for Zn (II) for an alteration in the initial concentration from 200-400 mg L^{-1}. Desorption investigations and the influence of other additives such as stabilizers and other complexing agents have not been addressed in the article.

The adsorption capacity of carboxyphenyl resorcinarene-impregnated Amberlite XAD-4 resin for Pb(II) affirmed a maximum adsorption capacity of 107.6-461.0 mg g^{-1} from aqueous nitrate solution and at an optimum pH of 6.5 (Zawierucha et al., 2014). Thereby, the article delineated on the critical role of pH enhancement for the maximization of adsorption capacity. Further, Pb (II) adsorption removal of 79 % has been reported for the sulfonic acid functional group based on Amberlite IR 120H (Naushad & Alothman, 2015). The efficacy of Lewatit CNP80 resin (with carboxylic acid functional group) for Pb (II) adsorptive removal has been inferred to be about 83.3 % and at 5 pH (Vergili et al., 2017). Another investigation targeted the recovery of Cu (II), Pb (II), and Zn (II) with Lewatit TP 260 (with aminomethyl phosphoric acid functional group), Lewatit

TP 208 (with iminosiacetic acid functional group) and Amberlite IRA743 (with N-methylglucamine functional group) from aqueous solutions. Among the chosen resins, Lewatit TP 260 exhibited the highest metal uptake for Pb (II) and Zn (II) and Lewatit TP 208 exhibited the highest metal uptake for Cu (II) (Nekouei et al., 2019). The recovery of Pb (II) from aqueous nitrate solution using Prosopis juliflora seed-modified Amberlite IRA-400 (with a carboxyl functional group) has been investigated by a research group (Anbazhagan et al., 2021). It was found that the maximum adsorption capacity of 106 mg g^{-1} was obtained at a solution pH of 6. For the Dowex Marathon C resin (with a sulfonic acid functional group), it was inferred that a good removal of 83.1 and 77.8 % can be achieved for Cu (II) and Zn (II) respectively from aqueous solutions (Taha, 2021).

A quantitative summary of the critical findings reported among the best available prior art with respect to Cu (II), Pb (II), Zn (II), and Fe (II) adsorption attributes has been presented in Table 1.2.

1.2.3 Adsorption Characteristics of Chitosan and Associated Derivatives

The adsorptive removal of Cu (II) with N-(2-hydroxy-3–mercapto-propyl) chitosan, N-(2-hydroxy-3–methyl aminopropyl) chitosan and 6 -O-(mercapto acetate–N-mercaptoacetyl chitosan has been studied from aqueous solutions (Cárdenas et al., 2001). For the chosen chitosan derivatives, N-(2-hydroxy-3–mercapto-propyl) chitosan exhibited the highest metal uptake of 238 mg g^{-1} for Cu (II) adsorption at an optimum pH of 4.5. Another research group synthesized the *N*-succinyl-chitosan derivative (with succinyl acid functional group) and investigated the adsorption of Pb (II) (S. Sun & Wang, 2006b). It was analyzed that the maximum adsorption capacity of 1.68 mmol g^{-1} can be achieved at an optimum pH of 5.8. In another article, the research group synthesized the Carboxymethyl-chitosan derivative (with the carboxylic acid functional group)

and investigated Zn (II) adsorption (S. Sun & Wang, 2006a). Thereby, the authors reported a maximum adsorption capacity of 2.04 mmol g^{-1} at an optimum pH of 6.32.

In a relevant prior art, the authors prepared a mixed metal solution of Cu (II), Cd (II), Ni (II), and Pb (II) using nitrate and sulphate systems and thereby studied the adsorptive characteristics of EDTA-modified crosslinked chitosan (Huacai Ge and Shiying Huang, 2010). At the optimal process condition, the adsorption capacity of the resin was inferred to be 2.11 mmol of Cu/g of resin, 1.28 mmol of Ni per g of resin, 1.29 mmol of Cd per g of resin, and 1.28 mmol of Pb per g of resin. Other researchers studied the adsorption of zinc from nitrate and sulphate solution of Cu (II), Cd (II), Ni (II), and Zn (II) using pristine chitosan (F. C. Wu et al., 2010). The authors reported an adsorption capacity of 4.42 mmol g^{-1} at an optimal pH of 2.0. The adsorption capacities of Cu (II), Ni (II), and Cd (II) have been as well examined. At optimal conditions, the adsorption capacity of these heavy metals was 3.13 mmol of Cu per g of resin, 2.33 mmol of Ni per g of resin, and 3.34 mmol of Cd per g of resin respectively. The investigations considered a fixed choice of pH and as the natural pH of the mixed metal solution. Considering the metal solution of Cu (II), Hg (II), Pb (II), and Zn (II), another research group studied the adsorption characteristics of chitosan (Benavente et al., 2011). The authors reported a maximum adsorption capacity of 79.94 mg L^{-1} for Cu (II), 109.55 mg L^{-1} for Hg (II), 58.71 mg L^{-1} for Pb (II), 47.15 mg/l for Zn (II) at an optimal pH of 6, 4, 6, 6 respectively. Also, it was analyzed that the maximum desorption was for the Cu (92 %).

For the adsorption of Pb (II), another research group synthesized EDTA-modified chitosan–silica hybrid derivative and conducted relevant studies (Repo et al., 2011). It was inferred that the maximum adsorption capacity was 0.62 mmol g^{-1} at an optimal pH of 3. Adsorption characteristics of Cu (II), Pb (II), and Cd (II) were examined for the nitrate solution (Ren et al., 2013). In the

article, the authors synthesized magnetic EDTA-modified chitosan adsorbent and found that the highest adsorption capacity of 0.70 mmol g^{-1} was achieved at an optimal pH of 5. Also, with complex EDTA eluent, the desorption was 75.73 %. In another article, chitosan-glutaraldehyde beads (with an amine functional group) were synthesized for the adsorption-based removal of Pb (II), Ni (II), Zn (II), and Cu (II). The initial metal ion concentration was altered as 9.1-90.72, 13.39-99.39, 11.31-92.32, and 14.58-108.8 mg L^{-1}, respectively. Thereby, maximum adsorption capacities of 67.19, 67.81, 72.71, and 79.18 mg g^{-1} respectively were reported (Busuioc et al., 2016).

Another research group synthesized chitosan-coated bentonite (with Si-O and amine functional group) for the adsorptive removal of Pb (II), Cu (II), and Ni (II). The work inferred that the maximum adsorption capacities were 13.49, 12.14, and 10.29 mg L^{-1}, respectively. Hence, the synthesized derivative functioned best for the Pb (II) removal (Tsai et al., 2016). Dev et al. (2020) examined the adsorption characteristics of Zwitterion-chitosan for Zn (II), Pb (II), and Cu (II) and found maximum adsorption capacity of 92.27, 127.91, and 123.50 mg g^{-1}, respectively at an optimal pH of 6 (Dev et al., 2020). For the adsorptive removal of Zn (II), Pb (II), and Cu (II), another research group attempted adsorption studies with carboxymethyl chitosan derivative (with carboxyl acid functional group) and found maximum removal of 65, 86 and 75 %, respectively at an optimal pH of 10 (Kavitha et al., 2020).

The pertinent information with respect to the Cu (II), Pb (II), Zn (II), and Fe (III) adsorption and desorption attributes of important alternate chitosan-based functional adsorbents have been quantitatively summarized in Table 1.3.

1.2.4 Adsorptive Performance of Other Chelating Resins

The adsorption characteristics of Cr (VI), Cu (II), and Zn (II) from their aqueous solution have been studied for the carrot residue adsorbent (Nasernejad et al., 2005). For an optimal pH of 4.5, the authors reported optimal adsorption capacities for Cr (VI), Cu (II), and Zn (II) as 45.09, 32.74, and 29.61 mg g^{-1}, respectively. Using cascade lime as an adsorbent, a research group studied sulfate and chloride solutions of Cu (II), Mn (II), Zn (II), and Ni (II) and found maximum removal of 99.30 % Cu (II) (pH 6) and 99.24 % Mn (II) (pH 11), respectively (Pavlović et al., 2007). Other researchers studied the adsorption characteristics of Cd (II), and Pb (II) and reported maximum removal of 89.2 % and 85.3 %, respectively using banana peel as an adsorbent (Anwar et al., 2010). A research group synthesized a novel Na Alginate Tricholoma Lobayense composite adsorbent for the removal of Pb (II), Cd (II), and Cu (II) from their aqueous solution. At an optimal pH of 5, the solution concentration was varied between 10-100 mg L^{-1}. It was found that the maximum adsorption capacity of Pb (II) was obtained as 526.3 mg g^{-1} with a single metal solution. However, after mixing with the other metal solutions, the maximum adsorption capacity was significantly reduced to 370.4 mg g^{-1} (Cao et al., 2010). Similarly, the desorption efficiency of Pb (II) was also reduced for the mixed metal solutions.

A novel poly(ethylenimine) grafted aerobic granular sludge adsorbent (with ethylenimine functional group) has been reported for the removal of Cu (II) and Cr (VI) from their aqueous solutions. For the system, the initial solution concentration was varied between 10-500 mg L^{-1}. At an optimum pH of 5.5, the maximum adsorption capacity of 71.24 and 348.12 mg g^{-1} was achieved for Cu (II) and Cr (VI) (X. F. Sun et al., 2011). For the sulfured orange peel adsorbent, a nitrate solution of Pb (II), and Zn (II) was considered (Liang et al., 2011). The authors reported a maximum adsorption capacity of 164 mg g^{-1} for Pb (II) and 80 mg g^{-1} for Zn (II) at an optimal pH

of 5. Other authors reported the efficacy of synthesized titanate nanotubes (with hydroxyl functional group) adsorbent for the recovery of Pb (II), Cu (II), Cd (II), and Cr (VI) from their aqueous chloride solution (Liu et al., 2013). The best desorption efficiencies of 98, 94, 91, and zero %, respectively have been reported for the EDTA eluent. For the cabbage waste adsorbent, an aqueous solution of Cu (II), Pb (II), Zn (II), and Cd (II) was studied (Liu et al. 2014). In this prior art, the authors examined both single-metal and mixed-metal solutions. It was reported that the maximum adsorption capacity was reduced for the metals in the mixed metal solution. However, the maximum adsorption capacity of Zn (II) remained unaltered (10.89-10.17 mg g^{-1}).

In another article, the authors reported a mixed metal solution of Zn (II), Cd (II), and Pb (II) using nitrate precursors of the metals and thereby studied the adsorptive efficacy of extracellular polymeric substance adsorbent. At optimal conditions (initial solution pH of 4.5 and initial concentration as 5-200 mg L^{-1}), the adsorption capacity of resin was analyzed to be 980.4 mg of Zn per g of resin, 1388.9 mg of Cd per g of resin and 1515.2 mg of Pb per g of resin. It was also reported that the maximum removal was 94.78 % for Pb (II) and 51.28 % for Cd (II) (Liu et al., 2015). For mixed clay adsorbents, a research group reported the adsorption characteristics of Cd (II), Co (II), and Cu (II) from their nitrate solution (Mnasri-Ghnimi & Frini-Srasra, 2019). The authors inferred that at optimal conditions (pH of 8 and initial concentration of 10-100 mg L^{-1}), the removal of Cd (II) was 74.29 %. Incidentally, this value was maximum among all other species in the solution.

A quantitative summary of the critical findings of adsorptive and desorptive attributes of the reported best resins and adsorbents in this section has been presented in Table 1.4.

Table 1.2: A summary of literature reported Cu (II), Pb (II), and Zn (II) adsorption and desorption characteristics of commercial resins.

Metal Ion	Adsorbent	pH	Conc. (mg L^{-1})	Ads. Caps. (mg g^{-1})	Removal (%)	Desorption (%)	References
Pb (II)	GMA/DVB magnetic resin	6	5 (mmol L^{-1})	2.68	-	96 (0.2M EDTA 5 Cycles)	(Atia et al., 2008)
Cd (II)		6.6		2.39			
Zn (II)		6.5		2.00			
Ca (II)		6.5		1.99			
Mg (II)		7.0		1.83			
Cu (II)	Lewatit TP 207 Lewatit TP 260 Lewatit SP 112	6.5	-	42.15 (ii)	-	-	(Hubicki et al., 2011)
Zn (II)				64.12			
Co (II)				80.61			
Ni (II)				68.33 (iii)			
Cr (VI)	Styrene –DVB copolymer	3.5	-	-	99.7	65	(Misra et al., 2011)
Ni (II)					65	70	
Pb (II)					59	45	
Cd (II)					28	(0.1N NaOH)	
Pb (II)	Polyvinyl tetrazole grafted PS resins	5	4 (mmol L^{-1})	1.52	26.3	94 (10 Cycle)	(Chen et al., 2014)
Cu (II)				2.65	39.8		
Cr (VI)				3.36	83.2 (Mixed)		
Al (III)	Lewatit TP 260	3.9	-	64.764	-	>90 (low molar Sulfuric Acid)	(Nekouei et al., 2019)
Cu (II)				1.749			
Ni (II)				3.247			
Pb (II)	Lewatit TP 208			66.67			
Zn (II)				1.681			
				2.740			
	Amberlite IRA743			35.3			
				1.337			
				1.183			
Mn (II)	Dowex Marathon C	-	20-300	9.6	77.1	-	(Taha, 2021)
Cu (II)				11.3	83.1		
Zn (II)				13.6	77.8		
Cd (II)				7.4	65.1		

Table 1.3: A summary of literature reported Cu (II), Pb (II), and Zn (II) adsorption and desorption characteristics of chitosan-based synthesized resins.

Metal Ion	Adsorbent	pH	Conc. (mmol L^{-1})	Ads. Caps. (mmol g^{-1})	Removal (%)	Desorption (%)	References
Pb (II)	EDTA modified crosslinked	5	-	1.28	-	95.8	(Huacai Ge, 2010)
Cd (II)				1.29		95.9	
Ni (II)				1.28		94.3	
Cu (II)				2.11		93.3	
Cu (II)	chitosan	6	5-50 (mg L^{-1})	79.94	96.3	92.0	(Benavente et al., 2011)
Hg (II)		4		109.55	93.6	1.6	
Pb (II)		6		58.71	73.5	29.6	
Zn (II)		6		47.15	95.9	72.3	
Cu (II)	magnetic EDTA-modified	5	1-7	0.10-0.70	-	90 Na_2EDTA	(Ren et al., 2013)
Pb (II)				0.10-0.60			
Cd (II)				0.08-0.56			
Pb (II)	chitosan-glutaraldehyde Beads	-	90.72	67.19	74.06	-	(Busuioc et al., 2016)
Ni (II)			99.39	67.81	73.45		
Zn (II)			92.32	72.71	73.16		
Cu (II)			108.8	79.18 (mg g^{-1})	72.77		
Zn (II)	zwitterion-chitosan	6	150 (mg L^{-1})	92.27	-	95 (4 cycles)	(Dev et al., 2020)
Cd (II)				108.42			
Pb (II)				127.91		71.2 (5 cycles)	
Cu (II)				123.50			
Cu (II)	carboxymethyl chitosan	10	20-70 (mg L^{-1})	-		75	(Kavitha et al., 2020)
Ni (II)						72	
Zn (II)						65	
Pb (II)						86	
Cu (II)	chitosan-coated perlite beads	5	50-200	128.20	-	Column study using 0.1 N NaOH	(Swayampakula et al., 2009)
Co (II)				35.21			
Ni (II)				30.487			

Table 1.4: A summary of literature reported Cu (II), Pb (II), and Zn (II) adsorption and desorption characteristics of other synthesized resins.

Metal Ion	Adsorbent	pH	Conc. (mg L^{-1})	Ads. Caps. (mg g^{-1})	Removal (%)	Desorption (%)	References
Pb (II) Cd (II) Cu (II)	Na Alginate Tricholoma Lobayense composite	5	10-100	526.3/370.4 769.2/22.1 92.6/91.7 (single/mixed)	-	24/12 8/2 10/5 (mg g^{-1}) (1M HNO_3)	(Cao et al., 2010)
Pb (II) Cd (II) Cu (II) Cr (III)	titanate nanotubes	5	0.1-3 (mmol L^{-1})	2.64 2.13 1.92 1.37	-	72/98 92/91 93/94 40/0 (HNO_3/EDTA)	(Liu et al., 2013)
Cu (II) Pb (II) Zn (II) Cd (II)	cabbage waste	6	1-500	12.95/2.415 61.27/15.08 10.89/10.17 22.12/8.69 (single/mixed)	-	-	(Liu et al., 2014)
Pb (II) Cd (II) Cr (III) Cu (II) Zn (II)	sesame straw biochar	7	5-40	104/88 86/5 65/21 55/40 34/7 (single/mixed)	-	-	(Park et al., 2016)

1.2.5 Ranking and Cost Efficacy of Chelating Resins for Adsorptive Removal of Heavy Metals

The technical proficiency of alternate adsorbents and chelating resins for heavy metal removal and resin reusage has been discussed in relevant sub-sections of the prior art. The commercial relevance of these materials crucially depends upon their cost efficacy and sustainable performance. Thereby, a conceptual cost analysis can serve as a crucial tool to support technical conclusions and thereby facilitate effective decision-making with respect to resin selection through a holistic and combinatorial analysis of process cost, threats to the ecosystem, and accompanying disposables.

Needless to infer, the adsorbent cost is an essential aspect in the decision-making process. The major deployed adsorbents for heavy metals removal are commercial resins, bio adsorbents, and functionally modified derivatives. Many of these are very expensive to afford in a developing country such as India. Thus, the wider utilization of such adsorbent materials is a serious issue to ponder upon. Thereby, resin selection and choice need to elucidate upon both resin reusage competence and its lower cost for the treatment of complex adsorbate systems being encountered in real-world scenarios.

For such contextual perspectives, it shall be noted that the reported commercial resins and chitosan derivatives have not been thoroughly analyzed for their cost efficacy. The available prior art provides dismally little knowledge in this regard. The vast literature database does not specify upon the relevance of stoichiometric quantities and their functional role in terms of functional group abundance, resin reusage efficacy based on cyclic adsorption-desorption data, and rigorous cost analysis based on retail prices of the deployed precursors, solvents, etc.

As a result, conceptual cost and performance-based conceptual profitability analysis has not been precisely highlighted in the prior art and this is to be addressed to a certain extent in the PhD thesis. Also, the commercial resin-based analysis conveys that while the Lewatit TP 214 is impressive, it is however expensive to afford for large-scale treatments. Thereby, other cost-efficient industrial resins need to be explored to conclude upon their efficacy for heavy metal removal. The basis for such studies is in terms of the effective resin reusage for complex wastewater systems that have closer semblance with the complex industrial effluents.

1.3 Possible scope for further research

1.3.1 Efficacy of Alternate Sorbent Materials for Multi-Heavy Metal Removal from Complex Adsorbate Systems

Removing heavy metals from contaminated streams has been the subject of a large number of reported prior art and ongoing research studies. Among these, major studies devoted to the heavy metal removal from simpler synthetic aqueous waste streams such as acidic or neutral solutions (Atia et al., 2008; Benavente et al., 2011; Busuioc et al., 2016; Cao et al., 2010; Chen et al., 2014; Dev et al., 2020; Huacai Ge, 2010a; Hubicki et al., 2011a; Kavitha et al., 2020a; LIU et al., 2014; Liu et al., 2013; Misra et al., 2011; Nekouei et al., 2019a; Park et al., 2016; Ren et al., 2013; Swayampakula et al., 2009; Taha, 2021). However, real-time scenarios involving industrial waste effluents possess enhanced complexity in terms of other coexisting heavy and conventional cations. Such systems have not been considered till date in the adsorption-desorption studies of even the best-mentioned prior art. An example of such a complex adsorbate system refers to the agricultural and industrial untreated wastewater that constitutes Na, Al, K, and Mg along with the targeted heavy metal ions namely Cu, Zn, Fe, and Pb (Morcali et al., 2014). For such cases, the

heavy metal removal can be detrimentally influenced due to the poor desorption performance of the chosen resins.

Regarding heavy metal recovery from such complex adsorbate systems, the adsorptive effectiveness of O, N, and S synthesized derivatives may be worth taking into consideration. According to the HSAB hypothesis, when all other variables are kept constant, weak acids respond faster and build stronger connections with weak bases, and vice-versa (i.e. strong acids respond faster and build stronger connections with strong bases). For highly complex adsorbate systems such as real-time-based industrial effluents, the hypothesis needs to be verified based on further investigations. Based on the HSAB, it is possible to analyze commercial resins and functionalized chitosan derivatives with respect to their efficacious heavy metal removal from intricate adsorbate systems. However, the role of other co-existing cations needs to be experimentally verified as they further complicate pertinent speciation and complexes.

In summary, it is noteworthy that commercial resins and chitosan derivatives possessing O and N functional groups have been examined for heavy metal removal. However, solutions with the least complexity of solution chemistry (for example, acidic and aqueous source solutions) were considered. The need of the hour is to consider solutions that constitute several other cations that may interfere and compete with the heavy metal adsorption characteristics. Also, few adsorbents have been studied in the context of pH and solute concentrate effects but not in conjunction with the pertinent speciation that critically catalyzes or detriments multi-heavy metal adsorption (Kavitha et al., 2020b; Ren et al., 2013). Also, the reusage of the mentioned resins is required in the midst of complex solutions and associated challenges. Such potential studies will be successful in promoting the commercial and industrial utility of the aforementioned resins and derivatives to concurrently reduce effluent threat through the sustainable removal of heavy metals from effluents.

Also, among many chitosan derivatives with O and N functional groups, modified chitosan derivatives with citric acid (Suc and Ly, 2013), polyvinyl alcohol (Trikkaliotis et al., 2020), and carboxymethyl (Abreu and Campana-Filho, 2005) precursors may be enticing for heavy metals removal from simulated industrial effluents. The chelation of N and O atoms that exist in the relevant functional groups will be of particular interest in an intricate adsorbate system. This is due to the emphasis on issues such as evaluation of adsorption mechanism, difficulties encountered in due course of the desorption characteristics and other peripheral issues such as lower resin fabrication cost and reusage efficacy of the deployed adsorbent.

1.3.2 Desorption Characteristics and Cost Efficacy of Eluents Deployed for Multi-Heavy Metal Removal

So far, several adsorptive investigations have been performed for the heavy metal removal from wastewater systems using various types of adsorbents. In many cases, researchers did not target upon the cyclic reusability characteristics of the spent adsorbents (Abo-Farha et al., 2009; Busuioc et al., 2016; Demirbas et al., 2005; Hubicki et al., 2011b; LIU et al., 2014; Mnasri-Ghnimi and Frini-Srasra, 2019; Niu et al., 2010; Pavlović et al., 2007; Pehlivan and Altun, 2006; Rengaraj et al., 2004; Taha, 2021; Zawierucha et al., 2014). In many studies, authors employed sophisticated and costly eluents such as Na_2EDTA, EDTA, and EDTA-HCl for heavy metal recovery from deployed adsorbents. These eluents are costlier, hazardous, and non-sustainable for large-scale scenarios that demand adsorption-based heavy metal removal and resin reusage (Atia et al., 2008; Liu et al., 2013; Ren et al., 2013). The possibility for desorption-based removal of heavy metal may be effectively targeted using simpler acidic and basic eluents. Consequently, cost-effective multi-heavy metal removal can be targeted. Ongoing research trends also advocate upon the need

for investigations with such simpler eluents (Benavente et al., 2011; Cao et al., 2010; Dev et al., 2020; Huacai Ge, 2010b; Kavitha et al., 2020b; Nekouei et al., 2019b). However, the mentioned prior art targeted wastewater systems of lower chemistry complexity. Thus, studies based on simple eluents (HCl, NaOH, HNO_3, KOH, etc.), and relevant studies have been scanty for more complex wastewater systems. Considering this aspect, the Ph.D. thesis needs to analyze the performance of a few promising commercial resins and chitosan derivatives.

1.3.3 Role of Chitosan Molecular Weight on Grafting and Multi-Heavy Metal Removal Efficacy for Intricate Adsorbate Systems

Numerous adsorbents have been reported for heavy metal removal from aqueous and acidic solutions. This has been vividly presented in the relevant prior-art sub-sections. However, no inputs have been provided to convey upon the role of the molecular weight of chitosan in influencing adsorptive and desorptive efficacy and resin reusability (Benavente et al., 2011; Busuioc et al., 2016; Cárdenas et al., 2001; Dev et al., 2020; Kavitha et al., 2020a; Repo et al., 2011). Also, the stoichiometry of chosen grafting and crosslinking agents need to be as well assessed. These were ignored in the mentioned prior art. Such directives will be useful to gain further useful insights into their role in influencing cost-effective and sustainable resin development and process optimization.

1.3.4 Cost Efficacy-based Sustainability of Adsorbents for Multi-Heavy Metal Removal

The relevant prior-art sections provided details with respect to experiments conducted to remove heavy metals from aqueous and acidic solutions. However, no inputs have been provided based on cost efficacy. For this reason, it is necessary to analyze the cost efficacy of various adsorbents for

the removal of heavy metals from complex and intricate adsorbate systems. Thereby, needful introspection into the most efficient resin identification and competitiveness-based benchmarks can be set to further enhance research quality in resin fabrication chemistry and resin application domain.

1.3.5 Scope for Targeted Commercial and Chitosan Derivative Resins

Based on the HSAB (Hard and soft acid and base) hypothesis, heavy metal ions have a greater affinity towards oxygen-containing functional groups. Thus, according to the HSAB hypothesis, commercial resins namely Amberlyst IR120H (containing sulfonic acid functional group) and Lewatit TP 260 (containing aminomethyl phosphonic acid functional group) were selected for adsorption-desorption studies in this PhD thesis. These resins were selected based on the combinatorial analysis involving the relevance of functional groups, processing, availability, and retail cost.

Along with these commercial resins, chitosan derivatives such as chitosan-PVA derivative, chitosan-citric acid derivative, and carboxymethyl chitosan were prepared for adsorption-desorption studies in this PhD thesis. These resins were once again chosen based on the combinatorial analysis involving the presence of excess oxygen functional groups in the said resins, the easy preparation process for the chosen resins, the non-toxic nature of the resins, and lower fabrication cost in conjunction with other derivatives. Many of these resins have a tendency towards the application of green chemistry due to the utilization of ingredients that may cause little harm to the environment even after disposal due to their higher bio-degradability status.

1.4 Thesis Objectives

Based on the aforementioned research gaps, the following objectives have been set for the PhD thesis:

a) Multi-metal adsorption, desorption, and cyclic efficacy of commercial Lewatit TP260, Amberlite IRA 120H for complex Zn and Cu-based synthetic wastewater solutions.

b) Effect of chitosan molecular weight on the polyvinyl alcohol-chitosan derivative performance attributes (adsorption, desorption, and cyclic efficacy) for complex Zn and Cu-based synthetic wastewater solutions.

c) Effect of chitosan molecular weight on the citric acid-chitosan derivative performance attributes (adsorption, desorption, and cyclic efficacy) for complex Zn and Cu-based synthetic wastewater solutions.

d) Effect of chitosan molecular weight on the carboxymethylated chitosan derivative performance attributes (adsorption, desorption, and cyclic efficacy) for complex Zn and Cu-based synthetic wastewater solutions.

e) Conceptual resin and processing cost analysis for the quantification of suitable cost-based benchmarks and identification of best-performing resin for the multi-heavy metal ion removal from complex adsorbate systems.

1.5 Organization of the Thesis

As elaborated in section 1.3 of the thesis, significant scope does exist for further research in the field of chelating and ion-exchange resins for multi-heavy metal adsorption from complex adsorption systems such as industrial wastewater solutions. The objectives mentioned in section 1.4 of the PhD thesis aim to gain deeper insights into such a central objective. In this section, a

brief summary of all subsequent chapters of the thesis has been presented in the following paragraphs.

Chapter 2 details upon the experimental and modeling approaches being addressed in the entire Ph.D. thesis. These include (a) preparation of simulated Cu and Zn dominant multi-heavy metal complex waste water solutions, (b) batch adsorption of multi-heavy metals onto the chosen commercial resins (Amberlite IR120H, and Lewatit TP260) followed with modeling approaches to represent evaluated adsorption characteristics, (c) preparation and characterization of chitosan based biosorbents (chitosan-polyvinyl alcohol derivative variants, chitosan-citric acid derivative variants, and chitosan-carboxy methyl derivative variants), (d) batch adsorption of multi-heavy metals on chitosan based biosorbents followed with modeling approaches to represent evaluated adsorption characteristics, (f) cyclic batch desorption efficacy of the commercial resins, (g) cyclic batch desorption efficacy of mentioned chitosan derivatives.

Chapter 3 addresses multi-heavy metals (Cu, Fe, Pb, and Zn) adsorption and desorption characteristics of commercial ion-exchange resins (such as Lewatit TP 260 and Amberlite IR 120H) with synthetic industrial wastewater solutions (Cu dominant and Zn dominant solutions). Results obtained from relevant modeling efforts have also been elucidated in the chapter to identify the best-fit models for various cases. Finally, batch desorption characteristics of said commercial resins with simple eluents such as NaOH, KOH, H_2SO_4, HNO_3, and HCl have been summarized to identify the best inexpensive eluent for heavy-metal removal and resin reuse from simulated industrial wastewater solutions. In addition, the chapter also summarizes a comparative assessment of multi-heavy metal adsorption using various other reported best-performing adsorbents in the prior art.

Chapter 4 details upon the results obtained for polyvinyl alcohol grafted chitosan derivatives. These refer to polyvinyl alcohol grafted low molecular weight chitosan (low CSPVA), polyvinyl

alcohol grafted medium molecular weight chitosan (medium CSPVA), and polyvinyl alcohol grafted high molecular weight chitosan (high CSPVA). Subsequently, multi-heavy metal batch adsorption characteristics and fitness of best equilibrium and kinetic models have been summarized for the mentioned polyvinyl alcohol grafted chitosan variant derivatives. Finally, cyclic batch desorption characteristics of the best polyvinyl alcohol grafted chitosan variant derivative have been summarized for simple eluents such as NaOH, KOH, H_2SO_4, HNO_3, and HCl. Thereafter, the chapter also summarizes a comparative assessment of best-assessed multi-heavy metal adsorption characteristics with those reported best in the relevant prior art.

Chapter 5 details upon the results obtained for citric acid-modified chitosan derivatives. These refer to citric acid-modified low molecular weight chitosan (low Cit-CS), citric acid-modified medium molecular weight chitosan (medium Cit-CS), and citric acid-modified high molecular weight chitosan (high Cit-CS). Subsequently, multi-heavy metal batch adsorption characteristics and fitness of best equilibrium and kinetic models have been summarized for the mentioned citric acid-modified chitosan derivatives. Finally, cyclic batch desorption characteristics of the best polyvinyl alcohol grafted chitosan variant derivative have been summarized for simple eluents such as NaOH, KOH, H_2SO_4, HNO_3, and HCl. Thereafter, the chapter also summarizes a comparative assessment of best-assessed multi-heavy metal adsorption characteristics with those reported best in the relevant prior art.

Chapter 6 details upon the results obtained for carboxymethylated chitosan derivatives. These refer to carboxymethylated low molecular weight chitosan (low CMCS), carboxymethylated medium molecular weight chitosan (medium CMCS), and carboxymethylated high molecular weight chitosan (high CMCS). Subsequently, multi-heavy metal batch adsorption characteristics and fitness of best equilibrium and kinetic models have been summarized for the mentioned carboxymethylated chitosan derivatives. Finally, cyclic batch desorption characteristics of the best

polyvinyl alcohol grafted chitosan variant derivative have been summarized for simple eluents such as NaOH, KOH, H_2SO_4, HNO_3, and HCl. Thereafter, the chapter also summarizes a comparative assessment of best-assessed multi-heavy metal adsorption characteristics with those reported best in the relevant prior art.

Chapter 7 elucidates upon the comparative assessment of the conceptual chitosan derivative fabrication cost with respect to the retail cost of the commercial resin and processing cost of all synthesized chitosan derivatives and commercial resins. Accordingly, the best-performing resin has been identified for the multi-heavy metal removal from two complex adsorbate systems that have a close resemblance with industrial heavy wastewater systems.

Chapter 8 addresses the conclusions deduced from the research findings of this work. Finally, possible research directions in the near future in the mentioned research theme have been presented in a dedicated section in the thesis.

Chapter 2:

Materials and Methods

Chapter 2

Materials and Methods

In six sections, the chapter presents a summary of the experimental and modeling approaches being adopted in the Ph.D. thesis. Among these, the first section (section 2.1) addresses the materials required for the preparation of Cu and Zn dominant simulated industrial wastewater solutions and the physicochemical properties of commercial resins. Thereafter, section 2.2 elaborates upon synthesis procedures associated to various chitosan derivatives. Following this, section 2.3 briefly presents surface characterization methodologies for commercial resins and chitosan derivatives. Sections 2.4 and 2.5 respectively delineate upon the procedures followed for batch adsorption and desorption studies. Finally, section 2.6 summarizes considered modeling methods for the evaluation of the fitness of well-known equilibrium and kinetic models to represent measured multi-heavy metal adsorption-based removal data for Cu and Zn dominant simulated wastewater solutions.

2.1 Materials

2.1.1 Commercial Resins and Chemicals

Amberlyst IR120H and Lewatit TP 260 commercial resins were procured from Sigma-Aldrich Corporation, Bangalore, India. Table 2.1 presents a summary of various physiochemical properties of these commercial resins. For adsorbent preparation, chitosan (7100, 220000, and 583000 g mol^{-1} for low, medium, and high molecular weight cases, respectively), polyvinyl alcohol $(C_2H_4O)_x$ (Cat No. 8.43866), and citric acid ($C_6H_8O_7$) (Cat No. 251275) were obtained from Sigma-Aldrich, Bangalore, India.

Table 2.1: Salient characteristics of Amberlite IR 120H and Lewatit TP 260 commercial resins.

Properties	Commercial resins used	
	Amberlite IR 120H	**Lewatit TP 260**
Active Group	Sulfonic acid	Aminomethyl phosphonic acid
Maximum operating range (^oC)	150	80
Purchased Form	As shipped H	As shipped Na
Particle size (mean) (mm)	0.5	0.5
Operation pH range	0-14	0-14
Total transferring capacity	1.9 meq mL^{-1} wet resin 4.50 mmol mL^{-1}	2.3 mmol g^{-1}

2.1.2 Copper and Zinc dominant simulated complex wastewater system precursors

Simulated wastewater solutions of desired heavy metal concentrations were prepared with metallic salts summarized in Table. 2.2. Furthermore, millipore water (Make: milliQ) was used for the preparation of solutions in aqueous media. The solution pH was measured with a pH meter (VSI-301).

Table 2.2: A summary of utilized chemicals for the preparation of a simulated complex wastewater adsorbate system.

S. No.	Chemical Name	Formula	Cat. No.	Seller
1.	Magnesium Sulfate	$MgSO_4$	M7506-500G	Sigma-Aldrich, Bangalore, India
2.	Zinc Sulfate	$ZnSO_4.7H_2O$	221376-500G	
3.	Potassium Sulfate	K_2SO_4	223492-500G	
4.	Lead Nitrate	$Pb(NO_3)_2$	228621-500G	
5.	Aluminum Sulfate	$Al_2(SO_4)_3.18H_2O$	227617-500G	
6.	Sodium Sulfate	Na_2SO_4	238597-500G	
7.	Ferric Sulfate	$Fe_2SO_4.xH_2O$	215422-250G	
8.	Copper Sulfate	$CuSO_4.5H_2O$	209198-500G	

2.1.3 Preparation of Copper and Zinc dominant simulated stock solutions

Real industrial wastewater and simulated wastewater are two alternate types of aqueous adsorbate systems. They are often used in the research associated to the development of sustainable wastewater treatment technologies. Real industrial wastewater is the wastewater being generated as a byproduct of the industrial processes. It is collected directly from industrial facilities and constitutes a highly complex combination of contaminants at their appropriate compositions. Thus, real industrial wastewater composition varies widely and is critically dependent upon the type of industry and the involved processes. Such systems constitute pollutants such as chemicals, heavy metals, organic compounds, and even particulate solids. Thereby, it is highly challenging to treat such complex wastewater systems.

Often ignored contaminants in the real wastewater system due to non-detailed characterization approaches in wastewater treatment research translate into severe challenges. Accordingly, they may demand specialized treatment processes. Research emphasis on real wastewater is mandatory as it provides the most authentic resolution of challenges being faced in real-world scenarios. Accordingly, outcomes of such research can effectively address compliance with stringent environmental regulations. Thereby, the discharge of treated wastewater becomes an easy task.

On the other hand, the simulated wastewater system is a simpler representation of the real wastewater system. It is often developed with the major characterization parametric data of real wastewater samples. Accordingly, all constituents of the real wastewater system are not characterized and only those characterized will be considered in the laboratory work environment to achieve adsorbate systems through the effective mixing of specific chemicals and contaminants. Henceforth, controlled and reproducible wastewater samples can be realized. Thus, while simulated wastewater may provide dividends in research, they may not provide effective solutions

for real wastewater treatment scenarios, as certain key constituents may not be included in the simulated system. Consequently, the developed technologies could be ineffective to meet the stringent environmental regulations. Thus, it is very important to conduct a detailed characterization of wastewater adsorbate systems. Thereby, prepared simulated wastewater systems can mimic real wastewater systems. Thus, addressing moderately the variability in the real wastewater system, the simulated wastewater system may provide isolated solutions that may work in real-world scenarios. However, such studies will be beneficial to serve as an intermediate platform between simplistic aqueous solutions and complex real wastewater systems.

The prior art often suggests alternate palette compositions of wastewater systems. However, it does not delineate upon the type of wastewater and variability in the constitution of the metal ions (Futalan et al., 2011; Li et al., 2011; Misra et al., 2011; Ren et al., 2013; Verma et al., 2022b, 2022c, 2022a). To overcome such lacunae in the prior art, this thesis attempted to identify a wastewater composition such that its source is known and it constitutes a variegated palette of metal ions in the aqueous media (Morcali et al., 2014). Additionally, a similar study (Singh, 2019) also affirmed upon the presence of multi-heavy metal ions in the wastewater system in the state of Meghalaya, India. Accordingly, Cu and Zn dominant adsorbate systems have been chosen in this work as representative wastewater systems that mimic real wastewater samples. The composition of these simulated wastewater systems is based on the detailed account presented in relevant prior art (Morcali et al., 2014).

The considered wastewater systems in the Ph.D. thesis constitute Cu, Pb, Fe, Zn, and Al as heavy metals and Mg, Na, and K as co-existent cations. The Ph.D. thesis involved the evaluation of Cu, Pb, Fe, and Zn heavy metals removal from the wastewater system and did not consider the removal studies for Mg, Na, K, and Al. Among these, Al could not be evaluated due to the limitations in

the available infrastructure at the institute. Given the higher constitution of Mg, Na, and K in the adsorbate system, assuming a removal efficiency of about 50% for these, their constitution after adsorption has been assumed to be effective to meet the discharge regulations set by EPA and WHO. Accordingly, the studies are confined to the mentioned heavy metal ions removal. Further studies in this direction will be beneficial to corroborate upon the separation efficacy trends of real wastewater and simulated wastewater systems.

In the considered adsorbate systems, no organic and inorganic anions existed. This has been the case even with the composition reported in the relevant prior art. The dominant metal ions refer to Cu, Zn, Pb, Fe, K, Al, Mg, and Na. To assess upon the role of interfering cations, a few experimental trials were conducted in a hierarchy mode for the visualization of the sensitive roles of the mentioned ions in influencing the adsorption-desorption characteristics of the resins. Among all mentioned non-heavy metal cations, it was found that the Al had a detrimental influence on the adsorption-desorption characteristics of CSPVA resins. Through the conduct of similar studies, the sustainability limits of the best-performing resin can be assessed and thereby the resin performance can be enhanced through the inclusion of appropriate remedial pre-treatment strategies. Similarly, even though the adsorbate systems did not contain organic contaminants, such hierarchy mode base design of experiments can be addressed for similar adsorbate systems that constitute organic and inorganic anions. Accordingly, remedial strategies can be designed and further sustainability of the best-performing resin can be assured.

Table 2.3 summarizes the compositions of the prepared synthetic wastewater solutions for adsorption and desorption investigations. In the mentioned prior art, these wastewater solution palettes have been conveyed to have originated from agricultural and mining waste streams

(Morcali et al., 2014). Thus, appropriate metal salt quantities have been measured and diluted in deionized water samples.

Table 2.3: Constitution of heavy and non-heavy metals in the simulated complex wastewater adsorbate systems and their permissible limits.

S. No.	Metals	Solutions		Max permissible limits (The Environment Protection Act, 2002)
		Copper dominant solution (mg L^{-1})	Zinc dominant solution (mg L^{-1})	
1.	Cu	**375.4**	6.1	**0.5**
2.	Zn	3.5	**389.8**	**2**
3.	Mg	98.6	77.4	-
4.	Al	201.2	168.8	5
5.	Na	497.6	366.9	200
6.	K	49.8	10.4	-
7.	Pb	**10.4**	**5.3**	**0.05**
8.	Fe	**123.7**	**209.6**	**2**

2.2 Synthesis of Alternate Chitosan Derivatives

To achieve oxygen and nitrogen-functionalized chitosan derivatives, polyvinyl alcohol, citric acid, and carboxy methyl groups were grafted onto glutaraldehyde-treated chitosan. The degree of acetylation (DA) of low molecular weight chitosan, medium molecular weight chitosan, and high molecular weight chitosan was >90 %, >80 %, and 75 % respectively. The DA in chitosan refers to the extent to which chitin, the precursor to chitosan, has been deacetylated through the removal of acetyl groups. Accordingly, an inverse relationship exists between the degree of acetylation and the molecular weight of chitosan. Thus, chitosan with higher DA tends to possess lower molecular weight and vice-versa for higher molecular weight chitosan. DA also affects the solubility of chitosan. For example, chitosan with higher DA possesses higher solubility (Lv, 2016).

Hard and Soft Acid and Base (HSAB) theory and available prior art data (Benavente et al., 2011; Dev et al., 2020; Huacai Ge, 2010; Kavitha et al., 2020; Ren et al., 2013) conveyed that heavy metal ions such as Cu, Pb, Zn, and Fe exhibit higher affinity towards oxygen-containing functional groups in comparison to the resins possessing nitrogen and sulphur containing functional groups. Among alternate oxygen functional groups containing adsorbents, carboxy methyl, citric acid, and polyvinyl alcohol are promising from the perspective of simpler and easy synthesis of chitosan derivative resins, utilization of minimal or no hazardous chemicals, and cost of the materials. For these resins, a detailed account of the synthesis procedure has been elaborated in the following sub-sections.

2.2.1 Chitosan-polyvinyl alcohol derivative (CSPVA) Resin

Firstly, 6 g of chitosan was mixed slowly with 20 % aqueous CH_3COOH (acetic acid) solution and the mixture was kept overnight on a magnetic stirrer to realize a thick solution. Thereafter, 4 g PVA was blended in 300 mL deionized water at 80 °C and the solution was subjected to slow and continuous mixing on a magnetic stirrer at 150 rpm for 300 min. Subsequently, the PVA solution was slowly added to the previously prepared chitosan solution and the mixture was subjected to stirring for 300 min at 298 K. Consequently, the solution was transferred to a syringe and was precipitated in 2M NaOH solution to realize small beads of PVA-chitosan. Eventually, the beads were separated from the NaOH solution with a 125 mm diameter Whatman filter paper. Thereby, the beads were washed several times with a mixture of ethanol and deionized water. Finally, the residue was dried in an oven at 70 °C for 24 h and the dried residue was ground to achieve powder samples (Trikkaliotis et al., 2020). Fig. 2.1 summarizes the process flow diagram for resin preparation. This resultant powder being named as the CSPVA resin was further subjected to characterization and adsorption-desorption investigations. Using alternate molecular weight

chitosan precursor, the synthesized resins have been further termed as high, medium, and low CSPVA resin. Relevant functional group interaction during the synthesis of the mentioned resin has been presented in Fig. 2.2.

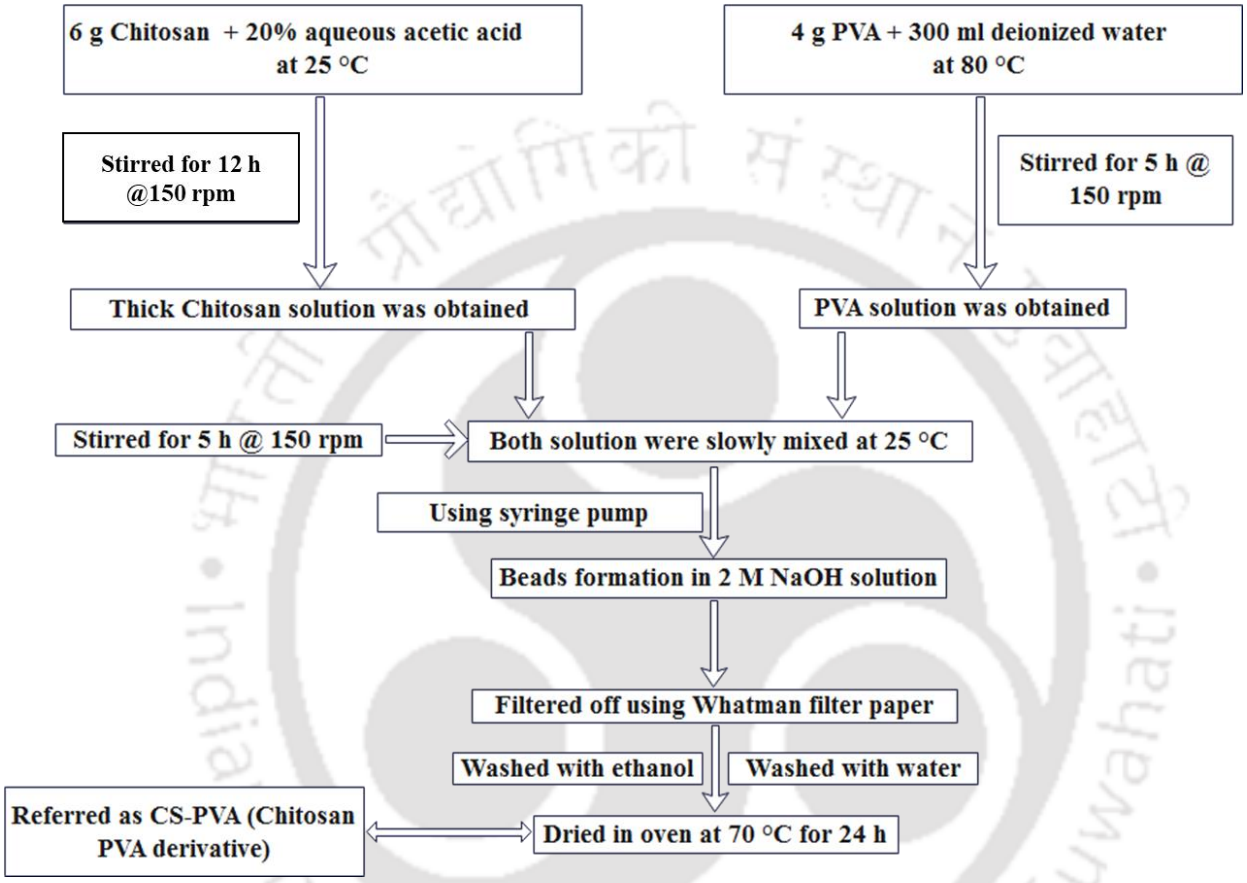

Fig. 2.1. Flowchart depicting the synthesis of CSPVA derivative resin.

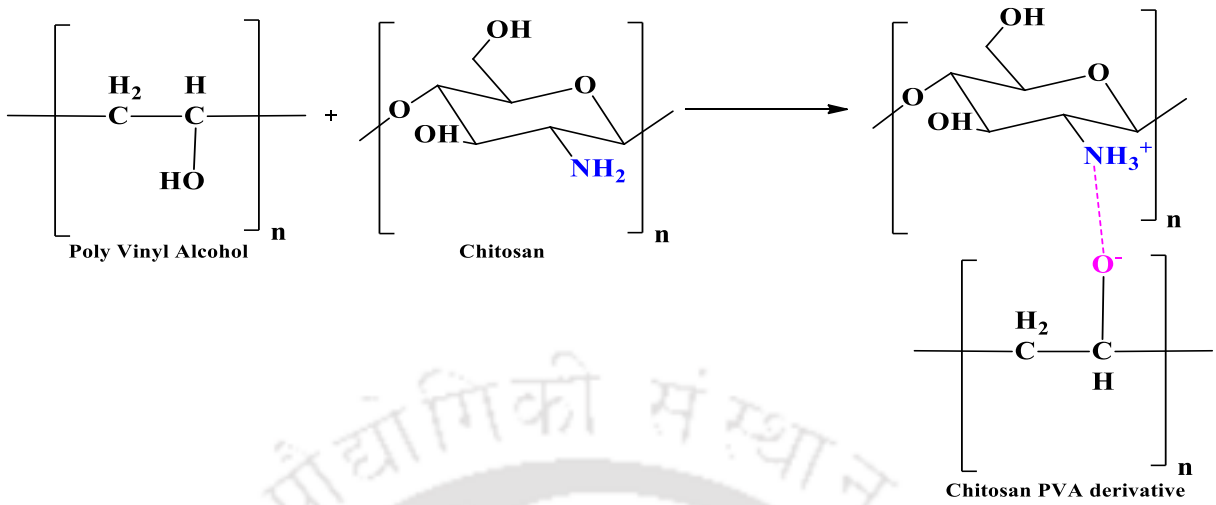

Fig. 2.2. Schematic depicting Chitosan-PVA structural interaction.

2.2.2 Chitosan-citric acid derivative (Cit-CS) Resin

To realize Cit-CS, firstly, 6 g of powdered chitosan was agitated in 600 mL of 20 % aqueous acetic acid solution for 12 h. Eventually, at room temperature, 96 mL of glutaraldehyde was added rapidly to the solution. After 1 h contact time, the reaction mixture turned to an orange color. Finally, the resulting mixture was treated with 0.2 M NaOH solution. Thereafter, the achieved solid product was rinsed repeatedly with deionized water and acetone. Subsequently, the product was dried overnight in a vacuum oven (56°C) (Nagireddi et al., 2017). Thereby, the obtained product refers to crosslinked chitosan. Thereafter, the crosslinked chitosan was soaked in an aqueous 5.0 % (w/v) citric acid solution for 24 h at 4 °C and at a pH of 5. Consequently, crosslinked chitosan being treated with the citric acid was dried thoroughly in an ambient environment and was dried thereafter in a vacuum oven at 60 °C. Deployed chitosan precursor with alternate molecular weight (low, high, and medium molecular weight), alternate resins have been realized by following relevant procedures mentioned in the prior art (Suc and Ly, 2013). A schematic of the Cit-CS resin

synthesis is depicted in Fig. 2.3. The developed resins were characterized further and were termed as high, medium, and low Cit-CS resin. Pertinent functional group interaction has been demonstrated in Fig. 2.4.

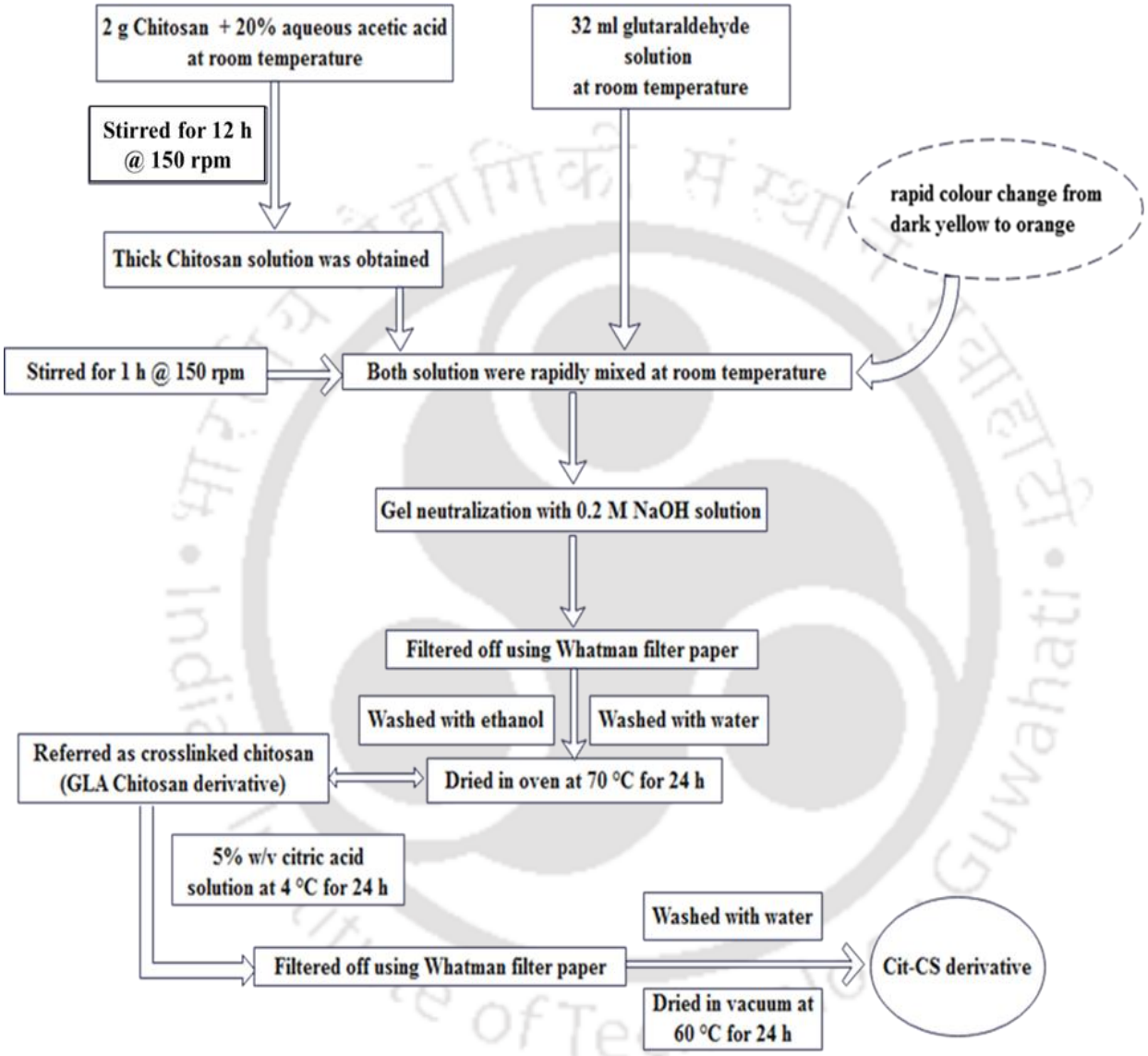

Fig. 2.3. Flowchart depicting the synthesis of Cit-CS derivative resin.

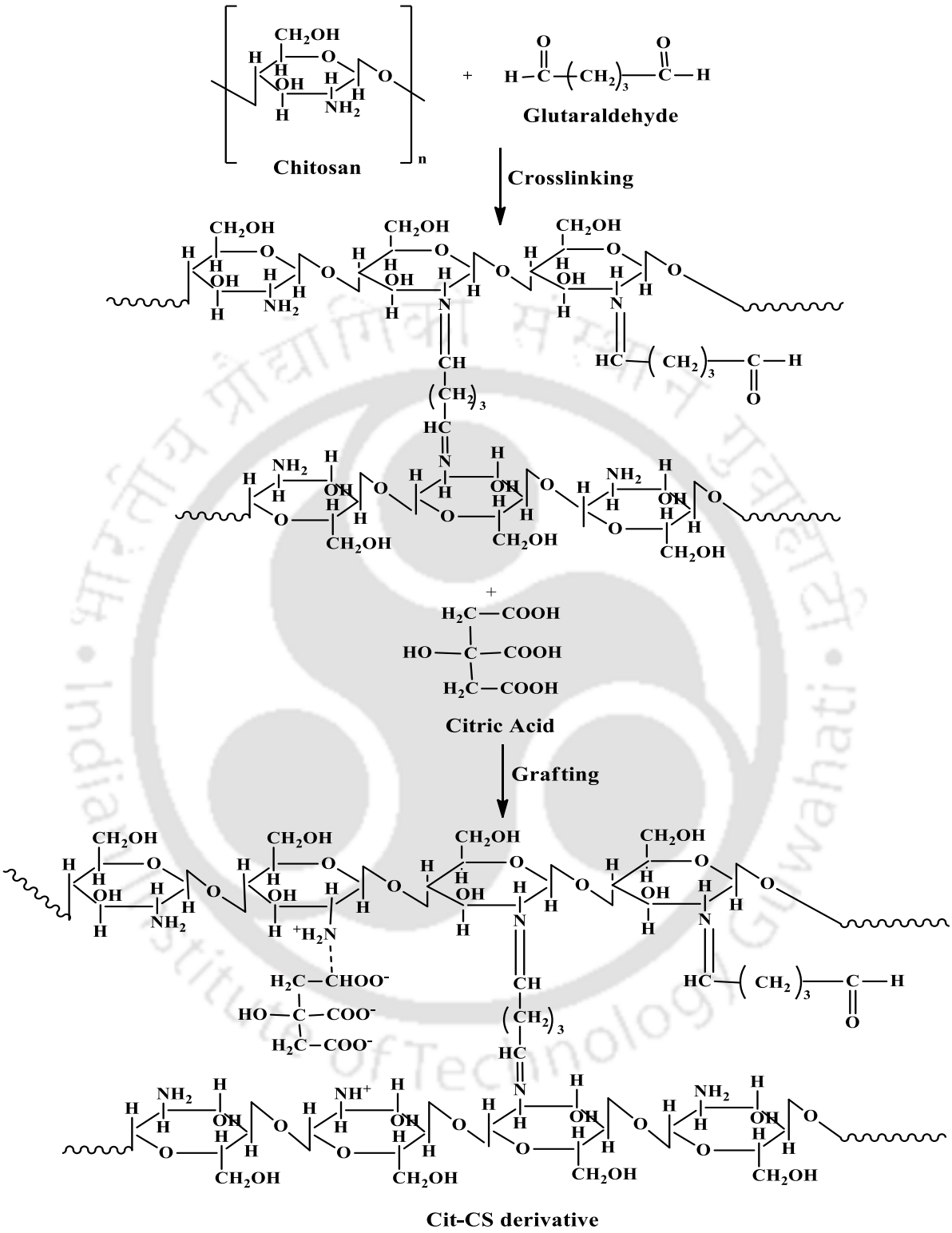

Fig. 2.4. Schematic depicting Chitosan-Citric acid structural interaction.

2.2.3 Chitosan-carboxymethyl derivative (CMCS) Resin

Adopting the procedure elucidated for the carboxymethylation of cellulose (Abreu and Campana-Filho, 2005), firstly, purified chitosan (3 g) was dispersed in 65 mL of isopropanol. After 20 minutes of magnetic stirring at room temperature, 20.4 g of aqueous NaOH (40 %) and 14.4 g of monochloroacetic acid/isopropanol solution (1:1 m:m) were added to the chitosan suspension. Thereby, the reaction occurred for 10 h at room temperature. Eventually, 48 mL of glutaraldehyde solution was added to the solution and the mixture was stirred 4 h to facilitate crosslinking in the system. Thereafter, the solid product was filtered and suspended in 150 mL of methanol. Finally, the product was extensively washed with 80% ethanol and was dried at room temperature. Alternate carboxymethyl chitosan derivative samples were realized by deploying alternate molecular weight chitosan precursors. These were appropriately labeled as low CMCS, high CMCS, and medium CMCS. The schematic for resin synthesis is shown in Fig. 2.5. Pertinent functional group interaction has been demonstrated in Fig. 2.6.

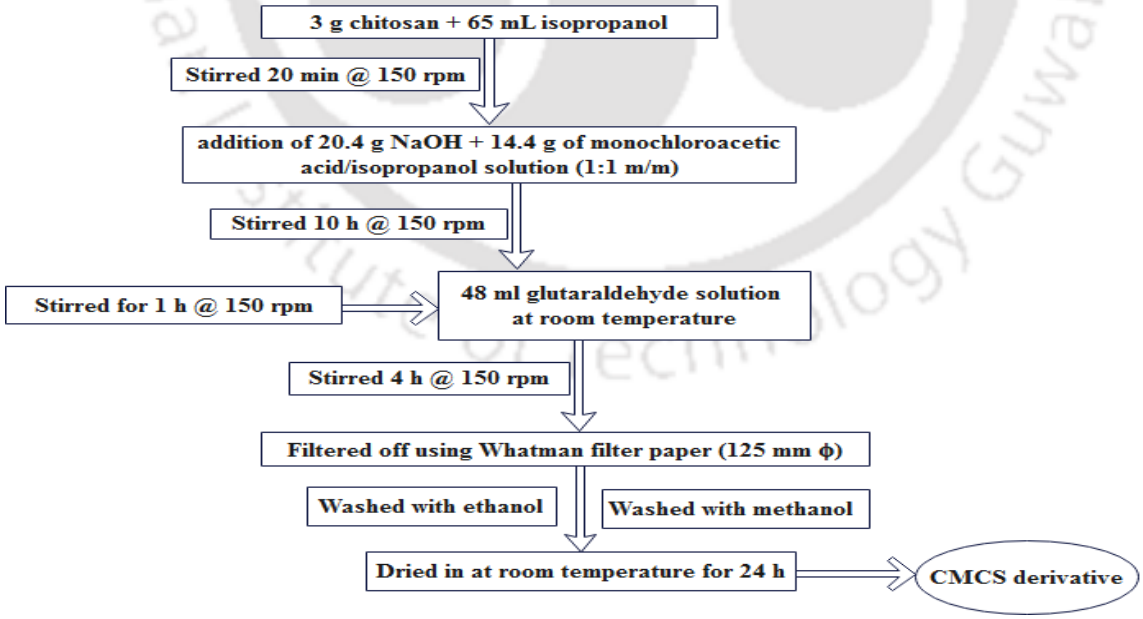

Fig. 2.5. Flowchart depicting the synthesis of CMCS derivative resin.

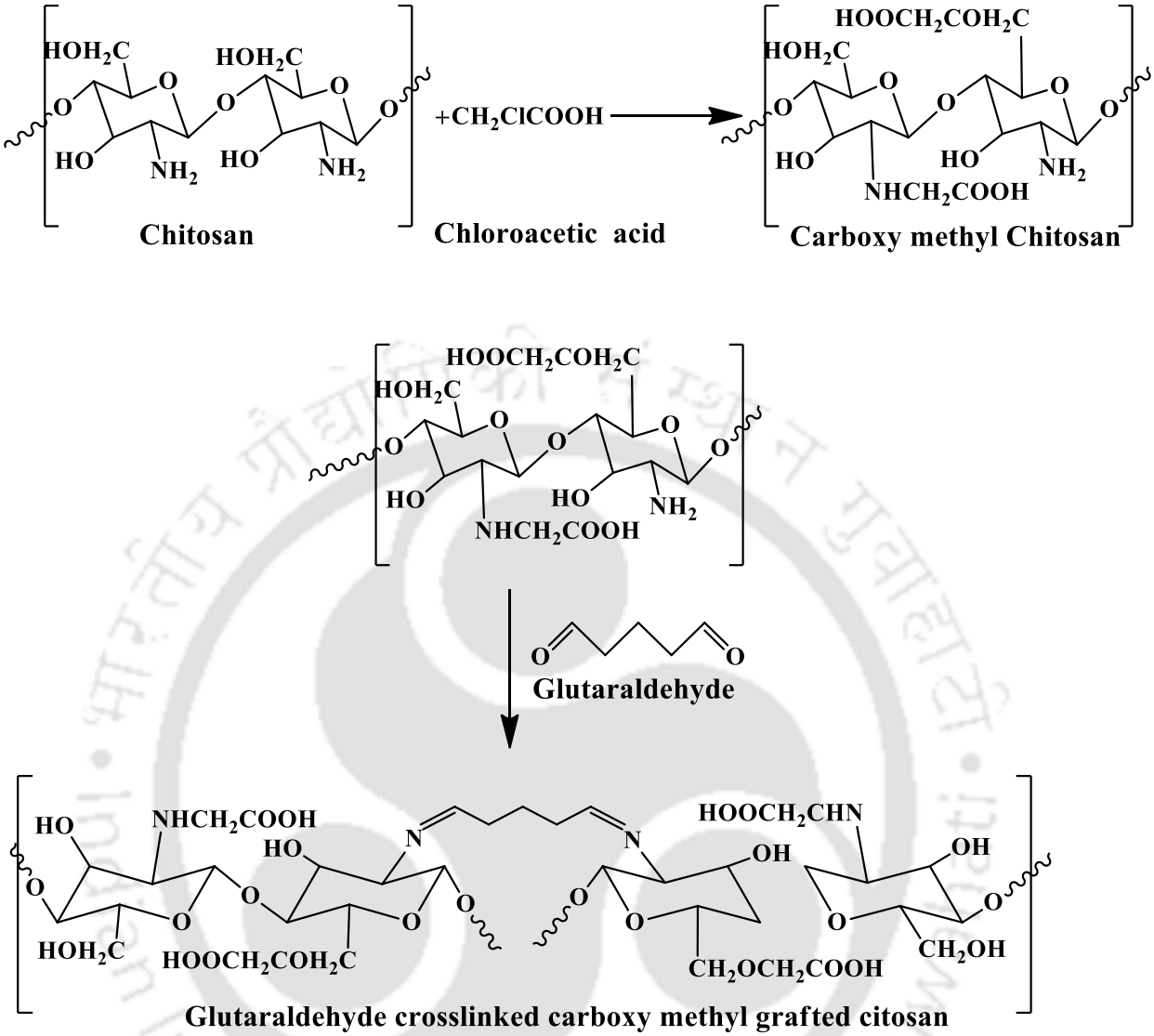

Fig. 2.6. Flowchart depicting chitosan-chloroacetic acid interaction.

2.3 Surface Characterization

The primary emphasis of surface characterization was to analyze and understand the surface properties of the investigated materials. Accordingly, the physical, chemical, and structural properties of the surface have been assessed. However, these characteristics may not delineate upon the overall characterization of the investigated materials. Henceforth, surface

characterization is a sub-set of the characterization techniques being adopted in the thesis. In the thesis, these refer to TGA, FESEM-EDX, and FTIR analyses.

The surface and thermal characterization studies for both raw and metal-loaded commercial resins, chitosan and its derivatives (prior to and after metal loading) were carried out using Fourier transform-infrared spectrophotometer (FTIR), Braummer-emmet-teller (BET) instrument, X-ray powder diffractometer (XRD), Thermo-gravimetric analyzer (TGA) and Field emission scanning microscope equipped energy dispersive X-Ray analyzer (FESEM-EDX). During adsorption and desorption experiments, the atomic absorption spectrophotometer (AAS; Varian; Spectra AA 220 FS; Netherlands) was operated at a wavelength of 324.8, 217.0, 213.9, and 248.3 nm for Cu, Pb, Zn, and Fe respectively to determine the initial and final metal solution concentrations. Sampling procedures involved collecting at least three samples and determining the mean value of all measurements. Such average values have been reported in the thesis. Nitrogen gas adsorption-desorption isotherm data were measured using relevant instruments (Quantachrome; Autosorb-IQ MP; USA) at 77 K for chitosan and its derivatives. Thereby, the pore size and surface area were determined. FTIR (Shimadzu; IR Affinity1; Japan) was used to determine prevalent functional groups in commercial resins, chitosan, modified chitosan derivatives, and metal-adsorbed chitosan derivative samples. The FTIR instrument was operated in the wavenumber range of 4000–400 cm^{-1}. XRD (Bruker; D8 Advance; Germany) was used to determine the crystalline properties of chitosan, chitosan derivatives, and metal-loaded chitosan derivatives. Thermal properties of chitosan and its derivatives were measured using TGA (Mettler Toledo; TGA 851e/LF/1100; Switzerland). FESEM-EDX (Zeiss; Sigma; Germany) was used to obtain an elemental composition for both raw and metal-loaded commercial resins, chitosan and its derivatives.

2.4 Batch adsorption studies

Deploying 50 mL of the mentioned solutions (Table 2), the chitosan derivatives were loaded into 250 mL conical flasks to achieve a dosage of 0.2-2 g L^{-1} (Nagireddi et al., 2017). Thereafter, batch adsorption experiments were conducted at 200 rpm and at 298 K. The considered synthetic wastewater system was analyzed to be highly sensitive to pH and precipitated below and above a pH range of 3 – 4. Hence, pH optimality could not be addressed in the thesis and all experiments were conducted at the natural pH of the solution system (3.82 for Cu and 3.64 for Zn dominant solution). Other than the pH, the optimality of contact duration, adsorbent dosage, and baseline metal ion concentration, was targeted through the consideration of only one adsorption process parameter for its optimality. Thereby, the process parameters have been altered in the range of 187.7-563.1 mg L^{-1} Cu for a contact time of 12 h. After adsorption, multi-heavy metal concentrations of the solutions were determined using AAS for Pb, Fe, and Cu from the Cu dominant solution and Zn, Fe, and Pb from the Zn dominant solution due to their existence beyond permissible limits as per the environmental legislations. The AAS instrument was used to measure the concentrations of Cu, Pb, Fe, and Zn in the adsorbate. Based on mean values deduced from triplicate runs, adsorption capacity (AC) and percentage removal (PR) were evaluated with the expressions (Kumar et al., 2022):

$$\text{Removal} = \frac{C_o - C_e}{C_o} \times 100 \quad (\%) \tag{2.1}$$

$$\text{Adsorption capacity}(q_e) = \frac{C_o - C_e}{W} \times V \quad (\text{mg g}^{-1}) \tag{2.2}$$

where V, C_o, C_e, and g are the volume of solution (L), baseline and equilibrium concentration (mg L^{-1}), and mass of adsorbent (g), respectively.

2.5 Batch desorption experiments

2.5.1 Batch desorption of multi-heavy metal-loaded commercial resins

Using heavy metal adsorbed Amberlyst IR 120H and Lewatit TP 260 commercial resins, eluents such as NaOH, KOH, HCl, H_2SO_4, and HNO_3 were deployed at the varied concentration range of 0.1-2M to determine desorption characteristics. Subsequently, precise quantities of resins were placed in stoppered reagent bottles, a specific quantity of the eluent (50 mL) was added and the mixture was subjected to mechanical shaking (200 rpm) for optimal contact duration (obtained from adsorption studies) at room temperature. Finally, the final metal solution concentration in the solution was measured for the evaluation of desorption-based heavy metal recovery. The metal removal characteristics were evaluated with a mass balance expression of the number of moles of heavy metal that exist before and after desorption.

In this Ph.D. thesis, cyclic adsorption and desorption studies were also performed upto three consecutive cycles using fresh adsorbate solutions and without washing the adsorbent after each cycle. After the third cycle of adsorption-desorption, some amount of eluent solution remains on the adsorbent surface which leads to the formation of a deposit in the fourth cycle. Thus, cyclic adsorption-desorption studies were difficult to conduct after the third cycle and were terminated after the third cycle. Appendix F delineates upon the procedures adopted for the determination of desorption efficiency and overall metal adsorption efficiency in the consecutive cycles.

2.5.2 Batch desorption of multi-heavy metal-loaded chitosan derivatives

Using heavy metal loaded chitosan derivatives (CSPVA, Cit-CS, and CMCS), NaOH, KOH and HCl, H_2SO_4, and HNO_3 solutions with variant concentrations (0.1, 0.5, 1, 1.5, and 2 M) were

deployed as the eluents. A detailed account of the adopted procedures for the batch desorption study has been similar to that presented in section 2.5.1 of the Ph.D. thesis.

Based on a three-cycle-based adsorption-desorption performance, Fig. 4.17 (chapter 4), Fig. 5.17 (chapter 5), and Fig. 6.17 (chapter 6) confirm upon the adsorbent stability of the relevant resins. Further studies involving about ten cycles of adsorption-desorption are often targeted. However, this is beyond the scope of the thesis and can be addressed in the near future. The stability of all chitosan derivative resins investigated in this work has been excellent and further studies on their stability will provide detailed insights into possible alterations in solution chemistry, adsorbent chemistry, and eluent chemistry for the effective and sustainable performance of the mentioned chitosan derivative resins.

The desorption mechanisms at the sites of $-NH_2$ (amine) and -OH (hydroxyl) groups in the chitosan derivative resins system involve the release of adsorbed heavy metal ions from the respective functional groups. These have been detailed as follows:

Desorption mechanism at $-NH_2$ (Amine) sites: The desorption mechanism at the amine sites has been elucidated for alternate cases namely ion-exchange and pH-dependent desorption and as follows:

a) Ion exchange-based desorption mechanism: Ion exchange exists as a primary mechanism for the heavy metal ion desorption from the $-NH_2$ sites. According to the ion exchange mechanism, during desorption, the proton of the eluent system replaces the heavy metal ion being adsorbed to the $-NH_2$ site of the chitosan derivative resin. Such a process occurs in a scenario that assures higher affinity of the proton for the NH_2 groups. Henceforth, the lower pH of the eluent system would be favorable for desorption.

b) pH-dependent desorption mechanism: Protonation degree or deprotonation of the -NH_2 groups prevalent in the chitosan derivative resin is strongly dependent upon the solution pH. At a lower pH, (acidic condition), -NH_2 groups undergo protonation (NH_3^+) and at a higher pH (alkaline condition), they undergo deprotonation (-NH_2) (Patrick, 2021). Thus, desorption occurs effectively through the solution pH adjustment and this assures protonation state alteration of the -NH_2 groups. Accordingly, the charge alteration at the -NH_2 site facilitates the release of the adsorbed species.

Desorption mechanism at -OH (Hydroxyl) sites: The desorption mechanism at the hydroxyl sites has been elucidated for alternate cases namely hydrogen bonding, competitive desorption, and pH-dependent desorption, and as follows:

a) Hydrogen bonding-based desorption mechanism: Hydroxyl (-OH) groups in the chitosan derivative resin form hydrogen bonds with the adsorbed heavy metal ions. Desorption at these sites involves the breakage of these hydrogen bonds. Such desorption occurs through the enhancement in the temperature or a reduction in the solution pH. Thus, environmental conditions prompt a hydrogen bonding-based desorption mechanism and accordingly, desorbed heavy metal ions do get released from the resin structure and enter the eluent system.

b) Competitive desorption-based mechanism: In some cases, the desorption of heavy metal ions at -OH sites may be influenced by the presence of other molecules in the solution. This is due to their better affinity to get adsorbed at the same site at which a heavy metal ion is adsorbed. Thus, an ion with higher affinity towards the hydroxyl site can replace the adsorbed heavy metal ion, and accordingly, the displaced heavy metal ion gets released from the resin structure and enters the eluent system. Thus, the strength or affinity of a

heavy metal ion towards the hydroxyl site dictates the competitive desorption mechanism (Ivanets et al., 2021; Zhao et al., 2022).

c) pH-dependent desorption mechanism: The mechanism is similar to that being elucidated for the pH-dependent desorption mechanism at the -NH_2 sites of the chitosan derivative resin. Thus, protonation or deprotonation can be driven with pH alteration that assures charge and reactivity alteration of the -OH sites with respect to the adsorbed heavy metal ions.

In summary, the desorption mechanisms at -NH_2 and -OH sites of the chitosan derivative resin are complex and do vary with respect to the adsorbate solution system conditions, functional group chemistry of the resins, and the interaction strength between the resin functional groups and the adsorbate systems. Thus, a deeper understanding of these mechanisms is important to custom design adsorbent materials such as chitosan derivative resins for applications such as wastewater treatment, heavy metal removal, and controlled drug release. Accordingly, optimality of desorption conditions can be sought for the effective regeneration of chitosan derivative resins. Such strategies enhance the sustainability characteristics of the mentioned resins for greater application perspectives in real-world scenarios.

2.6 Fitness of Equilibrium and Kinetic Models

2.6.1 Equilibrium models

The batch equilibrium adsorption data were analyzed first with the Langmuir isotherm model. The model hypothesizes monolayer metal adsorption onto the adsorbent active sites. The obtained batch adsorption data was also analyzed with the Freundlich isotherm model. This model hypothesizes multilayer metal adsorption due to the assumption of uniform energy of a

heterogeneous surface. The Langmuir isotherm equation (Eq. (2.3)) can be expressed as follows in the linear form (Langmuir, 1919):

$$\frac{C_e}{Q_e} = \frac{C_e}{Q_o} + \frac{1}{bQ_o} \tag{2.3}$$

where, Q_e and C_e are equilibrium adsorption capacity (mg g^{-1}) and equilibrium solution concentration (mg L^{-1}), respectively. In the above expression, Q_o and b are the maximum adsorption capacity (mg g^{-1}) and Langmuir adsorption constant, respectively. The values of Q_o and b were determined from the slope and intercept of the Langmuir plot of C_e versus C_e/Q_e. Based on the initial solution concentration C_o and Langmuir constant b, dimensionless equilibrium parameter R_L can be evaluated using the expression:

$$R_L = \frac{1}{1 + bC_o} \tag{2.4}$$

The magnitude of R_L affirms upon one of the following regimes:

Favorable adsorption: $0 < R_L < 1$, Unfavorable and linear adsorption: $R_L > 1$ and $R_L = 1$

Irreversible adsorption: $R_L = 0$

The linearized Freundlich isotherm model is expressed as (Freundlich 1906):

$$\log Q_e = \log K_f + \frac{1}{n} \log C_e \tag{2.5}$$

where, K_f and n are the Freundlich constants related to adsorption capacity and adsorption intensity, respectively.

The value of n has been inferred to indicate alternate regimes. For the case of the n value being one, the partition between the two phases is to be regarded as independent of the concentration. On the other hand, the case of 1/n being lower than one has been referred to as normal adsorption. Similarly, the case of the 1/n value being zero has been referred to cooperative adsorption

(Freundlich 1906). With increasing temperature, both k and n constants vary and indicate that the quantity adsorbed increases slowly, and a higher concentration is required to saturate the surface. However, due to K_f and n being characteristic parameters of the sorbent-sorbate system, they are to be determined through curve fitting techniques. To do so, linear regression with the least-squares method is generally adopted to determine the parameters of kinetic and isotherm models. Also, the term 1/n corresponds to the level of heterogeneity. Hence, a smaller value of 1/n indicates a greater degree of heterogeneity. Thus, the expression reduces to a linear adsorption isotherm in the case of a 1/n value of 1. Alternatively, for the n value between one and ten corresponds to a favorable adsorption process (Freundlich 1906).

2.6.2 Kinetic models

For all cases, the heavy metal adsorption kinetic analysis was conducted for 50 mg L^{-1} initial solution concentration, optimum adsorbent loading case, natural solution pH, 298 K, and 250 rpm operating condition. To conduct analytical characterization, liquid samples have been taken at precise time intervals until equilibrium contacting time was achieved. Thereby, the time-dependent heavy metal ion concentration in the adsorbate was determined. The metal adsorption kinetics data thus obtained were subjected to fitness studies with pseudo-first-order (Aharoni and Ungarish, 1976), and pseudo-second-order models (Y.S. Ho, 1999). These can be expressed as:

$$\log (Q_e - Q_t) = \log Q_e - \frac{K_1 t}{2.303} \tag{2.6}$$

$$\frac{t}{Q_t} = \frac{1}{K_2 Q_e^{\,2}} + \frac{t}{Q_e} \tag{2.7}$$

where Q_t and Q_e are time-dependent and equilibrium resin adsorption capacities (mg g^{-1}), respectively. The model constants in the above expressions are pseudo-first-order rate constant

(K_1, min^{-1}) and pseudo-second-order rate constant (K_2, g mg^{-1} min^{-1}). For the fitness of the pseudo-second-order model, the plot of t/Q_t against t needs to indicate a linear relationship. From such a plot, Q_e and K_2 can be respectively determined from the slope and intercept of the plot.

Appendix G delineates upon the error functions namely, Chi-square, Root mean square deviation, Residual sum of squares, and ANOVA analysis of CSPVA (Tables G1-G4), Cit-CS (Tables G5-G8), and CMCS derivative resins (Tables G9-G12) and for Cu and Zn dominant simulated adsorbate systems.

Also, the conducted investigations targeted the efficacy of alternate commercial resins and chitosan derivative sorbents for multi-heavy metals mitigation from simulated adsorbate systems that mimic real wastewater samples. Accordingly, the best-performing resins shall be identified. Since such samples are often found in the environment at ambient temperature conditions, the influence of temperature on the adsorption-desorption characteristics has not been targeted. However, such studies are beneficial and can be addressed in the near future for the best-performing resins in terms of cyclic adsorption-desorption characteristics. Further, pH alteration studies targeting optimality of pH and zeta potential characteristics have not been targeted in this work due to the very fact that the adsorbate system was unstable (through the formation of a deposit) for a pH above 4 and below 3. However, such studies can be considered for altered adsorbate systems constitutions that affirm solution stability in the desired pH range. Such studies shall be addressed in the near future. Consequently, various sorption process variables namely adsorbent loading, initial concentration, and adsorbent contact duration were optimized for the considered adsorbate systems at their natural solution pH (3.64 for Zn dominant solution and 3.82 for Cu dominant solution).

Chapter 3:

Cyclic Multi-Heavy Metal desorptive efficacy of Lewatit TP 260 and Amberlite IRA 120H Commercial Resins

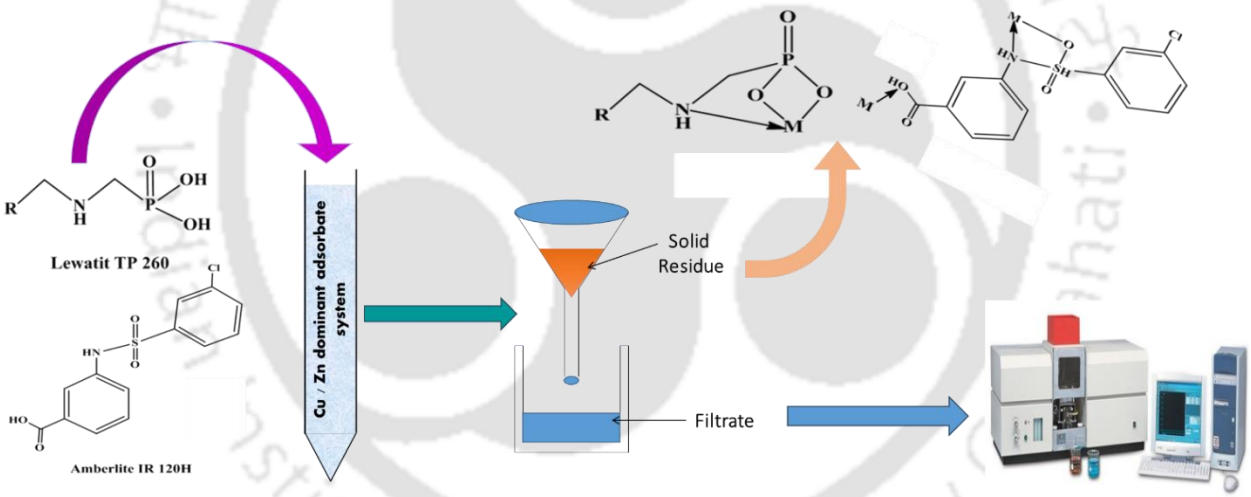

Cyclic Multi-Heavy Metal desorptive efficacy of Lewatit TP 260 and Amberlite IRA 120H Commercial Resins

Section 3.1 summarizes the background for the conducted work. Section 3.2 elaborates upon the multi-heavy metal batch adsorption characteristics of the mentioned commercial resins. Section 3.3 details upon the equilibrium, and kinetic model fitness for measured data. Section 3.4 presents surface characterization findings for fresh and metal-loaded resins. Sections 3.5 and 3.6 respectively detail upon the cyclic desorption characteristics of commercial resins and literature comparison of the best available prior art with the findings of this chapter. Finally, the chapter summary is presented in section 3.7.

3.1 Background

Prior to this work, no literature has been reported on the multi-heavy metal removal characteristics of commercial resins and real-world-based wastewater adsorbate systems. Till date, relevant prior art addressed heavy metal ion adsorption characteristics for aqueous solutions. Hence, the combinatorial influence of co-existent metal ions on the adsorption characteristics of targeted heavy metal ions for several inexpensive commercial resins has not been addressed in the prior art. Thereby, the central objective of this work is to investigate and achieve the simultaneous removal of targeted metal ions from real-world-based multi-heavy metal-containing wastewater adsorbate systems. Further, desorption characteristics with simple and cheaper eluents have not been investigated. With these limitations in the literature, the chapter focuses on the multi-heavy metal

adsorption characteristics for commercial resins and synthetic complex wastewater adsorbate systems. A deeper perspective of the investigations is to as well examine upon the influence of other co-existent multivalent metal ions on the adsorption characteristics of Cu, Zn, Fe, and Pb from Cu and Zn dominant complex synthetic adsorbate systems. Surface characterization studies have been carried out using Fourier transform infrared (FTIR) spectral analysis and Field Emission Scanning Microscopy equipped with energy dispersive X-ray analysis (FESEM-EDX). For the optimal set of pH, adsorbent dosage, and contact time, adsorption experiments were conducted for a wider range of heavy metal solution concentrations 187.7-563.1 mg L^{-1}, 5.2-15.6 mg L^{-1}, and 61.85-185.55 mg L^{-1} for Cu, Pb, and Fe, respectively for Cu dominant solution and 194.9-584.7 mg L^{-1}, 2.65-7.95 mg L^{-1}, and 104.8-314.4 mg L^{-1} for Zn, Pb, and Fe, respectively for Zn dominant solution. The specific influence of various co-existent metal ions such as Al, Mg, Na, and K on targeted heavy metal ion (Cu, Zn, Pb, and Fe) adsorption characteristics of commercial resins were thereby addressed for the mentioned adsorbate systems.

3.2 Batch Adsorption Characteristics

The batch adsorption studies were first conducted for a fixed choice of solution pH (3.82 for Cu dominant solution and 3.64 for Zn dominant solution), contact time 720 min, initial metal ion concentration (375.4 mg L^{-1} Cu, 10.4 mg L^{-1} Pb, 123.7 mg L^{-1} Fe for Cu dominant solution and 389.8 mg L^{-1} Zn, 5.3 mg L^{-1} Pb, 209.6 mg L^{-1} Fe for Zn dominant solution), agitation speed 200 rpm and variant range of adsorbent dosage (AD) (0.2–2 g L^{-1}), The findings have been depicted in Fig. 3.1 that infers upon the adsorbent dosage optimality for Fe, Cu and Pb adsorption on Amberlite IR 120H and Lewatit TP 260 and Cu dominant adsorbate system. With reference to optimal % removal and adsorption capacity, the optimal adsorbent dosage has been evaluated as 1.6 g L^{-1} for

Amberlite IR 120H resin and 1.2 g L^{-1} for Lewatit TP 260 resin. Corresponding batch adsorption data were 64.85 % and 152.14 mg g^{-1} for Cu; 87.4 % and 5.68 mg g^{-1} for Pb and 72.9 % and 56.4 mg g^{-1} for Fe for Amberlite IR 120H resin and 79.00 % and 247.17 mg g^{-1} for Cu; 78.17 % and 6.78 mg g^{-1} for Pb and 60.42 % and 62.28 mg g^{-1} for Fe for Lewatit TP 260 resin.

Similarly, Fig. 3.2 depicts adsorbent dosage optimality for Fe, Zn, and Pb adsorption onto Amberlite IR 120H resin and Lewatit TP 260 resin and Zn dominant adsorbate system. With respect to optimal % removal and adsorption capacity, the optimal adsorbent dosage has been evaluated as 1.4 g L^{-1} for Fe, Zn, and Pb for Amberlite IR 120H resin and 1.2 g L^{-1} for Fe, Zn, and Pb for Lewatit TP 260 resin. Corresponding batch adsorption data were 61.48 % and 171.19 mg g^{-1} for Zn; 73.21 % and 2.77 mg g^{-1} for Pb and 64.62 % and 96.74 mg g^{-1} for Fe for Amberlite IR 120H resin and 67.51 %, 219.32 mg g^{-1} for Cu, 62.08 %, 2.74 mg g^{-1} for Pb and 72.68 % and 126.95 mg g^{-1} for Fe for Lewatit TP 260 resin. As predicted, the adsorbent capacity enhanced for larger dosages due to the increased availability of active sites. As a consequence, a reduction in the adsorbed metals resulted in the reduced % removal of metals.

The second set of adsorption studies was conducted at a fixed choice of solution pH (3.82 for Cu dominant solution and 3.64 for Zn dominant solution), initial metal ion concentration (375.4 mg L^{-1} Cu, 10.4 mg L^{-1} Pb, 123.7 mg L^{-1} Fe for Cu dominant solution and 389.8 mg L^{-1} Zn, 5.3 mg L^{-1} Pb, 209.6 mg L^{-1} Fe for Zn dominant solution), agitation speed 200 rpm, adsorbent dosage (1.6 g L^{-1} for Amberlite IR 120H in Cu dominant solution, 1.4 g L^{-1} for Amberlite IR 120H resin in Zn dominant solution and 1.2 g L^{-1} for Lewatit TP 260 resin) and variant contact time (5-660 min). The findings have been depicted in Fig. 3.3.

Fig. 3.3 illustrates the contact time optimality graph associated to Fe, Cu, and Pb adsorption on Amberlite IR 120H resin and Lewatit TP 260 resin for Cu dominant solution. Thereby, based on

optimal removal efficiency and adsorption capacity, the optimal contact time has been evaluated as 420 min for Amberlite IR 120H resin and 300 min for Lewatit TP 260 resin.

Corresponding batch adsorption data were 65.2 % and 153.0 mg g^{-1} for Cu; 82.02 % and 5.5 mg g^{-1} for Pb and 71.5 % and 55.3 mg g^{-1} for Fe for Amberlite IR 120H resin and 77.5 % and 242.6 mg g^{-1} for Cu; 78.5 % and 6.8 mg g^{-1} for Pb and 58.7 % and 60.5 mg g^{-1} for Fe for Lewatit TP 260 resin.

Similarly, Fig. 3.4 depicts the contact time optimality graph associated to Fe, Zn, and Pb adsorption on Amberlite IR 120H resin and Lewatit TP 260 resin for Zn dominant solution. Thereby, based on optimal removal efficiency and adsorption capacity, the optimal contact time has been evaluated as 480 min for Amberlite IR 120H resin and 300 min for Lewatit TP 260 resin. Corresponding batch adsorption data are 61.7 % and 171.2 mg g^{-1} for Zn; 69.8 % and 2.6 mg g^{-1} for Pb and 62.2 % and 93.1 mg g^{-1} for Fe for Amberlite IR 120H resin and 67.0 % and 217.8 mg g^{-1} for Zn; 61.4 %, 2.3 mg g^{-1} for Pb and 72.1 % and 125.2 mg g^{-1} for Fe for Lewatit TP 260 resin. The third set of experiments was eventually performed for Cu dominant solution and for a fixed choice of adsorbent dosage (1.6 g L^{-1} for Amberlite IR 120H resin and 1.2 g L^{-1} for Lewatit TP 260 resin), initial solution pH (3.82) and contact period (420 min for Amberlite IR 120H and 300 min for Lewatit TP 260) and for altered initial solution concentrations (187.7-563.1 mg L^{-1} for Cu, 61.85-185.55 mg L^{-1} for Fe, and 5.2-15.6 mg L^{-1} for Pb). Fig. 3.5 depicts the influence of initial concentration on the removal of heavy metal ions for the copper-dominant simulated industrial wastewater adsorbate system. Corresponding removal efficiency and adsorption capacity altered as 85.14-48.61 % and 99.88-171.08 mg g^{-1} for Cu; 91.53-45.43 % and 35.38-52.68 mg g^{-1} for Fe and 92.31-42.24 % and 3.00-4.12 mg g^{-1} for Pb for Amberlite IR 120H resin and 85.14-50.55 % and 133.18-237.23 mg g^{-1} for Cu; 89.36-45.44 % and 46.06-70.26 mg g^{-1} for Fe and 82.88-48.65 % and 3.59-6.32 mg g^{-1} for Pb for Lewatit TP 260 resin.

Also, batch experiments were carried out for Zn dominant solution for a fixed choice of adsorbent dosage (1.4 g L^{-1} for Amberlite IR 120H and 1.2 g L^{-1} for Lewatit TP 260), initial solution pH (3.64) and contact period (480 min for Amberlite IR 120H resin and 300 min for Lewatit TP 260 resin) and for altered initial adsorbate systems concentrations (194.9-584.7 mg L^{-1} for Zn, 104.8-314.4 mg L^{-1} for Fe, and 2.65-7.95 mg L^{-1} for Pb). Fig. 3.6 depicts the influence of initial concentration on the removal of heavy metal ions for the zinc-dominant simulated industrial wastewater system. Corresponding removal efficiency and adsorption capacity altered as 91.36-48.46 % and 127.19-202.38 mg g^{-1} for Zn; 88.97-61.89 % and 66.61-139.00 mg g^{-1} for Fe and 84.91-38.36 % and 1.61-2.18 mg g^{-1} for Pb for Amberlite IR 120H resin and 92.45-46.77 % and 150.15-227.88 mg g^{-1} for Zn; 88.94-58.71 % and 77.67-153.83 mg g^{-1} for Fe, and 73.58-35.72 % and 1.63-2.37 mg g^{-1} for Pb for Lewatit TP 260 resin.

In the lower pH range of 1-6, heavy metals have been found to exist in their ionic forms (such as Pb++, Zn++, and Cu++). For the adsorbate systems at its natural pH (i.e. 3.82 for Cu dominant solution and 3.64 for Zn dominant solution), stronger interaction between metal ions with oxygen and nitrogen-containing groups in the resin is inevitable. Thus, $–NH_2$ groups may get protonated at lower pH levels and thereby allow the resin to adsorb more metal ions and hence have larger adsorption capabilities. Thus, the speciation has been in excellent accord with solution chemistry related to pH, species abundance, and important functional group interactions. Thus, the associated mechanism of the resin metal ion adsorption process can be deduced from such combinatorial analysis. Further, FESEM and EDX analysis will be required to affirm upon the hypothesis. The metal ion adsorption process at the solution system pH has been shown in Fig. 3.7 (based on the protonation of amine groups and oxygen-containing groups to generate a metal ion complex.

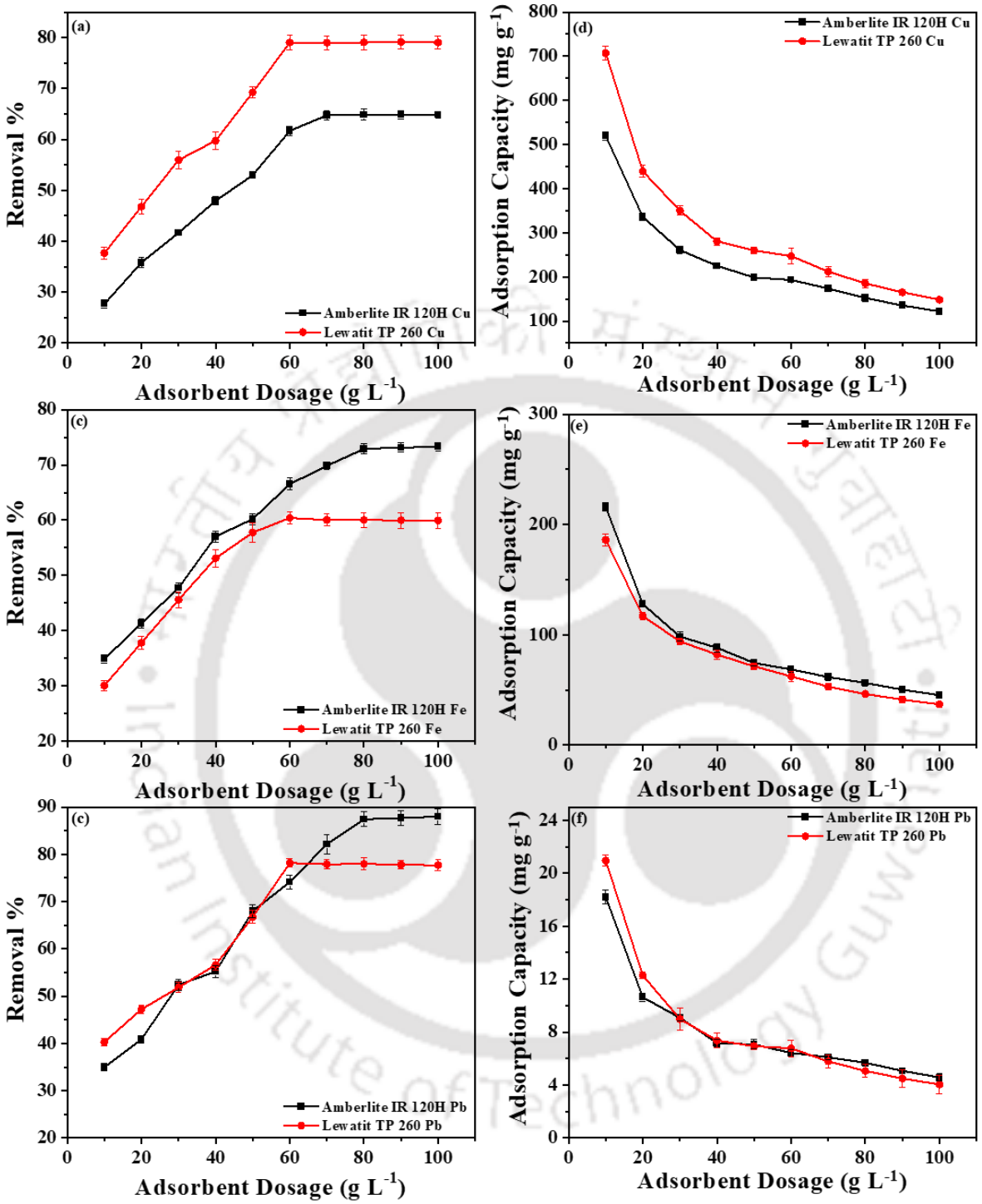

Fig. 3.1. Graphs depicting the influence of adsorbent dosage on adsorption characteristics of Amberlite IR 120H and Lewatit TP 260 commercial resins and Cu dominant adsorbate system.

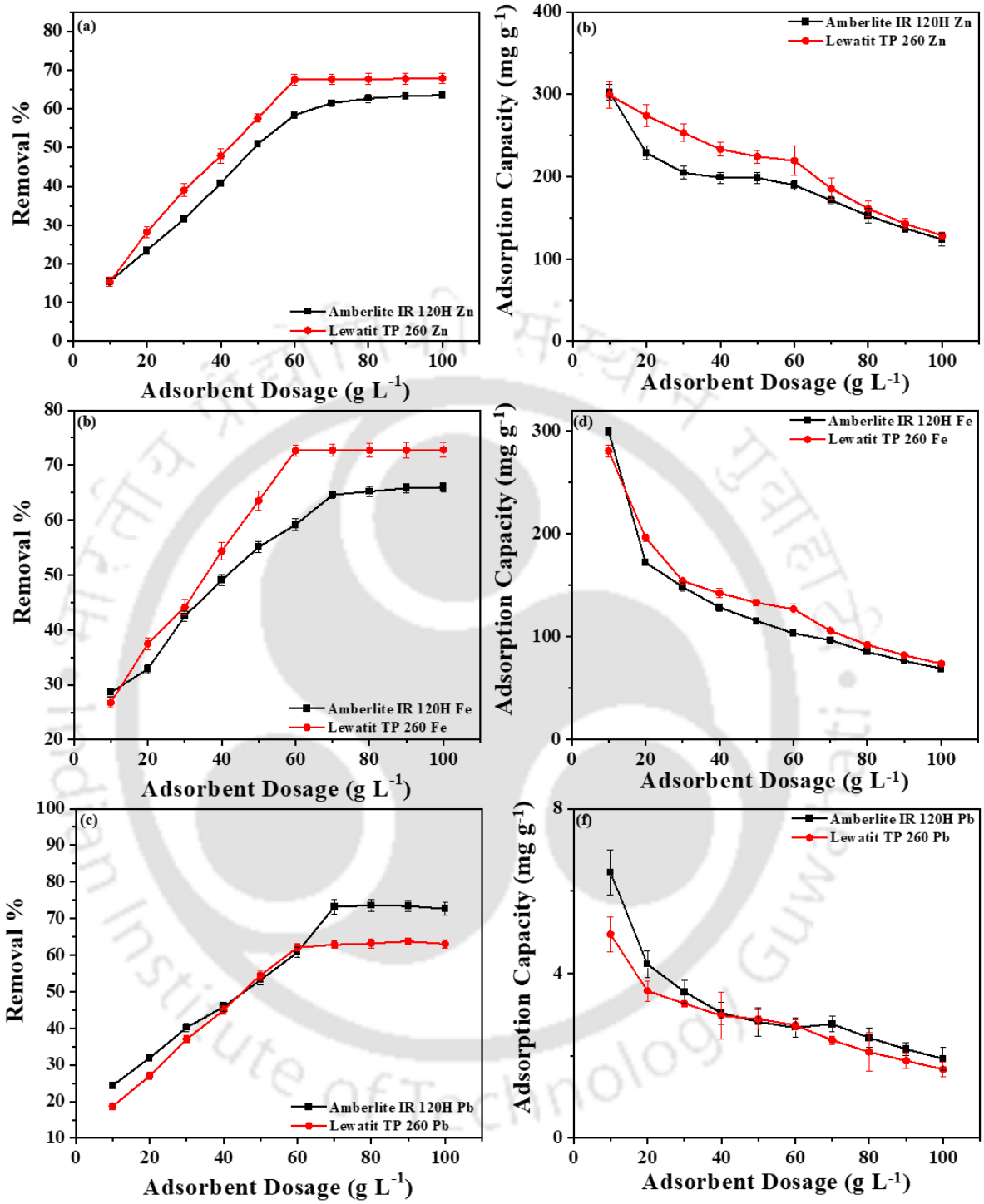

Fig. 3.2. Graphs depicting the influence of adsorbent dosage on adsorption characteristics of Amberlite IR 120H and Lewatit TP 260 commercial resins and Zn dominant adsorbate system.

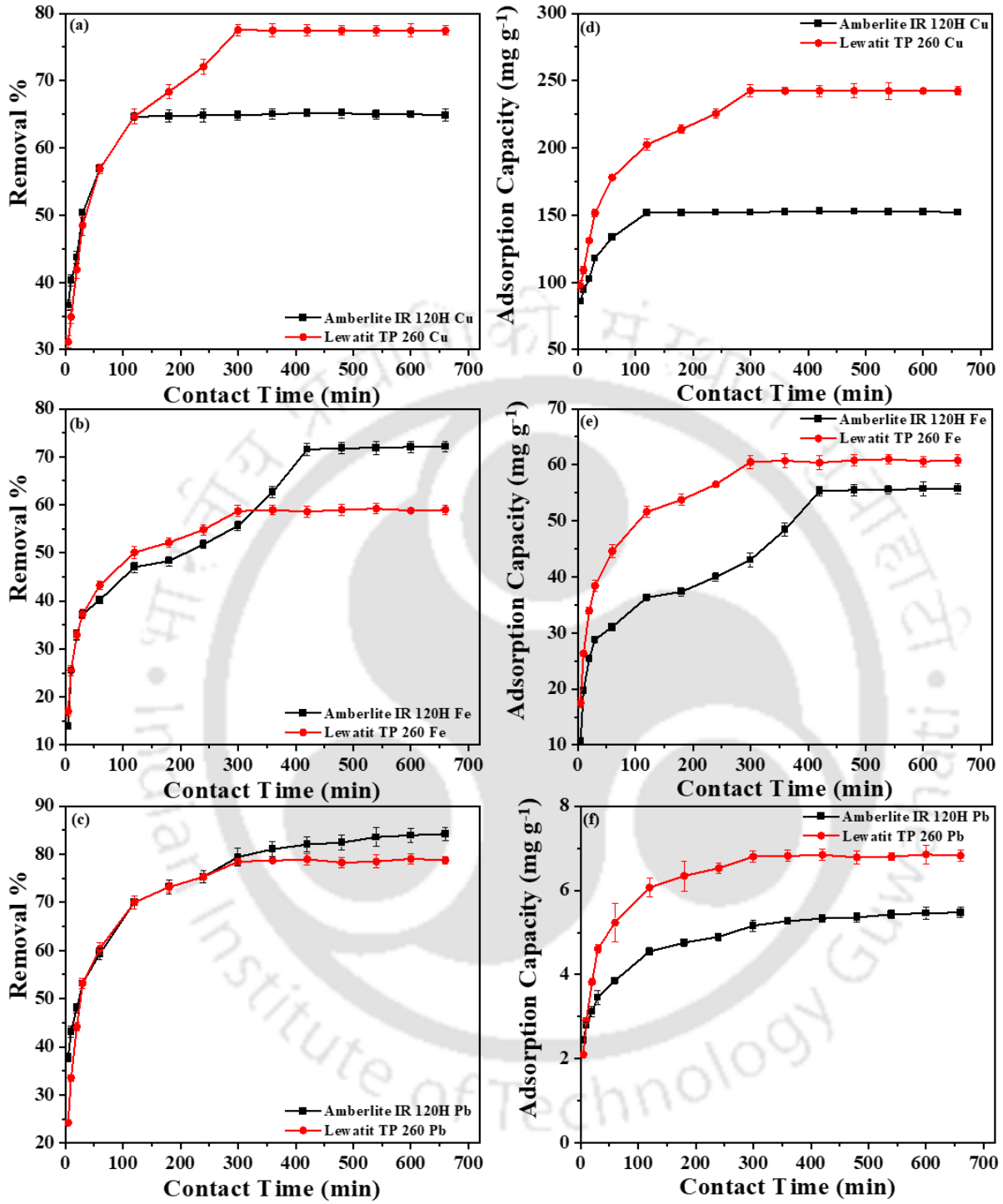

Fig. 3.3. Graphs depicting the influence of contact time on adsorption characteristics of Amberlite IR 120H and Lewatit TP 260 commercial resins and Cu dominant adsorbate system.

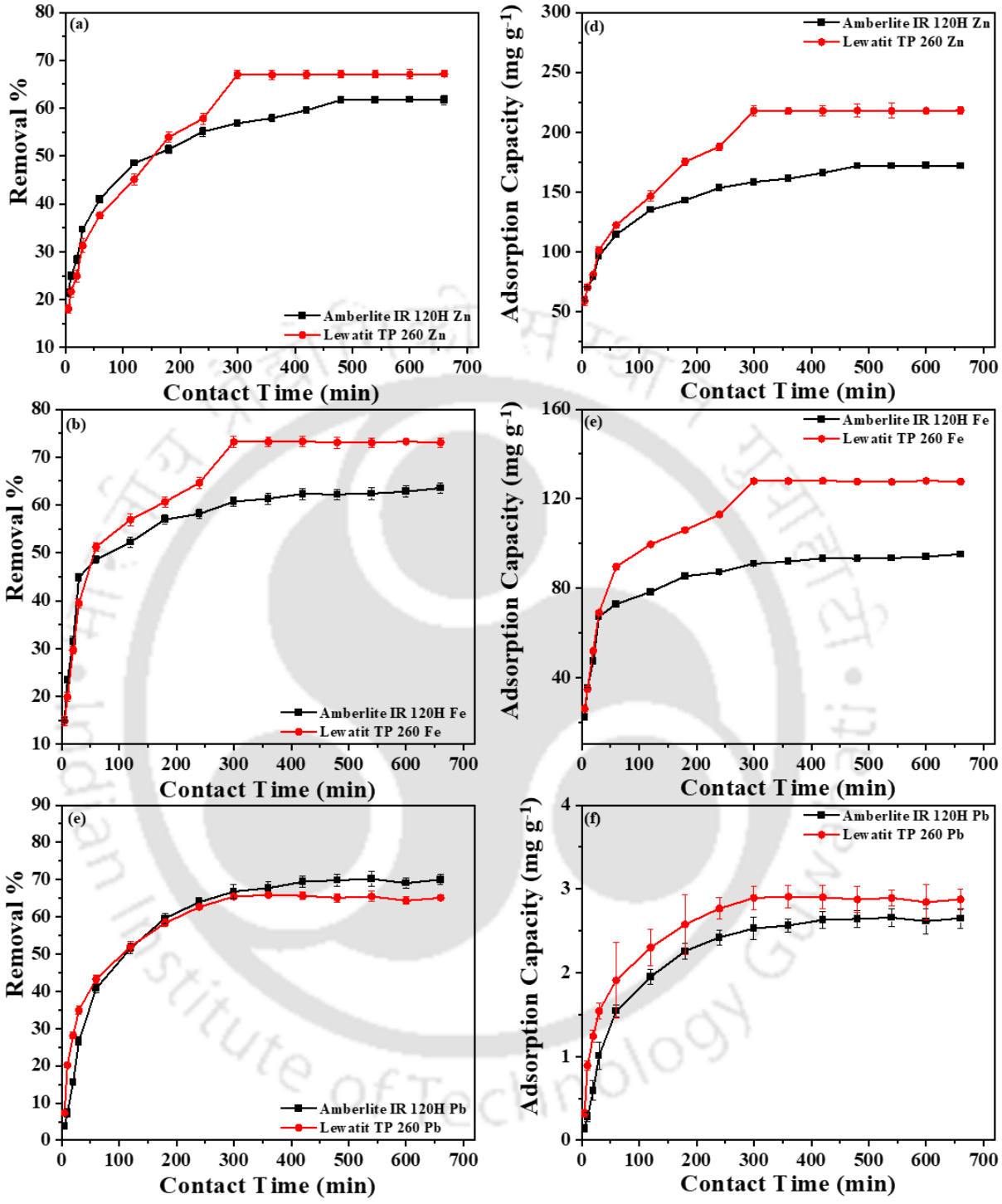

Fig. 3.4. Graphs depicting the influence of contact time on adsorption characteristics of Amberlite IR 120H and Lewatit TP 260 commercial resins and Zn dominant adsorbate system.

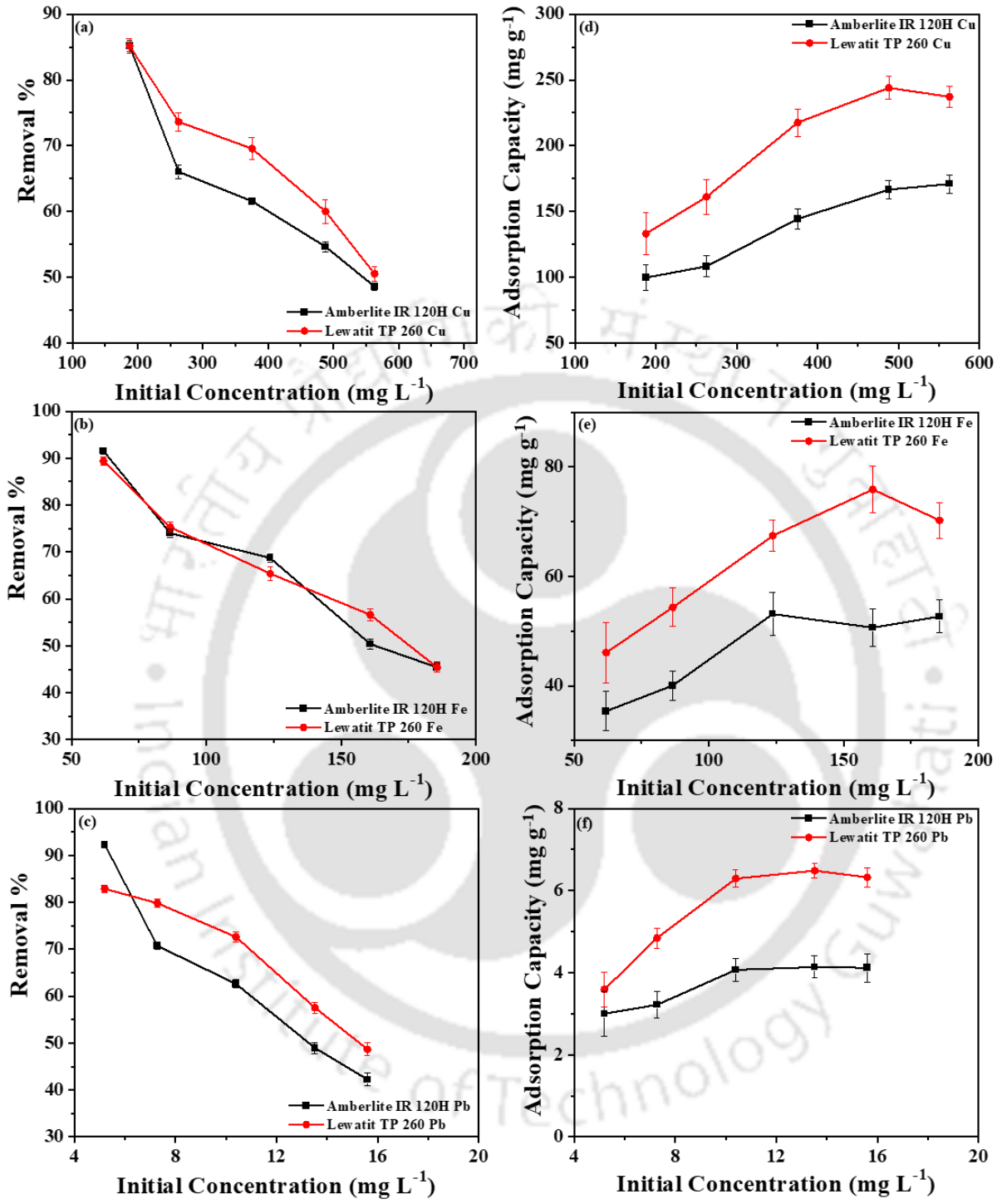

Fig. 3.5. Graphs depicting the influence of metal ion concentration on adsorption characteristics of Amberlite IR 120H and Lewatit TP 260 commercial resins and Cu dominant adsorbate system.

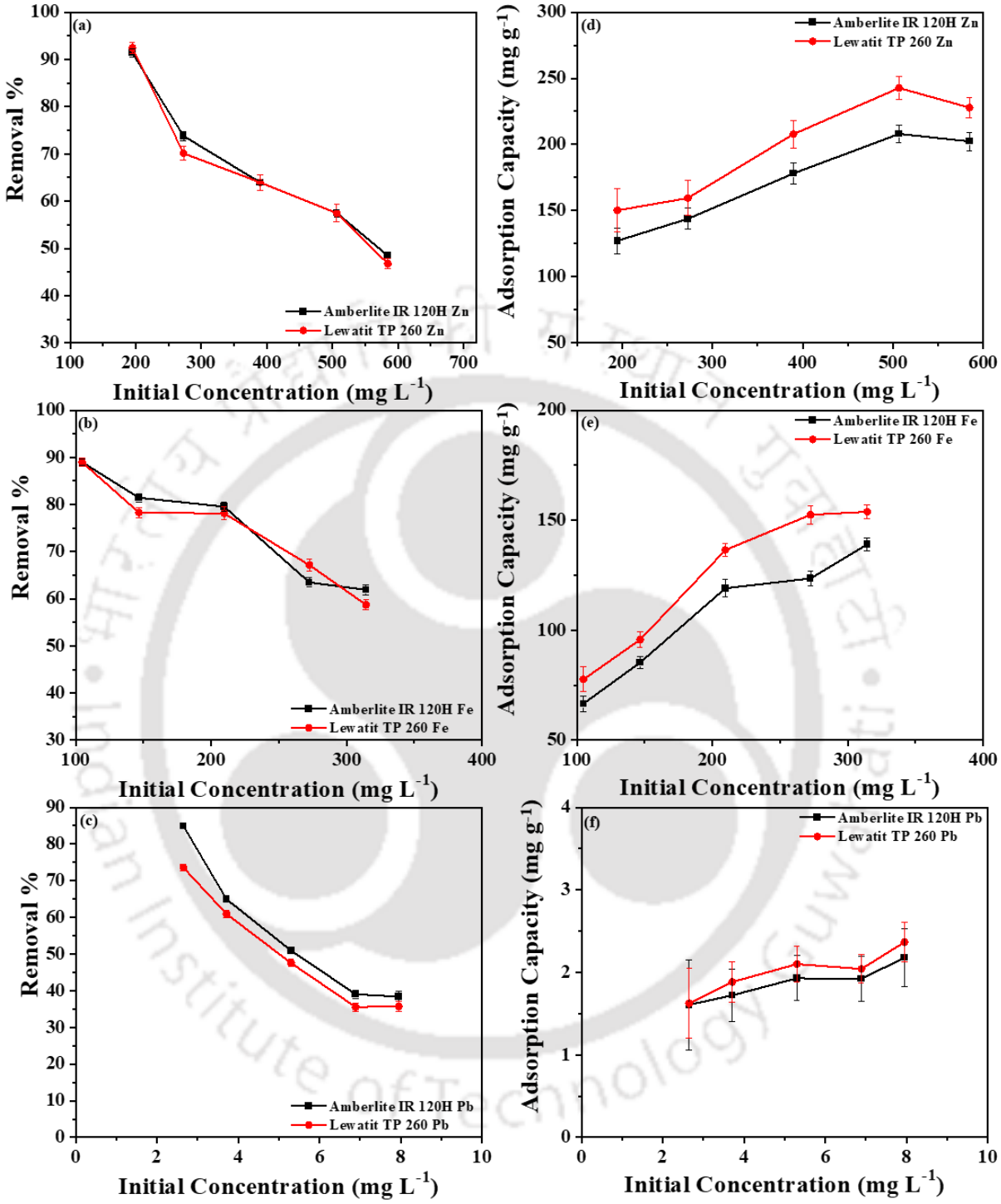

Fig. 3.6. Graphs depicting the influence of metal ion concentration on adsorption characteristics of Amberlite IR 120H and Lewatit TP 260 commercial resins and Zn dominant adsorbate system.

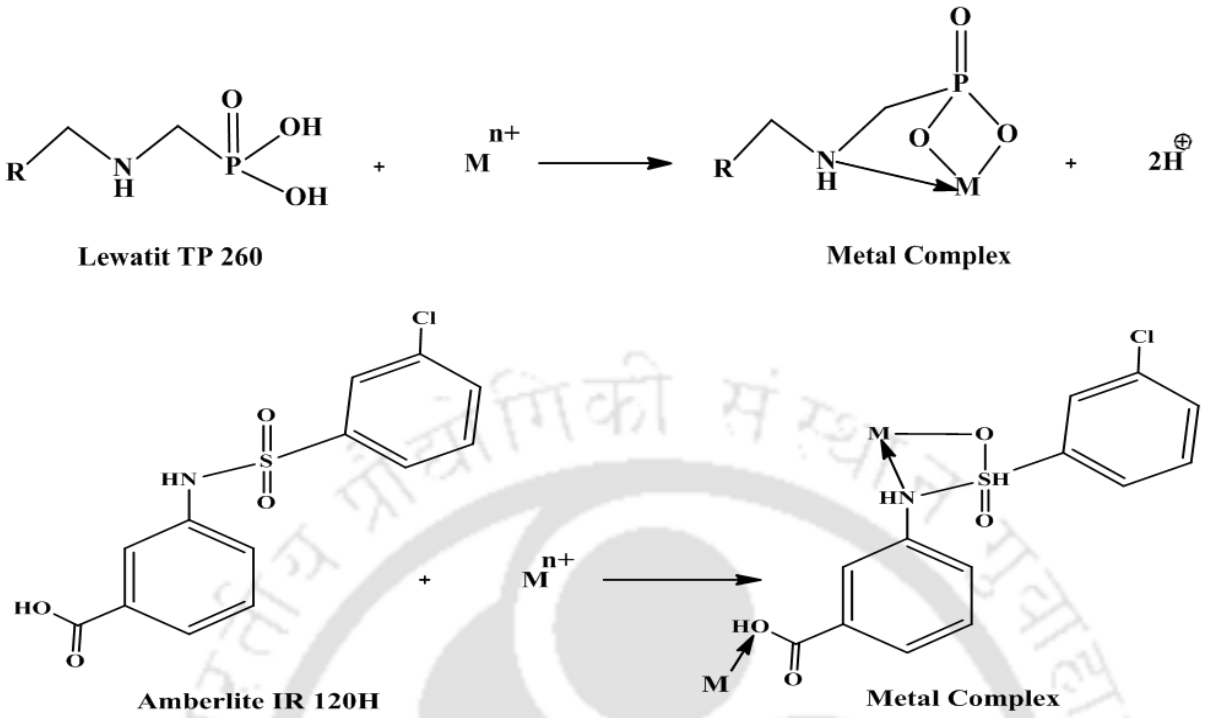

Fig. 3.7. Proposed heavy metal adsorption mechanism for commercial resins.

3.3 Fitness of Alternate Equilibrium and Kinetic Models

Fig. 3.8 and Fig. 3.10 illustrate the fitness plots of alternate equilibrium models namely Langmuir (Fig. 3.8a-3.8c and Fig. 3.10a-3.10c) and Freundlich isotherm (Fig. 3.8d-3.8f and Fig. 3.10d-3.10f) for Cu and Zn dominant solutions, respectively. The figures affirm the fitness of the Langmuir isotherm model to represent measured Cu, Pb, Zn, and Fe adsorption data for Amberlite IR 120H and Lewatit TP 260 resins. The R_L value reported in Table 3.1 is in the range of 0-1. Thereby it affirmed that both Amberlite IR 120H and Lewatit TP 260 resins are favorable for Cu, Pb, Zn, and Fe adsorption from Cu and Zn dominant simulated industrial wastewater solutions. The equilibrium model parameters for Cu, Pb, Zn, and Fe adsorption have been summarized in Table 3.1.

Fig. 3.9 and Fig. 3.11 depict the fitness plots for alternate kinetic models to represent the evaluated Cu, Pb, and Fe adsorption kinetics data of Amberlite IR 120H and Lewatit TP 260 resins. Table 3.2 summarizes the best results obtained for the said resins. Among all models, only the pseudo-second-order model provided very good fitness (R^2 = 0.99 for Amberlite IR 120H and Lewatit TP 260 resins). Similar fitness trends have been reported for the relevant data reported by the research groups for the CSPVA derivative (Karim et al., 2019; Trikkaliotis et al., 2020).

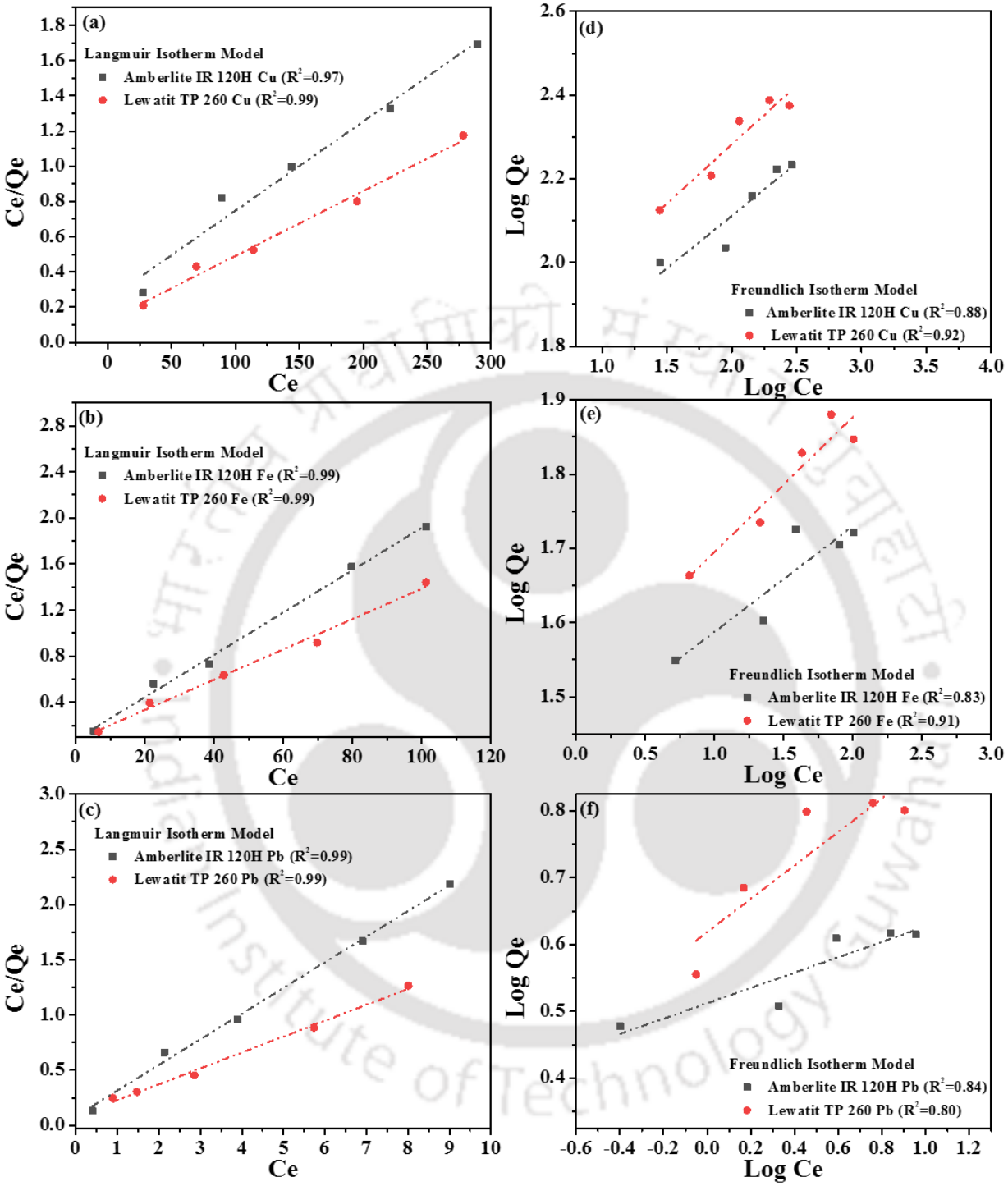

Fig. 3.8. Equilibrium models fitness plots (a-c: Langmuir isotherm model and d-f: Freundlich isotherm model) for Amberlite IR 120H and Lewatit TP 260 commercial resins and Cu dominant adsorbate system.

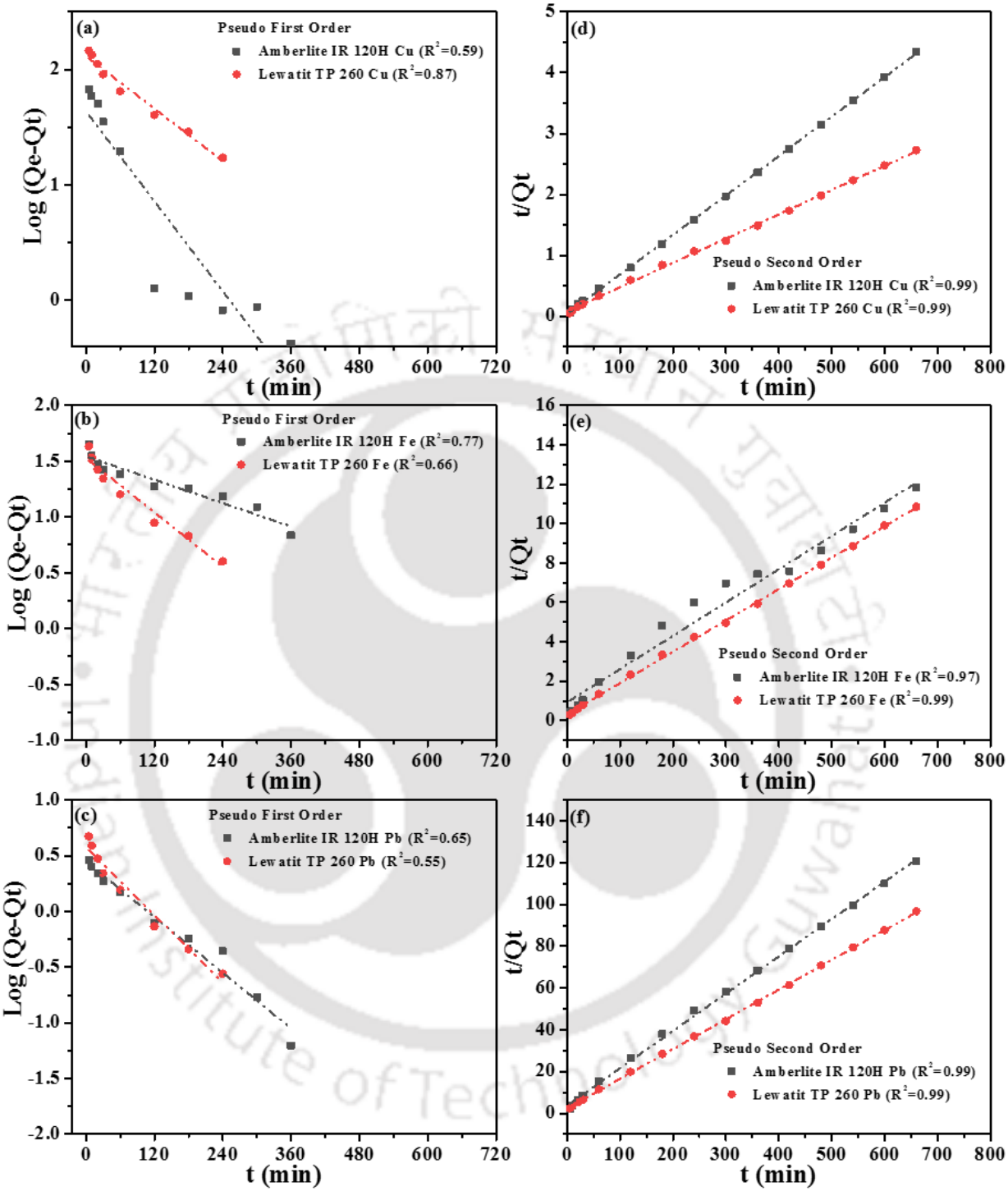

Fig. 3.9. Kinetic models fitness plots (a-c: Pseudo-first-order kinetic model, and d-f: Pseudo-second-order kinetic model) for Amberlite IR 120H and Lewatit TP 260 commercial resins and Cu dominant adsorbate system.

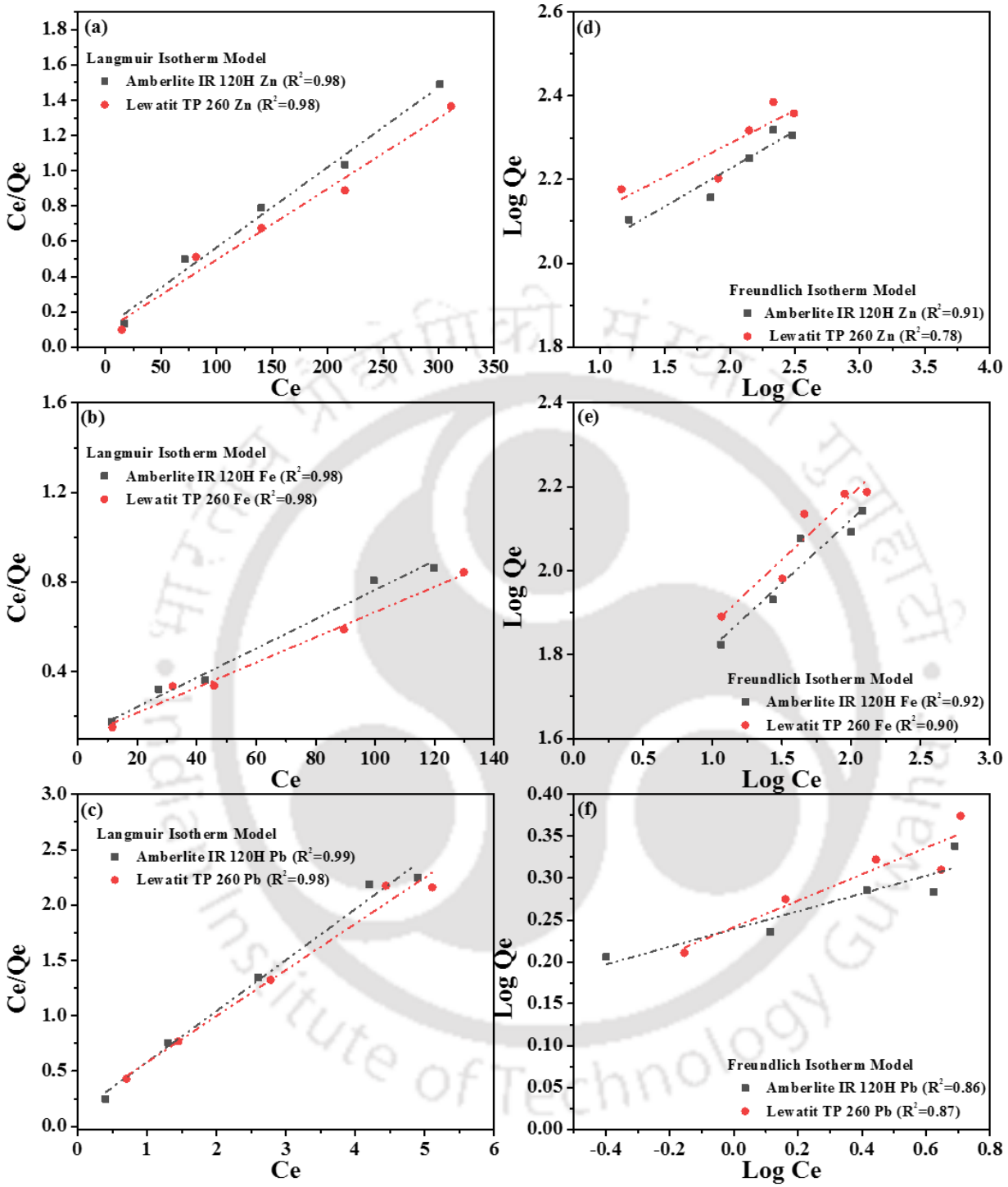

Fig. 3.10. Equilibrium models fitness plots (a-c: Langmuir isotherm model and d-f: Freundlich isotherm model) for Amberlite IR 120H and Lewatit TP 260 commercial resins and Zn dominant adsorbate system.

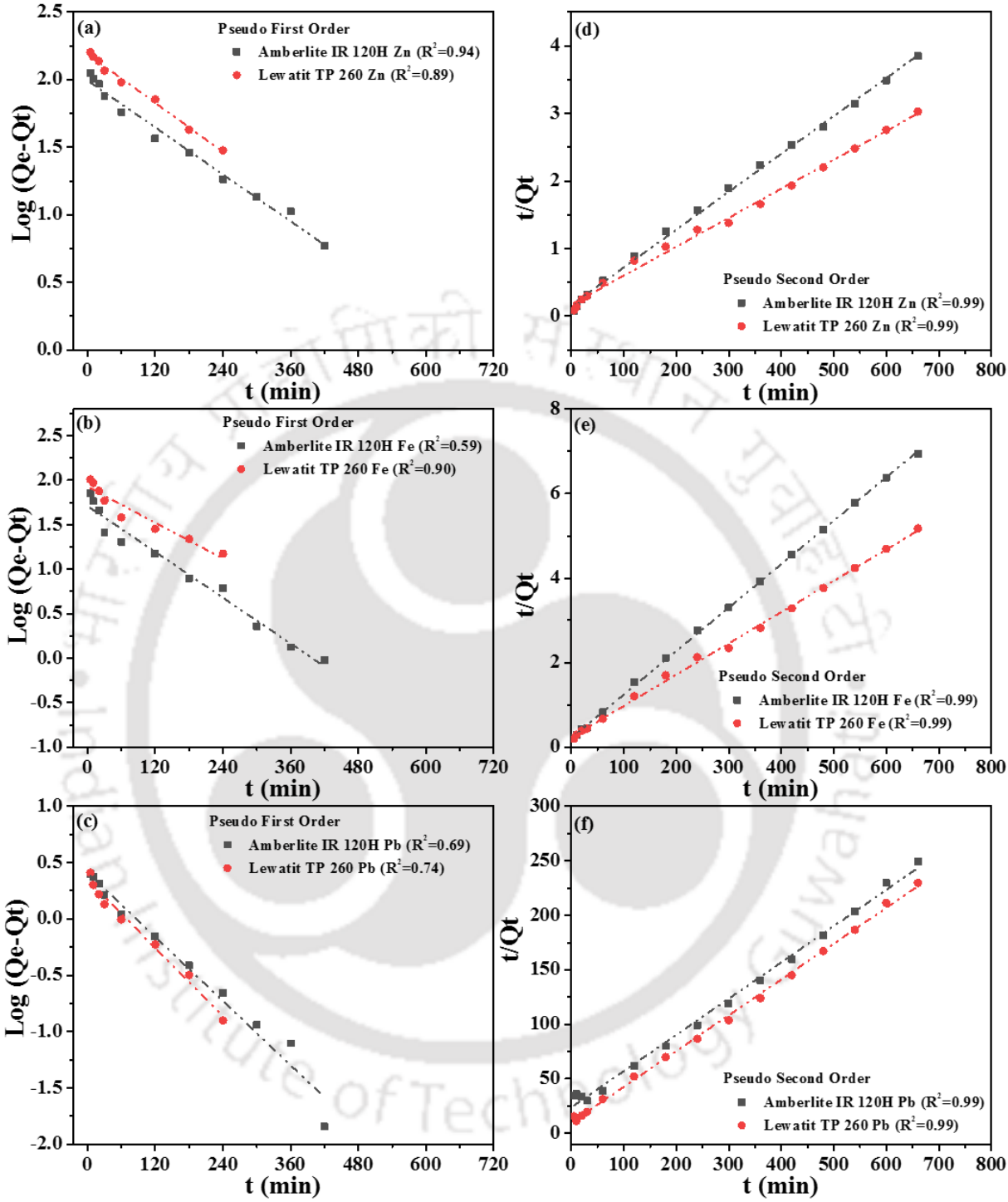

Fig. 3.11. Kinetic models fitness plots (a-c: Pseudo-first-order kinetic model, and d-f: Pseudo-second-order kinetic model) for Amberlite IR 120H and Lewatit TP 260 commercial resins and Zn dominant adsorbate system.

Table 3.1. Regressed model parameters representing heavy metal adsorption equilibrium data of commercial resins and Cu and Zn dominant adsorbate systems.

Metals	Commercial Resin	Solution	Langmuir parameters				Freundlich parameters		
			Q_o (mg g^{-1})	b (L mg^{-1})	R^2	R_L	K_f	n	R^2
Cu	Amberlite IR 120H	Cu dominant solution	196.1	0.02	0.97	0.2-0.07	40.6	3.98	0.88
Fe			54.3	0.24	0.99	0.06-0.02	27.9	7.03	0.83
Pb			4.3	2.78	0.99	0.06-0.02	3.3	8.7	0.84
Zn		Zn dominant solution	192.3	0.04	0.98	0.11-0.04	64.3	5.56	0.91
Fe			133.3	0.06	0.98	0.13-0.05	28.7	3.30	0.92
Pb			1.9	3.68	0.99	0.05-0.03	1.5	9.45	0.86
Cu	Lewatit TP 260	Cu dominant solution	204.1	0.03	0.99	0.15-0.06	39.2	3.54	0.92
Fe			57.1	0.19	0.99	0.08-0.03	24.5	5.50	0.91
Pb			5.2	1.67	0.99	0.10-0.04	3.1	4.00	0.80
Zn		Zn dominant solution	196.1	0.04	0.98	0.13-0.05	64.3	5.98	0.78
Fe			133.3	0.05	0.98	0.15-0.05	27.4	3.23	0.90
Pb			1.8	2.53	0.98	0.07-0.05	1.3	6.33	0.87

Table 3.2. Regressed model parameters representing heavy metal adsorption kinetic data of commercial resins and Cu and Zn dominant adsorbate systems.

Metals	Commercial Resin	Experimental Capacity (Q_{exp}, mg g^{-1})	Solution	Pseudo-first-order model			Pseudo-second-order model		
				Q_e (mg g^{-1})	K_1 (min^{-1})	R^2	Q_e (mg g^{-1})	K_2 (g mg^{-1} min^{-1})	R^2
Cu	Amberlite IR 120H	154.3	Cu dominant solution	35.4	0.013	0.59	156.25	0.0009	0.99
Fe		55.7		56.0	0.009	0.77	59.17	0.0003	0.97
Pb		5.5		2.1	0.005	0.65	5.60	0.0086	0.99
Zn		161.6	Zn dominant solution	148.2	0.012	0.94	169.49	0.0002	0.99
Fe		91.8		104.2	0.011	0.59	96.15	0.0003	0.99
Pb		2.6		1.8	0.006	0.69	2.97	0.0036	0.99
Cu	Lewatit TP 260	242.6	Cu dominant solution	114.8	0.011	0.87	250.0	0.0002	0.99
Fe		60.8		21.1	0.008	0.66	62.89	0.0008	0.99
Pb		6.8		2.2	0.006	0.55	7.02	0.0090	0.99
Zn		156.6	Zn dominant solution	100.4	0.009	0.89	166.67	0.0002	0.99
Fe		98.5		58.4	0.010	0.90	104.17	0.0003	0.99
Pb		2.2		1.2	0.006	0.74	2.28	0.0149	0.99

Isotherm models have been targeted to analyze the adsorption of studied heavy metal ions onto the surface of commercial resins (Amberlite IRA 120H and Lewatit TP 260) and at a constant temperature. Langmuir Isotherm model has been the best-fit isotherm model. It is based on the assumption that adsorption occurs at specific sites on the adsorbent surface, and once a site is occupied by an adsorbate molecule, no further adsorption can take place at that site. Also, the pseudo-second-order model has been inferred to be the best-fit model to represent the kinetics of

studied heavy metal ions adsorption from Cu and Zn dominant adsorbate systems and onto commercial resins (Amberlite IRA 120H and Lewatit TP 260). Thus, the model's basic assumption stated as follows is valid. The rate-limiting step could be the chemisorption involving valency forces through the sharing or exchange of electrons with the sulphonic acid functional group of Amberlite IRA 120H and the amino methyl phosphonic acid functional group of Lewatit TP 260. The fitness of the pseudo-second-order model is also justified with the FTIR analysis of metal-adsorbed commercial resins that inferred strong metal ions chemical interaction with the prevalent functional groups of the commercial resins.

3.4 Analytical Characterization

3.4.1 FTIR Analysis

Raw and metal-loaded commercialized resins were analyzed with Fourier transform infrared (FTIR) spectroscopy and in the 400–4000 cm^{-1} spectral range. Figs. 3.12 depicts the FTIR spectra of Amberlite IR 120H and Lewatit TP 260 resins. At high frequencies and between 3400– 3200 cm^{-1}, both anion-exchanging resins can be analyzed to exhibit a considerable and wider range of -OH stretching vibration. For pure Amberlite IR 120H, a peak exists between 2860-2930 cm^{-1} and thereby corresponds to symmetric or asymmetric stretching vibrations of the C−H bond. The band at 1630 cm^{-1} can be assigned to the vibration of the benzene ring. The bands observed at 1122 cm^{-1} and 1413 cm^{-1} corroborate with the -SO_2 groups of the sulfonic acid. A few peaks can be also observed in the spectra at 1002 cm^{-1}, 1038 cm^{-1}, 1134 cm^{-1}, and 1168 cm^{-1}. They convey upon the existence of sulfonic acid groups (Prekob et al. 2019). After metal adsorption, these peaks are shifted to 999 cm^{-1}, 1029 cm^{-1}, 1156 cm^{-1}. Such a peak shift has been due to heavy metal interaction with the Amberlite IR 120H resin.

For the raw Lewatit TP 260 resin, a strong band at 3420 cm^{-1} can be observed. This corroborates to the amine groups present in the resin. The compounds with P-OH groups affirm a broad band with medium intensity at 2732 cm^{-1} and 2323 cm^{-1}. These are due to the O-H stretching vibrations. Also, a strong band can be seen due to P-O stretching at 1220 cm^{-1} (Kołodyńska and Hubicki 2009). The bands at 1631 cm^{-1} and 1723 cm^{-1} have been assigned to the formation of the -NH bond. After metal adsorption, a strong band at 972 cm^{-1} disappeared. This is being assigned to the metal interaction with the resin.

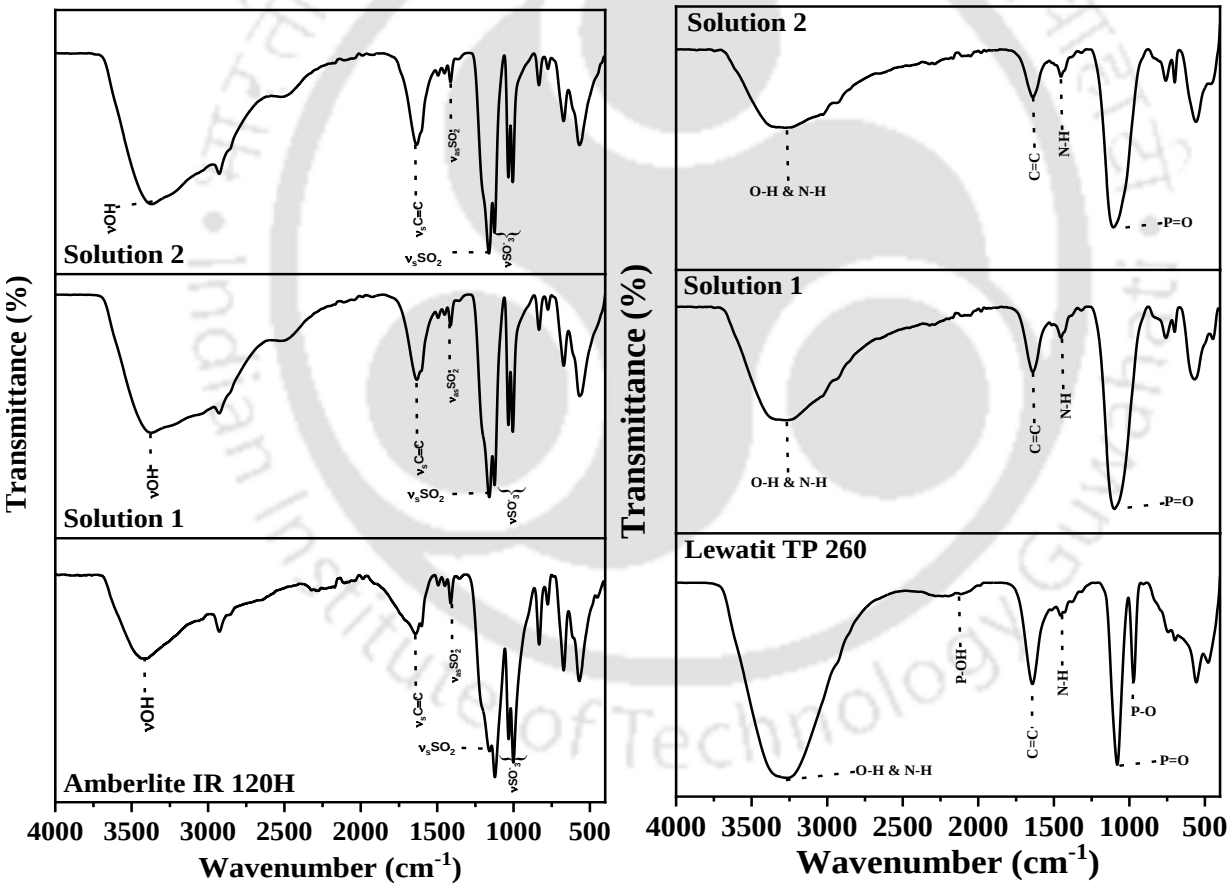

Fig. 3.12. FTIR spectra of raw and heavy metal loaded Amberlite IR 120H and Lewatit TP 260 resins.

3.4.2 EDX Analysis

EDX spectra obtained for pure Amberlite IR 120H and Lewatit TP 260 resins have been depicted in Figs. 3.13 and 3.14. The EDX spectra of Amberlite IR 120H resin (Fig. 3.13) confirm upon the presence of C (57.8 atomic weight %), O (24.8 atomic weight %), and S (13.1 atomic weight %). For Lewatit TP 260 resin (Fig. 3.14) pure resin, the EDX spectra refer to C (56.4 %), O (22.7 %) and P (9.8 %). After adsorption, the EDX spectra confirmed upon the presence of Cu, Fe, and Pb metal ions on the surface of both commercial resins.

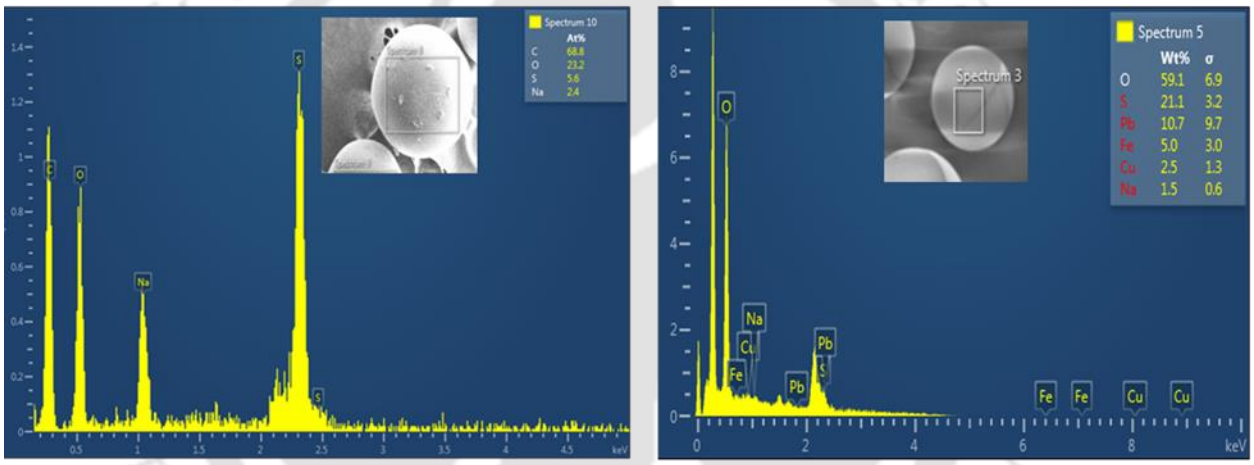

Fig. 3.13. FESEM-EDX spectra of raw and metals loaded Amberlite IR 120H resin.

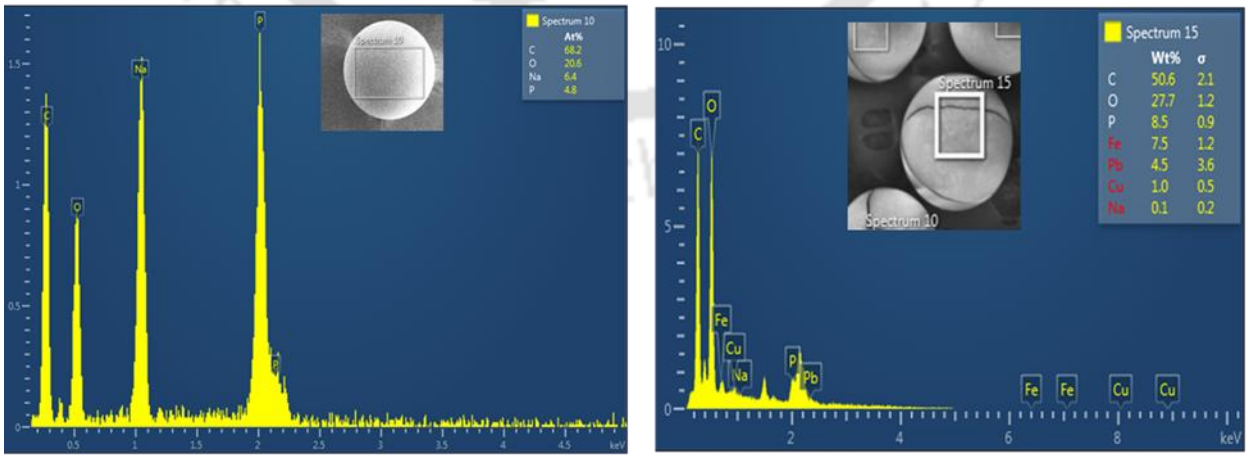

Fig. 3.14. FESEM-EDX spectra of raw and metals loaded Lewatit TP 260 resin.

3.5 Batch Desorption Studies

For the Cu dominant solution and for Amberlite IR 120H resin, the desorption efficiencies were the best for the 2M HCl case. For a variation in HCl concentration from 0.1-2M, the Cu recovery efficiencies varied as 25.11-53.88, 10.9-28.1, and 3.64-12.3 % for 1, 2 and 3 cycles, respectively. The desorption efficiencies of all tested acidic eluents followed the hierarchy as HCl > HNO_3 > H_2SO_4. Corresponding cycle efficiencies for HNO_3 and H_2SO_4 were comparatively lower and varied as 18.51-52.41, 5.27-25.8, and 1.72-11.3 %, and 16.74-49.59, 4.53-24.7, and 1.51-10.6 % for 1, 2 and 3 cycles, respectively. Thus, a significant reduction in cycle 2 and cycle 3 Cu desorption efficiencies was apparent in conjunction with the cycle 1 desorption efficiencies. The desorption efficiencies of Fe followed similar trends and correspondingly varied as 24.32-55.01, 10.34-25.98, and 6.35-16.47 % for 1, 2 and 3 cycles, respectively. For this case, the desorption efficiencies of all tested acidic eluents followed the hierarchy as HCl > H_2SO_4 > HNO_3. Corresponding cycle efficiencies for H_2SO_4 and HNO_3 were comparatively lower and varied as 22.0-47.06, 8.36-21.99, and 4.04-15.38 % and 24.24-44.28, 10.79-21.75, and 4.30-14.45 % for 1, 2 and 3 cycles, respectively. The desorption efficiencies of Pb followed similar trends and correspondingly varied as 13.36-56.46, 5.01-21.65, and 2.24-12.15 % for 1, 2 and 3 cycles, respectively. The Pb desorption efficiency of all tested acidic eluents followed the hierarchy as HCl > HNO_3 > H_2SO_4. Corresponding cycle efficiencies for HNO_3 and H_2SO_4 were comparatively lower and varied as 13.50-47.21, 5.73-24.5, and 1.70-11.92 %, and 21.72-42.97, 8.15-27.81, and 3.81-11.86 % for 1, 2 and 3 cycles, respectively.

For Cu dominant solution and for Amberlite IR 120H resin, the desorption efficiencies comparatively varied in the lower range for basic eluents in conjunction with the acidic eluents (0.1-2M). Corresponding cycle efficiencies for NaOH and KOH varied as 9.94-49.3.1, 3.81-21.0, and 1.49-8.46 % and 10.77-36.40, 4.29-16.3, and 1.81-7.33 % for 1, 2 and 3 cycles, respectively.

Thus, significant reductions in cycle 2 and cycle 3 Cu desorption efficiencies were observed with respect to cycle 1 desorption efficiencies. The desorption efficiencies of Fe followed a similar trend and the Fe desorption efficiency of tested basic eluents followed the hierarchy as KOH > NaOH. Corresponding cycle efficiencies for KOH and NaOH have been determined as 13.12-41.05, 5.69-18.51, and 3.81-13.07 % and 11.62-40.05, 5.06-17.98, and 3.42-11.32 % for 1, 2 and 3 cycles, respectively. Thus, a significant reduction in cycle 2 and cycle 3 Fe desorption efficiencies with respect to cycle 1 Fe efficiencies was observed. The desorption efficiencies of Pb followed a similar trend and the desorption efficiency of all tested basic eluents followed the hierarchy as NaOH > KOH. Corresponding cycle efficiencies for NaOH and KOH were 14.66-43.31, 6.08-24.36, and 3.21-13.08 % and 13.72-40.09, 5.64-21.16, and 2.18-10.05 % for 1, 2 and 3 cycles, respectively. Thus, a significant reduction in cycle 2 and cycle 3 Pb desorption efficiencies was apparent in comparison with the Pb cycle 1 desorption efficiencies.

For Cu dominant solution and for Lewatit TP 260 resin, the desorption efficiencies were obtained promising for the 2M HCl case. Corresponding variations in the Cu desorption efficiencies varied as 20.64-44.30 %, 8.62-21.2 %, and 2.64-8.24 % for 1, 2, and 3 cycles, respectively in the concentration range of 0.1-2 M. The desorption efficiency of all tested acidic eluents followed the hierarchy as HCl > HNO_3 > H_2SO_4. Corresponding cycle efficiencies for HNO_3 and H_2SO_4 have been determined as 15.22-43.08 %, 4.2-19.5 %, 1.27-7.63 %, and 13.77-40.78 %, 3.62-18.8 %, 1.12-7.2 % for 1, 2 and 3 cycles, respectively. Thus, a significant reduction in cycle 2 and cycle 3 Cu desorption efficiencies with respect to cycle 1 efficiencies was observed. The desorption efficiencies of Fe followed similar trends and varied as 15.12-47.18 %, 10.88-23.73 %, and 6.61-13.44 % for 1, 2, and 3 cycles, respectively in the concentration range of 0.1-2 M. The desorption efficiency of all tested acidic eluents followed the hierarchy as HCl > HNO_3 > H_2SO_4. Corresponding cycle efficiencies for HNO_3 and H_2SO_4 have been determined as 16.41-43.59 %,

9.43-20.86 %, 4.44-13.33 %, and 15.20-42.08 %, 10.11-21.62 %, 6.26-16.0 % for 1, 2 and 3 cycles, respectively. Thus, a significant reduction in cycle 2 and cycle 3 desorption efficiencies with respect to cycle 1 efficiencies was observed. The desorption efficiencies of Pb followed different trends with 2M HNO_3 and varied as 14.27-44.89 %, 6.25-24.81 %, and 1.84-12.01 % for 1, 2, and 3 cycles, respectively in the concentration range of 0.1-2 M. The desorption efficiency of all tested acidic eluents followed the hierarchy as HNO_3 > H_2SO_4 > HCl. Corresponding cycle efficiencies for H_2SO_4 and HCl have been determined as 22.5-43.7 %, 8.71-30.14 %, 4.04-12.87 %, and 14.09-39.32 %, 5.45-18.62 %, and 2.42-9.89 % for 1, 2 and 3 cycles, respectively. Thus, a significant reduction in cycle 2 and cycle 3 Pb desorption efficiencies with respect to cycle 1 efficiencies was observed.

For the Cu dominant solution and for Lewatit TP 260 resin, the Cu desorption efficiencies were best for the 2M NaOH case. Corresponding cycle efficiencies for NaOH and KOH have been determined as 16.24-51.06 %, 4.22-24.7 %, 2.43-12.0 %, and 8.87-33.29 %, 3.46-17.2 %, 1.35-8.55 % for 1, 2 and 3 cycles, respectively. Thus, a significant reduction in cycle 2 and cycle 3 Cu desorption efficiencies with respect to cycle 1 efficiencies was observed. The desorption efficiencies of Fe followed similar trends and the desorption efficiency of tested basic eluents followed the hierarchy as NaOH > KOH. Corresponding cycle efficiencies for NaOH and KOH have been determined as 13.78- 49.93 %, 5.79-26.09 %, 3.80-13.65 %, and 15.55-46.74 %, 6.52-22.01 %, 4.24-15.10 % for 1, 2 and 3 cycles, respectively. Thus, a significant reduction in cycle 2 and cycle 3 Fe desorption efficiencies with respect to cycle 1 efficiencies was observed. The desorption efficiencies of Pb followed similar trends and the desorption efficiency of all tested basic eluents followed the hierarchy as NaOH > KOH. Corresponding cycle efficiencies for NaOH and KOH have been determined as 15.77-47.63 %, 13.16-26.88 %, 7.38-20.13 %, and 14.30-41.91

%, 6.07-23.09 %, 2.32-11.81 % for 1, 2 and 3 cycles, respectively. Thus, a significant reduction in cycle 2 and cycle 3 Pb desorption efficiencies with respect to cycle 1 efficiencies was observed. For the Zn dominant solution and for Amberlite IR 120H resin, Zn recovery efficiencies were lesser (with respect to Pb and Fe) for acidic eluents in the concentration range of 0.1-2 M, and for all tested acidic eluents, the trend followed the hierarchy as HCl > HNO_3 > H_2SO_4. Corresponding cycle efficiencies for HCl, H_2SO_4 and HNO_3 have been determined as 23.71-48.9 %, 10.75-26.1 %, 3.5-12.4 %, 15.80-44.86 %, 4.5-25.31 %, 1.5-12.8 % and 17.10-47.6 %, 5.3-27.8 %, 1.7-12.1 % for 1, 2 and 3 cycles, respectively. Thus, a significant reduction in cycle 2 and cycle 3 Zn desorption efficiencies with respect to cycle 1 efficiencies was observed. The desorption efficiencies of Fe were highest for 2M HCl and varied as 14.95-40.31 %, 12.59-27.20 %, and 9.45-22.54 % for 1, 2, and 3 cycles, respectively in the concentration range of 0.1-2 M. The desorption efficiency of all tested acidic eluents followed the hierarchy as HCl > H_2SO_4 > HNO_3. Corresponding Fe cycle desorption efficiencies for H_2SO_4 and HNO_3 have been determined as 13.56-29.01 %, 10.37-22.8 %, 6.21-19.72 % and 14.93-27.18 %, 13.18-24.82 %, 6.4-21.4 % for 1, 2 and 3 cycles, respectively. Thus, a significant reduction in cycle 2 and cycle 3 desorption efficiencies with respect to cycle 1 Fe efficiencies was observed. The desorption efficiencies of Pb followed similar trends and varied as 21.87-52.01 %, 10.07-28.34 %, and 4.75-14.81 % for 1, 2, and 3 cycles, respectively in the concentration range of 0.1-2 M. The desorption efficiency of all tested acidic eluents followed the hierarchy as HCl > HNO_3 > H_2SO_4. Corresponding cycle efficiencies for HNO_3 and H_2SO_4 have been determined as 17.29-46.3 %, 7.07-26.8 %, 2.95-15.2 %, 17.5-44.4 %, 7.53-24.03 %, 3.46-13.17 % for 1, 2 and 3 cycles, respectively. Thus, a significant reduction in cycle 2 and cycle 3 Pb desorption efficiencies with respect to cycle 1 efficiencies was observed.

For the Zn dominant solution and for Amberlite IR 120H resin, Zn desorption efficiencies were the best for the 2M NaOH case. Corresponding cycle efficiencies for NaOH and KOH have been determined as 23.9-50.63 %, 10.7-28.1 %, 5.1-14.7 % and 10.24-43.5 %, 4.27-23.8 %, 1.8-10.4 % for 1, 2 and 3 cycles, respectively in the concentration range of 0.1-2 M. Thus, significant reduction in cycle 2 and cycle 3 Zn desorption efficiencies with respect to cycle 1 efficiencies was observed. The desorption efficiencies of Fe were comparatively lesser for basic eluents and the desorption efficiencies for KOH and NaOH have been achieved as 8.6-24.3 %, 7.3-20.5 %, 6.1-17.1 % and 7.18-24.6 %, 6.7-19.71 %, 5.6-14.8 % for 1, 2 and 3 cycles, respectively. Thus, a significant reduction in cycle 2 and cycle 3 Fe desorption efficiencies with respect to cycle 1 efficiencies was observed. The desorption efficiencies of Pb followed similar trends and the desorption efficiency of all tested basic eluents followed the hierarchy as KOH > NaOH. Corresponding cycle efficiencies for KOH and NaOH have been determined as 21.48-46.63 %, 10.55-24.9 %, 4.8-13.5 %, and 18.7-45.02 %, 7.9-26.0 %, 7.5-13.46 % for 1, 2 and 3 cycles, respectively. Thus, a significant reduction in cycle 2 and cycle 3 Pb desorption efficiencies with respect to cycle 1 efficiencies was observed.

For the Zn dominant solution and for Lewatit TP 260 resin, Zn recovery efficiencies were lesser (compared to Fe and Pb) for acidic eluents in the concentration range of 0.1-2 M. For all tested acidic eluents, the hierarchy was HNO_3 > HCl > H_2SO_4. Corresponding cycle efficiencies for HNO_3, HCl, and H_2SO_4 have been determined as 17.24-46.3 %, 5.2-25.2 %, 1.7-11.8 %, 23.1-46.1 %, 10.6-25.2 %, 3.5-11.2 % and 15.4-43.7 %, 4.4-24.8 %, 1.44-12.6 % for 1, 2 and 3 cycles, respectively. Thus, a significant reduction in cycle 2 and cycle 3 Zn desorption efficiencies with respect to cycle 1 efficiencies was observed. The desorption efficiencies of Fe were highest for the 2M HCl case and varied as 13.8-32.1 %, 11.8-23.7 %, and 8.3-20.2 % for 1, 2, and 3 cycles, respectively in the concentration range of 0.1-2 M. The desorption efficiency of all tested acidic

eluents followed the hierarchy as HCl > H_2SO_4 > HNO_3. Corresponding cycle efficiencies for H_2SO_4 and HNO_3 have been determined as 12.6-26.9 %, 9.7-21.3 %, 5.8-18.4 % and 13.8-25.2 %, 12.3-23.2 %, 6.1-20.1 % for 1, 2 and 3 cycles, respectively. Thus, a significant reduction in cycle 2 and cycle 3 Fe desorption efficiencies with respect to cycle 1 efficiencies was observed. The desorption efficiencies of Pb followed similar trends and varied as 26.02-41.4 %, 12.7-27.6 %, and 5.9-15.7 % for 1, 2, and 3 cycles, respectively in the concentration range of 0.1-2 M. The desorption efficiency of all tested acidic eluents followed the hierarchy as HCl > HNO_3 > H_2SO_4. Corresponding cycle efficiencies for HNO_3 and H_2SO_4 have been determined as 19.6-41.3 %, 8.5-24.4 %, 3.5-13.3 % and 20.2-39.2 %, 9.2-25.6 %, 4.1-15.03 % for 1, 2 and 3 cycles, respectively. Thus, a significant reduction in cycle 2 and cycle 3 Pb desorption efficiencies with respect to cycle 1 efficiencies was observed.

For the Zn dominant solution and for Lewatit TP 260 resin, Zn desorption efficiencies were the best for the 0.1M NaOH case. Corresponding cycle efficiencies for NaOH and KOH have been determined as 49.2-23.4 %, 27.4-10.5 %, 14.3-4.9 %, and 10.01-43.5 %, 4.2-23.8 %, 1.7-10.4 % for 1, 2 and 3 cycles, respectively in the concentration range of 0.1-2 M. Thus, a significant reduction in cycle 2 and cycle 3 Zn desorption efficiencies with respect to cycle 1 efficiencies was observed. The desorption efficiencies of Fe were lower for basic eluents and the desorption efficiencies for KOH and NaOH have been achieved as 7.9-29.0 %, 6.8-21.8 %, 5.7-18.6 %, and 9.9-31.8 %, 9.7-30.5 %, 6.6-23.6 % for 1, 2 and 3 cycles, respectively. Thus, a significant reduction in cycle 2 and cycle 3 Fe desorption efficiencies with respect to cycle 1 efficiencies was observed. The desorption efficiencies of Pb followed similar trends and the desorption efficiency of all tested basic eluents followed the hierarchy as NaOH > KOH. Corresponding cycle desorption efficiencies (Pb) for NaOH and KOH have been determined as 22.2-47.3 %, 9.7-26.3 %, 9.1-14.9 % and 25.5-

43.5 %, 13.2-25.05 %, 5.9-13.9 % for 1, 2 and 3 cycles, respectively. Thus, a significant reduction in cycle 2 and cycle 3 Pb desorption efficiencies with respect to cycle 1 efficiencies can be inferred. In summary, for Amberlite IR 120H commercial resin case and for a variation in number of cycles from 1-3, the cyclic desorption % reduced from 51.1-12.0 %, 49.9-13.7 %, and 47.6-20.1 %, respectively for Cu, Fe, and Pb from Cu dominant solution and 49.2-14.3 %, 31.8-23.6 %, and 47.3-14.9 %, respectively for Zn, Fe, and Pb from Zn dominant solution and with 2 M HCl eluent system. Incidentally, for the Cu dominant solution, the corresponding adsorptive removal was 65.10-37.90 %, 71.79-35.68 %, and 82.79-68.37 %, respectively. Also, the cyclic number (1-3) based adsorptive removal of 66.79-39.92 %, 68.49-38.31 %, and 77.55-68.11 %, respectively for Zn, Fe, and Pb respectively in the Zn dominant solution affirmed that the mentioned metals removal suffered detrimentally with cyclic adsorption. Further, the corresponding adsorption capacity reduced from 152.82-89.00 mg g^{-1}, 55.77-27.87 mg g^{-1}, and 5.38-4.44 mg g^{-1} from Cu dominant solution and 185.97-111.14 mg g^{-1}, 102.28 mg g^{-1}, and 2.94-1.84 mg g^{-1} from Zn dominant solution for a variation in cycle number from 1-3. This affirmed a natural reduction in adsorption capacity during cyclic adsorption-desorption studies.

Additionally, for Lewatit TP 260 commercial resin case and for a variation in number of cycles from 1-3, the cyclic desorption % reduced from 53.9-12.3 %, 55.0-12.2 %, and 56.5-12.2 %, respectively for Cu, Fe, and Pb from Cu dominant solution and 50.6-14.7 %, 40.31-22.5 %, and 51.96-14.8 %, respectively for Zn, Fe, and Pb from Zn dominant solution and for 2M NaOH solution. Incidentally, for the Cu dominant solution, the corresponding adsorptive removal was 79.20-59.70 %, 60.26-36.05 %, and 79.33-65.65 %, respectively. Also, the cyclic number (1-3) based adsorptive removal of 68.31-39.69 %, 73.91-40.12 %, and 66.79-43.87 %, respectively for Zn, Fe, and Pb respectively in the Zn dominant solution affirmed that the mentioned metals removal suffered detrimentally with cyclic adsorption. Further, the corresponding adsorption

capacity reduced from 247.78-186.78 mg g^{-1}, 62.12-37.16 mg g^{-1}, and 6.86-5.69 mg g^{-1} from Cu dominant solution and 190.19-110.50 mg g^{-1}, 129.10-70.07 mg g^{-1}, and 2.98-1.94 mg g^{-1} from Zn dominant solution for a variation in cycle number from 1-3. This affirmed a natural reduction in adsorption capacity during cyclic adsorption-desorption studies.

Thus, these findings confirm that both commercial resins (Amberlite IRA 120H and Lewatit TP 260) can further perform effectively in a hybrid adsorption process that targets the greater removal of Cu, Zn, Fe, and Pb. Such a hybrid process needs to address the pre-treatment technology for the mitigation of the Al, Mg, and Na constitutions in the mentioned simulated wastewater system.

3.6 Literature Comparison

A comparative summary of the best data of this work has been addressed in Table 3.3 along with that reported in the literature. Compared to the literature, the findings for Lewatit TP 260 resin were much superior. The literature refers to adsorption capacities of 64.8, 1.8, and 3.3 mg g^{-1} for Cu, Pb, and Zn solutions, respectively (Nekouei et al. 2019). In this work, for the synthetic Cu and Zn multi-metal wastewater, higher metal uptake values of 204.1 and 196.1 mg g^{-1} were obtained for the Cu and Zn dominant multi-metal wastewater solution. Thus, the adsorption properties of the Lewatit TP 260 resin were unaffected due to the presence of other metal ions such as Al, Na, and K. For comparison, no relevant literature data has been presented in the literature for the Amberlite IR 120H resin.

Table 3.3. Summary of the adsorption and desorption characteristics of alternate resins investigated in this study and prior art.

Adsorbent	Metal Ion		Conc. (mg/l)		pH		Ads. Caps. (mg/g)		Desorption (%)		Ref.
Amberlite IR 120H	**Pb** **Cu** **Fe**	**Pb** **Zn** **Fe**	10.4 375.4 123.7	5.3 389.8 209.6	3.8	3.6	4.3 196.1 54.3	1.9 192.3 133.3	47.6-20.1 51.1-12.0 49.9-13.7 (2 M HCl; 1-3 cycles)	47.3-14.9 49.2-14.3 31.8-23.6 (2 M HCl; 1-3 cycles)	Present study
Lewatit TP 260	**Pb** **Cu** **Fe**	**Pb** **Zn** **Fe**	10.4 375.4 123.7	5.3 389.8 209.6	3.8	3.6	5.2 204.1 57.1	1.8 196.1 133.3	56.5-12.2 53.9-12.3 55.0-12.2 (2 M NaOH; 1-3 cycles)	51.96-14.8 50.6-14.7 40.31-22.5 (2 M NaOH; 1-3 cycles)	Present study
Lewatit TP 260 Lewatit TP 208 Amberlite IRA743	Al **Cu** Ni **Pb** **Zn**		-		3.9		64.8 1.8 3.3	66.7 1.9 2.7	35.3 1.3 1.2	>90 (low molar Sulfuric Acid)	(Nekouei et al. 2019)
Styrene –DVB copolymer	Cr Ni Pb Cd		-		3.5		-		65 70 45 (0.1N NaOH) Cycles not given		(Misra et al. 2011)
Polyvinyl tetrazole grafted PS resins	Pb Cu Cr		4 (mmol/l)		5		1.5 2.6 3.4 (mmol/g)		94% 1M HCl (10 Cycle) 2 h desorption time		(Chen et al. 2014)
GMA/DVB magnetic resin	Pb Cd Zn Ca Mg		5 (mmol/l)		6 6.6 6.5 6.5 7.0		2.68 2.39 2.00 1.99 1.83		96 (0.2M EDTA 5 Cycles) Efficiency of each cycle given		(Atia et al. 2008)

3.7 Summary

For the studied commercial resins, a brief account of the key findings of cyclic multi-metal adsorption-desorption performance-based efficacy is as follows. Firstly, commercial resins Amerblite IR 120H and Lewatit TP 260 have been effective in removing Cu, Zn, Pb, and Fe from simulated multi-metal wastewater solutions. Thus, no inhibitory mechanisms existed due to other co-existent metals in the chosen adsorbate systems. Secondly, the optimal multi-heavy metal batch adsorption parameters for the Amberlite IR 120H resin for the Cu dominant solution were 3.82

pH, 1.6 g L^{-1} dosage, and 420 min contact time. Corresponding adsorption capacity and metal removal % of the resin were 99.88-171.08 mg g^{-1} and 85.14-48.61 % for Cu, 35.38-52.68 mg g^{-1} and 91.53-45.43 % for Fe and 3.00-4.12 mg g^{-1} and 92.31-42.24 % for Pb, respectively for the initial heavy metal ion concentration range of 187.7-563.1 mg L^{-1} for Cu, 61.85-185.55 mg L^{-1} for Fe, and 5.2-15.6 mg L^{-1} for Pb. On the other hand, the optimal heavy metal ion batch adsorption parameters for Amberlite IR 120H resin in Zn dominant solution were 3.64 pH, 1.4 g L^{-1} dosage, and 480 min contact time. Corresponding adsorption capacity and metal removal % of the resin were 127.19-202.38 mg g^{-1} and 91.36-48.46 % for Zn, 66.61-139.00 mg g^{-1} and 88.97-61.89 % for Fe, and 1.61-2.18 mg g^{-1} and 84.91-38.36 % for Pb, respectively in the initial heavy metal ion concentration range of 194.9-584.7 mg L^{-1} for Zn, 104.8-314.4 mg L^{-1} for Fe, and 2.65-7.95 mg L^{-1} for Pb. Similarly, the optimal multi-heavy metal batch adsorption parameters for the Lewatit TP 260 resin in Cu dominant solution were 3.82 pH, 1.2 g L^{-1} dosage, and 300 min contact time. Corresponding adsorption capacity and metal removal % of the resin were 133.18-237.23 mg g^{-1} and 85.14-50.55 % for Cu, 46.06-70.26 mg g^{-1} and 89.36-45.44 % for Fe and 3.59-6.32 mg g^{-1} and 82.88-48.65 % for Pb, respectively for the initial heavy metal ion concentration range of 187.7-563.1 mg L^{-1} for Cu, 61.85-185.55 mg L^{-1} for Fe, and 5.2-15.6 mg L^{-1} for Pb. On the other hand, the optimal heavy metal ion batch adsorption parameters for Lewatit TP 260 resin in Zn dominant solution were 3.64 pH, 1.2 g L^{-1} dosage, and 300 min contact time. Corresponding adsorption capacity and metal removal % of the resin were 150.15-227.88 mg g^{-1} and 92.45-46.77 % for Zn, 77.67-153.83 mg g^{-1} and 88.94-58.71 % for Fe, and 1.63-2.37 mg g^{-1} and 73.58-35.72 % for Pb, respectively in the initial heavy metal ion concentration range of 194.9-584.7 mg L^{-1} for Zn, 104.8-314.4 mg L^{-1} for Fe, and 2.65-7.95 mg L^{-1} for Pb. Hence, compared to the Zn dominant solution, the Amberlite IR 120H resin provided marginally higher removal efficiencies with the Cu dominant solution. Similarly, compared to the Cu dominant solution, the Lewatit TP 260 resin

provided marginally higher removal efficiencies with the Zn dominant solution. However, the Lewatit TP 260 resin exhibited higher regeneration characteristics for the Cu dominant solution in comparison with the Zn dominant solution. The desorption characteristics were 56.5, 53.9, and 55.0 % for Pb, Cu, and Fe, respectively for the Cu dominant solution and 51.96, 50.6, and 40.31 % for Pb Zn, and Fe, respectively for the Zn dominant solution. These indicate and confirm satisfactory heavy metal ion removal and resin regeneration. Further improvement in the heavy metal ion desorption characteristics of Lewatit TP 260 can be conveniently targeted through the suitable alteration in the abundance of the functional groups. Thirdly, the adsorption of Cu, Zn, Pb, and Fe with commercial resins exhibited a uniform adsorptive pattern and pseudo-second-order kinetic model. Fourthly, the speciation and functional group analyses enabled an easier understanding into the pertinent adsorption mechanism Cu, Zn, Pb, and Fe onto the commercial resin. Despite being expensive, the commercial resins provide satisfactory performance for multi-heavy metal removal with cyclic desorption. Hence, they shall not be ignored in conjunction with the synthesized derivatives.

Chapter 4:

Cyclic Multi-heavy metal adsorptive and desorptive characteristics of Polyvinyl alcohol-Chitosan derivative Resins

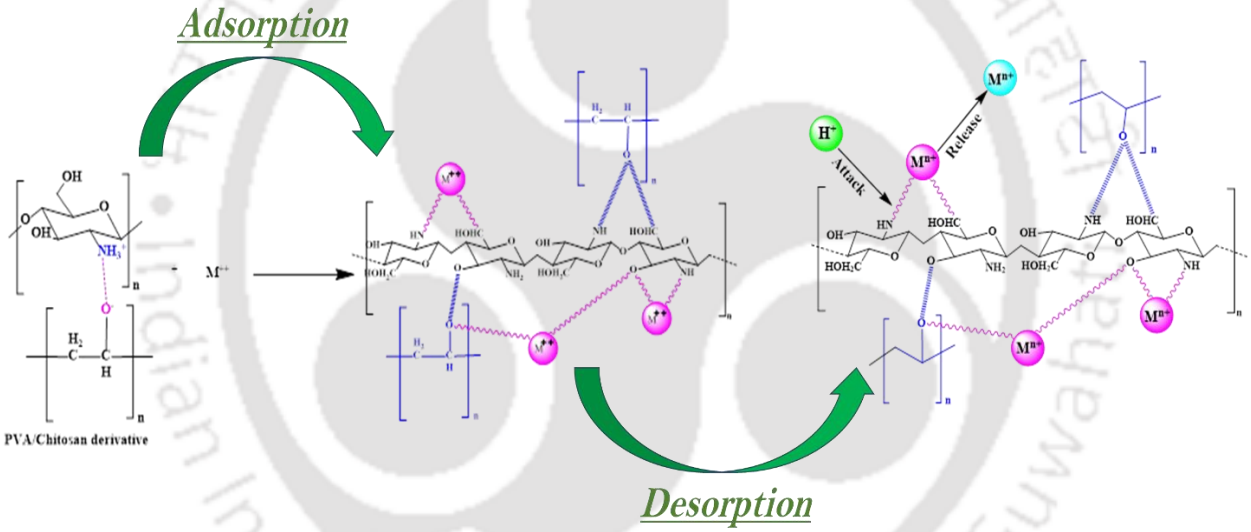

Chapter 4

Cyclic Multi-heavy metal adsorptive and desorptive characteristics of Polyvinyl alcohol-Chitosan derivative Resins

The chapter summarizes experimental and theoretical findings associated to multi heavy metal adsorption and desorption characteristics of polyvinyl alcohol grafted low molecular weight chitosan derivative (low CSPVA), polyvinyl alcohol grafted medium molecular weight chitosan derivative (medium CSPVA), and polyvinyl alcohol grafted high molecular weight chitosan derivative (high CSPVA). Section 4.1 presents relevant background followed by solubility resistance-related findings of the derivatives in section 4.2. Section 4.3 briefly presents the adsorption characteristics of the mentioned resins. Section 4.4 briefly describes the findings associated to surface characterizations of raw and metal-loaded derivative samples. Thereafter, section 4.5 presents heavy metal desorption characteristics of spent polyvinyl alcohol grafted high molecular weight chitosan derivative (high CSPVA) using various inexpensive eluents. Thereafter, section 4.6 presents the literature comparison of the best available prior art and the findings of this chapter. Finally, a summary of the key findings is presented in section 4.7.

4.1 Background

Prior to this work, the nitrogen, carboxyl, and hydroxyl functionalized adsorbents being evaluated for heavy metal ion removal and resin regeneration from multi-metal solutions refer to glutaraldehyde cross-linked chitosan derivative (Busuioc et al., 2016) and PVA/chitosan beads (Li

et al., 2011). However, many such resins have been evaluated for heavy metal removal from aqueous solutions. Therefore, the emphasis of the conducted research is to examine the role of chitosan molecular weight on the efficacy of the polyvinyl alcohol-chitosan derivative in terms of the multi-heavy metal adsorption characteristics from complex synthetic industrial wastewater adsorbate systems. Further, simple eluent-based desorption characteristics were targeted for these chitosan derivatives.

The heavy metal ion adsorption characteristics were evaluated for optimal combinations of contact time, adsorbent dosage, and initial heavy metal ion concentrations. Surface characterizations were conducted using a Fourier Transform-Infrared Spectrophotometer (FTIR), Braummer-Emmet-Teller (BET), X-ray diffractometer (XRD), Thermo Gravimetric Analyser (TGA), and Field Emission Scanning Microscopy equipped energy dispersive X-Ray analyzer (FESEM-EDX). For optimized adsorbent dosage and contact time, adsorption experiments were conducted for a wider range of initial metal ion concentrations (187.7-563.1 mg L^{-1} for Cu, 61.85-185.55 mg L^{-1} for Fe, and 5.2-15.6 mg L^{-1} for Pb) in Cu dominant and (194.9-584.7 mg L^{-1} for Zn, 104.8-314.4 mg L^{-1} for Fe, and 2.65-7.95 mg L^{-1} for Pb) Zn dominant solutions. Thereby, the specific influence of various coexisting ions such as K, Na, Al, and Mg on targeted heavy metal adsorption characteristics of low CSPVA, medium CSPVA, and high CSPVA derivatives were addressed.

4.2 Solubility Resistance of high CSPVA derivative Resin

The high CSPVA resin was subjected to stability studies prior to and after multi-heavy metal adsorption. To do so, firstly, the raw high CSPVA resin was placed in contact with 1 N HNO_3 and 1 N KOH solutions for 12 h, and a quantitative analysis of weight reduction was performed. Thereby, the weight loss % was 0.96 % for both cases and thereby confirming the very good stability of the resin in both acidic and basic media. Also, the heavy metal adsorbed high CSPVA

resin was also subjected to a similar stability test. It was found that the weight loss for the case was also similar (0.95 % for both cases of acidic and basic media). In summary, the high CSPVA derivative is stable at the mentioned process conditions (pH 3.64 and 360 min contact time) and in both acidic and basic media. These observations confirm upon its relevance for real-time applications.

4.3 Multi-Heavy Metal Adsorption Characteristics of low CSPVA, medium CSPVA, and high CSPVA derivative Resins

4.3.1 Optimality of batch adsorption process parameters

It is well known that pH has a strong influence on the adsorption behavior. Thus, pH optimization experiments were conducted for the copper-dominant solution. The adsorbate solution below 2 pH and above 4 pH was analyzed to be unstable and involved the formation of a precipitate. For this reason, altered pH studies could not be carried out. Therefore, other adsorption parameters were optimized for an initial solution pH (natural pH) of 3.82 for Cu and 3.64 for Zn dominant solutions. It has been hypothesized that the nitrogen atoms of the amino groups in the chitosan and the oxygen atoms of the hydroxyl groups in both chitosan and PVA would serve as adsorption sites for the chemisorption of mentioned metals in the crosslinked chitosan/PVA beads (Karim et al., 2019). Since each atom of nitrogen and oxygen has an extra electron, they may share an electron pair with a positively charged ion to form a stable ionic bond. Nitrogen serves as the primary binding site and creates a stable metal complex due to the ease with which lone pairs may be released from the atom. Based on this information, the following reactions have been suggested to explain the pertinent sorption process (Kumar et al., 2009):

$$R - NH_2 + H^+ \rightarrow R - NH_3^+ \quad (4.1)$$

$$R - NH_2 + M^{2+} \rightarrow R - NH_2M^{2+} \quad (4.2)$$

$$R - NH_3^+ + M^{2+} \rightarrow R - NH_2M^{2+} + H^+ \quad (4.3)$$

$$R - NH_2M^{2+} + H_2O \rightarrow MOH^+ + R - NH_3^+ \quad (4.4)$$

Relevant prior art conveys that heavy metal ion adsorption on the high CSPVA occurs through a combination of ion exchange, complexation, and electrostatic attraction (Li et al., 2022; Peng et al., 2022; Zhang et al., 2022). To further supplement such views, needful introspection has been addressed in this work to identify potential mechanisms of heavy metal adsorption on the CSPVA. Based on speciation results and solution pH, the mechanism has been deduced and presented in (Fig. 4.1) for the adsorption of heavy metal ions on the CSPVA derivative.

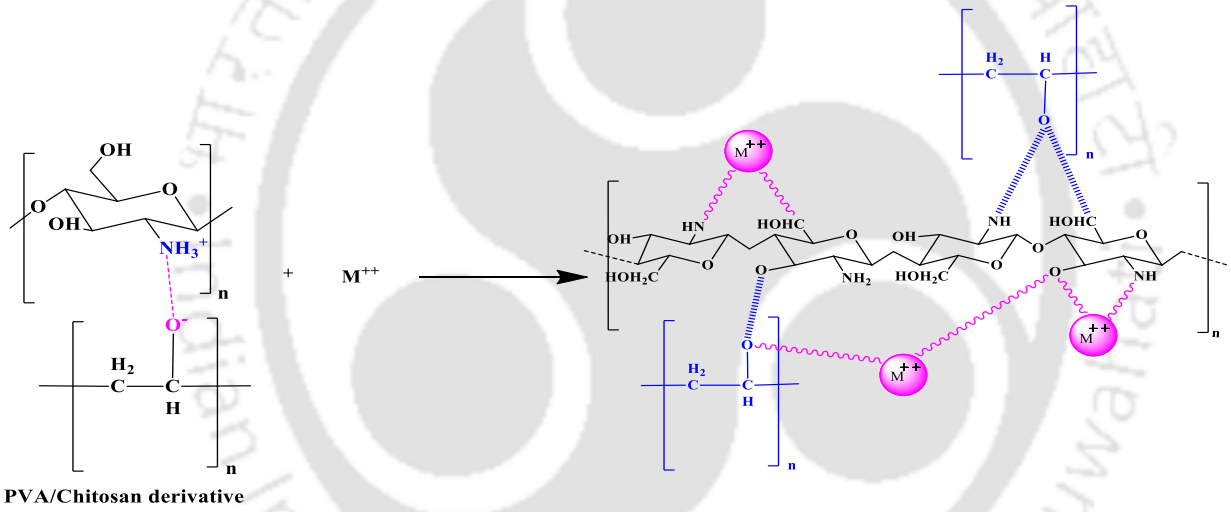

Fig. 4.1. Proposed heavy metal adsorption mechanism for CSPVA derivative.

The batch adsorption studies were conducted at specified combinations of contact period (720 min), fixed solution initial pH (3.82), and initial concentration (Cu 375.5 mg L^{-1}, Fe 123.7 mg L^{-1}, and Pb 10.4 mg L^{-1} for Cu dominant solution and Zn 389.8 mg L^{-1}, Fe 209.6 mg L^{-1}, and Pb 5.3 mg L^{-1} for Zn dominant solution) and altered adsorbent dosage values (0.2 g L^{-1} to 2 g L^{-1}). Fig. 4.2 depicts the influence of adsorbent dosage on the removal of heavy metal ions from the copper-dominant simulated industrial wastewater. Thereby, based on optimal adsorption capacity and %

removal, the optimum adsorbent dosage for low CSPVA, medium CSPVA, and high CSPVA was 1.6 g L^{-1} for optimal removal of all metal ions i.e., Cu, Fe, and Pb. Thereby, for Cu, at the optimal dosage, maximum adsorption capacities and removal % were 178.63 mg g^{-1} and 76.13 %; 203.72 mg g^{-1} and 86.86 %; and 209.66 mg g^{-1} and 89.35 % for low CSPVA, medium CSPVA and high CSPVA, respectively (Fig. 4.2a and 4.2d). Similarly, for Fe, maximum adsorption capacities and removal % were 49.0 mg g^{-1} and 63.39 %; 55.13 mg g^{-1} and 71.30 %; and 57.03 mg g^{-1} and 73.77 % for low CSPVA, medium CSPVA and high CSPVA, respectively (Fig. 4.2b and 4.2e). Also, for Pb, maximum adsorption capacities and removal % were 5.11 mg g^{-1} and 78.65 %; 5.41 mg g^{-1} and 83.17 %; and 5.50 mg g^{-1} and 84.55 % for low CSPVA, medium CSPVA and high CSPVA, respectively (Fig. 4.2c and 4.2f). Fig. 4.3 depicts the influence of adsorbent dosage on the removal of heavy metal ions from the zinc-dominant simulated industrial wastewater. Thereby, based on optimal adsorption capacity and % removal, the optimum adsorbent dosage of low CSPVA, medium CSPVA, and high CSPVA was 1.4 g L^{-1} for all metal ions i.e., Zn, Fe, and Pb. Thereby, for Zn, at the optimal dosage, maximum adsorption capacities and removal % were 139.01 mg g^{-1} and 49.92 %; 146.13 mg g^{-1} and 52.49 %; and 164.21 mg g^{-1} and 58.98 % for low CSPVA, medium CSPVA and high CSPVA, respectively (Fig. 4.3a and 4.3d). Similarly, for Fe, maximum adsorption capacities and removal % were 97.21 mg g^{-1} and 64.93 %; 102.47 mg g^{-1} and 68.44 %; and 106.28 mg g^{-1} and 70.99 % for low CSPVA, medium CSPVA and high CSPVA, respectively (Fig. 4.3b and 4.3e). Also, for Pb, maximum adsorption capacities and removal % were 2.69 mg g^{-1} and 71.00 %; 2.83 mg g^{-1} and 74.84 %; and 3.04 mg g^{-1} and 80.44 % for low CSPVA, medium CSPVA and high CSPVA, respectively (Fig. 4.3c and 4.3f). Based on these findings, the inferred optimal adsorbent dosage has been in good agreement with the value reported in the relevant prior art for the CSPVA derivative (Kumar et al., 2009; Li et al., 2012, 2011). Fig. 4.3 depicts the influence of adsorbent dosage on the removal of heavy metal ions from the zinc-dominant

simulated industrial wastewater. Initially, the removal % of Pb increases gradually with an increase in the adsorbent dosage from 0.2-1.4 g L^{-1} and after 1.4 g L^{-1} adsorbent dosage value, the alteration in removal % was not promising. Also, the high CSPVA resin possesses a greater constitution of relevant functional groups for heavy metal adsorption in comparison with the medium CSPVA resin. Accordingly, higher Pb removal has been achieved for the high CSPVA resin in comparison to the medium CSPVA resin. Such a hypothesis has been confirmed by the FTIR spectra of the raw samples of medium and high CSPVA resins (Fig. 4.14).

The next set of experiments were performed at specified combinations of adsorbent dosage (1.6 g L^{-1}), fixed solution initial pH (3.82) and initial concentration (Cu 375.5 mg L^{-1}, Fe 123.7 mg L^{-1}, and Pb 10.4 mg L^{-1} for Cu dominant solution and Zn 389.8 mg L^{-1}, Fe 209.6 mg L^{-1}, and Pb 5.3 mg L^{-1}) and altered contact period value range (5-720) min. Fig. 4.4 depicts the influence of the contact period on the removal of heavy metal ions from the copper-dominant simulated industrial wastewater. Thereby, based on optimal adsorption capacity and % removal, the optimum contact period has been inferred to be 360 min for both low CSPVA and medium CSPVA and 240 min for high CSPVA and for Cu, Fe, and Pb. For the Cu, rapid adsorption occurred on the adsorbent surface during the initial 120 min for low CSPVA and medium CSPVA and during 30 min for the high CSPVA adsorbent. During this phase, the adsorption capacity and % removal altered rapidly in the range of 96.25-137.825 mg g^{-1} and 41.02-58.74 %, respectively for low CSPVA case, 116.82-192.84 mg g^{-1} and 49.8-82.19 %, respectively for medium CSPVA case and 131.96-189.07 mg g^{-1} and 56.25-80.60 %, respectively for high CSPVA case. After this rapid phase, the adsorption process became slower and reached equilibrium after 360 min for low CSPVA and medium CSPVA derivatives, and 240 min for high CSPVA derivative. At equilibrium, the maximum adsorption capacity and % removal were 177.64 mg g^{-1} and 75.71 %; 204.37 mg g^{-1} and 87.10 %; and 208.30 mg g^{-1} and 88.78 % for low CSPVA, medium CSPVA, and high CSPVA

derivatives, respectively (Fig. 4.4a and 4.4d). Similarly for the Fe, rapid adsorption occurred on the adsorbent surface during the initial 60 min for low CSPVA and 30 min for medium CSPVA and high CSPVA adsorbent. During this phase, adsorption capacity and % removal altered rapidly in the range of 19.7-30.58 mg g^{-1} and 25.5-39.56 %, respectively for low CSPVA case, 18.78-47.9 mg g^{-1} and 24.3-62.01 %, respectively for medium CSPVA case and 25.9-51.56 mg g^{-1} and 33.6-66.70 %, respectively for high CSPVA case. After this rapid phase, the adsorption process became slower and reached equilibrium after 360 min for low CSPVA and medium CSPVA derivatives, and 240 min for high CSPVA derivative. At equilibrium, the maximum adsorption capacity and % removal were 49.69 mg g^{-1} and 64.28 %; 53.49 mg g^{-1} and 69.20 %; and 55.93 mg g^{-1} and 72.34 % for low CSPVA, medium CSPVA and high CSPVA derivatives, respectively (Fig. 4.4b and 4.4e). Also for the Pb, rapid adsorption occurred on the adsorbent surface during the initial 60 min for low CSPVA, during 120 min for medium CSPVA, and during 30 min for the high CSPVA adsorbent. During this phase, the adsorption capacity and % removal altered rapidly in the range of 1.94-3.2 mg g^{-1} and 29.9-49.23 %, respectively for low CSPVA cases; 2.47-4.83 mg g^{-1} and 37.98-74.32 %, respectively for medium CSPVA case and 2.86-4.32 mg g^{-1} and 44.13-66.44 %, respectively for high CSPVA case. After this rapid phase, the adsorption process became slower and reached equilibrium after 360 min for low CSPVA and medium CSPVA derivatives, and 240 min for high CSPVA derivative. At equilibrium, the maximum adsorption capacity and % removal were 5.06 mg g^{-1} and 77.80 %; 5.38 mg g^{-1} and 82.80 %; and 5.53 mg g^{-1} and 85.09 % for low CSPVA, medium CSPVA and high CSPVA derivatives, respectively (Fig. 4.4c and 4.4f). Fig. 4.5 depicts the influence of the contact period on the removal of heavy metal ions from the zinc-dominant simulated industrial wastewater. Thereby, based on optimal adsorption capacity and % removal, the optimum contact period has been inferred to be 480 min for low CSPVA and 360 min for medium CSPVA and high CSPVA and for Zn, Fe, and Pb. For the Zn, rapid adsorption

occurred on the adsorbent surface during the initial 180 min for low CSPVA and medium CSPVA and during 120 min for the high CSPVA adsorbent. During this phase, the adsorption capacity and % removal altered rapidly in the range of 40.58-111.65 mg g^{-1} and 14.57-40.10 %, respectively for low CSPVA case, 56.15-119.57 mg g^{-1} and 20.17-42.94 %, respectively for medium CSPVA case and 56.99-135.07 mg g^{-1} and 20.47-48.51 %, respectively for high CSPVA case. After this rapid phase, the adsorption process became slower and reached equilibrium after 480 min for low CSPVA, and 360 min for medium CSPVA and high CSPVA derivatives. At equilibrium, the maximum adsorption capacity and % removal were 139.43 mg g^{-1} and 50.08 %, 144.54 mg g^{-1} and 51.92 %, and 159.08 mg g^{-1} and 57.13 % for low CSPVA, medium CSPVA and high CSPVA derivatives, respectively (Fig. 4.5a and 4.5d). Similarly for the Fe, rapid adsorption occurred on the adsorbent surface during the initial 120 min for low CSPVA, medium CSPVA, and high CSPVA adsorbent. During this phase, adsorption capacity and % removal altered rapidly in the range of 29.31-72.27 mg g^{-1} and 19.58-48.27 %, respectively for low CSPVA case; 30.45-80.02 mg g^{-1} and 20.34-53.45 %, respectively for medium CSPVA case and 28.08-78.22 mg g^{-1} and 18.75-52.25 %, respectively for high CSPVA case. After this rapid phase, the adsorption process became slower and reached equilibrium after 480 min for low CSPVA, and 360 min for medium CSPVA and high CSPVA derivatives. At equilibrium, the maximum adsorption capacity and % removal were 96.80 mg g^{-1} and 64.65 %; 104.28 mg g^{-1} and 69.65 %; and 107.36 mg g^{-1} and 71.71 % for low CSPVA, medium CSPVA and high CSPVA derivatives, respectively (Fig. 4.5b and 4.5e). Also for the Pb, rapid adsorption occurred on the adsorbent surface during the initial 180 min for low CSPVA, medium CSPVA, and high CSPVA adsorbents. During this phase, the adsorption capacity and % removal altered rapidly in the range of 0.34-1.64 mg g^{-1} and 9.02-43.24 %, respectively for low CSPVA cases; 0.51-2.05 mg g^{-1} and 13.46-54.34 %, respectively for medium CSPVA case and 0.32-2.18 mg g^{-1} and 8.48-57.60 %, respectively for high CSPVA case.

After this rapid phase, the adsorption process became slower and reached equilibrium after 480 min for low CSPVA and medium CSPVA derivatives, and 360 min for high CSPVA derivatives. At equilibrium, the maximum adsorption capacity and % removal were 2.70 mg g^{-1} and 71.28 %; 2.82 mg g^{-1} and 74.60 %; and 3.02 mg g^{-1} and 79.70 % for low CSPVA, medium CSPVA, and high CSPVA derivatives, respectively (Fig. 4.5c and 4.5f). The obtained contact period in this work has been better in corroboration to the reported findings for the CSPVA derivative (Fato et al., 2019; Trikkaliotis et al., 2020).

Eventually, batch experiments were performed at specified combinations of adsorbent dosage (1.6 g L^{-1}), fixed solution initial pH (3.82) and contact period (360 min for low CSPVA and medium CSPVA, and 240 min for high CSPVA) and for altered initial concentrations of 187.7-563.1 mg L^{-1} for Cu, 61.85-185.55 mg L^{-1} for Fe, and 5.2-15.6 mg L^{-1} for Pb. Fig. 4.6 depicts the influence of initial concentration on the removal of heavy metal ions for the copper-dominant simulated industrial wastewater. For the Cu, CSPVA derivative variants exhibit enhanced adsorption capacity and % removal at the highest concentration and altered as 101.28-192.36 mg g^{-1} and 86.33-54.66 %; 110.6-226.25 mg g^{-1} and 94.3-64.31 %; and 111.47-230.91 mg g^{-1} and 95.01-65.61 % for low CSPVA, medium CSPVA and high CSPVA derivatives, respectively (Fig. 4.6a and 4.6d). Similarly for the Fe, CSPVA derivative variants exhibit enhanced adsorption capacity and % removal at the highest concentration and altered as 30.31-55.72 mg g^{-1} and 78.40-48.04 %; 31.56-65.02 mg g^{-1} and 81.63-56.07 %; and 32.14-71.48 mg g^{-1} and 83.14-61.64 % for low CSPVA, medium CSPVA and high CSPVA derivatives, respectively (Fig. 4.6b and 4.6e). Also for the Pb, CSPVA derivative variants exhibit enhanced adsorption capacity and % removal at the highest concentration and altered as 2.84-5.66 mg g^{-1} and 87.44-58.01 %; 3.0-5.9 mg g^{-1} and 92.11-60.32 %; and 3.02-6.27 mg g^{-1} and 92.88-64.27 % for low CSPVA, medium CSPVA and high CSPVA derivatives, respectively (Fig. 4.6c and 4.6f). Eventually batch experiments were

performed at specified combinations of adsorbent dosage (1.4 g L^{-1}), fixed solution initial pH (3.64) and contact period (480 min for low CSPVA and medium CSPVA, and 360 min for high CSPVA) and for altered initial concentrations of 194.9-584.7 mg L^{-1} for Zn, 104.8-314.4 mg L^{-1} for Fe, and 2.65-7.95 mg L^{-1} for Pb.

Fig. 4.7 depicts the influence of initial concentration on the removal of heavy metal ions for the zinc-dominant simulated industrial wastewater. For the Zn, CSPVA derivative variants exhibit enhanced adsorption capacity and % removal at the highest concentration and altered as 107.49-173.70 mg g^{-1} and 77.21-41.59 %; 110.12-179.76 mg g^{-1} and 79.10-43.04 %; and 115.88-203.20 mg g^{-1} and 83.24-48.65 % for low CSPVA, medium CSPVA and high CSPVA derivatives, respectively (Fig. 4.7a and 4.7d). Similarly for the Fe, CSPVA derivative variants exhibit enhanced adsorption capacity and % removal at the highest concentration and altered as 63.55-112.94 mg g^{-1} and 84.90-50.29 %; 65.86-121.29 mg g^{-1} and 87.98-54.01 %; and 66.74-126.37 mg g^{-1} and 89.15-56.27 % for low CSPVA, medium CSPVA and high CSPVA derivatives, respectively (Fig. 4.7b and 4.7e). Also for the Pb, CSPVA derivative variants exhibit enhanced adsorption capacity and % removal at the highest concentration and altered as 1.68-3.25 mg g^{-1} and 88.68-57.27 %; 1.74-3.42 mg g^{-1} and 91.95-60.25 %; and 1.78-3.42 mg g^{-1} and 94.21-60.29 % for low CSPVA, medium CSPVA and high CSPVA derivatives, respectively (Fig. 4.7c and 4.7f).

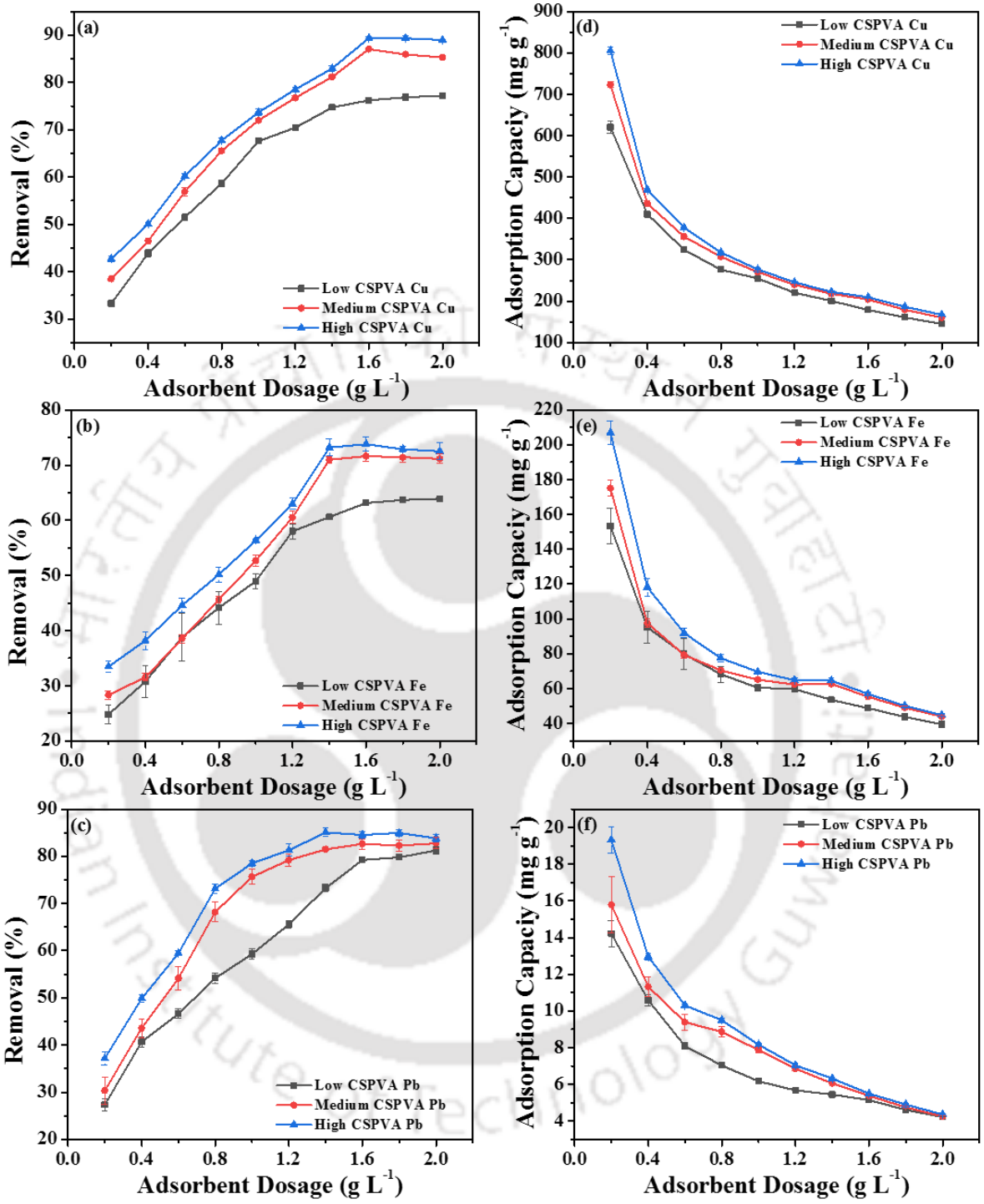

Fig. 4.2. Graphs depicting the influence of adsorbent dosage on adsorption characteristics of CSPVA derivatives and Cu dominant adsorbate system.

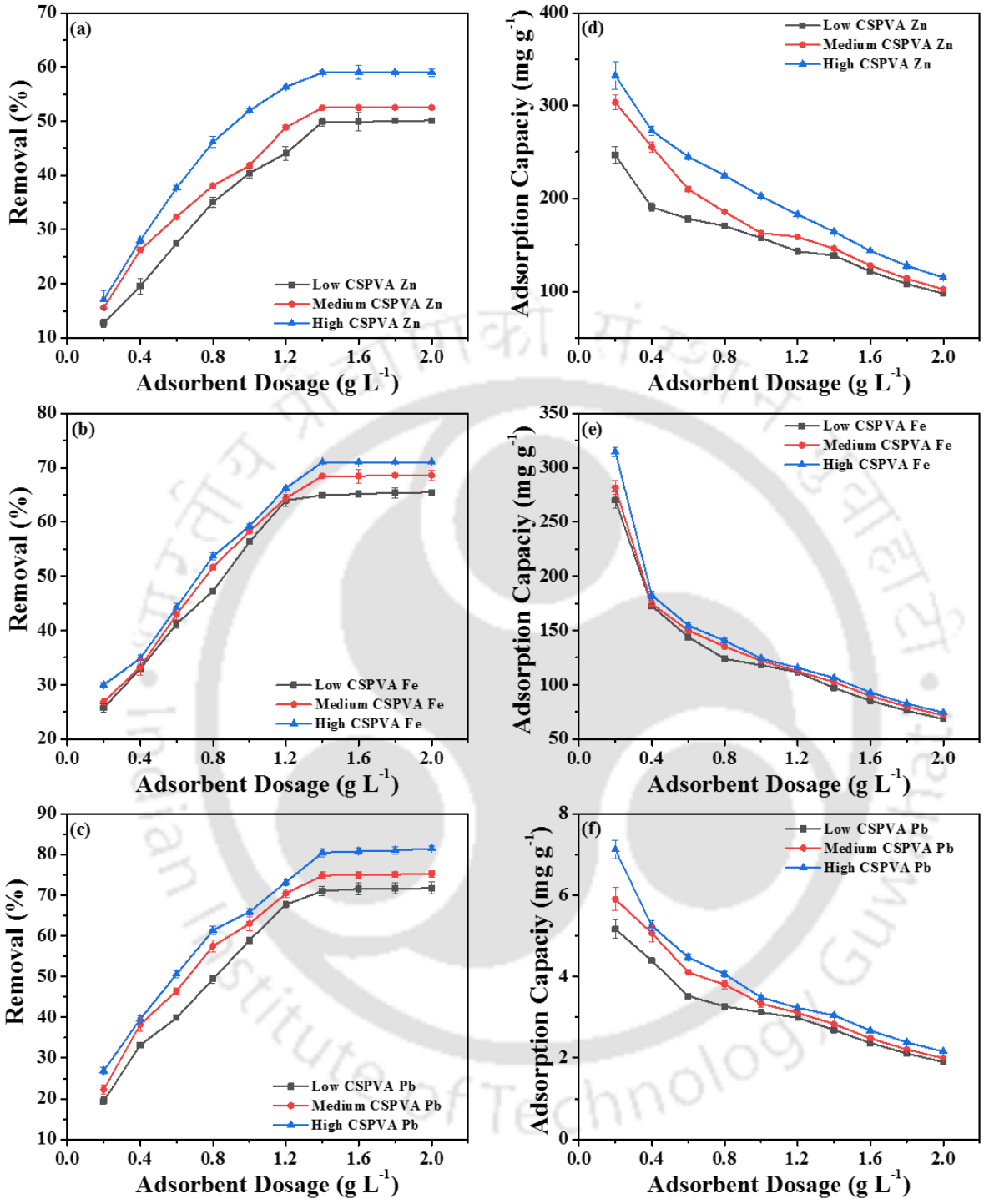

Fig. 4.3. Graphs depicting the influence of adsorbent dosage on adsorption characteristics of CSPVA derivatives and Zn dominant adsorbate system.

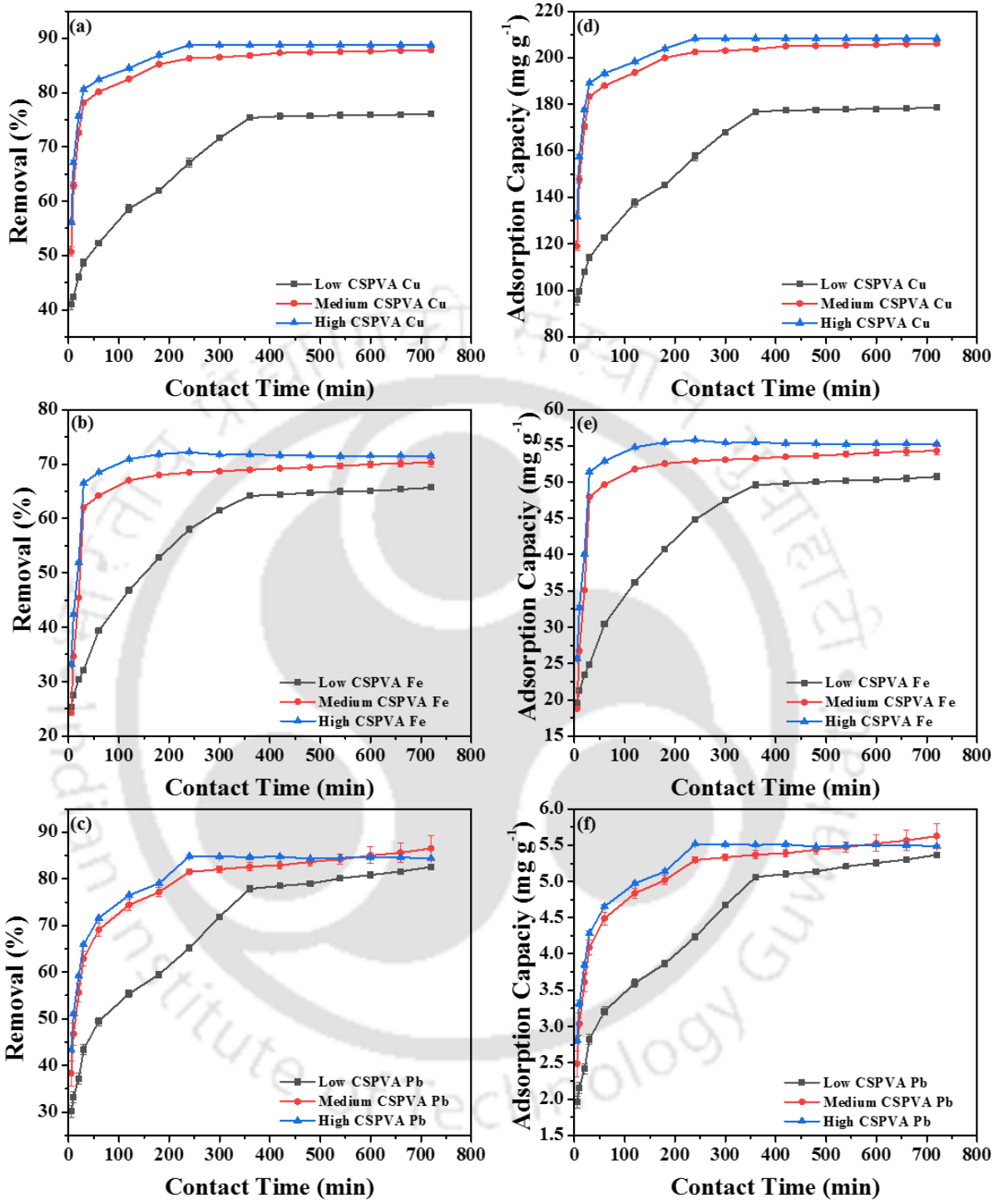

Fig. 4.4. Graphs depicting the influence of contact time on adsorption characteristics of CSPVA derivatives and Cu dominant adsorbate system.

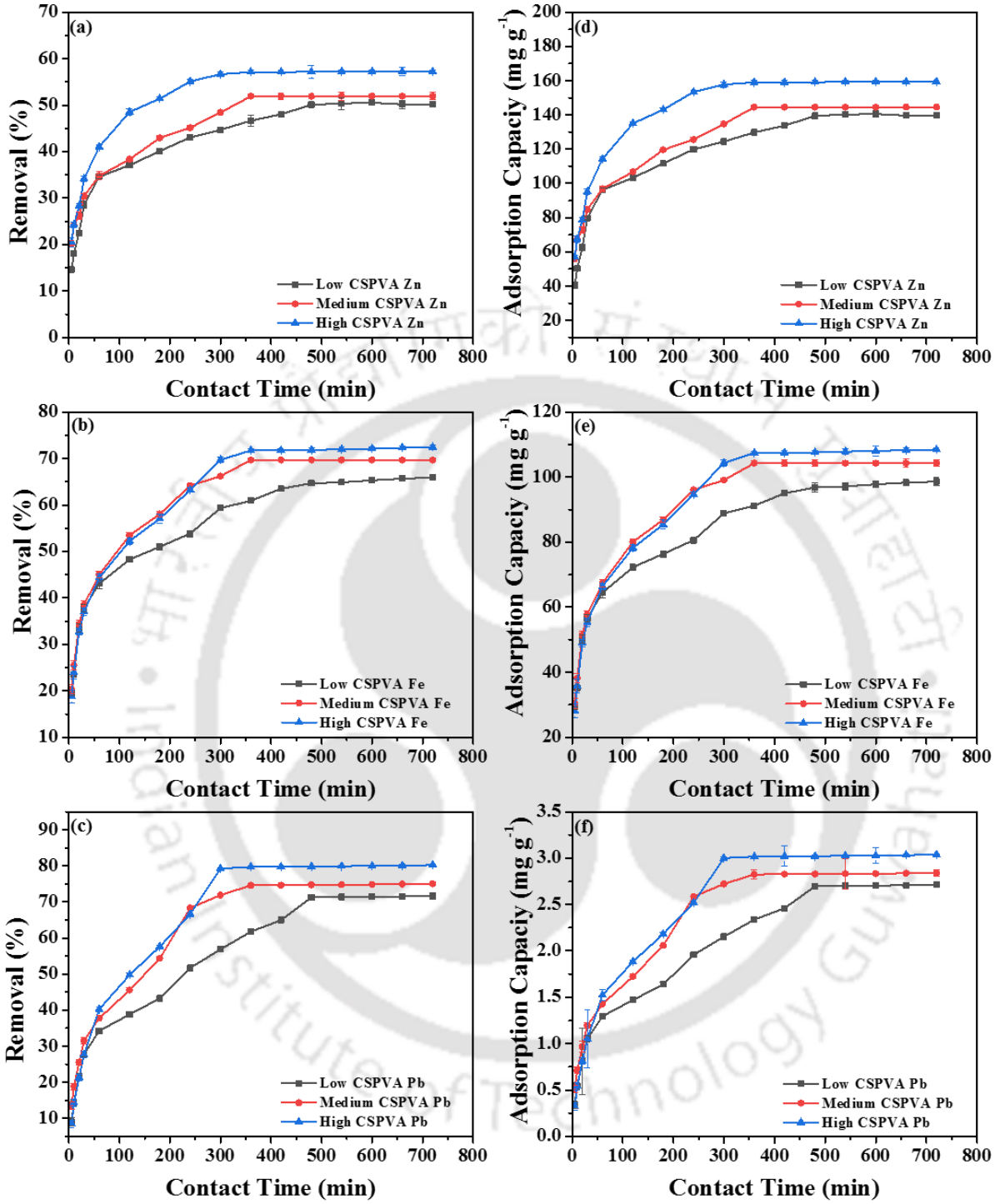

Fig. 4.5. Graphs depicting the influence of contact time on adsorption characteristics of CSPVA derivatives and Zn dominant adsorbate system.

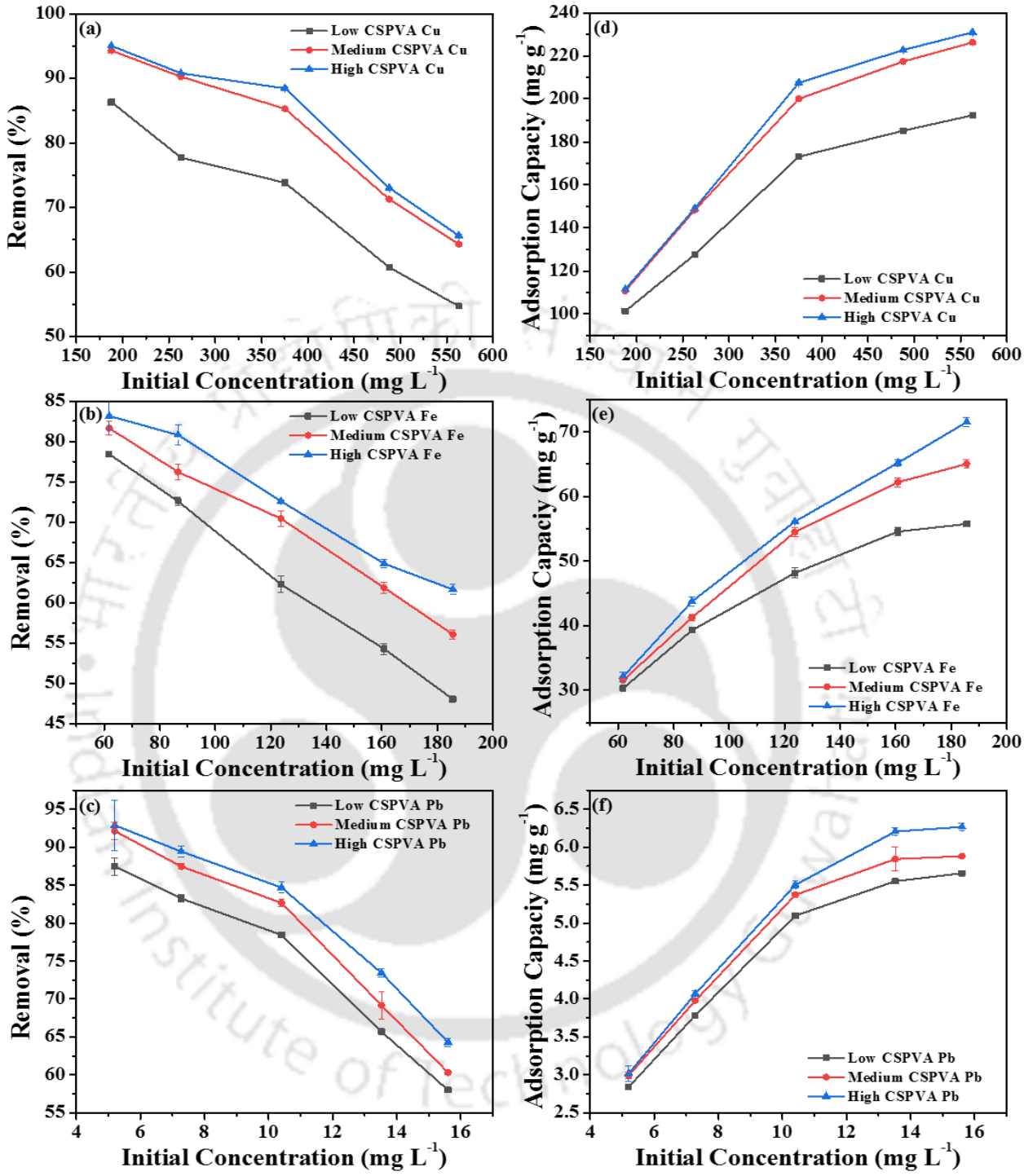

Fig. 4.6. Graphs depicting the influence of metal ion concentration on adsorption characteristics of CSPVA derivatives and Cu dominant adsorbate system.

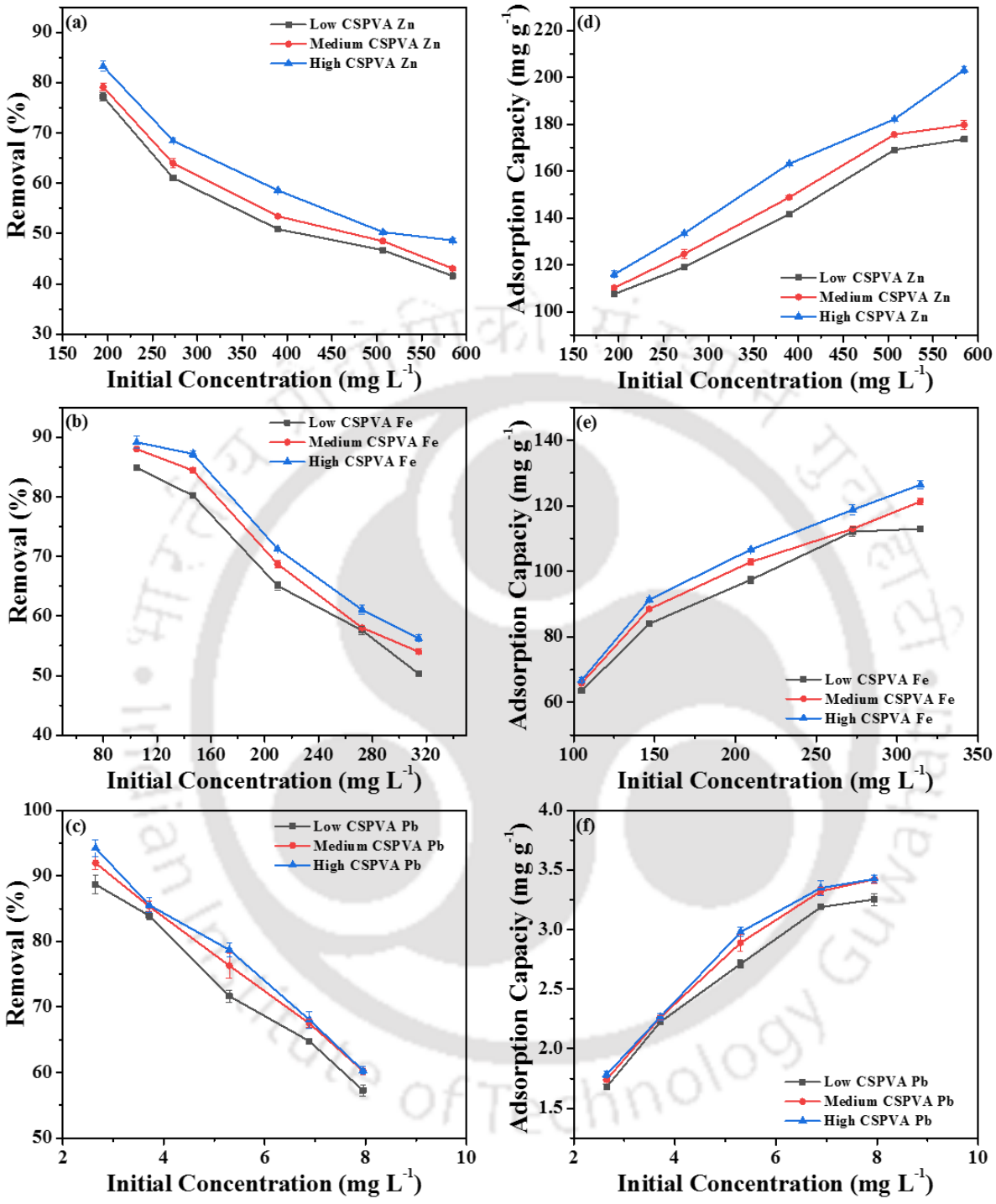

Fig. 4.7. Graphs depicting the influence of metal ion concentration on adsorption characteristics of CSPVA derivatives and Zn dominant adsorbate system.

4.3.2 Fitness of alternate Equilibrium and Kinetic models

Fig. 4.8 and Fig. 4.10 illustrate the fitness plots of alternate equilibrium models namely Langmuir (Fig. 4.8a-4.8c and Fig. 4.10a-4.10c) and Freundlich isotherm (Fig. 4.8d-4.8f and Fig. 4.10d-4.10f) for Cu and Zn dominant solutions, respectively. The figures affirm the fitness of the Langmuir isotherm model to represent measured Cu, Pb, Zn, and Fe adsorption data for the CSPVA derivative variants. The R_L value reported in Table 4.1 is in the range of 0-1 and thereby affirmed that the CSPVA adsorbents are favorable for Cu, Pb, Zn, and Fe adsorption from Cu and Zn dominant simulated industrial wastewater solutions. Equilibrium model parameters for Cu, Pb, Zn, and Fe adsorption have been summarized in Table 4.1 and Table 4.3. Fig. 4.9 and Fig. 4.11 depict the fitness plots for alternate kinetic models to represent the evaluated Cu, Pb, and Fe adsorption kinetics data of the CSPVA derivative variants. Among all models, only the pseudo-second-order model provided very good fitness (R^2 = 0.99 for low CSPVA, medium CSPVA, and high CSPVA, respectively). Further, Table 4.2 and Table 4.4 summarized that the best results have been obtained for the high CSPVA derivative. Thereby, the evaluated pseudo-second-order model-based adsorption capacity (208.35 mg g^{-1} for Cu, 55.87 mg g^{-1} for Fe and 5.59 mg g^{-1} for Pb from Cu dominant and 208.35 mg g^{-1} for Zn, 55.87 mg g^{-1} for Fe and 5.59 mg g^{-1} for Pb from Zn dominant solutions) has been in agreement with the experimentally determined adsorption capacity (159.08 mg g^{-1} for Cu, 107.36 mg g^{-1} for Fe and 3.02 mg g^{-1} for Pb for Cu dominant and 163.93 mg g^{-1} for Zn, 113.64 mg g^{-1} for Fe and 3.37 mg g^{-1} for Pb from Zn dominant solution). Similar fitness trends have been reported for the relevant data reported by the research groups for the CSPVA derivative (Karim et al., 2019; Trikkaliotis et al., 2020).

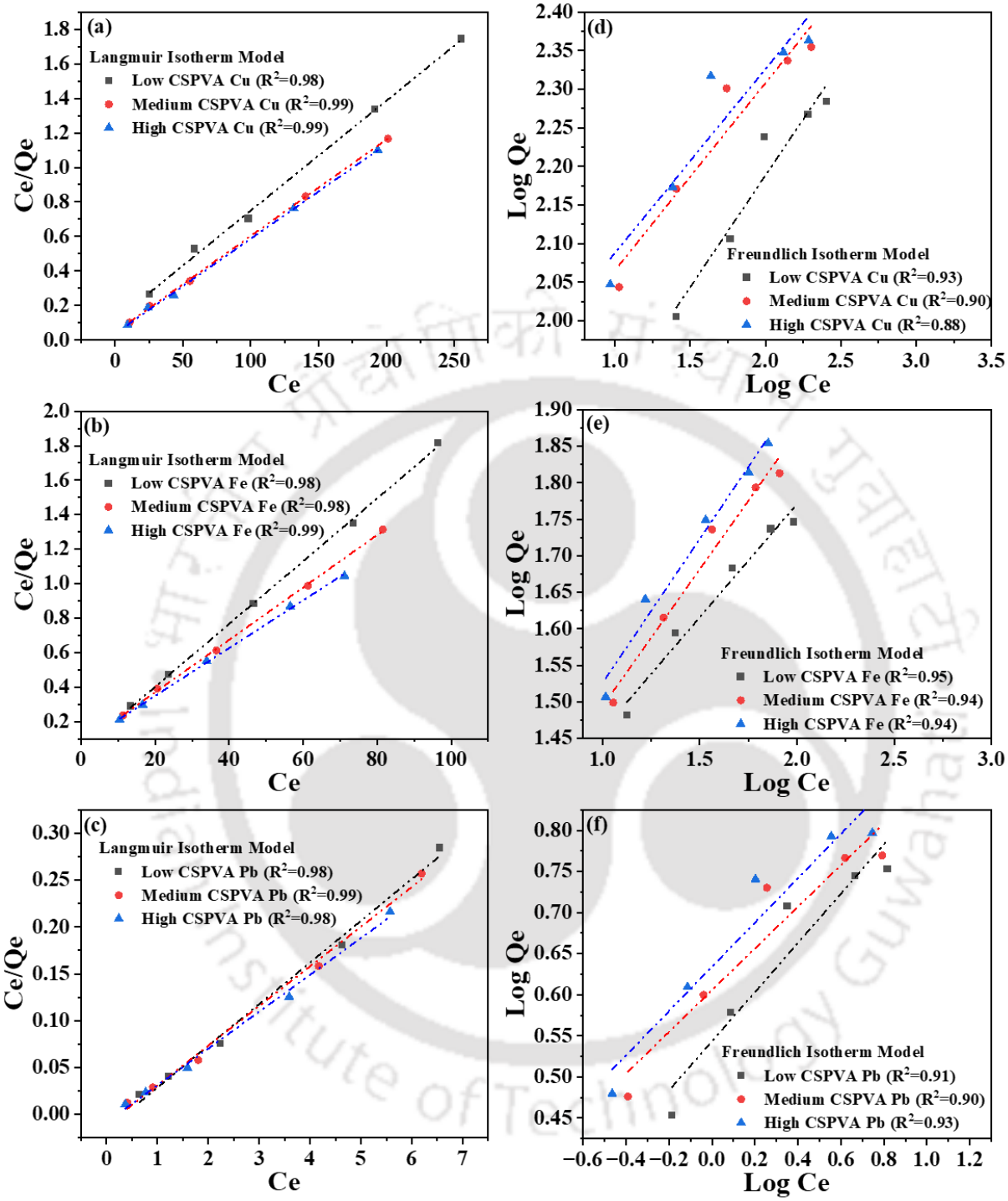

Fig. 4.8. Equilibrium models fitness plots (a-c: Langmuir isotherm model and d-f: Freundlich isotherm model) for CSPVA derivatives and Cu dominant adsorbate system.

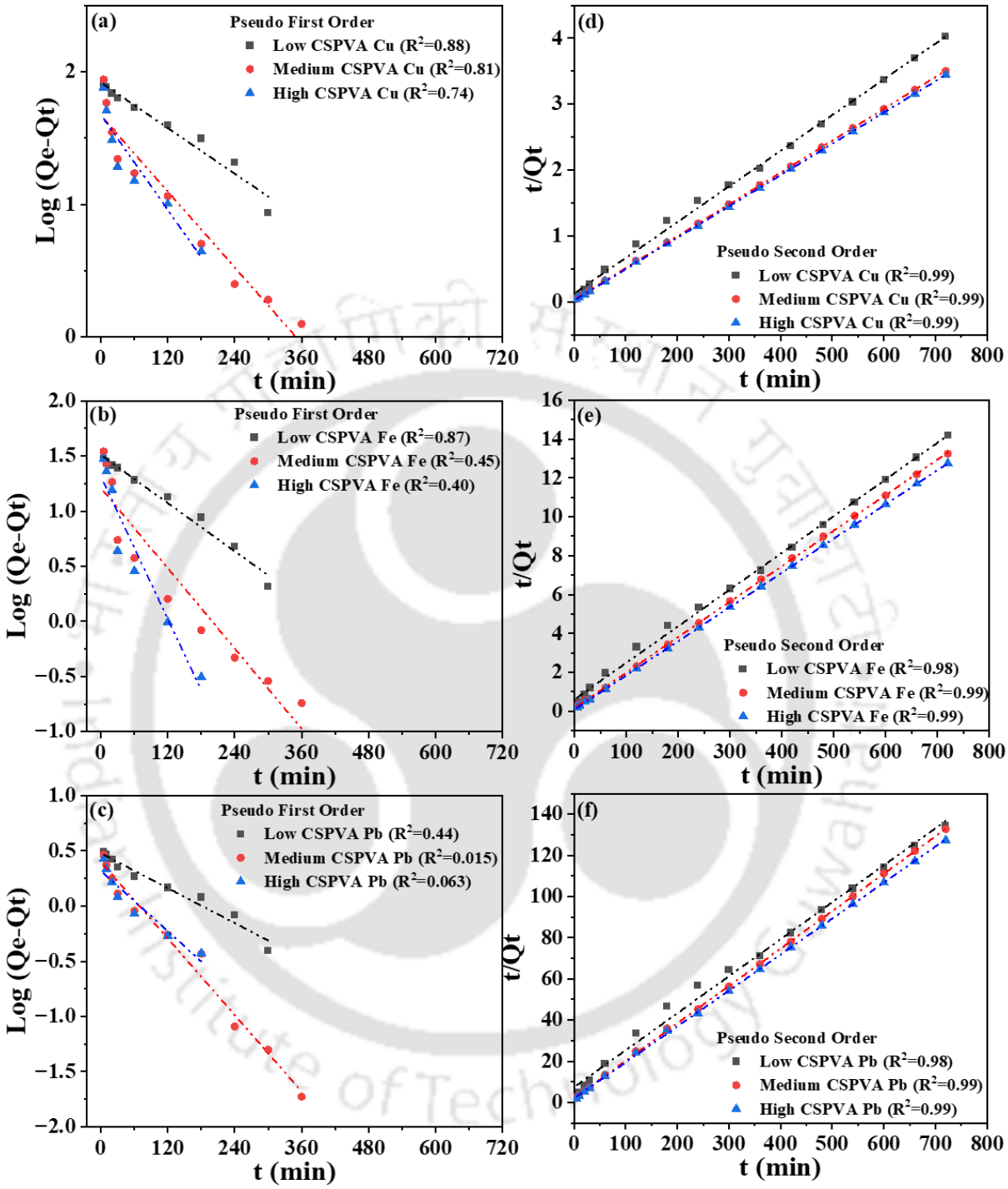

Fig. 4.9. Kinetic models fitness plots (a-c: Pseudo-first-order kinetic model, and d-f: Pseudo-second-order kinetic model) for CSPVA derivatives and Cu dominant adsorbate system.

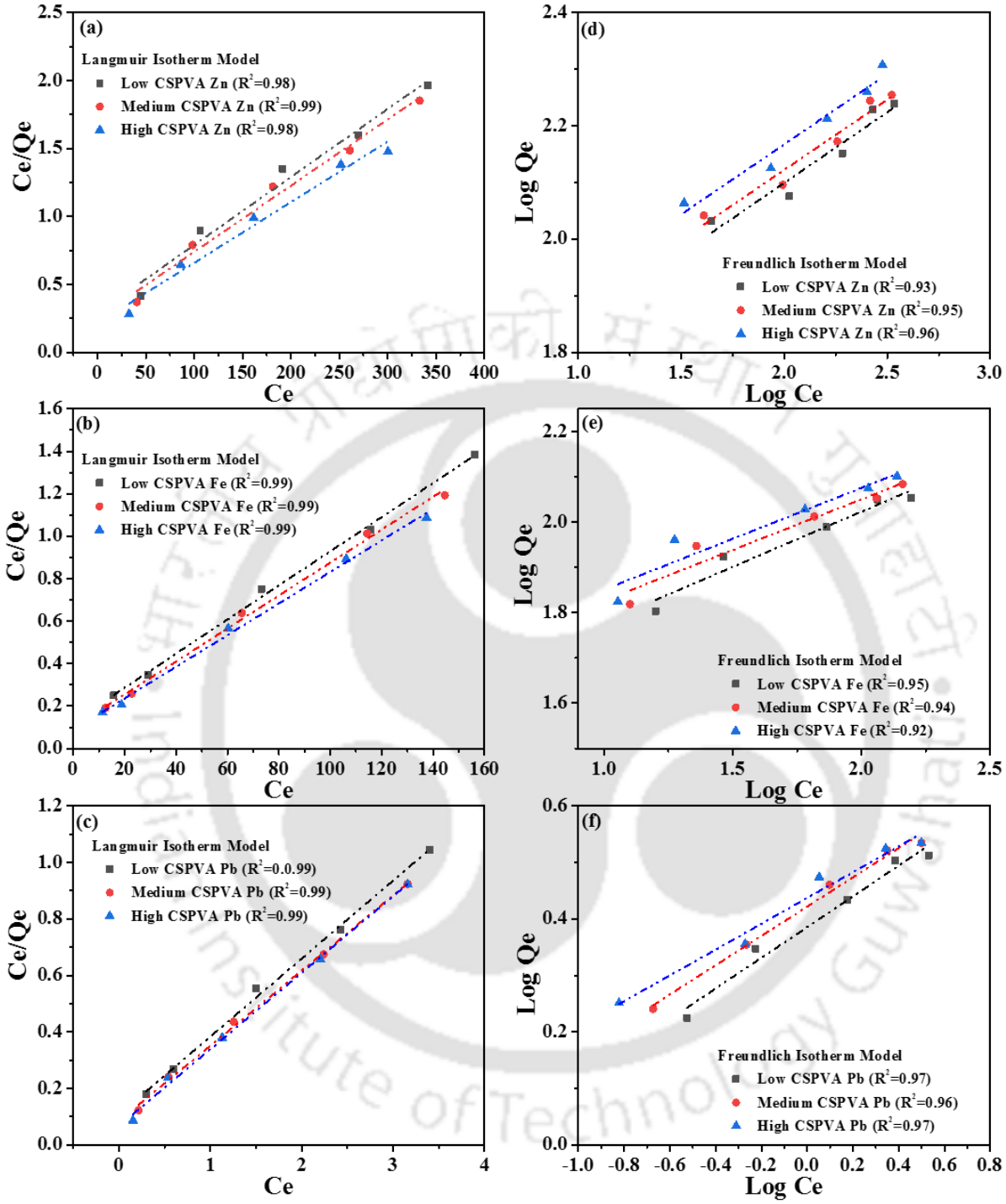

Fig. 4.10. Equilibrium models fitness plots (a-c: Langmuir isotherm model and d-f: Freundlich isotherm model) for CSPVA derivatives and Zn dominant adsorbate system.

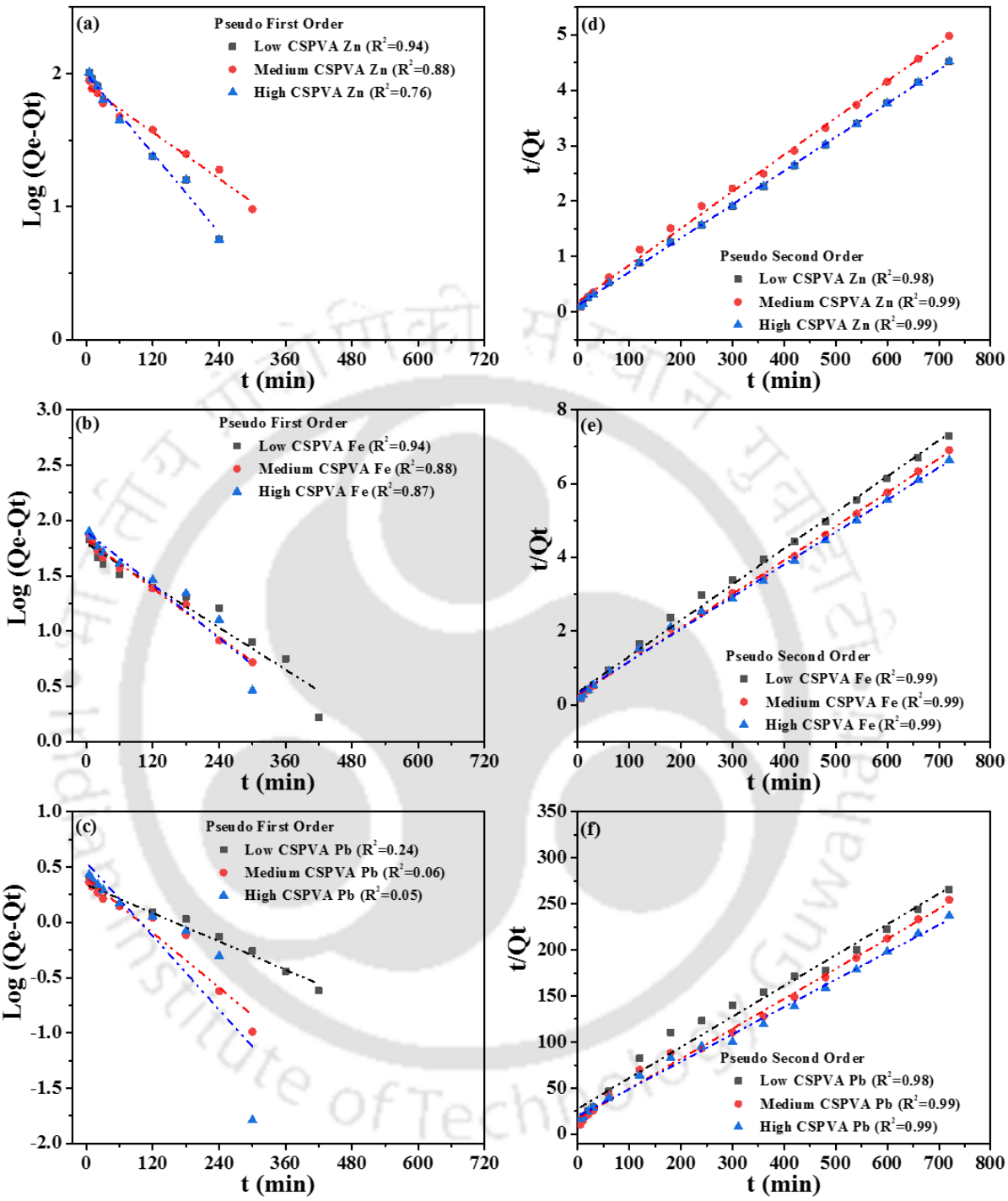

Fig. 4.11. Kinetic models fitness plots (a-c: Pseudo-first-order kinetic model, and d-f: Pseudo-second-order kinetic model) for CSPVA derivatives and Zn dominant adsorbate system.

Table 4.1: Regressed model parameters representing heavy metal adsorption equilibrium data of CSPVA derivatives and Cu dominant adsorbate system.

PVA/Chiosan derivatives	Langmuir parameters				Freundlich parameters		
	Q_o (mg g^{-1})	b (L mg^{-1})	R^2	R_L	K_f	n	R^2
Cu							
Low CSPVA	217.39	0.03	0.98	0.05-0.15	43.74	3.68	0.93
Med CSPVA	238.09	0.07	0.99	0.02-0.07	66.31	4.11	0.90
High CSPVA	243.90	0.085	0.99	0.02-0.05	70.58	4.19	0.88
Fe							
Low CSPVA	64.94	0.06	0.98	0.07-0.20	14.14	3.22	0.95
Med CSPVA	79.37	0.06	0.98	0.09-0.20	13.14	2.67	0.94
High CSPVA	87.72	0.05	0.99	0.08-0.23	13.54	2.54	0.94
Pb							
Low CSPVA	6.37	1.35	0.98	0.004-0.012	3.50	3.34	0.91
Med CSPVA	6.36	2.25	0.99	0.004-0.007	4.03	3.94	0.90
High CSPVA	6.85	2.20	0.98	0.002-0.008	4.30	3.71	0.93

Table 4.2: Regressed model parameters representing heavy metal adsorption kinetic data of CSPVA derivatives and Cu dominant adsorbate system.

Experimental capacity (Q_{exp}, mg g^{-1})	CSPVA derivatives	Pseudo-first-order model			Pseudo-second-order model		
		Q_e (mg g^{-1})	K_1 (min^{-1})	R^2	Q_e (mg g^{-1})	K_2 (g mg^{-1} min^{-1})	R^2
Cu							
177.64	Low CSPVA	73.62	0.007	0.88	178.57	0.00026	0.99
203.11	Med CSPVA	26.39	0.0078	0.81	205.33	0.00098	0.99
208.30	High CSPVA	21.39	0.016	0.74	208.35	0.0013	0.99
Fe							
49.70	Low CSPVA	22.23	0.0055	0.87	52.91	0.00059	0.98
53.24	Med CSPVA	5.17	0.0046	0.45	55.86	0.0051	0.99
55.93	High CSPVA	5.74	0.005	0.40	55.87	0.005	0.99
Pb							
5.06	Low CSPVA	1.98	0.0014	0.44	5.56	0.0044	0.98
5.36	Med CSPVA	1.24	0.0076	0.015	5.58	0.021	0.99
5.53	High CSPVA	1.23	0.0074	0.063	5.59	0.022	0.99

Table 4.3: Regressed model parameters representing heavy metal adsorption equilibrium data of CSPVA derivatives and Zn dominant adsorbate system.

PVA/Chiosan derivatives	Langmuir parameters				Freundlich parameters		
	Q_o (mg g^{-1})	b (L mg^{-1})	R^2	R_L	K_f	n	R^2
Zn							
Low CSPVA	200.01	0.01	0.98	0.09-0.23	39.81	4.01	0.93
Med CSPVA	204.08	0.01	0.99	0.08-0.21	42.41	4.04	0.95
High CSPVA	222.21	0.02	0.98	0.07-0.19	46.96	4.03	0.96
Fe							
Low CSPVA	125.01	0.06	0.99	0.05-0.13	34.32	4.1	0.95
Med CSPVA	128.21	0.07	0.99	0.04-0.11	40.06	4.47	0.94
High CSPVA	135.14	0.08	0.99	0.04-0.10	42.26	4.44	0.92
Pb							
Low CSPVA	3.62	2.58	0.99	0.05-0.07	2.43	3.68	0.97
Med CSPVA	3.72	3.16	0.99	0.04-0.05	2.64	3.86	0.91
High CSPVA	4.02	3.69	0.99	0.03-0.05	2.73	4.38	0.97

Table 4.4: Regressed model parameters representing heavy metal adsorption kinetic data of CSPVA derivatives and Zn dominant adsorbate system.

Experimental capacity (Q_{exp}, mg g^{-1})	CSPVA derivatives	Pseudo-first-order model			Pseudo-second-order model		
		Q_e (mg g^{-1})	K_1 (min^{-1})	R^2	Q_e (mg g^{-1})	K_2 (g mg^{-1} min^{-1})	R^2
Zn							
139.43	Low CSPVA	87.41	0.0071	0.94	144.93	0.00021	0.99
144.54	Med CSPVA	70.99	0.0073	0.88	147.06	0.00025	0.99
159.08	High CSPVA	50.55	0.0074	0.76	163.94	0.00032	0.99
Fe							
96.79	Low CSPVA	54.59	0.0067	0.94	102.04	0.00028	0.99
104.28	Med CSPVA	49.44	0.0069	0.88	108.69	0.00033	0.99
107.36	High CSPVA	55.31	0.0071	0.87	113.64	0.00026	0.99
Pb							
2.70	Low CSPVA	1.43	0.0011	0.24	2.99	0.0040	0.98
2.82	Med CSPVA	1.20	0.00069	0.06	3.07	0.0063	0.99
3.02	High CSPVA	1.29	0.0009	0.05	3.37	0.0045	0.99

Isotherm models have been targeted to analyze the adsorption of studied heavy metal ions onto the surface of PVA-chitosan derivative (low CSPVA, medium CSPVA, high CSPVA) and at a constant temperature. Langmuir Isotherm model has been the best-fit isotherm model. It is based on the assumption that adsorption occurs at specific sites on the adsorbent surface, and once a site is occupied by an adsorbate molecule, no further adsorption can take place at that site. Also, the pseudo-second-order model has been inferred to be the best-fit model to represent the kinetics of studied heavy metal ions adsorption from Cu and Zn dominant adsorbate systems and onto PVA-chitosan derivative (low CSPVA, medium CSPVA, high CSPVA). Thus, the model's basic assumption stated as follows is valid. The rate-limiting step could be the chemisorption involving valency forces through the sharing or exchange of electrons with the prevalent functional groups of the PVA-chitosan derivative resin. The fitness of the pseudo-second-order model is also justified with the FTIR analysis of the metal-adsorbed PVA-chitosan derivative that inferred strong metal ions chemical interaction with the prevalent functional groups of the PVA-chitosan derivative resin.

4.4 Analytical Characterization

4.4.1 BET Surface Area Analysis

For the raw high molecular weight chitosan, the BET surface area and total pore volume are 0.05 $m^2\ g^{-1}$ and 4 $\times 10^4$ cc g^{-1}, respectively. For the high CSPVA, the BET surface area and total pore volume are 1.96 $m^2\ g^{-1}$ and 1.13 $\times 10^2$ cc g^{-1}, respectively. Thus, chitosan structural modification with the PVA is apparent in the pertinent alterations and increment in the surface area of the high CSPVA.

4.4.2 Thermo gravimetric Analysis

Fig. 4.12 presents the thermo-gravimetric assessment patterns for the higher molecular weight chitosan and high CSPVA derivative. Two distinct phases of weight reduction can be seen for the high molecular weight chitosan (Nagireddi et al., 2019). However, three distinct phases of weight reduction can be seen for the high CSPVA derivative. The initial phase of the weight loss for both high molecular weight chitosan and high CSPVA derivative has been due to the elimination of physically adsorbed and partially hydrogen-bound water. This amounts to a significant 11 % for high CSPVA at 226 °C and 12.0 % for high molecular weight chitosan at 130 °C. The following phase could have entailed the dewatering of saccharide rings, depolymerization, and breakdown of deacetylated and acetylated chitosan. These would have occurred due to the disintegration of the high molecular weight chitosan. At 700 °C, 51.0 % of the mass has been lost in the second stage for high molecular weight chitosan. For the high CSPVA derivative, the second stage of mass loss (40%) starts at about 220 °C and relates to the breakdown of the side chain of polyvinyl alcohol. Further breakdown of polyene remnants occurs in the final and concluding phase that occurred from 400 °C. Such a phase eventually involves the formation of carbon and hydrocarbons. For the high CSPVA derivative, the phase mass loss is 11 %. A comparative evaluation of the TGA plots of high molecular weight chitosan and high CSPVA conveys that the high CSPVA derivative possessed marginally greater thermal stability than the high molecular weight chitosan. These findings and patterns are in excellent accord with those being presented in the relevant prior art (Hassiba et al., 2017).

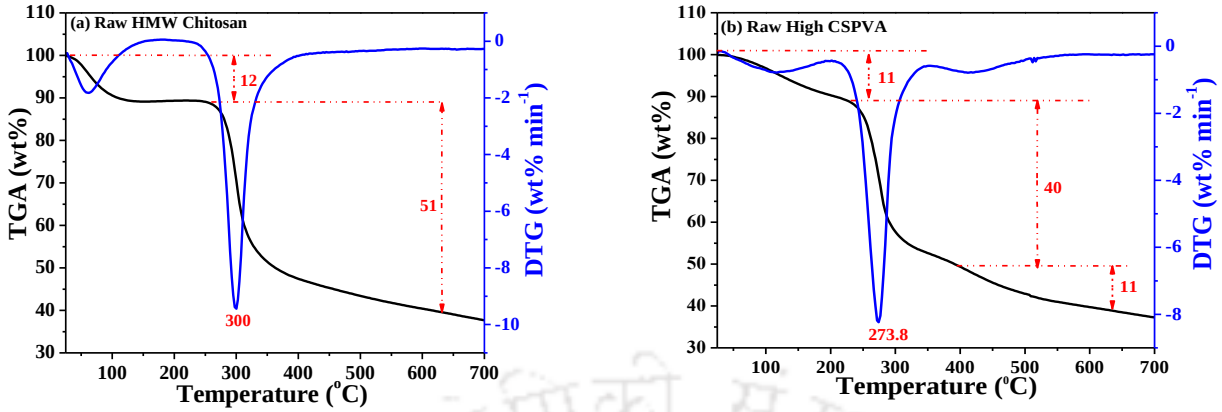

Fig. 4.12. TGA spectra of raw samples of high molecular weight chitosan and raw high CSPVA derivative resin.

4.4.3 Crystallinity Analysis

Fig. 4.13 illustrates the X-ray diffraction patterns of raw high molecular weight chitosan, high CSPVA, and metal sorbed high CSPVA. In accordance with the existing literature, the XRD spectra of chitosan (Fig. 4.13a) exhibited large and strong peaks at 9.18 and 19.85° and a higher crystallinity (Kanai et al., 2008; Nagireddi et al., 2019; Zhou et al., 2009). This is due to the abundance of hydroxyl and amino groups that produce stronger intra and intermolecular hydrogen interactions (Abdeen et al., 2015; Li et al., 2011). Additionally, chitosan's regular structure leads to its greater level of crystallinity. Due to the modification with polyvinyl alcohol, the raw high CSPVA derivative's XRD spectrum confirmed a reduced crystallinity (Fig. 4.13b), and a larger existence of the amorphous structure. However, after metal sorption, the resin became more amorphous (Fig. 4.13c).

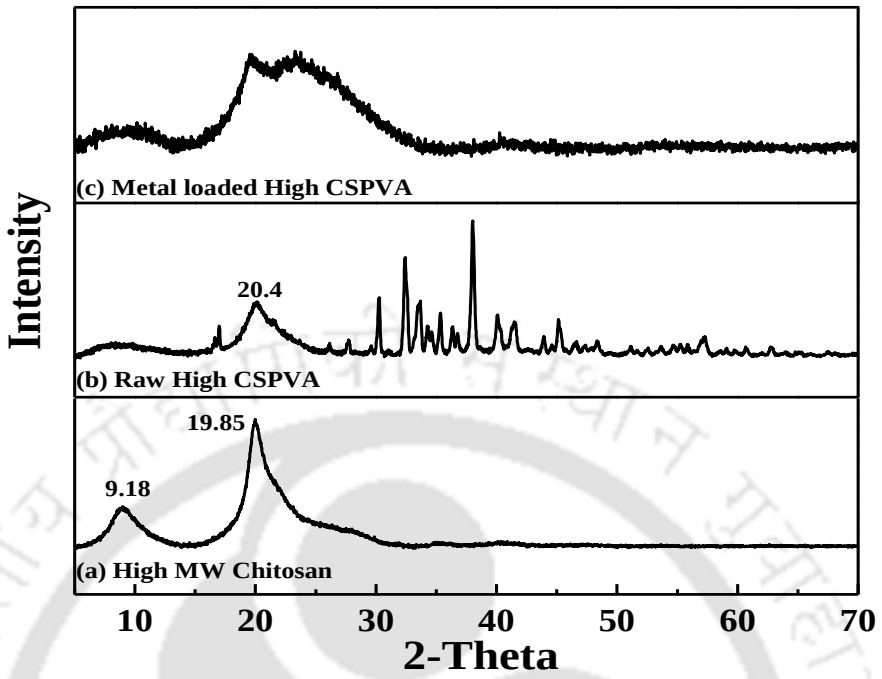

Fig. 4.13. XRD spectra of raw samples of high molecular weight chitosan and raw high CSPVA derivative resin.

4.4.4 FTIR Analysis

Fig. 4.14 exhibits the FTIR spectra of PVA, chitosan, and CSPVA derivative. The occurrence of characteristic peaks that corroborate with various functional groups in Fig. 4.14a did confirm that the metals interact significantly with the derivative. The stretching vibrations of -OH and -NH_2 groups and the overlap of intermolecular hydrogen bonds do corroborate with the peaks at 3400 cm^{-1} in the unprocessed chitosan sample. In addition, the presence of one amine spike near this peak lends credence to the theory that there is an amino group. The peaks at 1655 cm^{-1}, 1152 cm^{-1}, and 1060 cm^{-1} respectively confirm that the stretched amide I, CH, and –CONH groups do exist (Nagireddi et al., 2019). The FTIR spectrum of PVA shown in Fig. 4.14b refers to all significant peaks being linked to the hydroxyl and acetate groups. Notably, the O-H stretch from

intermolecular and intramolecular hydrogen bonding has been responsible for the wider band between 3550 and 3200 cm^{-1}. The C-H stretching of alkyl groups caused the vibrational band between 2840 and 3000 cm^{-1}. However -OH bending and C-O stretching of the remaining acetate groups enabled pertinent peaks between 1083 and 1138 cm^{-1} in the PVA. This is due to the saponification reaction of polyvinyl acetate (Mozafari et al., 2012). In addition to those associated to the ionization of the major amino groups of chitosan, the FTIR spectra of the CSPVA fibers (Fig. 4.14c and 4.14d) do indicate distinctive peaks of PVA and chitosan. The peaks have been located at 1408 and 1548-1560 cm^{-1}. Fig. 4.14c confirms the FTIR spectra of medium CSPVA resin with low peak intensities and Fig. 4.14d shows the FTIR spectra of high CSPVA resin with higher peak intensities. Carboxylic acid has been responsible for the peak at 1408 cm^{-1} and the symmetric deformation of $-NH_3^+$ groups can be considered to be relevant for the peak at 1552-1558 cm^{-1}. Carboxylic acid dimers do corroborate with the peaks at 1700 and 1725 cm^{-1} (Mozafari et al., 2012). After metal adsorption (Fig. 4.14e), compared to the raw adsorbent, the characteristic peaks of carboxylic acid got reduced and the intensity of the amine group was also minimized.

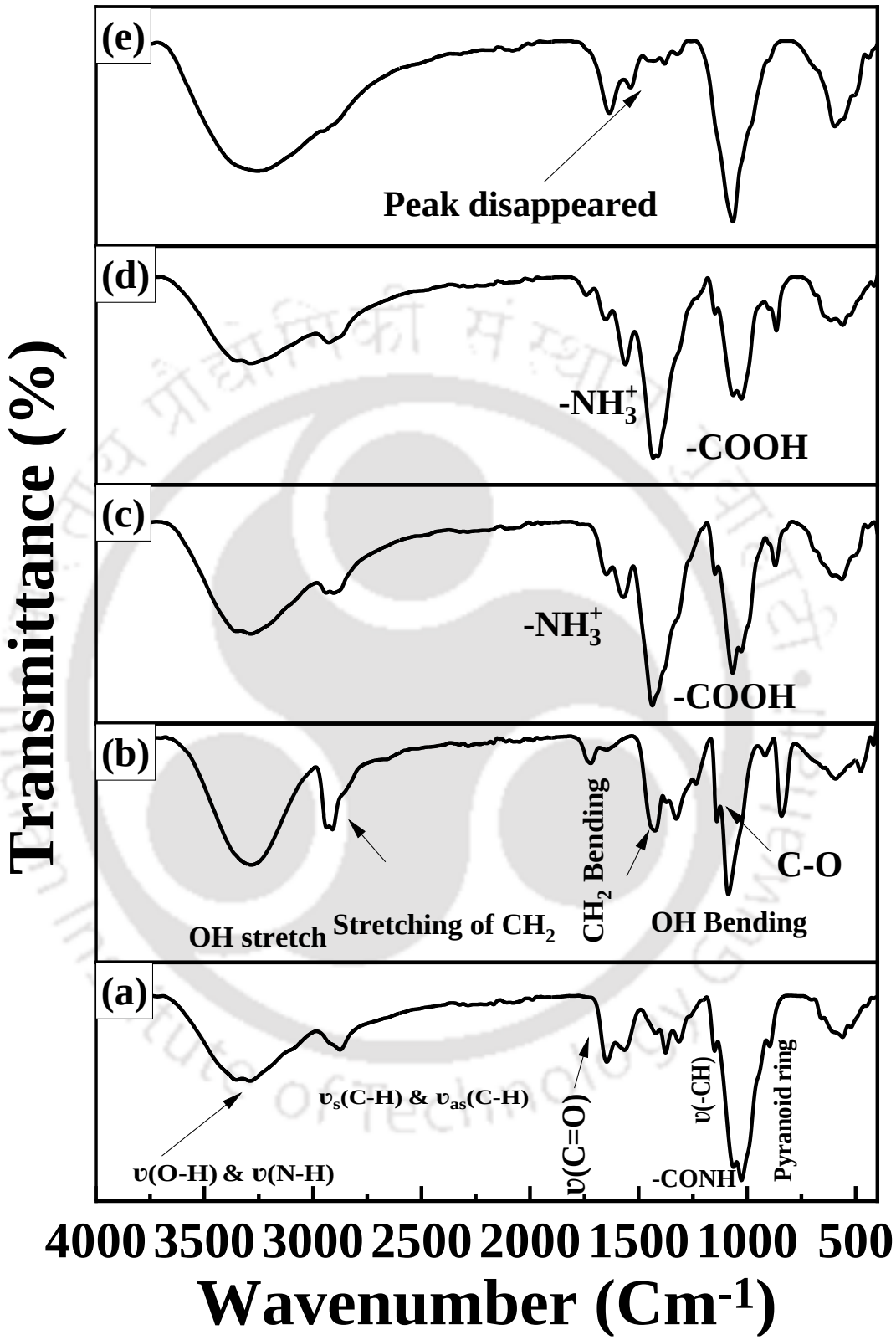

Fig. 4.14. FTIR spectra of raw and heavy metal loaded high CSPVA derivative resin samples.

4.4.5 EDX Analysis

Fig. 4.15 depicts FESEM and EDX spectra of raw high CSPVA and metal-loaded high CSPVA samples. For the raw high CSPVA derivative, the EDX pattern (Fig. 4.15a) affirmed the existence of C (25.5 %), O (65.4 %), and N (9.1 %). The metal-loaded high CSPVA sample confirmed the significant existence of several metals (Cu (2.9 %), Pb (19.5 %), Fe (1.2 %) and Al (9.6 %) and (Zn (1.8 %), Pb (16.5 %), Fe (2.4 %) and Al (13.2 %)) on the high CSPVA surface (Fig. 4.15b and Fig. 4.15c respectively).

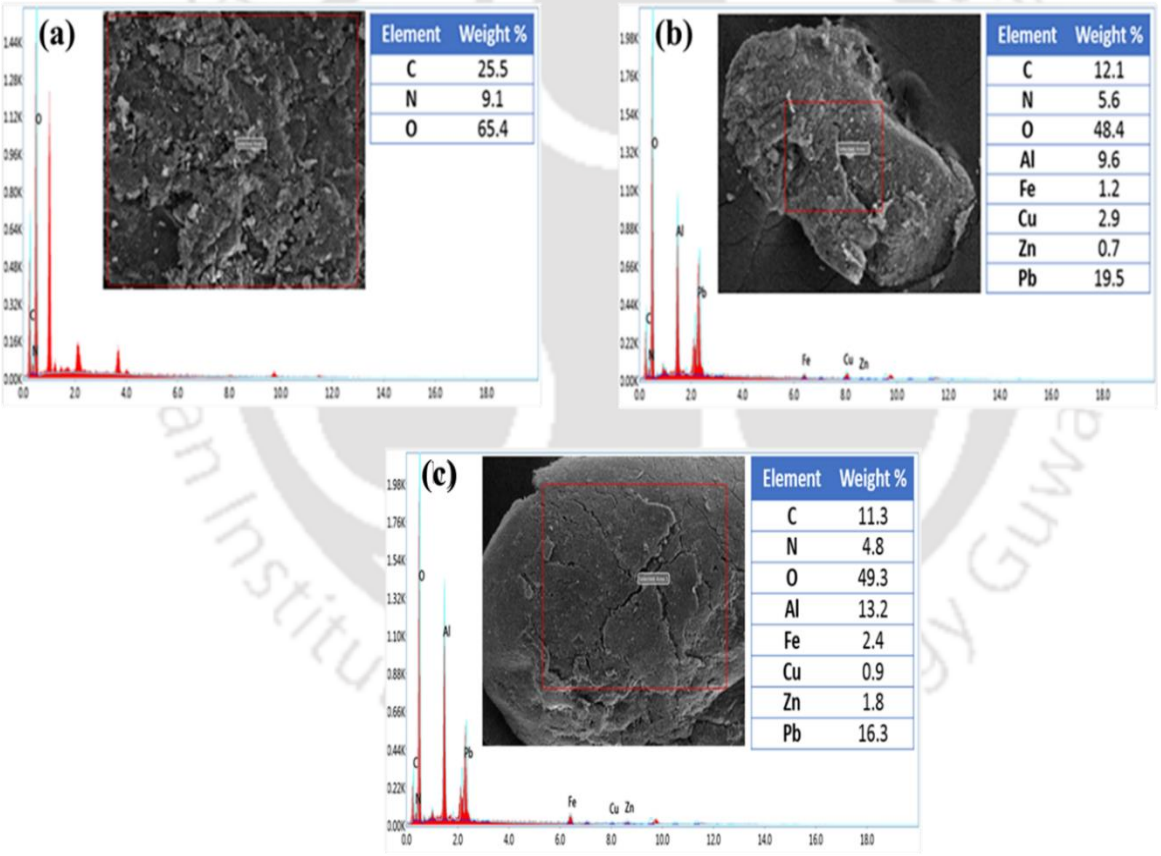

Fig. 4.15. FESEM-EDX spectra of raw and heavy metals loaded high CSPVA derivative resin samples.

4.5 Cyclic Multi-Heavy Metal Desorption Characteristics

For the high CSPVA, the cyclic desorption removal (%), adsorptive removal (%), and adsorption capacity have been depicted in Fig. 4.16a, b, and c, respectively for Cu dominant solution and Fig. 4.17a-c for Zn dominant solution. For a variation in the number of cycles from 1-3, the cyclic desorption % reduced from 69.25-44.3 %, 65.83-53.73 %, and 57.71-47.37 %, respectively for Cu, Fe, and Pb from Cu dominant solution and 60.95-51.89 %, 66.71-59.94 %, and 60.14-53.70 %, respectively for Zn, Fe, and Pb from Zn dominant solution. Incidentally, for the Cu dominant solution, the corresponding adsorptive removal was 89.01-75.39 %, 70.71-57.35 %, and 82.98-68.75 %, respectively. Thus, Cu and Pb removal suffered detrimentally with cyclic adsorption and this was not the case for the Fe. This confirmed greater irreversible chemisorption of Cu and Pb but not Fe from Cu dominant solution. Also, the cyclic number (1-3) based adsorptive removal of 59.08-48.86 %, 70.52-59.51 %, and 81.89-71.90 %, respectively for Zn, Fe, and Pb respectively in the Zn dominant solution affirmed that the mentioned metals removal suffered detrimentally with cyclic adsorption and confirmed greater irreversible chemisorption of Zn, Fe, and Pb. Further, the corresponding adsorption capacity reduced from 208.83-176.88 mg g^{-1}, 54.66-44.34 mg g^{-1}, and 5.39-4.47 mg g^{-1} from Cu dominant solution and 164.51-136.03 mg g^{-1}, 105.57-89.10 mg g^{-1}, and 3.10-2.72 mg g^{-1} from Zn dominant solution for a variation in cycle number from 1-3. This affirmed a natural reduction in adsorption capacity during cyclic adsorption-desorption studies. Also, after cycle 3, the desorption % of 44.3, 53.73, and 47.37 for Cu, Fe, and Pb, respectively for Cu dominant solution and 51.89, 59.94, and 53.70 for Zn, Fe, and Pb, respectively Zn dominant solution affirmed a good performance with the fact that the adsorbate had several heavy metals and co-existent cations.

Thus, these findings confirm that the high CSPVA derivative can further perform effectively in a hybrid adsorption process that targets the greater removal of Cu, Zn, Fe, and Pb through a pre-treatment methodology.

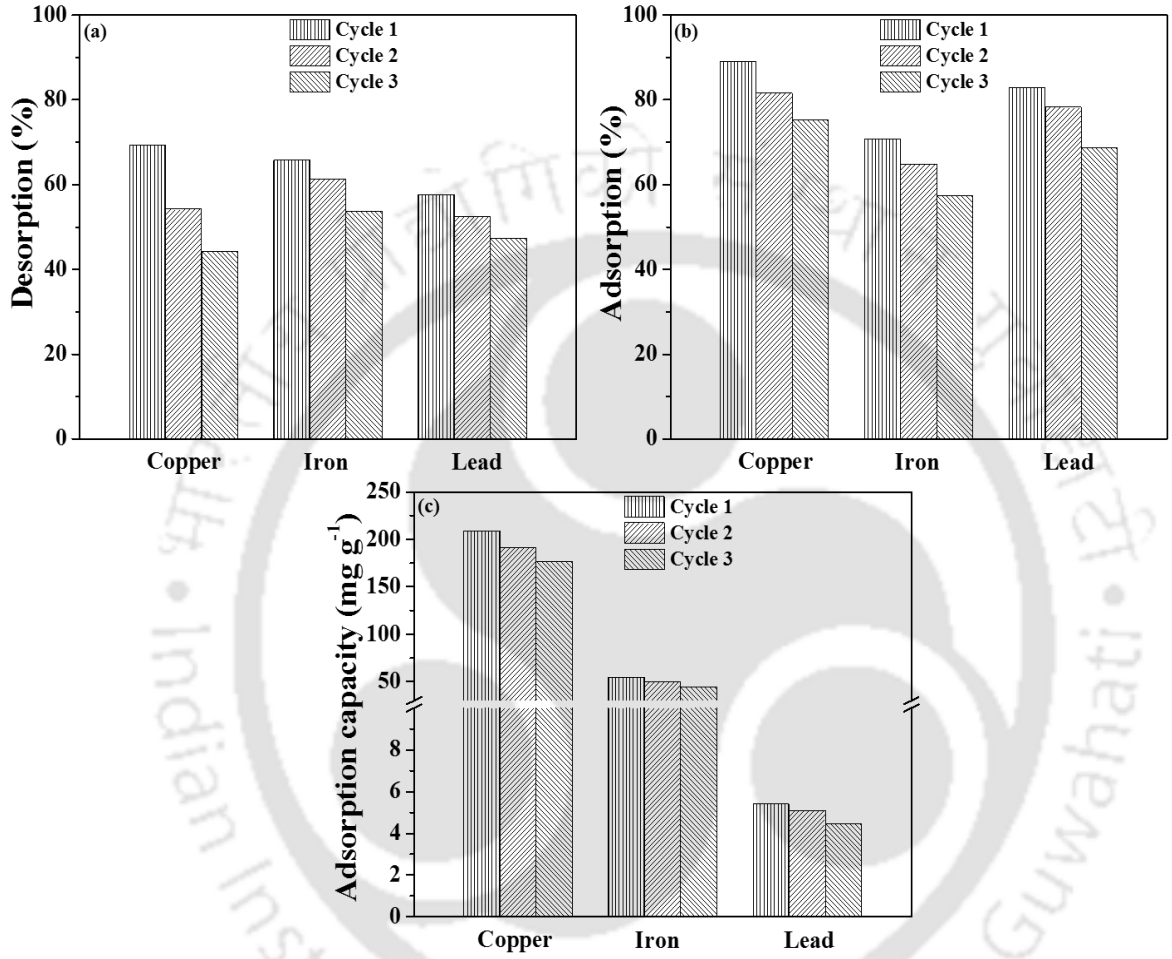

Fig. 4.16. Multi-heavy metal cyclic performance characteristics of high CSPVA derivative resin with Cu dominant adsorbate system (a) desorption % (b) adsorption % and (c) adsorption capacity.

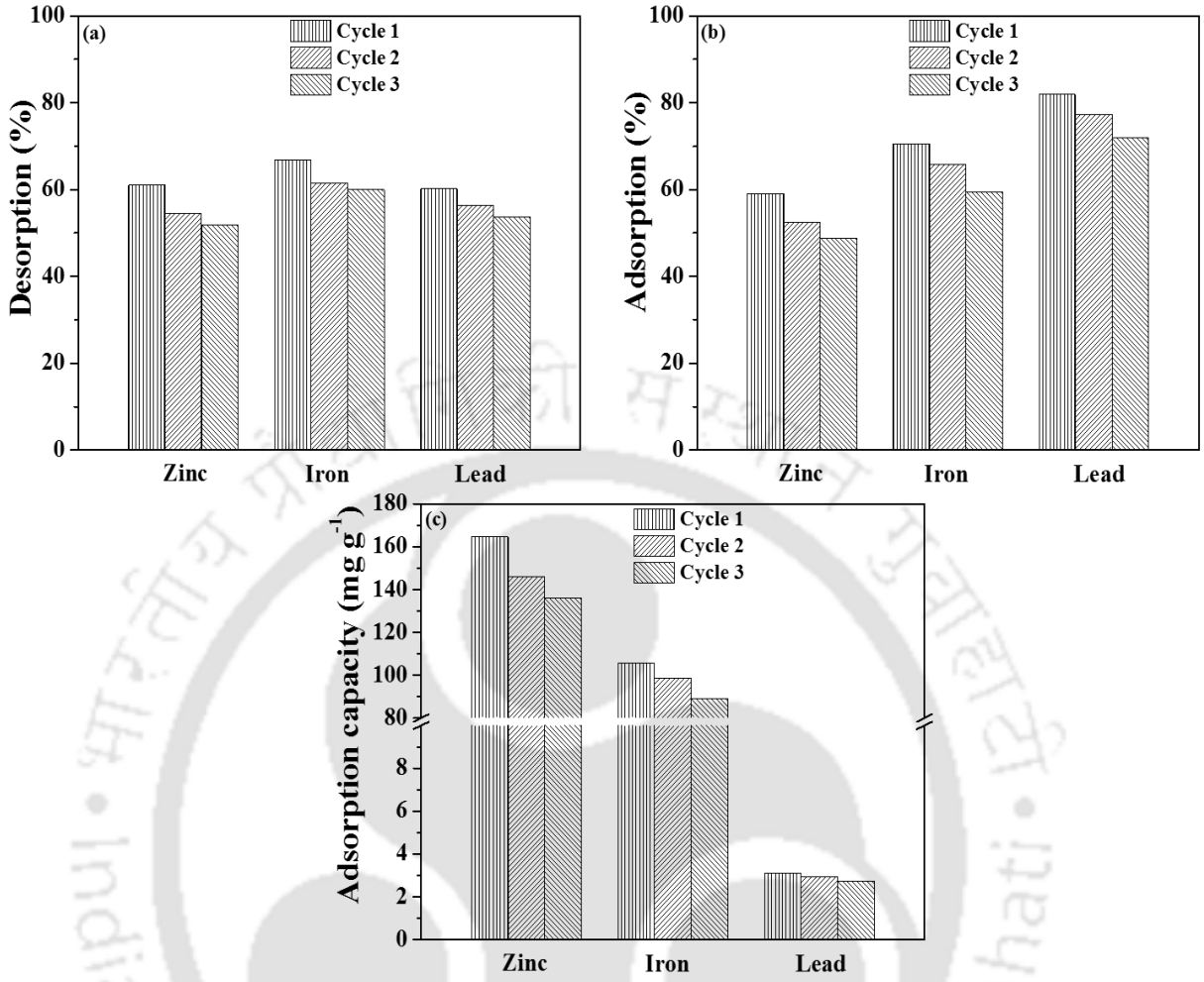

Fig. 4.17. Multi-heavy metal cyclic performance characteristics of high CSPVA derivative resin with Zn dominant adsorbate system (a) desorption % (b) adsorption % and (c) adsorption capacity.

Fig. 4.18 depicts the proposed desorption mechanism of exhausted high CSPVA derivative resin. Eluent solution would provide free H^+ ions for their reaction with the high CSPVA adsorbent exhausted adsorption sites. Accordingly, the adsorbed multi-heavy metal ions were released from the spent sorbent surface. However, to validate the hypothesis, additional insights are necessary from further characterization such as FTIR, EDX, and XRD analysis of the regenerated adsorbent. Such studies were beyond the scope of the Ph.D. thesis that primarily aims to screen and scope

upon the competence of chitosan derivatives for cyclic desorption-based multi-heavy metal removal from complex adsorbate systems. However, these could be addressed in the near future.

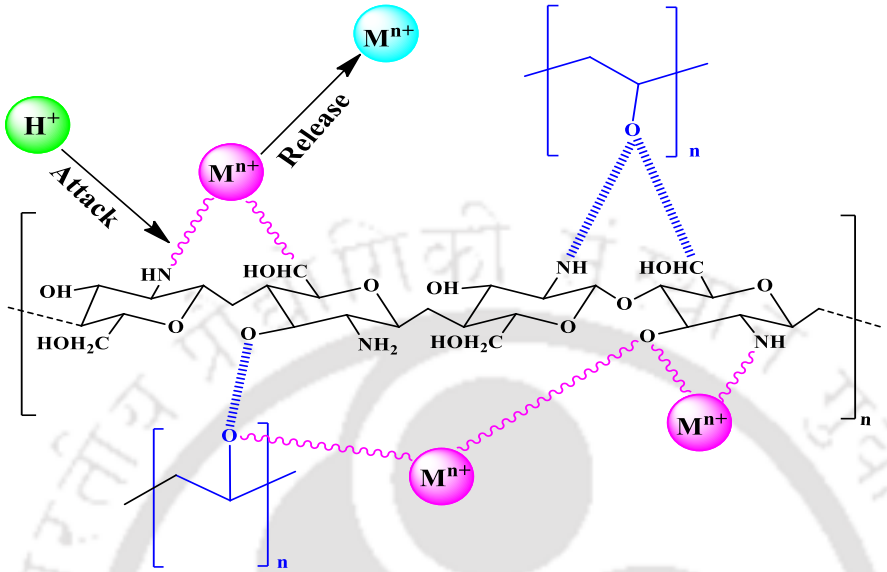

Fig. 4.18. Proposed desorption mechanism of heavy metals loaded with high CSPVA resin.

4.6 Literature Comparison

The experimental findings with respect to optimality of adsorption parameters, adsorption and desorption characteristics of low CSPVA, medium CSPVA, and high CSPVA derivatives have been compared with the best available literature for most relevant adsorbate (multi-heavy metal solution) and adsorbent systems (chitosan-derivatives). A summary of these findings is presented in Table 4.5. For complex industrial wastewater adsorbate systems, the reported data in the Ph.D. thesis is the only relevant data to compare adsorbent performance, as other relevant literature reported data for only aqueous acidic solutions. Based on the data summarized in the table, the following can be inferred:

a) From Zn and Cu removal perspective and for synthetic complex industrial wastewater and among chitosan derivatives, high CSPVA performed promising in comparison with the

glutaraldehyde cross-linked chitosan (adsorption capacity of 222.21 mg g^{-1} for 194.9-584.7 mg L^{-1} initial Zn solution concentration range in comparison to the 72.71 mg g^{-1} for 11.3-92.3 mg L^{-1} initial Zn solution concentration range). Similarly, the corresponding adsorption capacity of Cu was 243.9 mg g^{-1} for the 187.7-563.1 mg L^{-1} initial Cu solution concentration range in comparison to 79.18 mg g^{-1} for the 14.6-108.8 mg L^{-1} initial Cu solution concentration range. Hence, the performance of high CSPVA derivatives is comparable with the both adsorption and desorption characteristics of glutaraldehyde cross-linked chitosan resin. The high CSPVA derivative studied in this work performed excellent in terms of heavy metal removal but satisfactory in terms of metal desorption and derivative regeneration after three cycles.

b) From the perspective of the regeneration of the chitosan derivatives after multi-heavy metal desorption from complex synthetic industrial wastewater adsorbate solutions, the high CSPVA derivative can be concluded to have promising performance (69.25, 60.14 and 60.95 compared to 98.4, 96.7 and 98.5 aqueous solution desorption % for Cu, Pb, and Zn, respectively). In addition, the desorption efficiency is significantly better than that of styrene DVB copolymer. Hence, from a heavy metal removal and derivative regeneration perspective and complex adsorbate systems, high CSPVA is the best among PVA/Chitosan beads, EDTA-modified Chi/SiO_2/Fe_3O_4, and PVA/Chitosan foam.

c) All other literature data cannot be compared with the data obtained in this work, as these literature targets heavy metal removal from aqueous solutions with lesser solution complexity.

Table 4.5: Summary of the adsorption and desorption characteristics of alternate CSPVA derivatives investigated in this study and prior art.

Adsorbent	Metal Ions	Solution	Dose ($g\ L^{-1}$)	Contact time (min)	Conc. range ($mg\ L^{-1}$)	Adsorption capacity ($mg\ g^{-1}$)	Removal efficacy (%)	Desorption (%)	Eluents	Ref.
Chitosan immobilized Bentonite	Cu Ni Pb	Aqueous binary solution	-	240-360 240-360 240-360	25-200 25-200 25-200	17.09 12.61 20.8	51.41 39.04 80	-	-	(Futalan et al., 2011)
Styrene DVB Copolymer	Cr Ni Pb Cd	Aqueous mixed solution	10	210	-	-	99.7 65 59 28	65 70 45 0	0.1N NaOH	(Misra et al., 2011)
PVA/Chitosan Beads	Cu Pb Zn Cd	Multi metal solution	2	660 540 660 540	50-500	238.45 166.44 74.18 126.06 (Single solution)	93.90 77.85 10.93 21.31 (Multi-metal solution)	98.4 96.7 98.5 98.5 (Single solution)	0.1M EDTA for Cu 0.1 M HCl for Pb, Zn, Cd	(Li et al., 2011)
PVA/Chitosan Foam	MG dye Cu	Binary solution	2	360 480	50-800	227.02 111.85	-	97	0.1 M Na_2EDTA	(Li et al., 2012)
EDTA modified Chi/SiO_2/Fe_3O_4	Cu Pb Cd	Mixed solution	1	360 180 360	0.2-5 (mM)	0.699 0.596 0.563	-	75.73	0.01 M Na_2EDTA	(Ren et al., 2013)
GLA/Chitosan	Pb Ni Zn Cu	Multi metal solution	1	420 360 420 360	9.1-90.72 13.4-99.4 11.3-92.3 14.6-108.8	67.17 67.81 72.71 79.18	74.06 73.45 73.16 72.77	-		(Busuioc et al., 2016)
High CSPVA	Cu Pb Fe	Multi metal solution	1.6	240	187.7-563.1 5.2-15.6 61.9-185.5	243.9 6.65 87.72	88.78 85.09 72.34	69.25-44.3 57.7-31.9 65.8-53.7	0.1M HCl	This study
High CSPVA	Zn Pb Fe	Multi metal solution	1.4	360	194.9-584.7 2.65-7.95 104.8-314.4	222.21 4.02 135.14	58.98 80.44 71.71	60.95-51.89 60.14-53.70 66.71-59.94	0.1M HCl	This study

4.7 Summary

Several useful insights can be deduced from the best findings achieved in this work in the field of heavy metal adsorption and desorption characteristics of low CSPVA, medium CSPVA, and high CSPVA derivatives with synthetic complex industrial adsorbate systems. Firstly, the optimal

multi-heavy metal batch adsorption parameters for the high CSPVA derivative in Cu dominant solution are 3.82 pH, 1.6 g L^{-1} dosage, and 240 min contact time. Corresponding adsorption capacity and metal removal % of the resin are 111.47-230.91 mg g^{-1} and 95.01-65.61 % for Cu, 32.14-71.48 mg g^{-1} and 83.14-61.64 % for Fe and 3.02-6.27 mg g^{-1} and 92.88-64.27 % for Pb, respectively for the initial heavy metal ion concentration range of 187.7-563.1 mg L^{-1} for Cu, 61.85-185.55 mg L^{-1} for Fe, and 5.2-15.6 mg L^{-1} for Pb. On the other hand, the optimal heavy metal ion batch adsorption parameters for high CSPVA in Zn dominant solution are 3.64 pH, 1.4 g L^{-1} dosage, and 360 min contact time. Corresponding adsorption capacity and metal removal % of the resin is 115.88-203.20 mg g^{-1} and 83.24-48.65 % for Zn, 66.74-126.37 mg g^{-1} and 89.15-56.27 % for Fe, and 1.78-3.42 mg g^{-1} and 94.21-60.29 % for Pb, respectively in the initial heavy metal ion concentration range of 194.9-584.7 mg L^{-1} for Zn, 104.8-314.4 mg L^{-1} for Fe, and 2.65-7.95 mg L^{-1} for Pb. Hence, compared to the Zu dominant solution, the high CSPVA derivative provided marginally higher removal efficiencies with the Cu dominant solution. However, the high CSPVA resin exhibited higher regeneration characteristics in the Zn dominant solution in comparison with the Cu dominant solution. Secondly, after the three cycles, the desorption characteristics are 44.3, 31.9, and 53.7 % for Cu, Fe, and Pb, respectively for the Cu dominant solution and 51.89, 53.70, and 59.94 % for Zn, Fe, and Pb, respectively for the Zn dominant solution. These indicate and confirm satisfactory heavy metal ion removal and resin regeneration. Further improvement in the heavy metal ion desorption characteristics of high CSPVA can be conveniently targeted through the suitable alteration in functional groups abundance. This can be achieved through stoichiometric and resin synthesis variations. The surface analysis with FTIR, BET, TGA, XRD FESEM-EDX, etc., are in good agreement with apparent functional interactions between various chemical species.

From the perspective of heavy metal ion removal and resin reusability, compared to the available prior art based on aqueous solution, high CSPVA derivative performed better for complex synthetic industrial wastewater adsorbate systems. With respect to chitosan, all adsorbents exhibited excellent desorption characteristics and thereby confirmed upon the greater role of chelating functional groups in achieving improved resin reusability for multi-heavy metal removal from synthetic industrial wastewater adsorbate systems.

Chapter 5:

Cyclic Multi-heavy metal adsorptive and desorptive characteristics of Citric acid-Chitosan derivative Resins

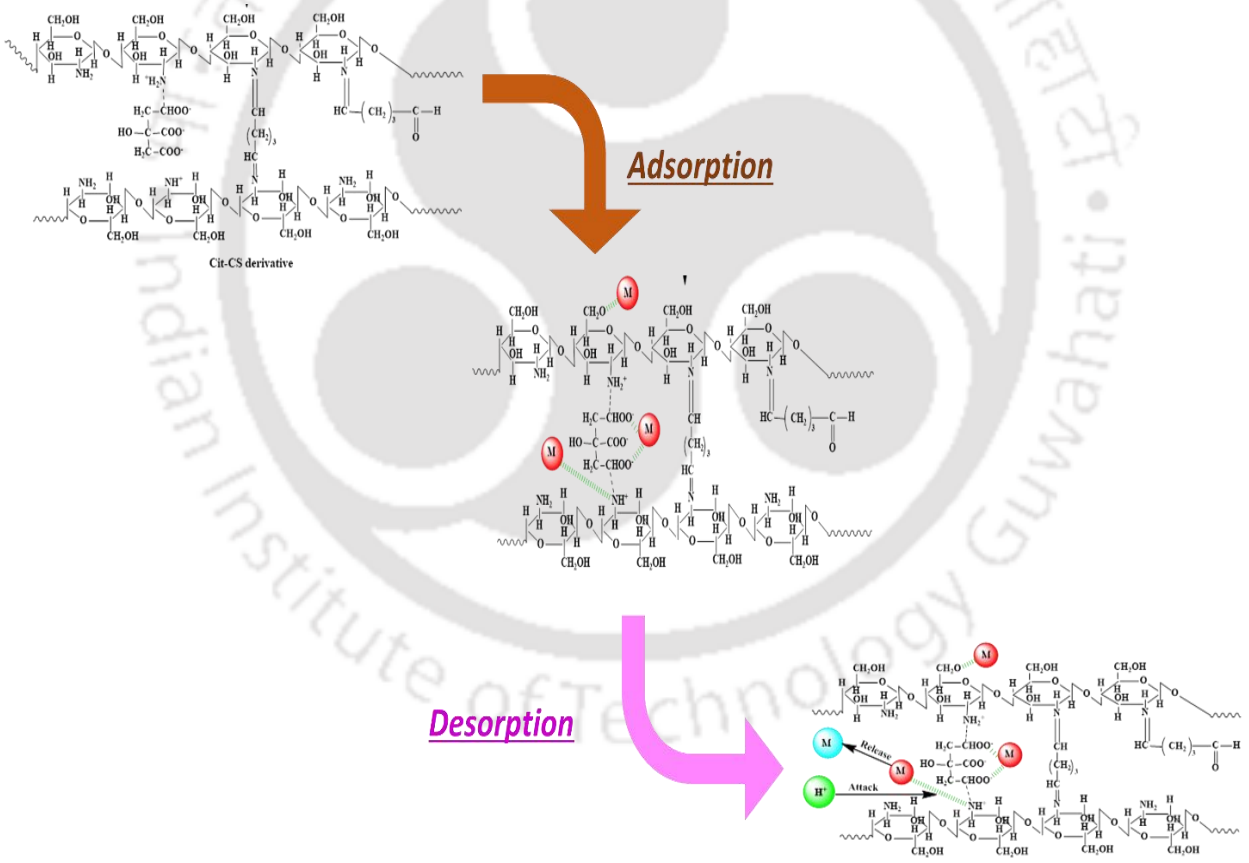

Chapter 5

Cyclic Multi-heavy metal adsorptive and desorptive characteristics of Citric acid-chitosan derivative Resins

The chapter summarizes experimental and theoretical findings associated to multi heavy metal adsorption and desorption characteristics of citric acid grafted low molecular weight chitosan derivative (low Cit-CS), citric acid grafted medium molecular weight chitosan derivative (medium Cit-CS), and citric acid grafted high molecular weight chitosan derivative (high Cit-CS) resins. Section 5.1 presents the relevant background followed with the solubility resistance of the medium Cit-CS derivative in section 5.2. Section 5.3 elucidates upon the adsorption characteristics of the mentioned resins. Section 5.4 briefly describes the findings associated to surface characterizations of raw and metal-loaded chitosan derivatives. Thereafter, section 5.5 presents heavy metal desorption characteristics of spent citric acid grafted medium molecular weight chitosan derivative (medium Cit-CS) using various inexpensive eluents. Thereafter, section 5.6 presents the literature comparison of the best available prior art and the findings of this chapter. Finally, a summary of the findings is presented in section 5.7 of the chapter.

5.1 Background

Prior to this thesis work, the nitrogen, carboxyl, and hydroxyl functionalized adsorbents being evaluated for heavy metal ion removal and resin regeneration from multi-metal solutions were glutaraldehyde cross-linked chitosan derivative (Busuioc et al., 2016) and PVA/chitosan beads (Li et al., 2011). However, such resins have been evaluated for heavy metal removal from aqueous solutions. Considering the relevant critical research gap, the emphasis of the conducted research

in the thesis was to examine the role of molecular weight of chitosan on the citric acid-chitosan derivative to influence multi-heavy metal adsorption characteristics from complex synthetic industrial wastewater adsorbate systems. Further, simple eluent-based desorption was targeted for these chitosan derivatives.

The multi-heavy metal ion adsorption characteristics were evaluated for optimal combinations of contact time, adsorbent dosage, and initial heavy metal ion concentrations. Surface characterizations were conducted with Fourier Transform-Infrared Spectrophotometer (FTIR), Braummer-Emmet-Teller (BET), X-ray diffractometer (XRD), Thermo Gravimetric Analyser (TGA), and Field Emission Scanning Microscopy equipped energy dispersive X-Ray analyzer (FESEM-EDX). For optimized adsorbent dosage and contact time, adsorption experiments were conducted for a wider range of initial metal ion concentrations 187.7-563.1 mg L^{-1} for Cu, 61.85-185.55 mg L^{-1} for Fe, and 5.2-15.6 mg L^{-1} for Pb in Cu dominant solution and 194.9-584.7 mg L^{-1} for Zn, 104.8-314.4 mg L^{-1} for Fe, and 2.65-7.95 mg L^{-1} for Pb in Zn dominant solution. Thereby, the specific influence of various co-existent ions such as K, Na, Al, and Mg on targeted heavy metal adsorption characteristics of low Cit-CS, medium Cit-CS, and high Cit-CS derivatives were addressed.

5.2 Solubility resistance of medium Cit-CS derivative Resin

The medium Cit-CS resin has been subjected to stability studies prior to and after multi-heavy metal adsorption. Similar resistance trends were observed for low Cit-CS and high Cit-CS resins. To do so, firstly, the raw medium Cit-CS resin was placed in contact with 1 N HNO_3 and 1 N KOH solutions for 12 h. Thereafter, the quantitative analysis through weight reduction was carried out. Thereby, the weight loss % was 0.96 % for both cases and thereby confirmed the very good

stability of the resin in both acidic and basic media. Also, the heavy metal adsorbed medium Cit-CS resin has been also subjected to a similar stability test. It was found that the weight loss for the case was also similar (0.95 % for both cases of acidic and basic media). In summary, the medium Cit-CS derivative is stable at the mentioned conditions and also in both acidic and basic media. These observations confirm upon its relevance for real-time applications.

5.3 Multi-heavy metal adsorption characteristics of low Cit-CS, medium Cit-CS, and high Cit-CS derivative resins

5.3.1 Optimality of batch adsorption process parameters

The performance of sorption is highly controlled by the solution pH. Therefore, experiments can be carried out to determine the ideal pH value for the simulated adsorbate system. However, it was observed that the complex adsorbate system at a pH above 4 and below 2 was unstable and enabled the formation of a precipitate. Henceforth, pH optimality could not be addressed and experiments were further conducted at the natural pH of the adsorbate system. Consequently, various sorption process variables namely sorbent contact time, sorbent dosage, and initial concentration were optimized for the natural pH of the solution (3.82 for Cu dominant solution and 3.64 for Zn dominant solution). Further, relevant prior art suggests that heavy metals may exist in their +2 ionic forms in the acidic pH range (Benavente et al., 2011). It was hypothesized that for both adsorbate systems, hydroxyl, and amino groups integrated with the Cit-CS resin's surface would be functional to serve as sorption sites for the multi-heavy metal adsorption. As a result, the following delineated chemical reaction mechanism has been proposed to represent the heavy metal adsorption (Patel et al., 2023):

$$R - NH_2 + H^+ \rightarrow R - NH_3^+ \quad (5.1)$$

$$R - NH_2 + M^{2+} \rightarrow R - NH_2M^{2+} \quad (5.2)$$

$$R - NH_3^+ + M^{2+} \rightarrow R - NH_2M^{2+} + H^+ \quad (5.3)$$

$$R - NH_2M^{2+} + H_2O \rightarrow MOH^+ + R - NH_3^+ \quad (5.4)$$

The mechanism through which the heavy metals adsorb onto the resin has been shown in Fig. 5.1. Thus, the dominant metal ions at the solution pH of 3.82 and 3.64 do have an influence on the adsorption process.

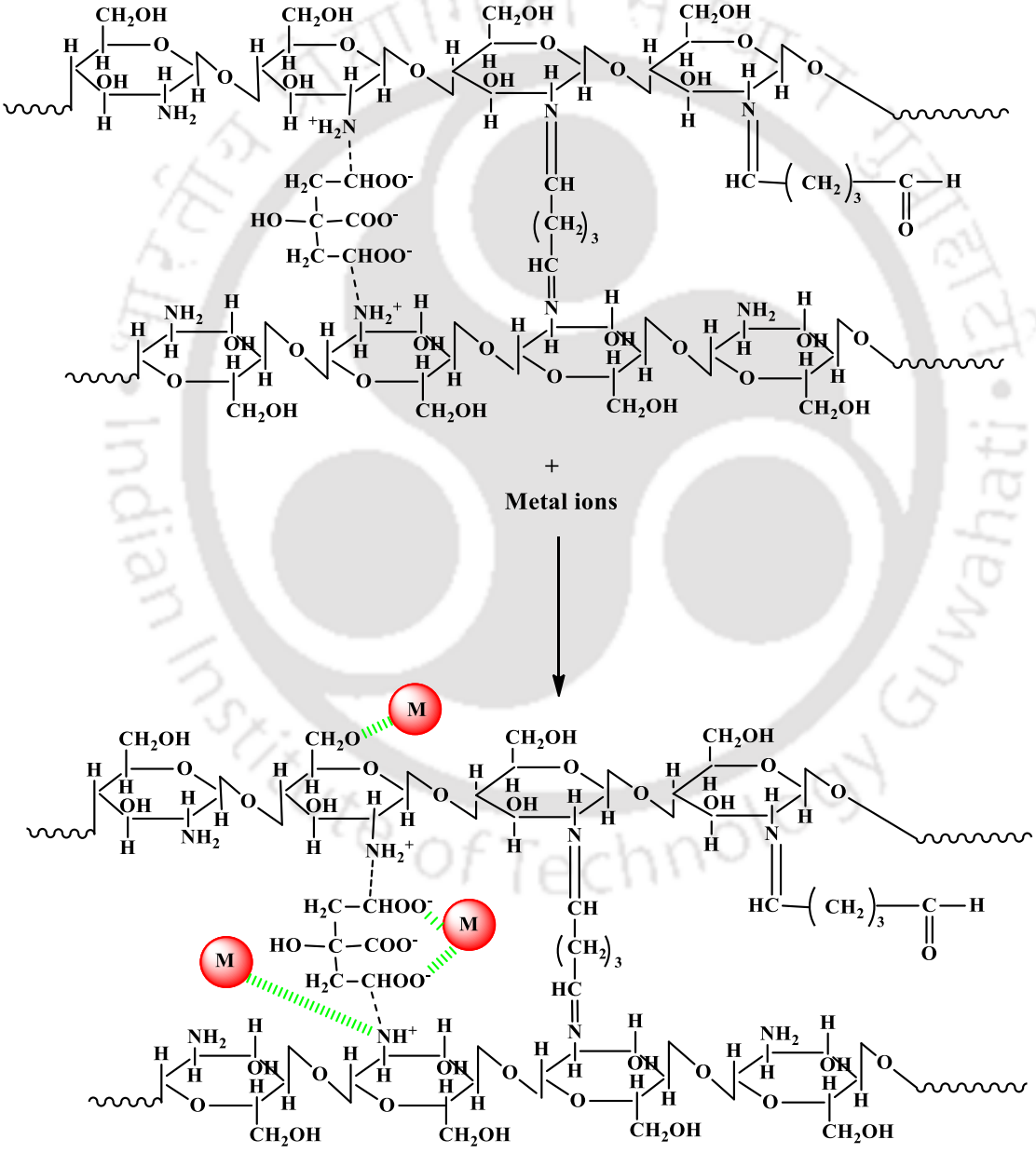

Fig. 5.1. Proposed heavy metal adsorption mechanism for Cit-CS derivative.

For a fixed choice of relevant sorption parameters (3.82, 12 h, 25°C, 200 rpm for initial pH, contact time, temperature, and shaking speed respectively) and initial heavy metal ion concentrations (10.4 mg L^{-1} Pb, 123.7 mg L^{-1} Fe, and 375.4 mg L^{-1} Cu for Cu dominant and 389.8 mg L^{-1} Zn, 209.6 mg L^{-1} Fe, and 5.3 mg L^{-1} Pb for Zn dominant solution), the alteration of metal adsorption patterns with adsorbent dosage for Cu dominant solution is shown in Fig. 5.2. The maximum dosage (1.8 g L^{-1} for low Cit-CS resin) has been inferred to be the ideal adsorbent dosage at which the optimal adsorption properties (139.42, 41.00, and 4.26 mg g^{-1} adsorption capacity and 66.85, 59.67, and 73.65% removal efficiency for Cu, Fe, Pb respectively) have been achieved. Also, for medium and high Cit-CS resins, maximum dosage (1.4 g L^{-1}) facilitated optimal adsorption properties (216.32, 65.21, 6.55 mg g^{-1} and 217.00, 65.61, 6.56 mg g^{-1} adsorption capacity and 80.67, 73.81, 88.17% and 80.93, 74.26, 88.30% removal efficiency for Cu, Fe, Pb respectively).

Similarly, the alteration of metal adsorption patterns with an alteration in adsorbent dosage for Zn dominant solution has been depicted in Fig. 5.3. The maximum adsorbent dosage (1.6 g L^{-1} for low Cit-CS resin) can be inferred to be the optimal adsorbent loading at which the optimal adsorption properties (125.26, 81.87, and 2.37 mg g^{-1} AC and 51.42, 62.50, and 71.54 % PR for Zn, Fe, Pb respectively) have been achieved. Also, for medium and high Cit-CS resins and at maximum loading (1.4 g L^{-1}), the optimal adsorption properties (175.13, 108.51, 3.05 and 177.98, 109.85, 3.03 mg g^{-1} AC and 62.90, 72.48, 80.50 % and 63.92, 73.37, 80.06 % PR for Zn, Fe, Pb respectively) have been achieved. The reduced heavy metal sorption at increased adsorbent dosage has been due to an increment in the sites available for metal sorption. Simultaneously, adsorption capacity reached a lower value due to reduced adsorbed mass per unit weight of adsorbent. Due to the presence of multiple functional groups, the Cit-CS resin affirmed higher removal efficacy in conjunction with other chitosan derivatives (Li et al., 2012, 2011).

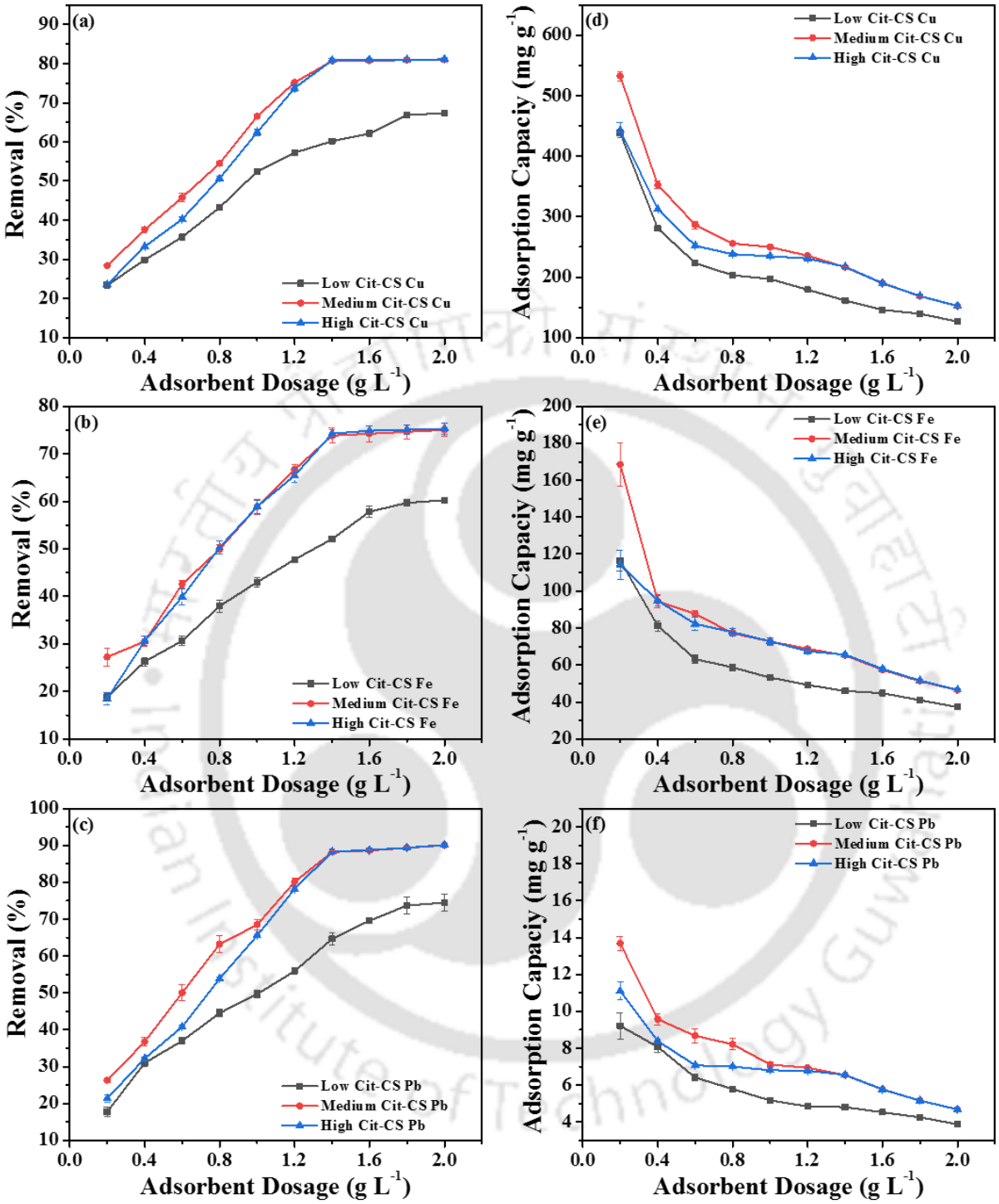

Fig. 5.2. Graphs depicting the influence of adsorbent dosage on adsorption characteristics of Cit-CS derivatives and Cu dominant adsorbate system.

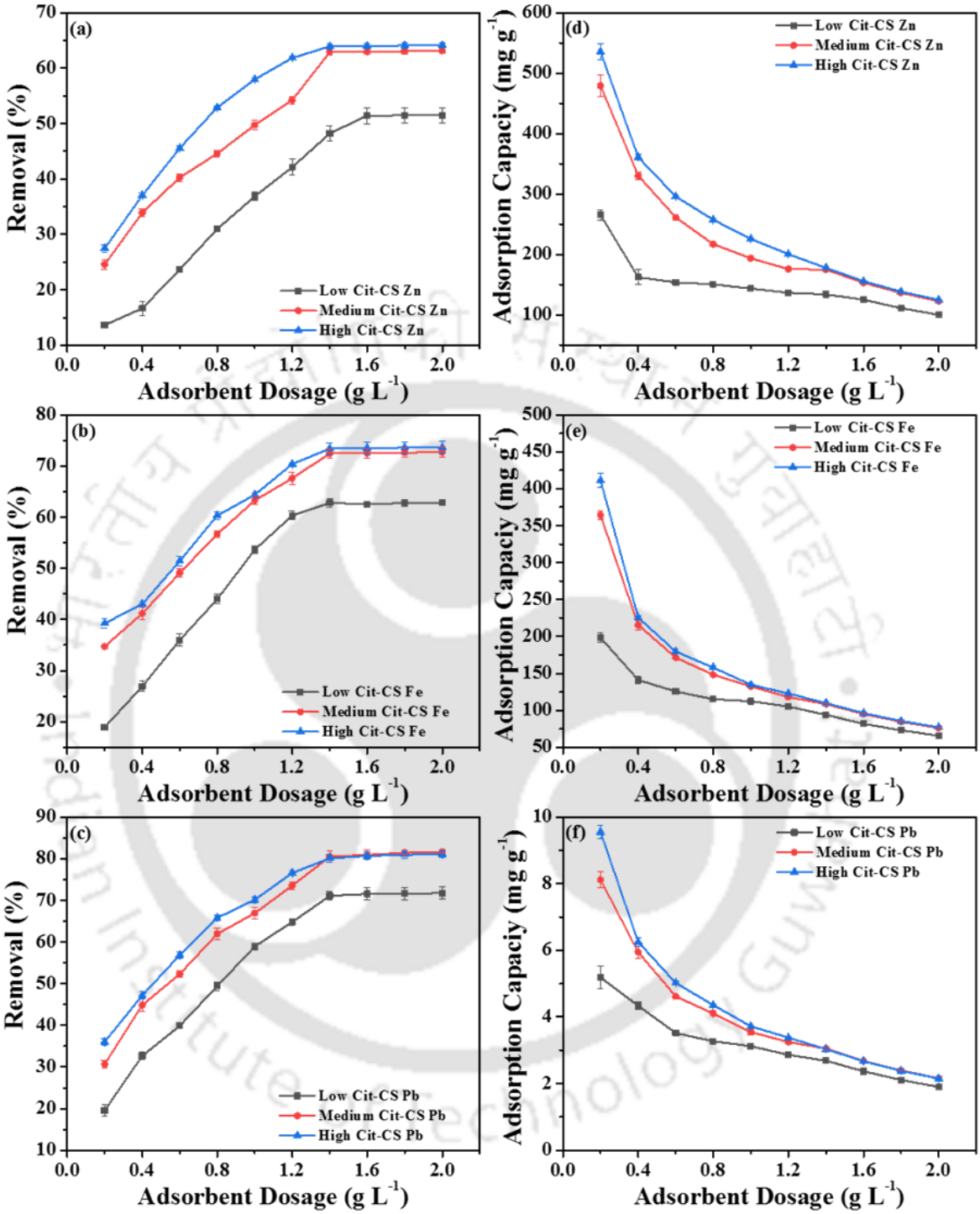

Fig. 5.3. Graphs depicting the influence of adsorbent dosage on adsorption characteristics of Cit-CS derivatives and Zn dominant adsorbate system.

For a fixed choice of other sorption process parameters (3.82, 25°C, 200 rpm for initial pH, temperature, and shaking speed respectively), adsorbent dosage (1.8 g L^{-1} for low Cit-CS resin and 1.4 g L^{-1} for medium and high Cit-CS derivative for Cu dominant solution and 1.6 g L^{-1} for low Cit-CS resin and 1.4 g L^{-1} for medium and high Cit-CS derivatives for Zn dominant solution) and heavy metal ion concentration (10.4 mg L^{-1} Pb, 123.7 mg L^{-1} Fe, and 375.4 mg L^{-1} Cu for Cu dominant and 389.8 mg L^{-1} Zn, 209.6 mg L^{-1} Fe, and 5.3 mg L^{-1} Pb for Zn dominant solution), the alteration of metal adsorption patterns with adsorbent contact time for Cu dominant solution has been shown in Fig. 5.4. The figure depicts that the adsorption rate was quick upto 120 min and reached equilibrium at 480 min for low Cit-CS resin and 420 min for high and medium Cit-CS resins. Thereby, the maximum removal efficiency and adsorption capacity of 76.89, 58.81, 67.24 %, and 4.44, 40.42, and 140.24 mg g^{-1} for Pb, Fe, and Cu respectively were realized with low Cit-CS resin. For medium Cit-CS resin, corresponding values were obtained as 89.26, 74.6, 80.37 %, and 6.63, 65.91, and 215.51 mg g^{-1} for Pb, Fe, and Cu respectively. Also, for the high Cit-CS resin, corresponding values were obtained as 89.52, 74.73, 80.75 %, and 6.65, 66.03, 216.52 mg g^{-1} for Pb, Fe, and Cu respectively.

Similarly, the alteration of metal adsorption patterns with an alteration in adsorbent contact time for the Zn dominant solution has been shown in Fig. 5.5. The figure shows that the adsorption rate was fast upto 180 min and eventually approached equilibrium at 480 min for low Cit-CS resin resin and 420 min for medium and high Cit-CS resins. Thereby, a maximum removal efficacy and adsorption capacity of 51.12, 62.36, 70.50 %, and 124.54, 81.70, 2.36 mg g^{-1} for Zn, Fe, and Pb respectively were achieved for low Cit-CS resin. For medium Cit-CS resin, corresponding values were 62.65, 72.93, 79.69 %, and 174.45, 109.19, 3.02 mg g^{-1} for Zn, Fe, and Pb respectively. Also, for the high Cit-CS resin, corresponding values were 63.43, 72.63, 79.62 %, and 176.59, 108.73,

3.01 mg g^{-1} for Zn, Fe, and Pb respectively. These findings corroborate with the prior art-based inference for the CSPVA resin (Trikkaliotis et al., 2020).

For a fixed combination of other sorption process parameters (3.82, 25°C, 200 rpm for initial pH, temperature, and shaking speed respectively), contact time (480 min for low Cit-CS resin and 420 min for high and medium Cit-CS resins) and adsorbent dosage (1.8 g L^{-1} for low Cit-CS resin and 1.4 g L^{-1} for medium and high Cit-CS resins), the alteration of metal adsorption patterns with heavy metal ion concentration (187.7-563.1 mg L^{-1} for Cu, 61.85-185.55 mg L^{-1} for Fe, and 5.2-15.6 mg L^{-1} for Pb) has been shown in Fig. 5.6. For the Cu, adsorption capacity and removal efficiency varied as 81.68-166.42 mg g^{-1} and 78.33-53.20 % for low Cit-CS resin; 119.50-258.58 mg g^{-1} and 89.12-64.29 % for medium Cit-CS resin and 120.19-260.27 mg g^{-1} and 89.64-64.71 % for high Cit-CS resin for mentioned alteration in initial metal ion concentration. Similarly, for the Fe, adsorption capacity and removal efficiency varied as 27.90-51.86 mg g^{-1} and 81.19-50.31 % respectively for low Cit-CS resin; 37.70-74.31 mg g^{-1} and 85.33-56.06 % respectively for medium Cit-CS resin and 39.49-75.48 mg g^{-1} and 89.38-56.95 % respectively for high Cit-CS resin with respect to the mentioned alteration in the initial heavy metal ion concentration of the system. Also, for the Pb, adsorption capacity and removal efficiency varied as 2.51-5.03 mg g^{-1} and 87.05-58.01 % respectively for low Cit-CS resin; 3.42-7.43 mg g^{-1} and 92.12-66.64 % respectively for medium Cit-CS resin and 3.56-7.47 mg g^{-1} and 95.83-67.07 % respectively for high Cit-CS resin and for mentioned alteration in the initial metal ion concentration of the system.

Similarly, for a fixed choice of other adsorption process parameters (3.64, 25°C, 200 rpm for initial pH, temperature, shaking speed), contact duration (CT) (480 min for low Cit-CS resin and 420 min for medium and high Cit-CS resins) and AD (1.6 g L^{-1} for low Cit-CS resin and 1.4 g L^{-1} for medium and high Cit-CS resins), the alteration of metal adsorption patterns for an alteration in MC (194.9-584.7 mg L^{-1} for Zn, 2.65-7.95 mg L^{-1} for Pb, and 104.8-314.4 mg L^{-1} for Fe) has been

illustrated in Fig. 5.7. For the Zn, adsorption capacity and removal efficacy varied as 94.05-151.99 mg g^{-1} and 77.21-41.60 % respectively for low Cit-CS resin; 110.36-205.17 mg g^{-1} and 79.27-49.13 % respectively for medium Cit-CS resin and 117.38-206.62 mg g^{-1} and 84.32-49.47 % respectively for high Cit-CS resin with respect to the alteration in the MC. Similarly, for the Fe, adsorption capacity and removal efficacy varied as 57.91-113.46 mg g^{-1} and 77.36-50.52 % respectively for low Cit-CS resin; 61.85-122.37 mg g^{-1} and 82.63-54.49 % respectively for medium Cit-CS resin and 62.85-124.89 mg g^{-1} and 83.96-55.61 % respectively for high Cit-CS resin with respect to the MC alteration. Additionally, for the Pb, adsorption capacity and removal efficacy varied as 1.65-3.33 mg g^{-1} and 87.42-58.66 % respectively for low Cit-CS resin; 1.68-3.41 mg g^{-1} and 88.55-60.13 % respectively for medium Cit-CS resin and 1.80-3.62 mg g^{-1} and 95.09-63.69 % respectively for high Cit-CS resin with respect to the MC alteration.

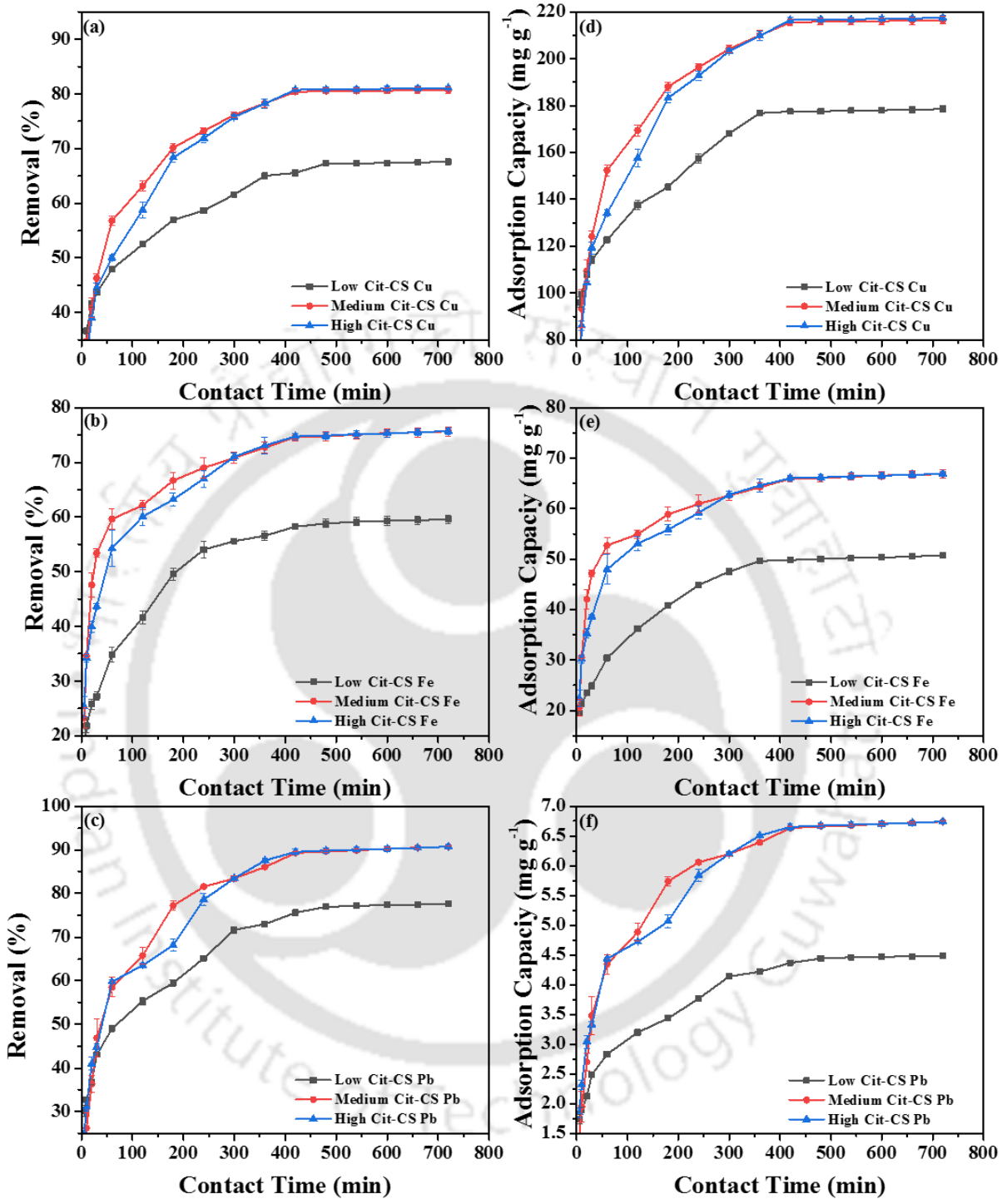

Fig. 5.4. Graphs depicting the influence of contact time on adsorption characteristics of Cit-CS derivatives and Cu dominant adsorbate system.

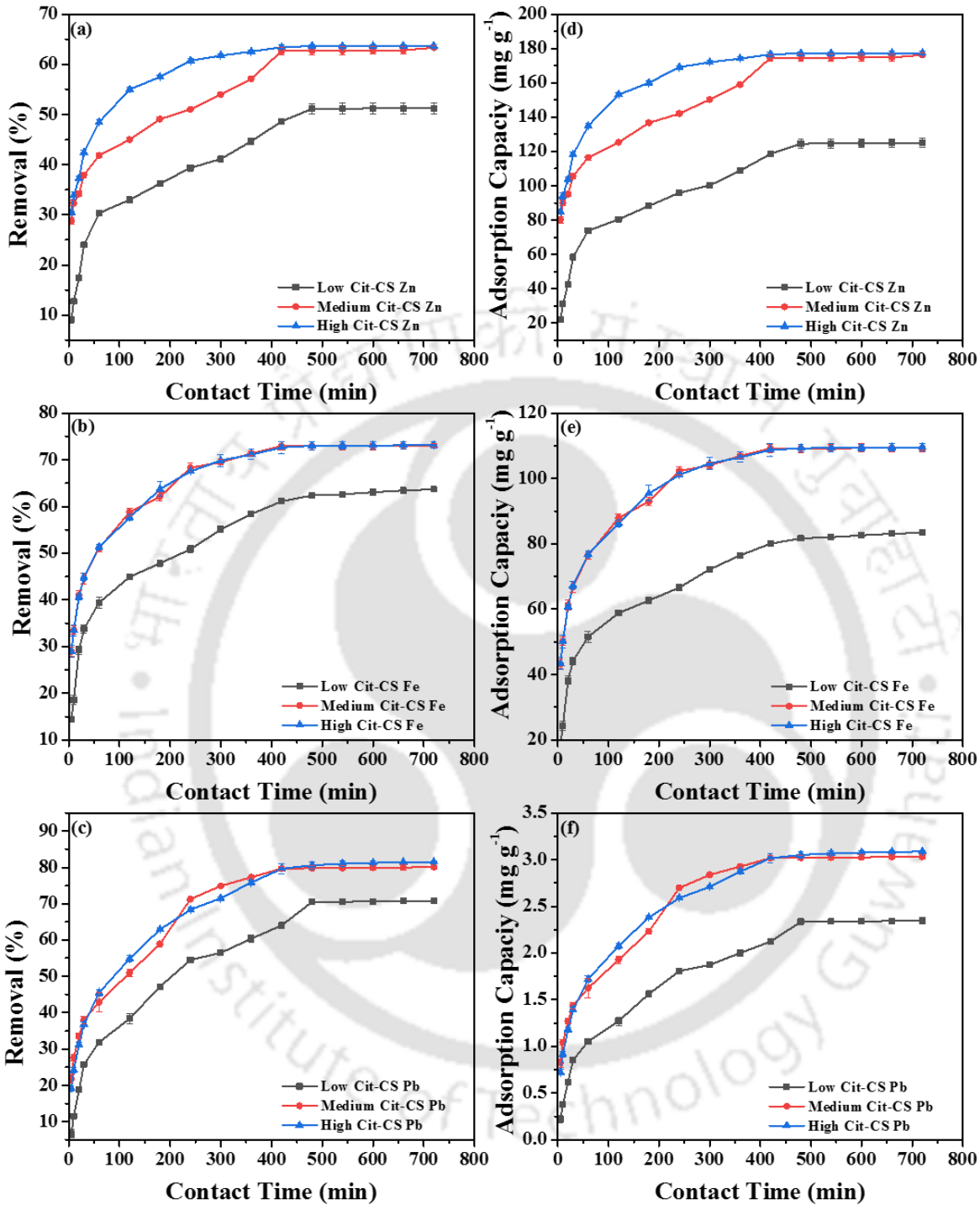

Fig. 5.5. Graphs depicting the influence of contact time on adsorption characteristics of Cit-CS derivatives and Zn dominant adsorbate system.

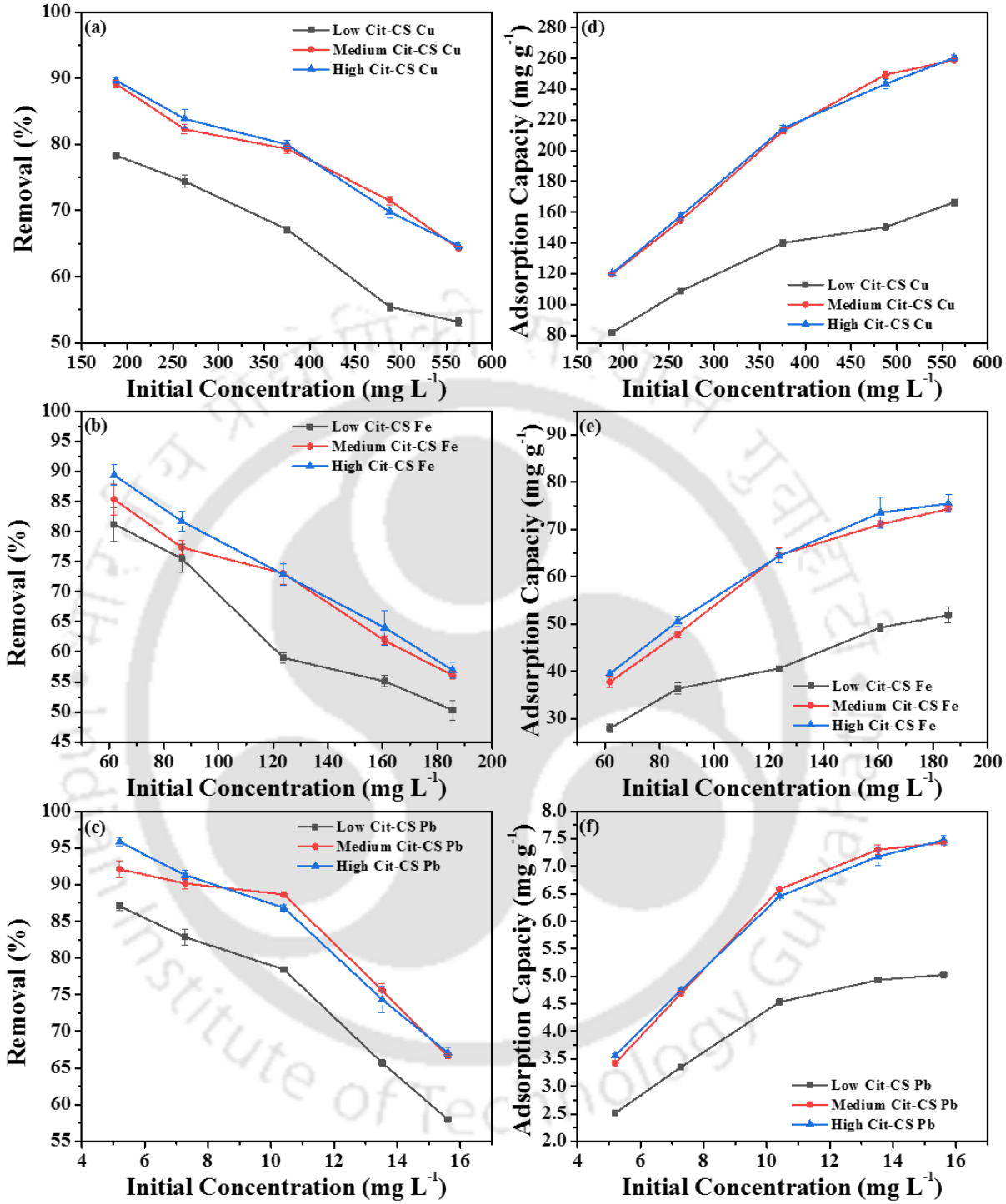

Fig. 5.6. Graphs depicting the influence of metal ion concentration on adsorption characteristics of Cit-CS derivatives and Cu dominant adsorbate system.

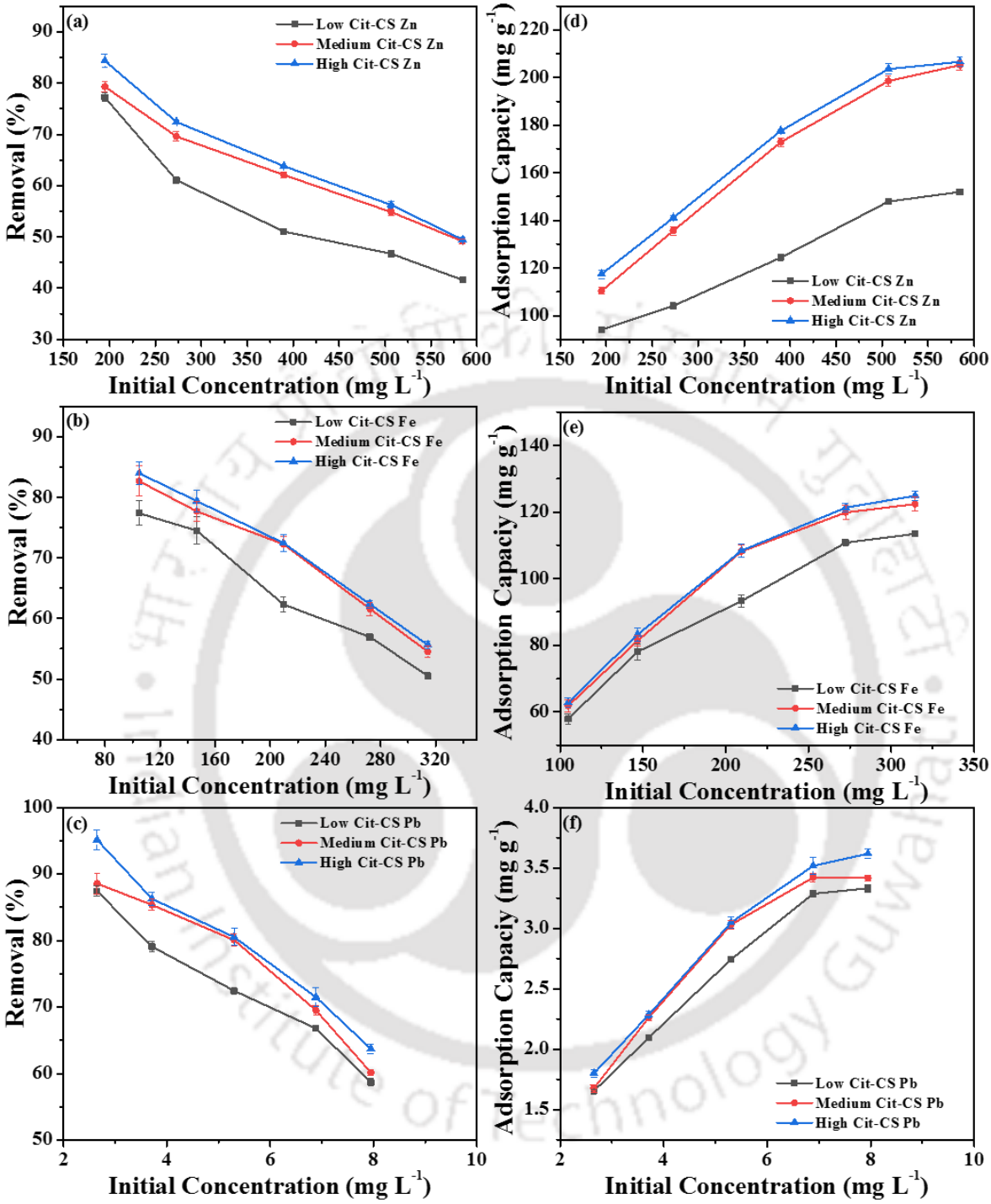

Fig. 5.7. Graphs depicting the influence of metal ion concentration on adsorption characteristics of Cit-CS derivatives and Zn dominant adsorbate system.

5.3.2 Fitness of alternate Equilibrium and kinetic models

In order to assess upon the pertinent mechanism of the Fe, Pb, and Cu sorption process, the Langmuir isotherm model was deployed to examine its fitness with the batch equilibrium sorption dataset (Fig. 5.8a–c). Thereby, the findings conveyed monolayer metal sorption onto the sorbent active sites. Furthermore, the findings were also evaluated with the Freundlich isotherm model (Fig. 5.8d-f) that hypothesizes multilayer metal sorption due to heterogeneous surfaces with uniform energy. Since Langmuir isotherm offered the best response for the measured dataset, monolayer adsorption has been inferred to best represent the adsorption mechanism. Table 5.1 summarizes equilibrium model parameter values for the sorption of Cu, Pb, and Fe onto Cit-CS derivatives.

Table 5.1: Regressed model parameters representing heavy metal adsorption equilibrium data of Cit-CS derivatives and Cu dominant adsorbate system.

Cit-CS derivatives	Langmuir isotherm variables				Freundlich isotherm variables		
	Q_o (mg g^{-1})	b (L mg^{-1})	R^2	R_L	K_f	n	R^2
Cu							
Low Cit-CS	196.08	0.018	0.99	0.09-0.23	23.12	2.8	0.95
Medium Cit-CS	312.5	0.026	0.99	0.06-0.17	40.15	2.75	0.96
High Cit-CS	303.03	0.03	0.99	0.06-0.15	45.06	2.95	0.97
Fe							
Low Cit-CS	58.82	0.067	0.98	0.07-0.2	14.45	3.57	0.95
Medium Cit-CS	86.21	0.078	0.99	0.06-0.17	19.03	3.12	0.96
High Cit-CS	84.03	0.11	0.99	0.05-0.13	19.78	3.13	0.97
Pb							
Low Cit-CS	5.69	1.29	0.99	0.004-0.012	3.07	3.27	0.90
Medium Cit-CS	8.18	2.16	0.99	0.002-0.007	5.09	3.44	0.83
High Cit-CS	7.94	2.96	0.99	0.002-0.005	5.35	4.17	0.95

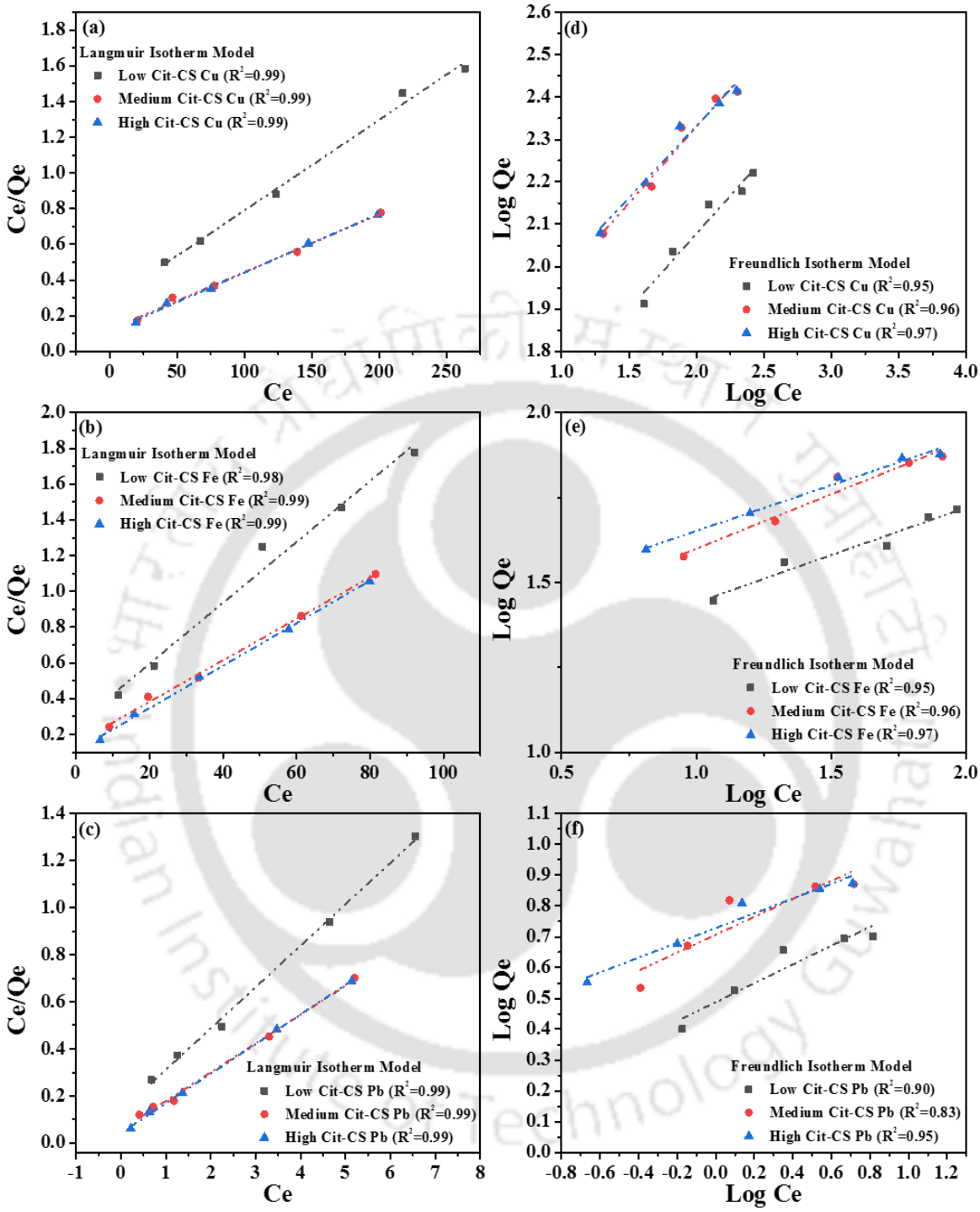

Fig. 5.8. Equilibrium models fitness plots (a-c: Langmuir isotherm model and d-f: Freundlich isotherm model) for Cit-CS derivatives and Cu dominant adsorbate system.

In order to assess upon the equilibrium characteristics of the resin-based Zn, Pb, and Fe sorption process, the Langmuir isotherm model was considered to examine the batch equilibrium sorption dataset. The isotherm postulates monolayer metal sorption onto the sorbent active sites. Relevant findings have been depicted in Fig. 5.9a-c. Furthermore, the findings were also evaluated using the Freundlich isotherm model which hypothesizes multilayer metal sorption based on the uniform energy surface heterogeneity. These findings have been depicted in Fig. 5.9d-f. Since Langmuir isotherm provided the best fit for the data collected monolayer adsorption has been assumed to represent the relevant mechanism (for Zn, Pb, and Fe sorption). Table 5.2 summarises the equilibrium model fit parametric data for the sorption of Zn, Pb, and Fe onto Cit-CS derivatives.

Table 5.2: Regressed model parameters representing heavy metal adsorption equilibrium data of Cit-CS derivatives and Zn dominant adsorbate system.

Cit-CS derivatives	Langmuir parameters				Freundlich parameters		
	Q_o (mg g^{-1})	b (L mg^{-1})	R^2	R_L	K_f	n	R^2
			Zn				
Low Cit-CS	175.44	0.017	0.98	0.09-0.23	34.79	4.0	0.93
Medium Cit-CS	243.90	0.017	0.99	0.09-0.23	32.82	3.06	0.98
High Cit-CS	232.56	0.025	0.99	0.06-0.17	46.39	3.74	0.97
			Fe				
Low Cit-CS	136.99	0.032	0.99	0.09-0.23	20.60	2.89	0.94
Medium Cit-CS	144.93	0.043	0.99	0.07-0.18	24.73	2.97	0.91
High Cit-CS	144.93	0.047	0.99	0.06-0.17	26.52	3.06	0.93
			Pb				
Low Cit-CS	3.23	1.774	0.99	0.06-0.10	2.36	3.03	0.97
Medium Cit-CS	3.86	2.850	0.99	0.04-0.06	2.64	3.26	0.88
High Cit-CS	3.93	3.820	0.99	0.03-0.05	2.89	4.19	0.96

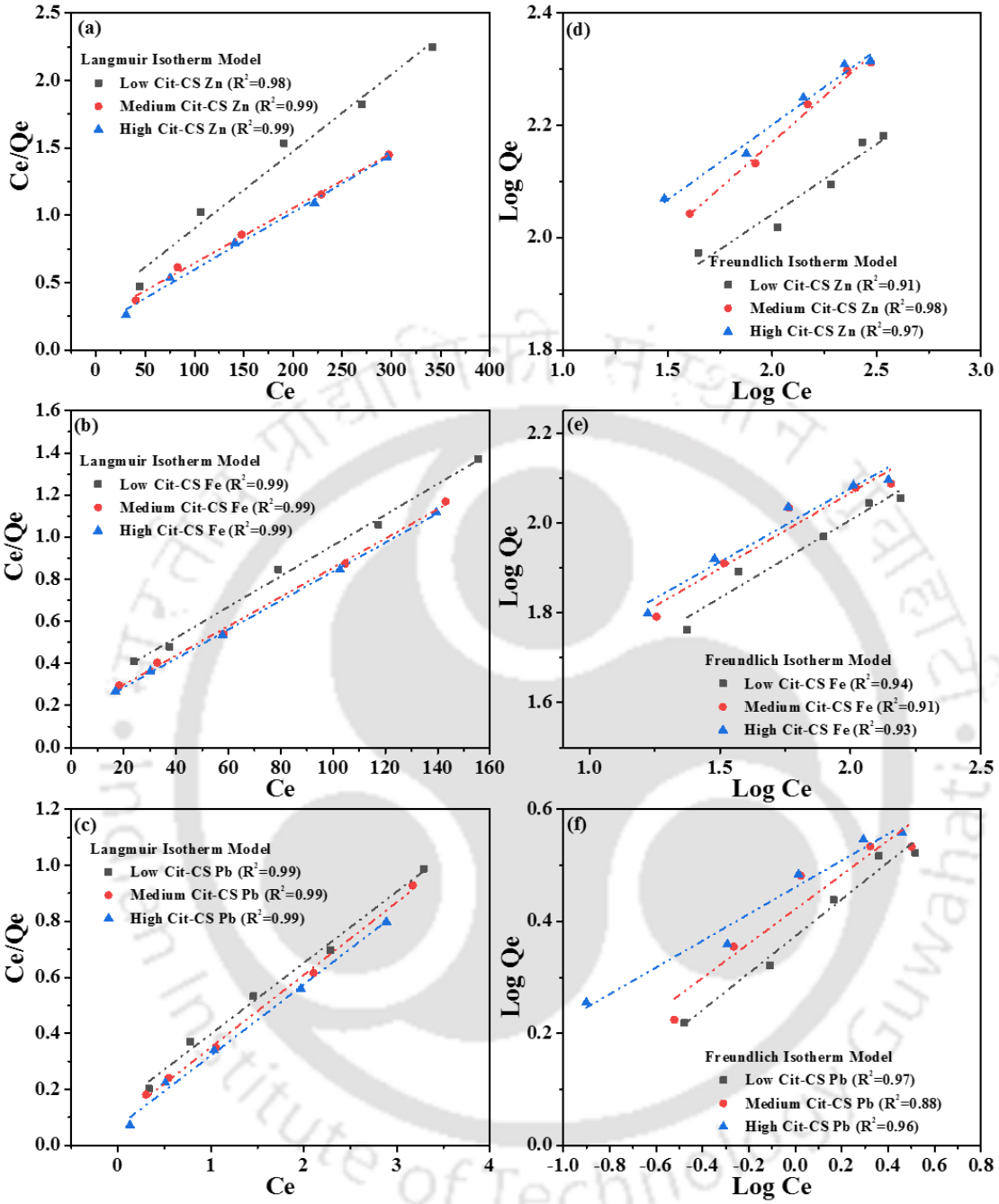

Fig. 5.9. Equilibrium models fitness plots (a-c: Langmuir isotherm model and d-f: Freundlich isotherm model) for Cit-CS derivatives and Zn dominant adsorbate system.

In order to assess upon Cu, Pb, and Fe sorption kinetics of Cit-CS derivative variants, the fitness plots for alternate kinetic models were prepared (Fig. 5.10). Thereby, among all models, the pseudo-second-order model was identified to be the best to represent kinetics data associated to

Pb, Cu, and Fe sorption onto Cit-CS resin. Table 5.3 summarizes the kinetic model parameters for all Cit-CS resins and for Pb, Cu, and Fe cases.

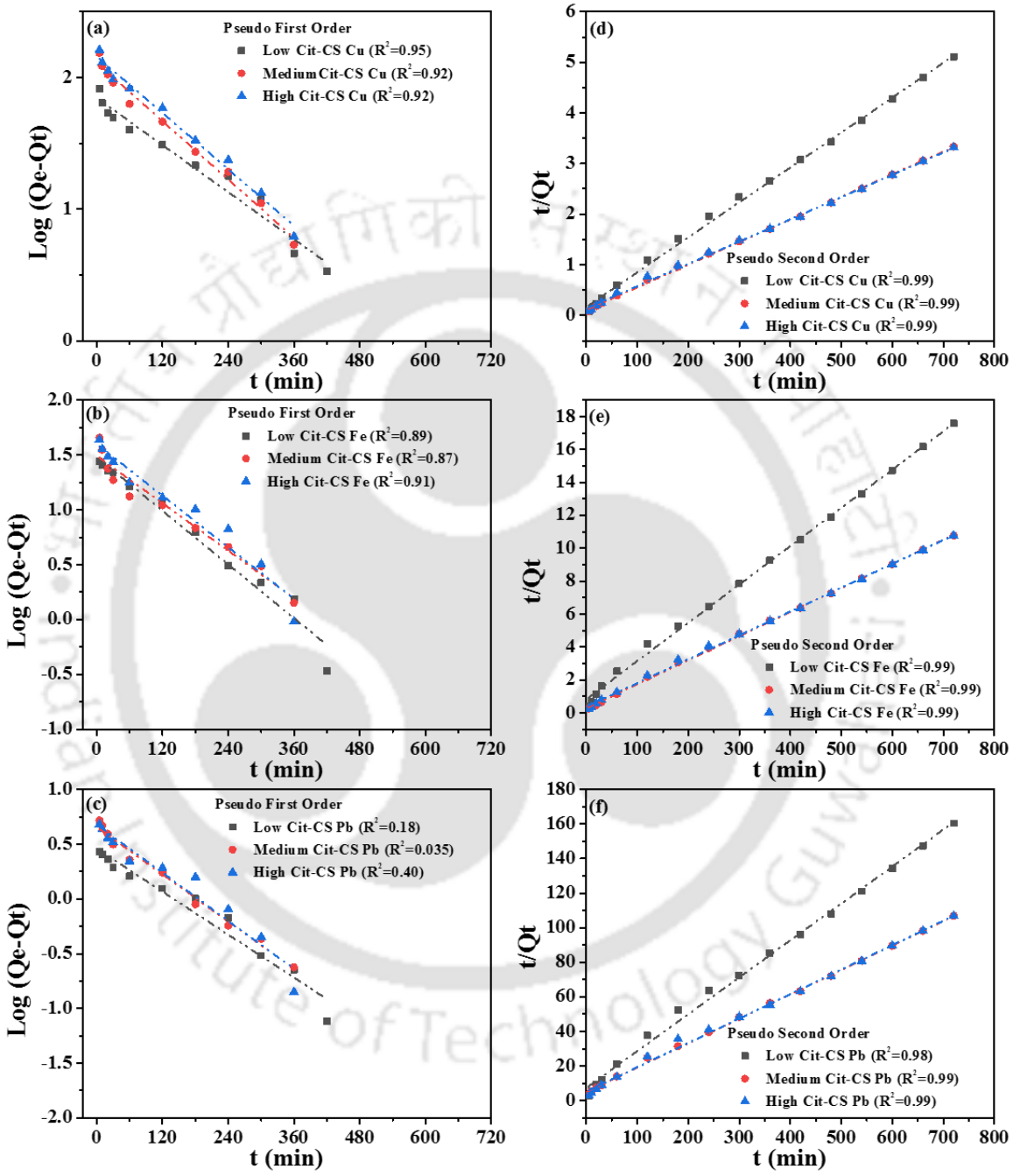

Fig. 5.10. Kinetic models fitness plots (a-c: Pseudo-first-order kinetic model, and d-f: Pseudo-second-order kinetic model) for Cit-CS derivatives and Cu dominant adsorbate system.

Table 5.3: Regressed model parameters representing heavy metal adsorption kinetic data of Cit-CS derivatives and Cu dominant adsorbate system.

Experimental capacity (Q_{exp}, mg g^{-1})	Cit-CS derivatives	Pseudo-first-order model			Pseudo-second-order model		
		Q_e (mg g^{-1})	K_1 (min^{-1})	R^2	Q_e (mg g^{-1})	K_2 (g mg^{-1} min^{-1})	R^2
Cu							
140.24	Low Cit-CS	66.81	0.0067	0.95	144.93	0.00029	0.99
215.51	Medium Cit-CS	103.15	0.0078	0.92	222.22	0.00019	0.99
216.52	High Cit-CS	130.23	0.0080	0.93	227.27	0.00014	0.99
Fe							
40.42	Low Cit-CS	20.96	0.0053	0.89	43.69	0.0006	0.99
65.91	Medium Cit-CS	21.50	0.0055	0.87	68.03	0.0008	0.99
66.03	High Cit-CS	28.56	0.0058	0.91	69.44	0.0006	0.99
Pb							
4.44	Low Cit-CS	2.66	0.0025	0.18	4.64	0.0065	0.99
6.63	Medium Cit-CS	2.44	0.0021	0.35	7.09	0.0039	0.99
6.65	High Cit-CS	2.61	0.0023	0.40	7.13	0.0038	0.99

Table 5.4: Regressed model parameters representing heavy metal adsorption kinetic data of Cit-CS derivatives and Zn dominant adsorbate system.

Experimental capacity (Q_{exp}, mg g^{-1})	Cit-CS derivatives	Pseudo-first-order model			Pseudo-second-order model		
		Q_e (mg g^{-1})	K_1 (min^{-1})	R^2	Q_e (mg g^{-1})	K_2 (g mg^{-1} min^{-1})	R^2
Zn							
124.54	Low Cit-CS	105.90	0.0074	0.92	133.33	0.00013	0.99
174.45	Medium Cit-CS	103.39	0.0076	0.89	181.82	0.00017	0.99
176.59	High Cit-CS	59.27	0.0071	0.91	181.81	0.00035	0.99
Fe							
81.70	Low Cit-CS	51.02	0.0006	0.94	87.72	0.0003	0.99
109.19	Medium Cit-CS	45.13	0.0067	0.91	112.36	0.0004	0.99
108.73	High Cit-CS	43.92	0.0067	0.91	113.64	0.0004	0.99
Pb							
2.33	Low Cit-CS	1.21	0.009	0.15	2.61	0.0045	0.98
3.02	Medium Cit-CS	1.11	0.009	0.07	3.21	0.0075	0.99
3.01	High Cit-CS	1.17	0.009	0.09	3.29	0.0067	0.99

In order to determine and assess upon Zn, Pb, and Fe sorption kinetics of the Cit-CS derivative variants, fitness plots were prepared for two well-known kinetic models and have been depicted in

Fig. 5.11. Among all models, the Pseudo-second-order model was identified to provide the best fit to characterize the kinetics of Pb, Zn, and Fe sorption onto Cit-CS resin from the Zn dominant adsorbate system. For both models, Table 5.4 summarizes the kinetic parametric dataset for Pb, Zn, and Fe sorption.

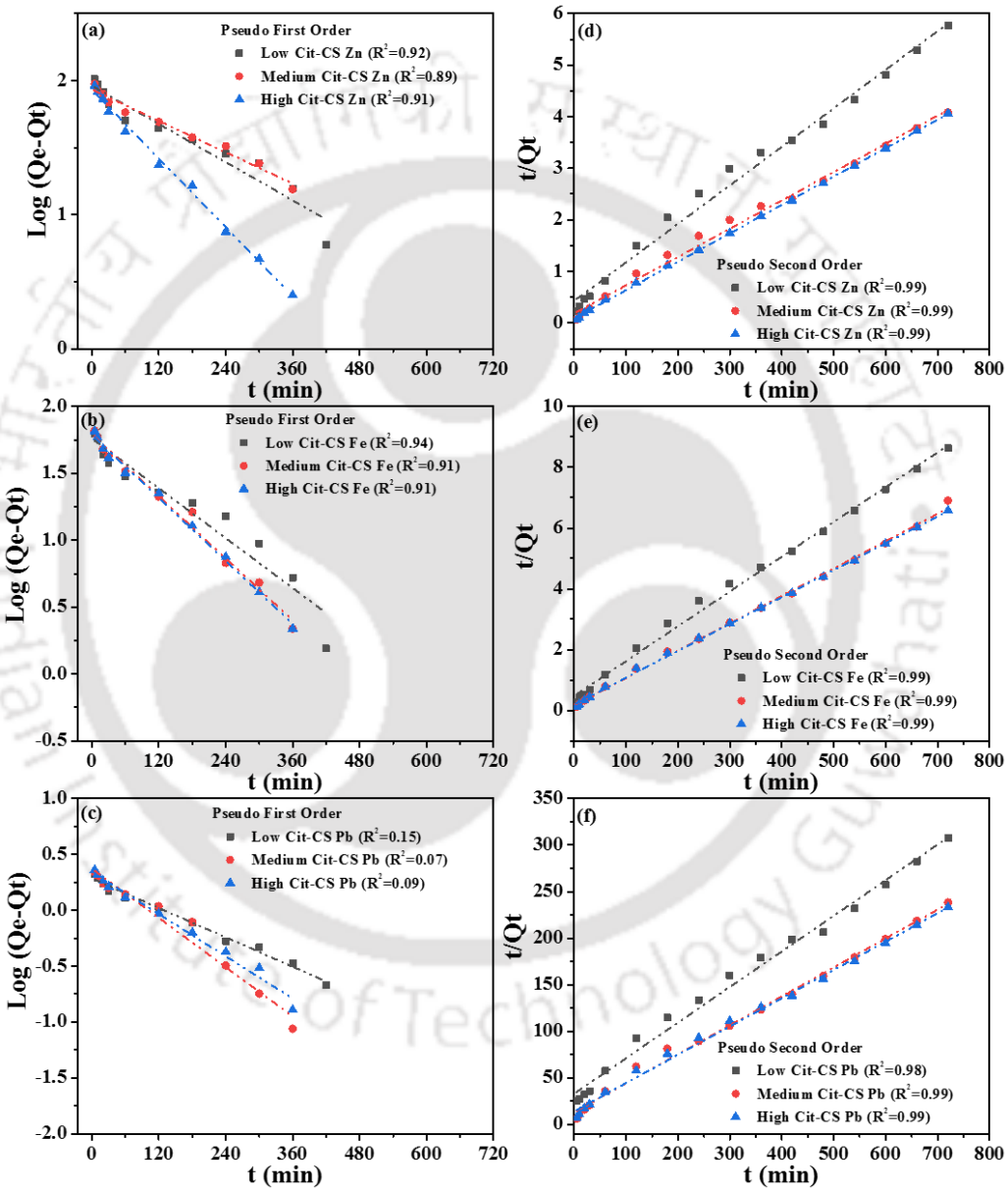

Fig. 5.11. Kinetic models fitness plots (a-c: Pseudo-first-order kinetic model, and d-f: Pseudo-second-order kinetic model) for Cit-CS derivatives and Zn dominant adsorbate system.

Isotherm models have been targeted to analyze the adsorption of studied heavy metal ions onto the surface of citric acid-chitosan derivative (low Cit-CS, medium Cit-CS, high Cit-CS) and at a constant temperature. Langmuir Isotherm model has been the best-fit isotherm model. It is based on the assumption that adsorption occurs at specific sites on the adsorbent surface, and once a site is occupied by an adsorbate molecule, no further adsorption can take place at that site. Also, the pseudo-second-order model has been inferred to be the best-fit model to represent the kinetics of studied heavy metal ions adsorption from Cu and Zn dominant adsorbate systems and onto citric acid-chitosan derivative (low Cit-CS, medium Cit-CS, high Cit-CS). Thus, the model's basic assumption stated as follows is valid. The rate-limiting step could be the chemisorption involving valency forces through the sharing or exchange of electrons with the prevalent functional groups of the citric acid-chitosan derivative resin. The fitness of the pseudo-second-order model is also justified with the FTIR analysis of metal-adsorbed citric acid-chitosan derivative that inferred strong metal ions chemical interaction with the prevalent functional groups of the citric acid-chitosan derivative resin.

5.4 Analytical characterization

5.4.1 Thermo gravimetric Analysis

Fig. 5.12 illustrates the TGA curve for medium molecular weight chitosan and medium Cit-CS derivative. As shown in Fig. 5.12a, significant weight loss (10.5 %) occurred in the chitosan below 150 °C and this was due to free water loss. However, the weight remained fairly constant upto 250 °C. Thereby, significant weight loss occurred upto 700 °C (66.9 % of total weight loss). In summary, for the medium Cit-CS resin, the total weight loss corresponds to 71.9 % and thereby confirmed almost similar thermal stability of the resin in comparison with the chitosan.

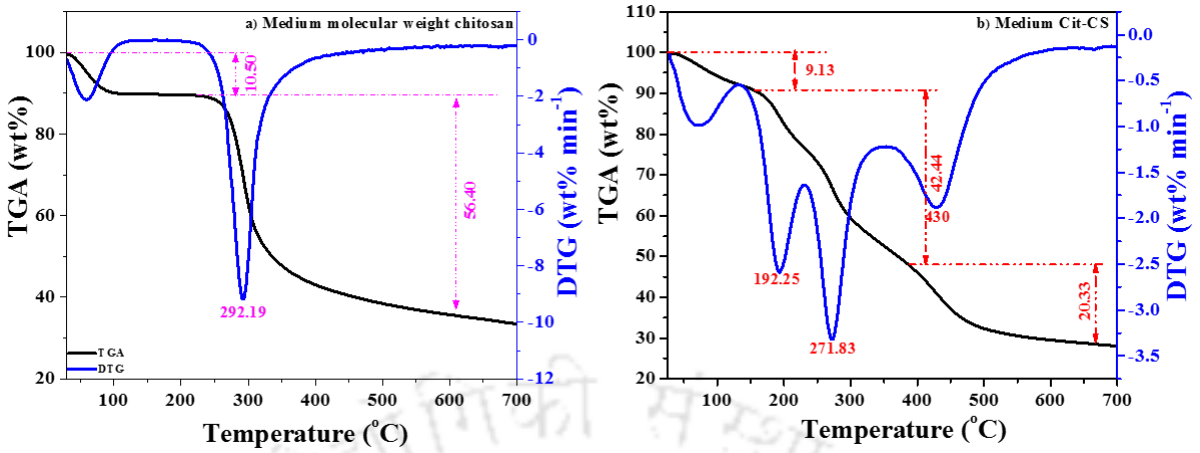

Fig. 5.12: TGA spectra of raw samples of medium molecular weight chitosan and raw medium Cit-CS derivative resin.

5.4.2 BET Surface Area Analysis

For the raw sample of the medium molecular weight chitosan, the BET surface area was 21.45 m^2 g^{-1}. For the medium Cit-CS sample, the BET surface area was 60.94 m^2 g^{-1}. Thus, the structural modification of chitosan with citric acid has been apparent in the pertinent alterations. Thereby, an increment in the surface area has been evident in the medium Cit-CS resin.

5.4.3 Crystallinity Analysis

Fig. 5.13 illustrates the X-ray diffraction patterns of the raw sample of medium molecular weight chitosan, citric acid, the raw sample of medium Cit-CS derivative, and metal sorbed medium Cit-CS derivative. Corroborating with the recent literature findings, the XRD results for medium molecular weight chitosan (Fig. 5.13a) reveal significant and prominent peaks at 9.18 and 20.19° and a greater degree of crystallinity. This has been attributed to the prevalent hydroxyl and amino groups. Both groups provided stronger intramolecular and intermolecular hydrogen bonds (Nagireddi et al., 2019). Further, the XRD pattern of citric acid (Fig. 5.13b) with various strong peaks affirmed a greater degree of crystallinity. The citric acid alteration resulted in a varied Cit-CS derivative's XRD pattern (Fig. 5.13c). Thereby, it confirmed upon a reduced crystallinity or

greater amorphiety. Also, the same resin structure had even greater amorphiety due to the sorption of the heavy metal ions onto the Cit-CS derivative surface (Fig. 5.13d).

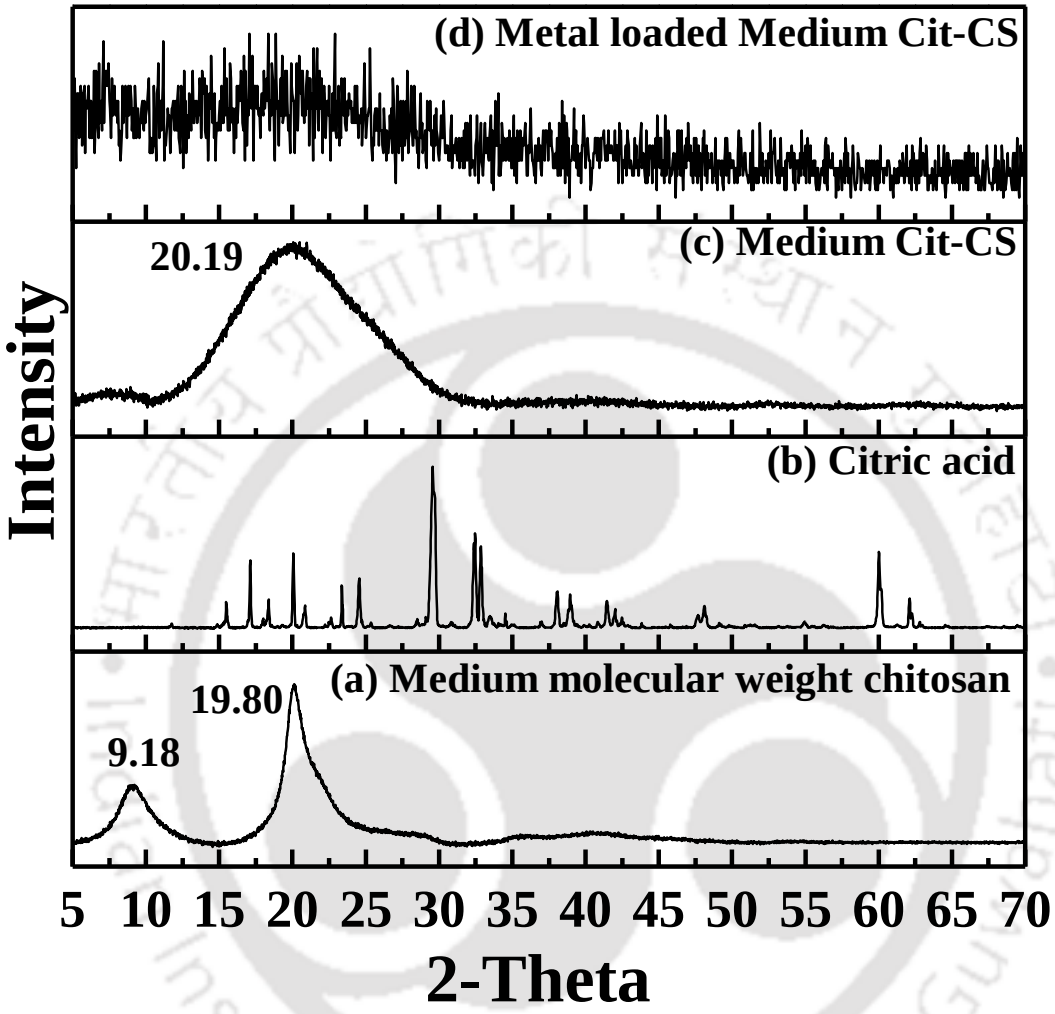

Fig. 5.13: XRD spectra of raw samples of medium molecular weight chitosan and raw medium Cit-CS derivative resin.

5.4.4 FTIR Analysis

The FTIR spectra of medium molecular weight chitosan, glutaraldehyde crosslinked chitosan, and glutaraldehyde crosslinked citric acid grafted chitosan (Cit-CS) have been illustrated in Fig. 5.14. In Fig. 5.14a, a band around 3390 cm^{-1} can be seen. This is due to –NH and hydroxyl groups. Also, the peak at 2910 cm^{-1} has been attributed to the CH_3 symmetrical stretching. Similarly, a peak at

1642 cm^{-1} corroborates with the C-N stretching vibration of amide I. The peak at 1367 cm^{-1} is due to the CH_3 bending vibration and a peak at 1142 cm^{-1} is due to the C-O-C bending vibration. The C-OH stretching is associated to the peak at 1069 cm^{-1}. The FTIR spectra of glutaraldehyde crosslinked chitosan (Fig. 5.14b) affirm that the peak at 1642 cm^{-1} was shifted to 1652 cm^{-1} and the peak at 1596 cm^{-1} was shifted to 1560 cm^{-1}. Thereby, these peak shifts convey glutaraldehyde crosslinking (Nagireddi et al., 2017; Suc and Ly, 2013). The intensity of the peaks at 1380 cm^{-1}, 1584 cm^{-1}, and 1637 cm^{-1} (Fig. 5.14c) convey carboxylic groups in the Cit-CS resin (Suc and Ly, 2013). The band at 1380 cm^{-1} corresponds to the carboxylic group of the Cit-CS resin. However, after metal adsorption, the peaks weakened and shifted to 1392 cm^{-1} (Fig. 5.14d). This confirms upon the emergence of new bonds between the carboxyl group and adsorbed heavy metal ions.

5.4.5 EDX Analysis

The FESEM and EDX spectra of raw and metal-loaded medium Cit-CS resin samples have been presented in Fig. 5.15. The EDX trends (Fig. 5.15a) confirmed upon the presence of C (51.4%), O (42.3%), and N (6.3%) in the raw medium Cit-CS derivative samples. The medium Cit-CS derivative with metal ions demonstrated a considerable presence of various metals namely Cu (1.2%), Fe (1.1%), and Pb (8.3%) on the medium Cit-CS resin surface (Fig. 5.15b) and Zn (1.2%), Fe (2.2%) and Pb (10.7%) on the medium Cit-CS resin surface (Fig. 5.15c).

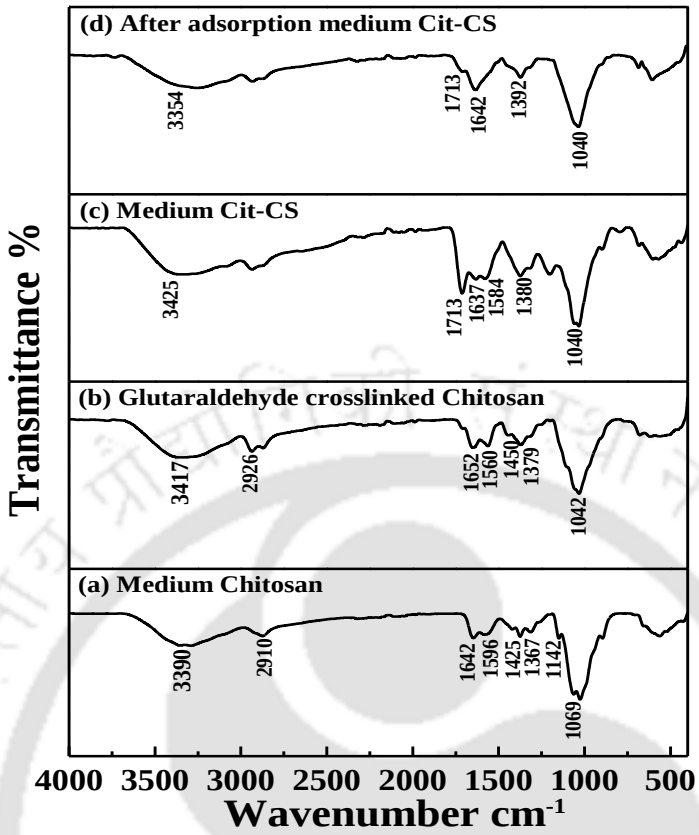

Fig. 5.14. FTIR spectra of raw and heavy metal loaded medium Cit-CS derivative resin samples.

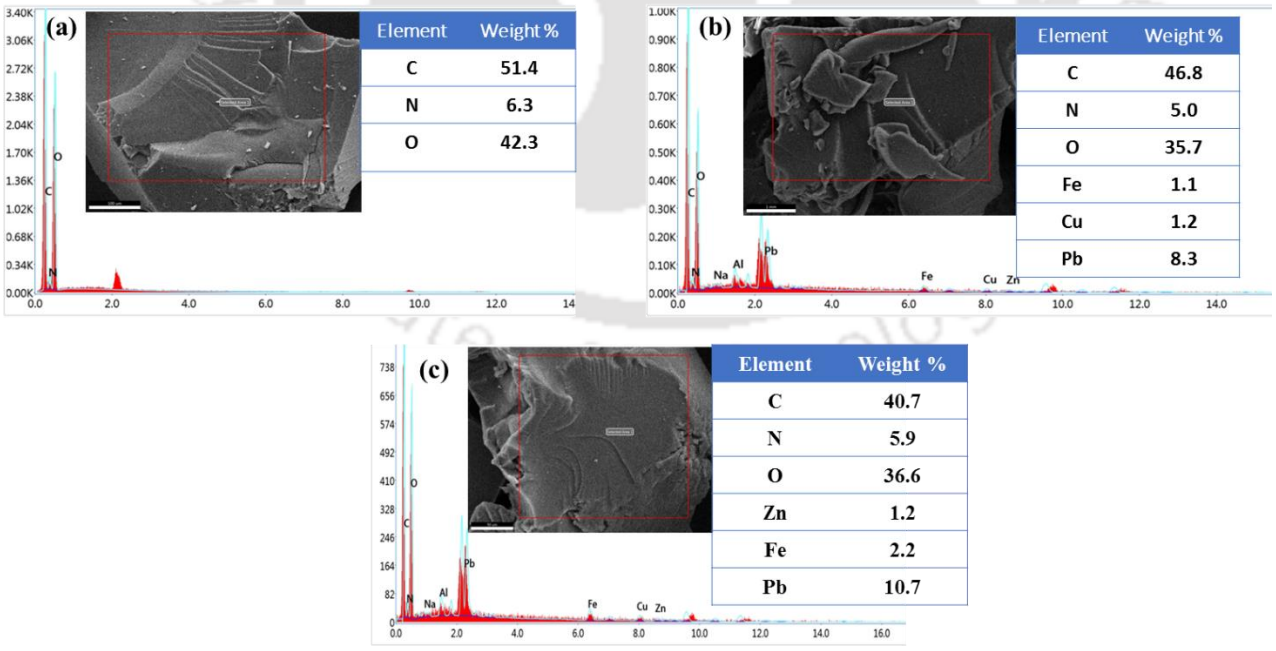

Fig. 5.15. FESEM-EDX spectra of raw and heavy metals loaded medium Cit-CS derivative resin samples.

5.5 Cyclic Multi-Heavy Metal Desorption Characteristics

The reusability and desorption efficiency of Cit-CS resin were examined to analyze the performance of the chitosan derivative as a low-cost and effective material for reversible adsorption technology. Adsorption experiments confirmed that the medium Cit-CS and high Cit-CS resins were better in comparison to low Cit-CS resins. Also, the regenerative ability of medium Cit-CS resin with easy-to-use and low-cost eluents (such as H_2SO_4, HNO_3, HCl, NaOH, and KOH in the broader range of concentrations (0.1-2M)) as well demonstrated effective desorptive performances.

For the Cu dominant solution and for the 2 M HCl eluent case, the desorption performances were the best for the simulated wastewater system. Thereby, the Cu desorption performance altered as 78.69-58.9% for a cycle number range from 1-3. Similarly, corresponding desorption performances of Fe varied as 75.31-53.78% and corresponding Pb desorption performance ranged as 69.63-49.40%. The order of eluent-based heavy metal desorption efficiencies was as follows: HCl > HNO_3 > H_2SO_4. Consequently, both cycle desorption efficiency and overall metal sorption efficacies decreased significantly for the later and consecutive cycles.

Desorption efficacies were comparatively lower for the basic solutions (0.1-2M). For KOH and NaOH, cycle efficiencies respectively varied as 39.46-23.02% and 36.65-16.28% for 1-3 cycles. Similarly, the desorption performances of Fe for KOH and NaOH have been respectively obtained as 28.69-20.43% and 32.82-21.67% for 1-3 cycles. Also, the respective desorption performances of Pb for KOH and NaOH were 41.39-37.88% and 42.19-39.10% respectively 1-3 cycles. Consequently, both cycle desorption and overall metal desorption-based performances decreased significantly in consecutive cycles. For the medium Cit-CS resin, the adsorption capacity, adsorptive removal (%), and cyclic desorption removal (%) have been illustrated in Fig. 5.16. For

Cu, Pb, and Fe, the cyclic desorption % reduced from 78.69-58.9%, 75.31-53.78%, and 69.63-49.40% respectively for a cycle number alteration from 1 to 3. Corresponding adsorption removal trends were 80.25-64.56%, 74.08-48.80%, and 88.65-63.17%. Hence, cyclic adsorption had a detrimental influence on Fe and Pb removal but not on Cu. Thereby, the observation conveyed that while iron and lead exhibited more irreversible chemisorption, copper did not. Furthermore, the adsorption capacity reduced from 215.19-173.12 mg g^{-1}, 65.46-43.11 mg g^{-1}, and 6.59-4.69 mg g^{-1}, respectively for a cycle number alteration from 1 to 3.

Similarly, for the Zn dominant solution and 2M HCl eluent case, the desorption performances were the best for the simulated wastewater system. Thereby, the Zn desorption performances ranged as 75.65-57.76% for the 1-3 desorption cycle range. Similarly, the corresponding desorption performances of Fe varied as 79.14-58.35% and the corresponding Pb desorption performance ranged as 68.59-49.83%. The order of eluent-based heavy metal desorption efficiencies was as follows: HCl > H_2SO_4 > HNO_3. Consequently, both cycle desorption efficiency and overall metal adsorption efficiencies decreased significantly in the consecutive cycles.

Desorption efficiencies were comparatively lower for the basic solutions (0.1-2M). For KOH and NaOH, cycle efficiencies respectively varied as 37.60-25.72% and 34.94-24.63% for 1-3 desorption cycle range. Similarly, the desorption performances of Fe for KOH and NaOH have been respectively obtained as 39.45-20.21% and 36.65-19.72% for 1-3 cycles. Also, the respective desorption performances of Pb for KOH and NaOH were 27.61-17.45% and 25.87-16.54% for 1-3 cycles. Consequently, both cycle desorption and overall metal desorption removal indices decreased significantly in consecutive cycles. For the medium Cit-CS resin, the adsorption capacity, adsorptive removal (%), and cyclic desorption (%) have been illustrated in Fig. 5.17. For Zn, Pb, and Fe, the cyclic desorption % respectively decreased from 75.65-57.76%, 79.14-58.35%, and 68.59-49.83% for 1-3 cycles. In addition, the associated respective adsorption removal

was 63.12-46.46%, 71.54-49.14%, and 81.70-66.79%. Hence, cyclic adsorption had a detrimental influence on iron and zinc removal but not lead. Thereby, the observation conveyed that both Fe and Zn but not Pb exhibited better irreversible chemisorption. Furthermore, the adsorption capacity decreased from 175.74-129.56 mg g^{-1}, 107.10-73.56 mg g^{-1}, and 3.09-2.53 mg g^{-1}, respectively for the 1-3 cycles. Thus, it can be confirmed that the adsorption capacity reduced naturally with repetitive phases of adsorption-desorption cycles. Thus, as expected, the adsorption capacity reduced with increasing number of adsorption-desorption cycles.

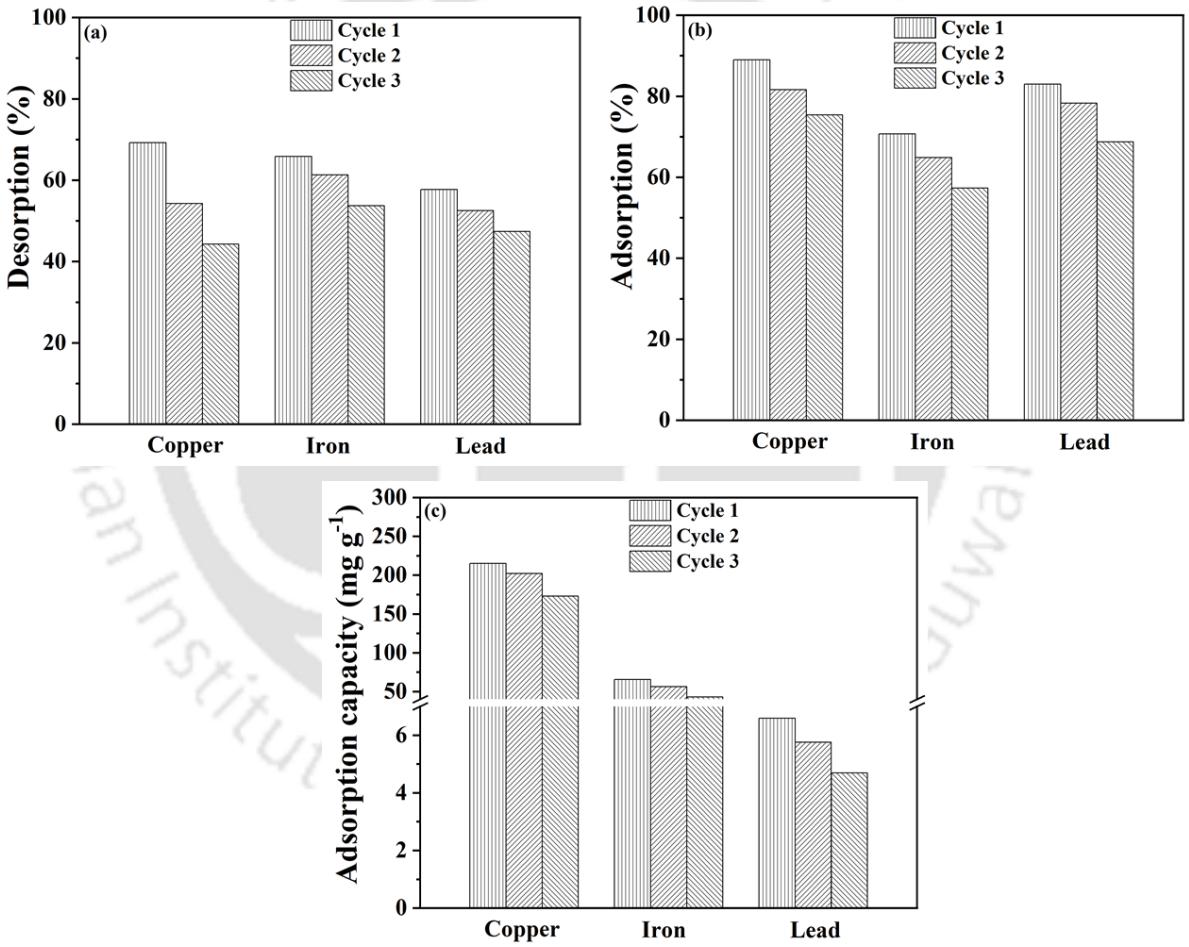

Fig. 5.16. Multi-heavy metal cyclic performance characteristics of medium Cit-CS derivative resin with Cu dominant adsorbate system (a) desorption % (b) adsorption % and (c) adsorption capacity.

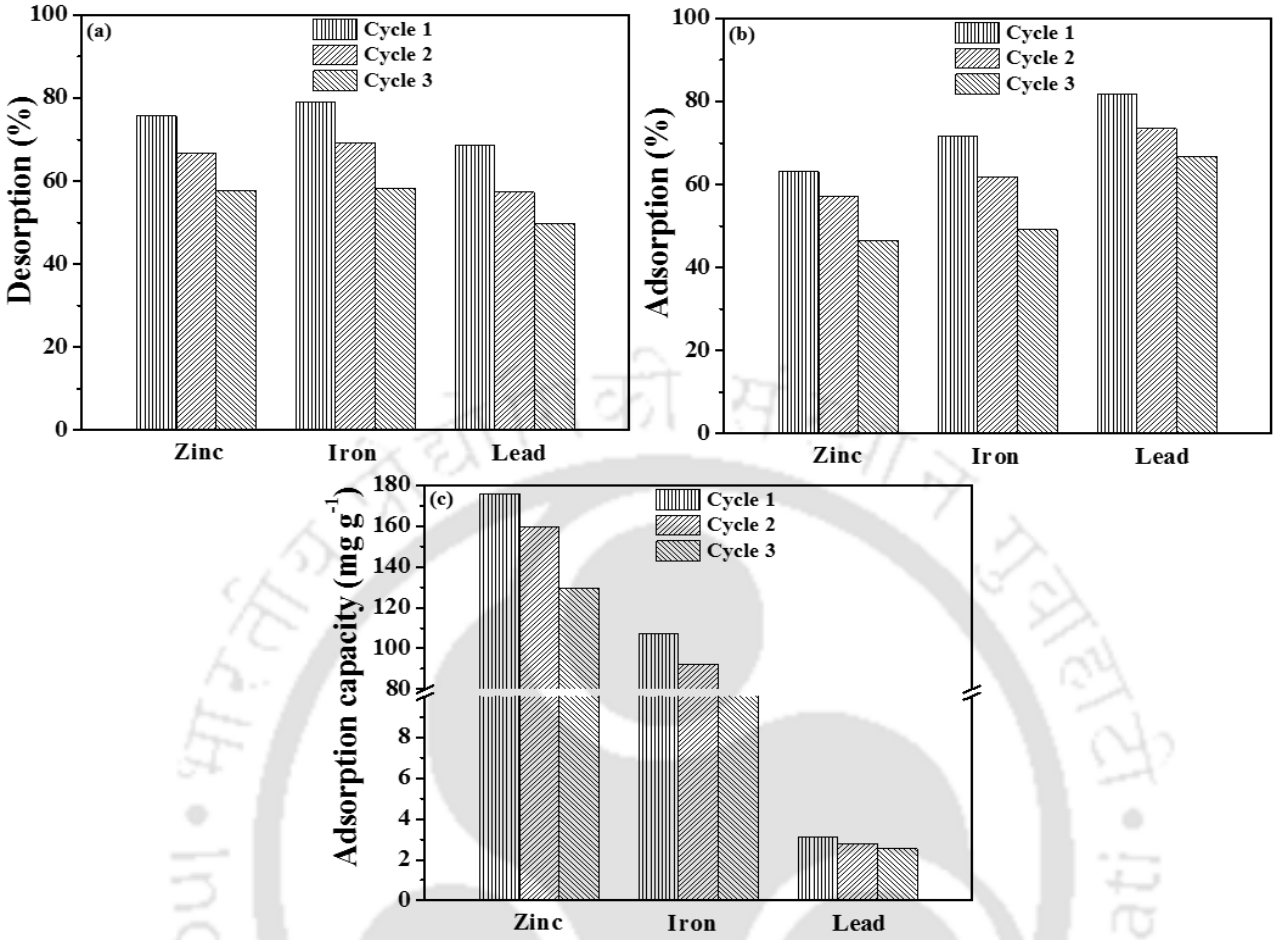

Fig. 5.17. Multi-heavy metal cyclic performance characteristics of medium Cit-CS derivative resin with Zn dominant adsorbate system (a) desorption % (b) adsorption % and (c) adsorption capacity.

In summary, after 3rd desorption cycle, 58.9%, 53.78%, and 49.40% removal for Cu, Fe, and Pb, respectively were obtained for the Cu dominant solution and 57.76%, 58.35%, and 49.83% removal for Zn, Fe, and Pb, respectively were obtained for the Zn dominant solution. These values convey satisfactory performance even in the presence of co-existent cations. Consequently, the results demonstrated that the medium Cit-CS derivative may perform more successfully in a modified adsorption method that emphasizes on the increased removal of Pb and Cu through a pre-treatment technique. Alternately, the functional role of the constituent cations can be investigated.

However, theoretical and conceptual cost assessment in terms of resin expenditure per unit mol of total heavy metal elimination provides useful inferences due to their relevant insights on sustainable operation. This can be addressed by our group of researchers in the near future. Relatively lower operating costs and applicability for commercial processes may be apparent for the Cit-CS resin due to its ability to renew itself with excellent desorption performances up to the 3rd cycle. Hence, Cit-CS resin can be considered as a trustworthy and recyclable adsorbent for the treatment of effluent systems polluted with mentioned toxic heavy metals.

Fig. 5.18 depicts the proposed desorption mechanism of exhausted medium Cit-CS derivative resin. Eluent solution would provide free H^+ ions for their reaction with the medium Cit-CS adsorbent exhausted adsorption sites. Accordingly, the adsorbed multi-heavy metal ions were released from the spent sorbent surface. However, to validate the hypothesis, additional insights are necessary from further characterization such as FTIR, EDX, and XRD analysis of the regenerated adsorbent. Such studies were beyond the scope of the Ph.D. thesis that primarily aims to screen and scope upon the competence of chitosan derivatives for cyclic desorption-based multi-heavy metal removal from complex adsorbate systems. However, these could be addressed in the near future.

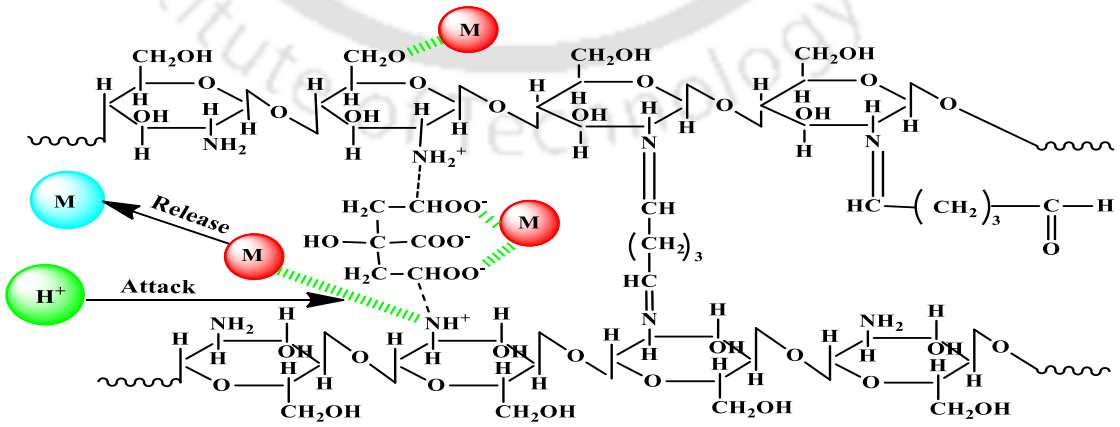

Fig. 5.18. Proposed desorption mechanism of heavy metals loaded medium Cit-CS resin.

5.6 Literature Comparison

The experimental findings with respect to optimality of adsorption parameters, adsorption and desorption characteristics of low Cit-CS, medium Cit-CS, and high Cit-CS derivatives have been compared with the best available literature for most relevant adsorbate (multi-heavy metal solution) and adsorbent systems (chitosan-derivatives). A summary of these findings has been presented in Table 5.5. For complex industrial wastewater adsorbate systems, the reported data in the Ph.D. thesis is the only relevant data to compare adsorbent performance, as other relevant literature reported data for only aqueous acidic solutions. Based on the data summarized in the table, the following can be inferred:

a) From Zn and Cu removal perspective and for synthetic complex industrial wastewater and among chitosan derivatives, medium Cit-CS resin affirmed promising performance in comparison with the glutaraldehyde cross-linked chitosan. Incidentally, for the thesis case, the adsorption capacity was 243.90 mg g^{-1} for 194.9-584.7 mg L^{-1} initial Zn solution concentration range and the literature data was the 72.71 mg g^{-1} for 11.3-92.3 mg L^{-1} initial Zn solution concentration range. Similarly, for the thesis case, the corresponding adsorption capacity of Cu was 312.50 mg g^{-1} for 187.7-563.1 mg L^{-1} initial Cu solution concentration range in comparison to the literature data of 79.18 mg g^{-1} for 14.6-108.8 mg L^{-1} initial Cu solution concentration range. Hence, the performance of medium Cit-CS derivative is comparable with both adsorption and desorption characteristics of literature reported glutaraldehyde cross-linked chitosan resin. The medium Cit-CS derivative studied in this work performed excellently in terms of heavy metal removal but was satisfactory in terms of metal desorption and derivative regeneration after three cycles.

Table 5.5: Summary of the adsorption and desorption characteristics of alternate Cit-CS derivatives investigated in this study and prior art.

Adsorbent	Metal Ions	Solution	Dose (g L^{-1})	Contact duration (min)	Conc. range (mg L^{-1})	Adsorption capacity (mg g^{-1})	Removal efficacy (%)	Desorption (%)	Eluents	Ref.
Medium Cit-CS	Zn Pb Fe	Multi metal solution	1.4	420	194.9 - 584.7 2.65-7.95 104.8 - 314.4	243.90 3.93 144.93	62.65 80.50 72.93	75.65-57.76 68.59-49.83 79.14-58.35 (1-3 cycles)	2.0 M HCl	This study
Medium Cit-CS	Cu Pb Fe	Multi metal solution	1.4	420	187.7 - 563.1 5.2-15.6 61.9-185.5	312.5 8.17 86.21	80.67 88.17 73.81	78.69-58.9 69.63-49.40 75.31-53.78 (1-3 cycles)	2.0 M HCl	This study
PVA/Chitosan Beads	Cu Pb Zn Cd	Multi metal solution	2	660 540 660 540	50-500	238.45 166.44 74.18 126.06 (Single solution)	93.90 77.85 10.93 21.31 (Multi-metal solution)	98.4 96.7 98.5 98.5 (Single solution)	0.1M EDTA for Cu 0.1 M HCl for Pb, Zn, Cd	(Li et al., 2011)
GLA/Chitosan	Pb Ni Zn Cu	Multi metal solution	1	420 360 420 360	9.1-90.72 13.4-99.4 11.3-92.3 14.6-108.8	67.17 67.81 72.71 79.18	74.06 73.45 73.16 72.77	-		(Busuioc et al., 2016)
PVA/Chitosan Foam	MG dye Cu	Binary solution	2	360 480	50-800	227.02 111.85	-	97	0.1 M Na_2EDTA	(Li et al., 2012)
EDTA modified Chi/SiO_2/Fe_3O_4	Cu Pb Cd	Mixed solution	1	360 180 360	0.2-5 (mM)	0.699 0.596 0.563	-	75.73	0.01 M Na_2EDTA	(Ren et al., 2013)
Chitosan immobilized Bentonite	Cu Ni Pb	Aqueous binary solution	-	240-360 240-360 240-360	25-200 25-200 25-200	17.09 12.61 20.8	51.41 39.04 80	-	-	(Futalan et al., 2011)

b) From the perspective of the regeneration of the chitosan derivatives after multi-heavy metal desorption from complex synthetic industrial wastewater adsorbate solutions, the medium Cit-CS derivative can be concluded to be the best (78.69, 69.63 and 75.65 for the thesis case in comparison to the literature data of 98.4, 96.7 and 98.5 aqueous solution desorption % for Cu, Pb, and Zn, respectively). In addition, the desorption efficiency is significantly better than that of styrene DVB copolymer. Hence, from a heavy metal removal and derivative regeneration perspective and complex adsorbate systems, medium Cit-CS resin is the best among PVA/Chitosan beads, EDTA-modified Chi/SiO_2/Fe_3O_4, and PVA/Chitosan foam.

c) All other literature data cannot be compared with the data obtained in this work, as these literature targeted heavy metal removal from aqueous solutions with lesser solution complexity.

5.7 Summary

Several useful insights can be deduced from the best findings achieved in this work in the field of heavy metal adsorption and desorption characteristics of low Cit-CS, medium Cit-CS, and high Cit-CS derivatives with synthetic complex industrial adsorbate systems. Firstly, the optimal multi-heavy metal batch adsorption parameters for the medium Cit-CS resin in Cu dominant solution were 3.82 pH, 1.4 g L^{-1} dosage, and 420 min contact time. Corresponding adsorption capacity and metal removal % of the resin was 119.50-258.58 mg g^{-1} and 89.12-64.29 % respectively for Cu, 37.70-74.31 mg $g^{-1,}$ and 85.33-56.06 % respectively for Fe and 3.42-7.43 mg g^{-1} and 92.12-66.64 % respectively for Pb for the initial heavy metal ion concentration range of 187.7-563.1 mg L^{-1} for Cu, 61.85-185.55 mg L^{-1} for Fe, and 5.2-15.6 mg L^{-1} for Pb. On the other hand, the optimal heavy metal ion batch adsorption parameters for medium Cit-CS resin in Zn dominant solution were 3.64

pH, 1.4 g L^{-1} dosage, and 420 min contact time. Corresponding adsorption capacity and metal removal % of the resin were 110.36-205.17 mg g^{-1} and 79.27-49.13 % respectively for Zn, 61.85-122.37 mg g^{-1} and 82.63-54.49 % respectively for Fe and 1.68-3.41 mg g^{-1} and 88.55-60.13 % respectively for Pb in the initial heavy metal ion concentration range of 194.9-584.7 mg L^{-1} for Zn, 104.8-314.4 mg L^{-1} for Fe, and 2.65-7.95 mg L^{-1} for Pb. Hence, compared to the Zn dominant solution, the medium Cit-CS derivative provided higher removal efficiencies for the Cu dominant solution. Also, the medium Cit-CS resin also exhibited higher regeneration characteristics in the Cu dominant solution in comparison with the Zn dominant solution.

Secondly, after the three desorption cycles, the desorption characteristics were 58.9, 53.78, and 49.40 % for Cu, Fe, and Pb, respectively for the Cu dominant solution and 57.76, 58.35, and 49.83 % for Zn, Fe, and Pb, respectively for the Zn dominant solution. These indicate and confirm satisfactory heavy metal ion removal and resin regeneration. Further improvement in the heavy metal ion desorption characteristics of medium Cit-CS resin can be conveniently targeted through the suitable alteration in the abundance of functional groups. This can be achieved through stoichiometric and resin synthesis variations. The surface analysis with FTIR, BET, TGA, XRD FESEM-EDX, etc., have been in good agreement with apparent functional interactions between various chemical species.

From the perspective of heavy metal ion removal and resin reusability, compared to the available prior art based on aqueous solution, medium Cit-CS derivative performed better for complex synthetic industrial wastewater adsorbate systems. With respect to chitosan, all adsorbents exhibited excellent desorption characteristics and thereby confirmed upon the greater role of chelating functional groups in achieving improved resin reusability for multi-heavy metal removal from synthetic industrial wastewater adsorbate systems.

Chapter 6:

Cyclic Multi-heavy metal adsorptive and desorptive characteristics of Carboxymethyl-Chitosan derivative Resins

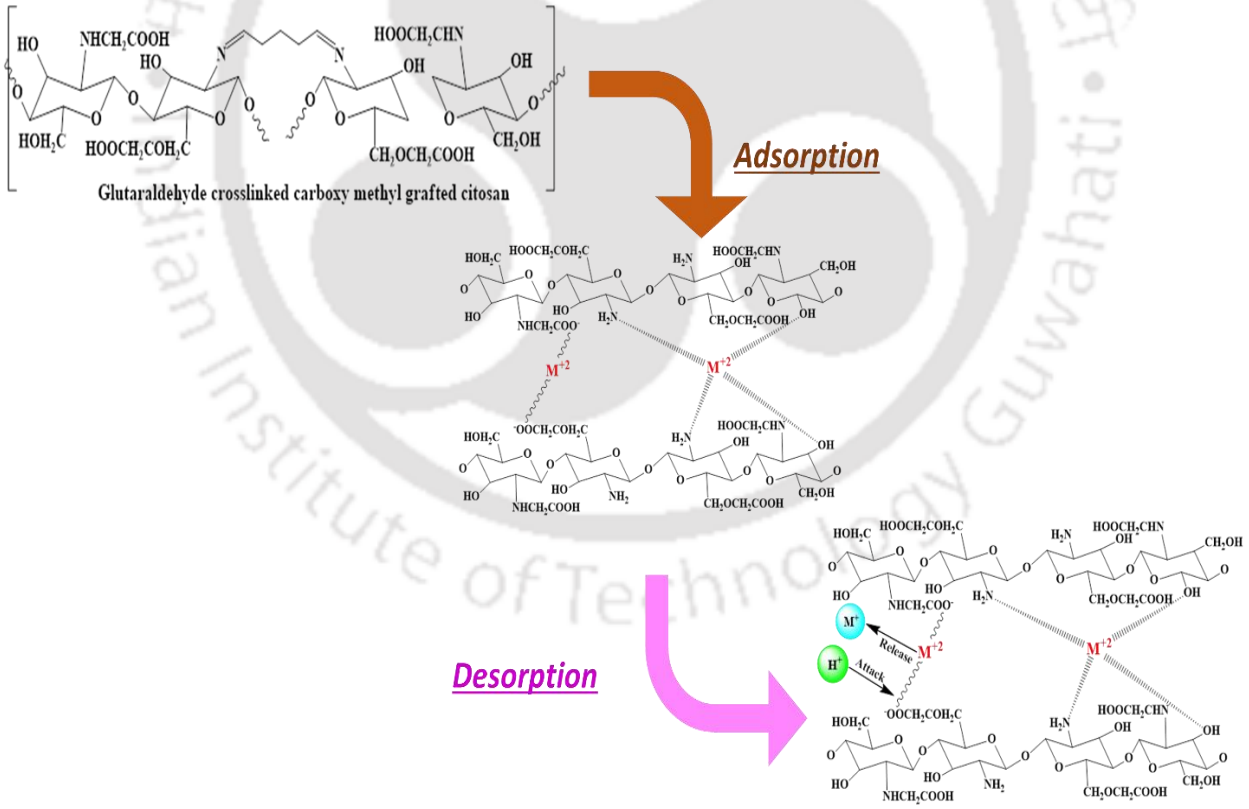

Chapter 6

Cyclic Multi-heavy metal adsorptive and desorptive characteristics of Carboxymethyl-Chitosan derivative Resins

The chapter summarizes experimental and theoretical findings associated to multi heavy metal adsorption and desorption characteristics of carboxy methyl grafted glutaraldehyde crosslinked low molecular weight chitosan derivative (low CMCS), carboxy methyl grafted glutaraldehyde crosslinked medium molecular weight chitosan derivative (medium CMCS), and carboxy methyl grafted glutaraldehyde crosslinked high molecular weight chitosan derivative (high CMCS). Firstly, section 6.1 elucidates on the relevant background. Following this, the findings of medium CMCS resin's solubility characteristics have been briefly outlined in section 6.2. The next section (section 6.3) addresses the adsorption characteristics. Section 6.4 briefly describes the findings associated to surface characterizations of raw and metal-loaded derivatives. Section 6.5 presents heavy metal desorption characteristics of spent carboxy methyl grafted glutaraldehyde crosslinked medium molecular weight chitosan derivative (medium CMCS) using various inexpensive eluents. Thereafter, section 6.6 presents the literature comparison of the best available prior art and the findings of this chapter. Finally, a summary of the findings has been presented in the last section (section 6.7) of the chapter.

6.1 Background

Prior to this work, oxygen/nitrogen functionalized chitosan derivatives were investigated for heavy metal ion adsorption characteristics by a few research groups that targeted hydroxyl, Si-

O, amine group, carboxyl, and EDTA functionalized adsorbents (Kavitha et al., 2020; Liu et al., 2013; Ren et al., 2013; Tsai et al., 2016). However, the authors deployed simple adsorption systems of aqueous solutions. On the other hand, the CMCS resin was deployed for applications other than multi-heavy heavy metal removal and adsorbent regeneration. Thus, moderate and highly complex solution systems with other co-existent ions were not targeted for said derivatives. Further, desorption characteristics were not targeted as well. Considering these limitations, multi-heavy metal adsorption and desorption characteristics were targeted for CMCS variant derivatives with Cu dominant and Zn dominant simulated complex wastewater adsorbate systems. For the said resin, conducted surface characterizations refer to FTIR, BET, XRD, TGA, and FESEM-EDX. The specific role of other co-existent ions on targeted multi-heavy metal ions removal and regeneration characteristics of the said resin was targeted for detailed investigations.

6.2 Solubility resistance of medium CMCS derivative Resin

The medium CMCS resin has been subjected to stability studies prior to multi-heavy metal adsorption. To do so, firstly, the raw medium CMCS resin was placed in contact with 1 N HNO_3 and 1 N KOH solutions for 12 h. Thereafter, the quantitative analysis of weight reduction was performed. Eventually, the weight loss % was 0.96 % for both cases and confirmed very good stability of the resin in both acidic and basic media. Such findings assure the relevance of the CMCS resin for real applications that involve the adsorbate system with acidic and basic pH.

6.3 Multi-heavy metal adsorption characteristics of low CMCS, medium CMCS, and high CMCS derivative resins

6.3.1 Optimality of batch adsorption process parameters

With the well-known influence of sorption being influenced with the pH, it is obvious to optimize and infer upon the best pH for optimal (highest) multi-heavy metal removal from the chosen adsorbate system. However, it was noticed that the adsorbate system was not at all stable above 4 and below 2 pH value range. This is due to the formation of a deposit that prompted all investigations at the natural solution pH (3.82 for Cu dominant solution and 3.64 for Zn dominant solution). Thus, the optimality of all other adsorption process parameters but not pH was targeted. Consequently, the well-known adsorption process parameters (sorbent loading, sorbent contact duration, and initial concentration) were optimized. Given that the prior art (Benavente et al., 2011) conveyed the existence of multi-heavy metals in +2 ionic forms at the solution's natural pH, it can be presumed that the amino and hydroxyl groups of chitosan interacted with the carboxylic group of the carboxymethyl chitosan derivative to serve as the crosslinking based sorption sites. Thus, the adsorption of the multi-heavy metals on the CMCS resin follows as per the reactions (Patel et al., 2023):

$$R - NH_2 + H^+ \rightarrow R - NH_3^+ \quad (6.1)$$

$$R - NH_2 + M^{2+} \rightarrow R - NH_2M^{2+} \quad (6.2)$$

$$R - NH_3^+ + M^{2+} \rightarrow R - NH_2M^{2+} + H^+ \quad (6.3)$$

$$R - NH_2M^{2+} + H_2O \rightarrow MOH^+ + R - NH_3^+ \quad (6.4)$$

The mechanism with which heavy metals get adsorbed on the adsorbent has been shown in Fig. 6.1. The dominant metal ions at pH of 3.82 and 3.64 do have an influence in the depicted heavy metal adsorption process:

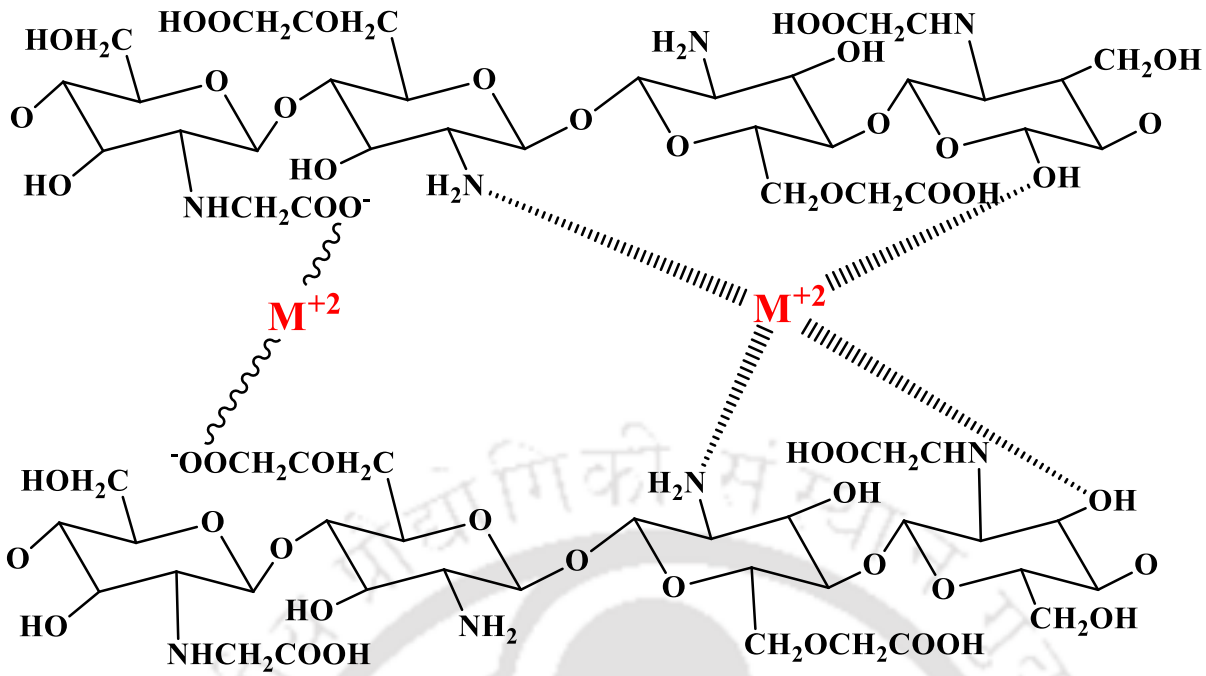

Fig. 6.1. Proposed heavy metal adsorption mechanism for CMCS derivative.

For a fixed choice of relevant sorption process parameters (3.82, 12 h, 25°C, 200 rpm for initial pH, contact time, temperature, and shaking speed respectively) and initial heavy-metal ion concentrations (Pb 10.4 mg L^{-1}, Fe 123.7 mg L^{-1}, and Cu 375.4 mg L^{-1}), the alteration of metal adsorption patterns with adsorbent dosage has been illustrated in Fig. 6.2. The maximum dosage (2 g L^{-1} for low CMCS resin) has been inferred to be the ideal adsorbent dosage at which the optimum adsorption characters (116.74, 39.84, and 4.195 mg g^{-1} adsorption capacity and 62.20, 64.41, and 80.67 % metal removal for Cu, Fe, Pb respectively) have been achieved. Also, for medium and high CMCS resins, maximum dosage (1.2 g L^{-1}) facilitated optimum adsorption characters (238.46, 79.68, 7.20 mg g^{-1} and 275.01, 80.16, 7.34 mg g^{-1} adsorption capacity and 76.23, 77.30, 83.10 % and 87.91, 77.76, 84.65 % metal removal for Cu, Fe, Pb respectively).

Similarly, the alteration of metal adsorption patterns with an alteration in adsorbent dosage for the Zn dominant solution is shown in Fig. 6.3. The maximum dosage (1.8 g L^{-1} for low CMCS) has been inferred to be the ideal adsorbent dosage at which the optimum adsorption properties

(132.07, 76.98, and 2.12 mg g^{-1} adsorption capacity and 60.99, 66.11, and 72.08 % metal removal for Zn, Fe, Pb respectively) have been achieved. Also, for medium and high CMCS, maximum dosage (1.4 g L^{-1}) facilitated optimum adsorption properties (194.19, 106.6, and 3.07 mg g^{-1} and 201.18, 108.61, and 3.08 mg g^{-1} adsorption capacity and 69.74, 71.20, and 81.00 % and 72.26, 72.54, and 81.45 % metal removal for Zn, Fe, Pb respectively). The reduced heavy metal sorption for the case of increased adsorbent dosage is due to an increment in the sites favorable for metal sorption on the adsorbent surface. Consequently, adsorption capacity got lowered due to the reduced mass of species adsorbed per unit weight of the adsorbent. Due to the presence of multiple functional groups, the CMCS affirmed higher removal efficacy in conjunction with other chitosan derivatives (Li et al., 2012, 2011).

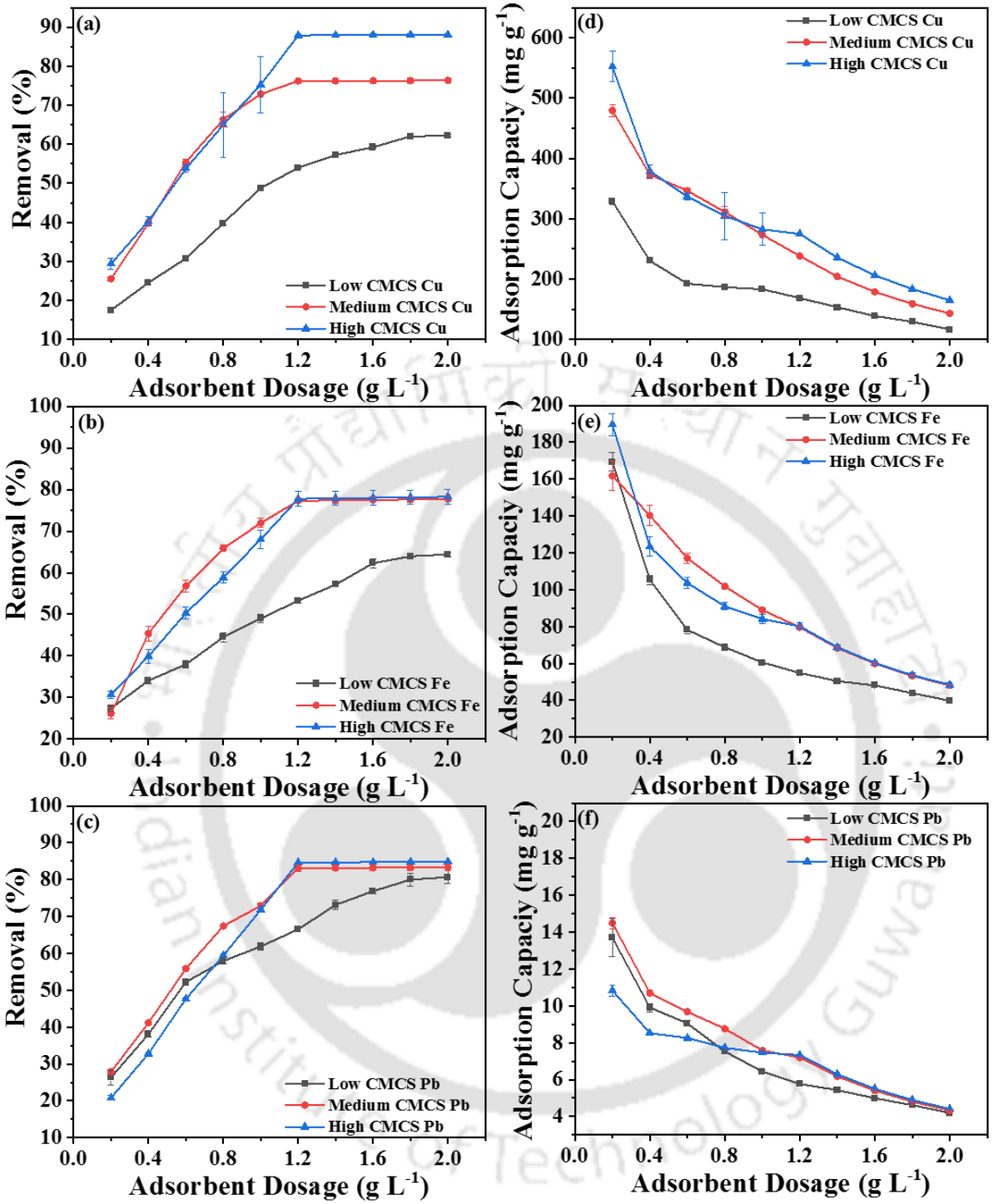

Fig. 6.2. Graphs depicting the influence of adsorbent dosage on adsorption characteristics of CMCS derivatives and Cu dominant adsorbate system.

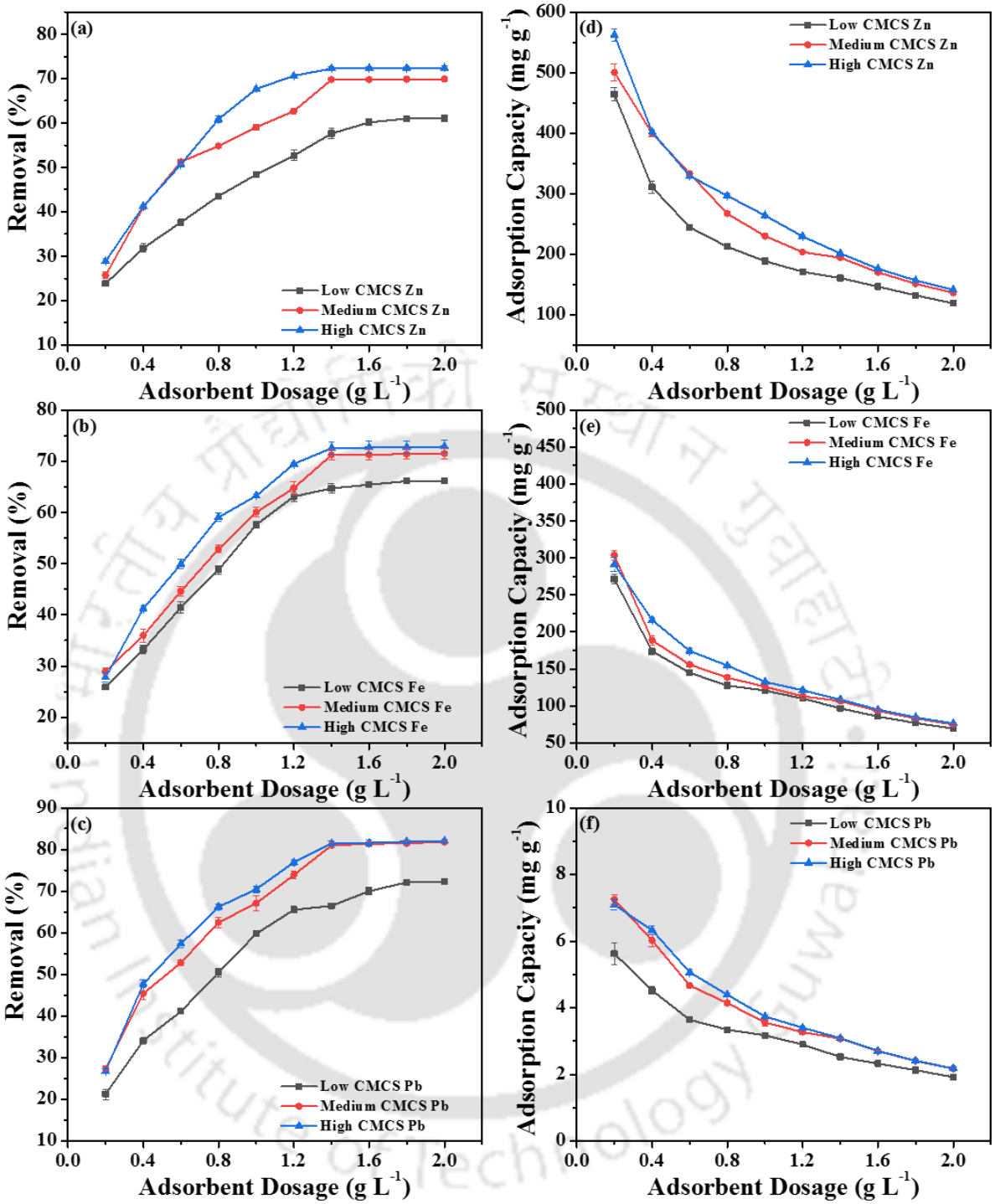

Fig. 6.3. Graphs depicting the influence of adsorbent dosage on adsorption characteristics of CMCS derivatives and Zn dominant adsorbate system.

For a fixed choice of relevant sorption process parameters (3.82, 25°C, 200 rpm for initial pH, temperature, and shaking speed respectively), adsorbent dosage (2 g L^{-1} for low CMCS and 1.2 g L^{-1} for medium and high CMCS derivative) and initial metal ion concentration (Pb 10.4 mg

L^{-1}, Fe 123.7 mg L^{-1}, and Cu 375.4 mg L^{-1}), the alteration of metal adsorption patterns with adsorbent contact time has been shown in Fig. 6.4. The figure shows that the adsorption rate was faster upto 180 min and reached equilibrium at 660 min for low CMCS resin and 540 min for high and medium CMCS resins. Thereby, a maximum % metal removal and adsorption capacity of 81.83, 65.85, 62.74 %, and 4.26, 40.73, 117.76 mg g^{-1} for Pb, Fe, and Cu respectively were realized with low CMCS resin. For medium CMCS resin, corresponding values were obtained as 85.71, 79.09, 77.39 %, and 7.44, 81.53, 242.10 mg g^{-1} for Pb, Fe, and Cu respectively. Also, for high CMCS resin, corresponding values were obtained as 83.59, 77.42, 86.99 %, and 7.24, 79.81, 272.14 mg g^{-1} for Pb, Fe, and Cu respectively.

Similarly, the alteration of metal adsorption patterns with an alteration in adsorbent contact time for the Zn dominant solution is shown in Fig. 6.5. The figure shows that the adsorption rate was quick upto 180 min and reached equilibrium at 660 min for low CMCS and 420 min for high and medium CMCS. Thereby, a maximum % metal removal and adsorption capacity of 72.77, 66.56, and 62.93 % and 2.14, 77.50, and 136.28 mg g^{-1} for Pb, Fe, and Zn respectively were realized with low CMCS. For medium CMCS, corresponding values were obtained as 80.82, 71.24, and 70.13 % and 3.06, 106.66, and 195.25 mg g^{-1} for Pb, Fe, and Zn respectively. Also, for high CMCS, corresponding values were obtained as 80.83, 73.05, and 71.22 % and 3.06, 109.36, and 198.29 mg g^{-1} for Pb, Fe, and Zn respectively. These findings corroborate with the prior art-based inference for the CSPVA resin (Trikkaliotis et al., 2020).

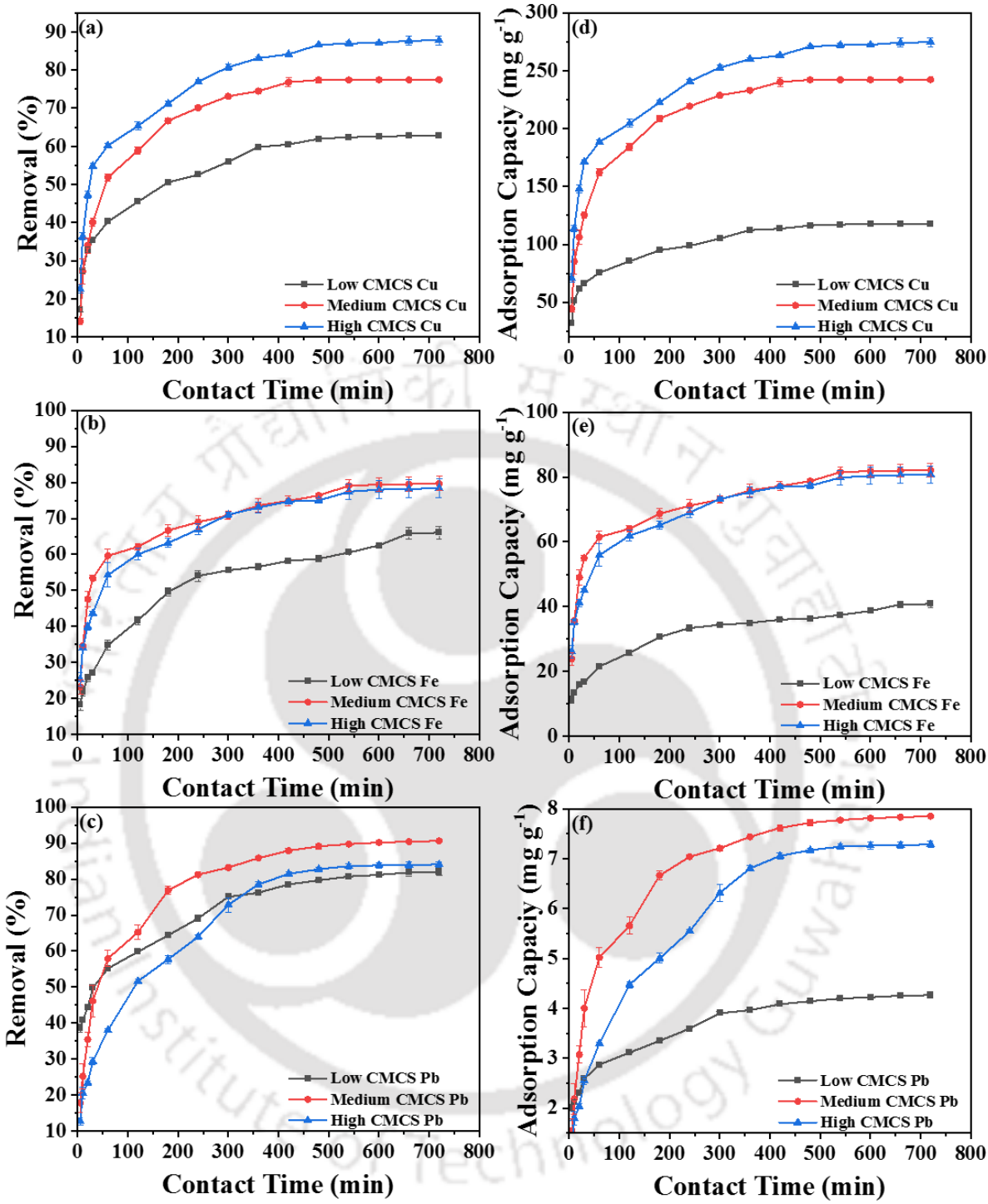

Fig. 6.4. Graphs depicting the influence of contact time on adsorption characteristics of CMCS derivatives and Cu dominant adsorbate system.

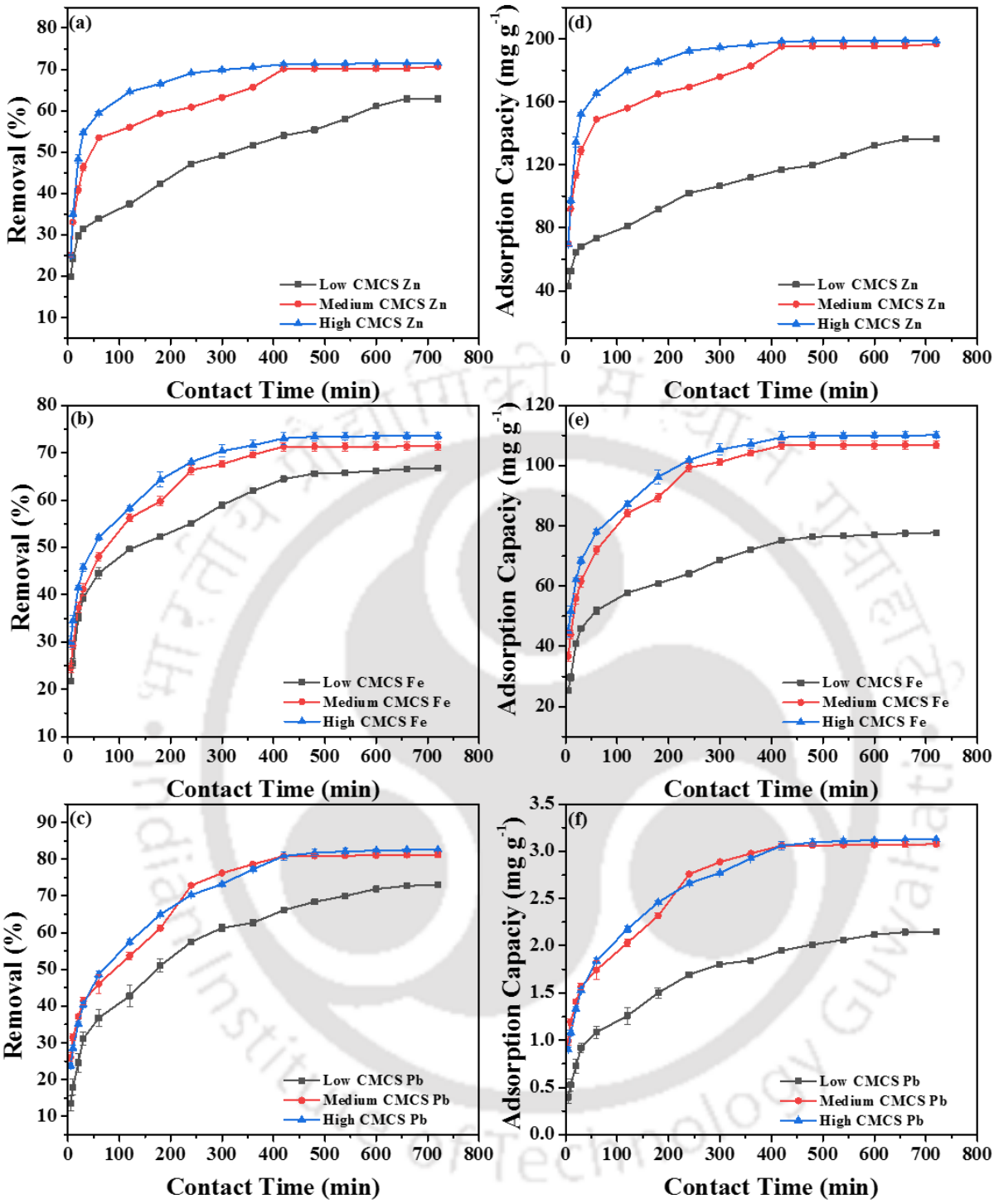

Fig. 6.5. Graphs depicting the influence of contact time on adsorption characteristics of CMCS derivatives and Zn dominant adsorbate system.

For a fixed choice of relevant sorption process parameters (3.82, 25°C, 200 rpm for initial pH, temperature, and shaking speed respectively), adsorbent contact time (660 min for low CMCS resin and 540 min for high and medium CMCS resins) and adsorbent dosage (2 g L^{-1} for low

CMCS resin and 1.2 g L^{-1} for medium and high CMCS derivatives), the alteration of metal adsorption patterns with initial metal ion concentration (187.7-563.1 mg L^{-1} for Cu, 61.85-185.55 mg L^{-1} for Fe, and 5.2-15.6 mg L^{-1} for Pb) has been illustrated in Fig. 6.6. For the Cu, adsorption capacity and % metal removal varied as 77.18-133.97 mg g^{-1} and 82.23-47.58 % respectively for low CMCS resin; 144.69-300.57 mg g^{-1} and 92.50-64.05 % respectively for medium CMCS resin; and 147.72-308.37 mg g^{-1} and 94.44-65.72 % respectively for high CMCS resin and for mentioned alteration in initial metal ion concentration. Similarly, for the Fe, adsorption capacity and % metal removal varied as 26.3-46.53 mg g^{-1} and 85.04-50.16 % respectively for low CMCS resin; 46.70-84.21 mg g^{-1} and 90.61-54.46 % respectively for medium CMCS resin; and 48.28-94.45 mg g^{-1} and 93.68-61.08 % respectively for high CMCS resin with respect to the mentioned alteration in the initial metal ion concentration of the system. Also, for the Pb, adsorption capacity and % metal removal varied as 2.41-4.525 mg g^{-1} and 92.69-58.03 % respectively for low CMCS resin; 4.04-8.68 mg g^{-1} and 93.33-66.73 % respectively for medium CMCS resin; and 4.15-9.19 mg g^{-1} and 95.83-70.66 % respectively for high CMCS resin and for mentioned alteration in the initial metal ion concentration of the system.

Similarly, for a fixed choice of other adsorption parameters (3.64, 25°C, 200 rpm for initial pH, temperature, shaking speed), adsorbent contact time (480 min for low CMCS and 420 min for medium and high CMCS) and adsorbent dosage (1.6 g L^{-1} for low CMCS and 1.4 g L^{-1} for medium and high CMCS derivative), the alteration of metal adsorption patterns with an alteration in initial metal ion concentration (194.9-584.7 mg L^{-1} for Zn, 2.65-7.95 mg L^{-1} for Pb, and 104.8-314.4 mg L^{-1} for Fe) is shown in Fig. 6.7. For the Zn, adsorption capacity and % metal removal varied as 88.60-146.40 mg g^{-1} and 81.83-45.07 % respectively for low CMCS; 115.84-208.98 mg g^{-1} and 83.21-50.04 % respectively for medium CMCS; and 120.95-215.92 mg g^{-1} and 86.88-51.70 % respectively for high CMCS for mentioned alteration in initial metal ion concentration. Similarly, for the Fe, adsorption capacity and % metal removal varied as

46.71-91.77 mg g^{-1} and 80.22-52.54 % respectively for low CMCS; 61.85-123.56 mg g^{-1} and 82.63-55.02 % respectively for medium CMCS; and 63.33-130.37 mg g^{-1} and 84.60-58.05 % respectively for high CMCS with respect to the mentioned alteration in the initial metal ion concentration of the system. Also, for the Pb, adsorption capacity and % metal removal varied as 1.25-2.66 mg g^{-1} and 84.65-60.29 % respectively for low CMCS; 1.67-3.82 mg g^{-1} and 88.05-67.34 % respectively for medium CMCS; and 1.74-3.84 mg g^{-1} and 92.08-67.59 % respectively for high CMCS and for mentioned alteration in the initial metal ion concentration of the system.

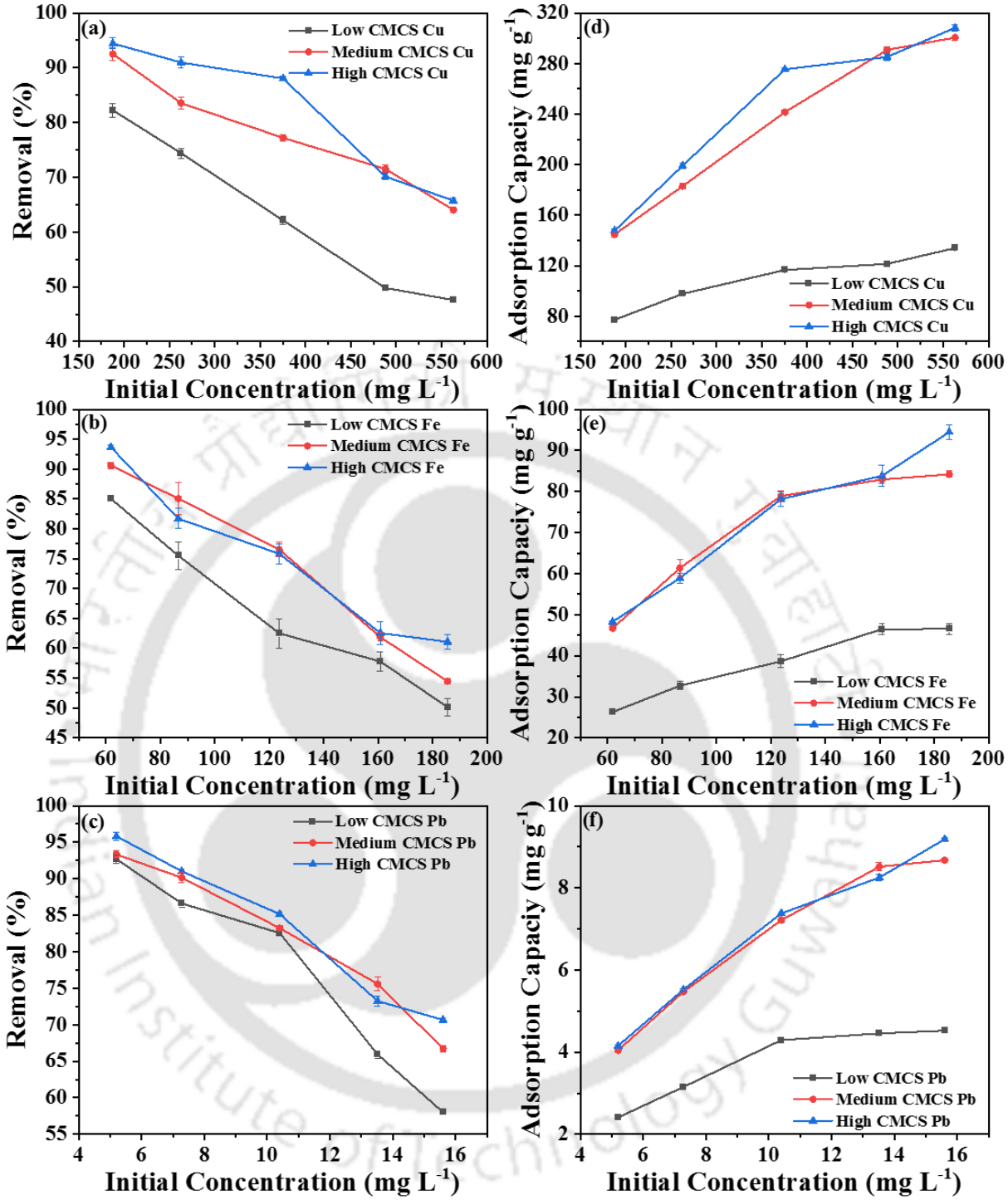

Fig. 6.6. Graphs depicting the influence of metal ion concentration on adsorption characteristics of CMCS derivatives and Cu dominant adsorbate system.

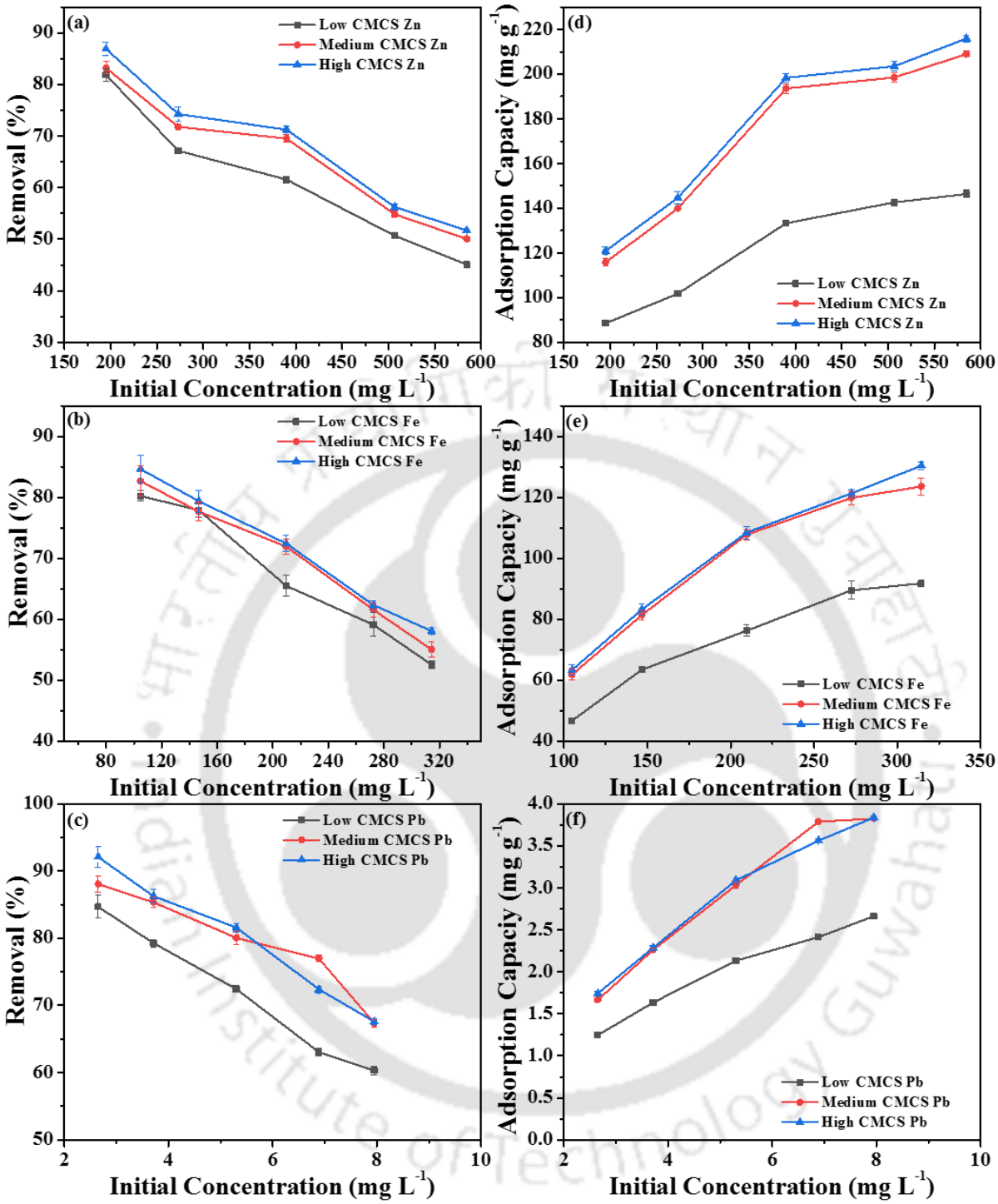

Fig. 6.7. Graphs depicting the influence of metal ion concentration on adsorption characteristics of CMCS derivatives and Zn dominant adsorbate system.

6.3.2 Fitness of alternate Equilibrium and Kinetic models

To assess upon the pertinent mechanism of the sorption process, the Langmuir isotherm model was deployed to examine its fitness with the batch equilibrium sorption dataset (Fig. 6.8a–c). Thereby, the findings conveyed monolayer metal sorption onto the sorbent active sites. Furthermore, the findings were also evaluated with the Freundlich isotherm model (Fig. 6.8d-f). The model presumes multilayer metal sorption due to the uniform energy surface heterogeneity hypothesis. Since Langmuir isotherm offered the best response for the measured dataset, monolayer adsorption has been hypothesized to represent the relevant mechanism. Table 6.1 summarizes the data for the equilibrium model terms for the sorption of Cu, Pb, and Fe onto CMCS derivatives.

Table 6.1: Regressed model parameters representing heavy metal adsorption equilibrium data of CMCS derivatives and Cu dominant adsorbate system.

CMCS derivatives	Langmuir isotherm variables				Freundlich isotherm variables		
	Q_o (mg g^{-1})	b (L mg^{-1})	R^2	R_L	K_f	n	R^2
Cu							
Low CMCS	142.86	0.032	0.99	0.05-0.14	35.14	4.27	0.96
Medium CMCS	344.83	0.034	0.99	0.05-0.14	65.01	3.42	0.97
High CMCS	322.58	0.081	0.99	0.02-0.06	93.91	4.27	0.87
Fe							
Low CMCS	52.36	0.085	0.99	0.06-0.16	14.79	3.86	0.97
Medium CMCS	90.09	0.192	0.99	0.03-0.08	33.84	4.54	0.91
High CMCS	100.0	0.129	0.99	0.04-0.11	34.34	4.41	0.95
Pb							
Low CMCS	5.69	1.29	0.99	0.004-0.002	3.07	3.27	0.88
Medium CMCS	9.59	1.96	0.99	0.003-0.008	5.81	3.46	0.96
High CMCS	9.69	2.33	0.99	0.002-0.007	6.21	3.93	0.97

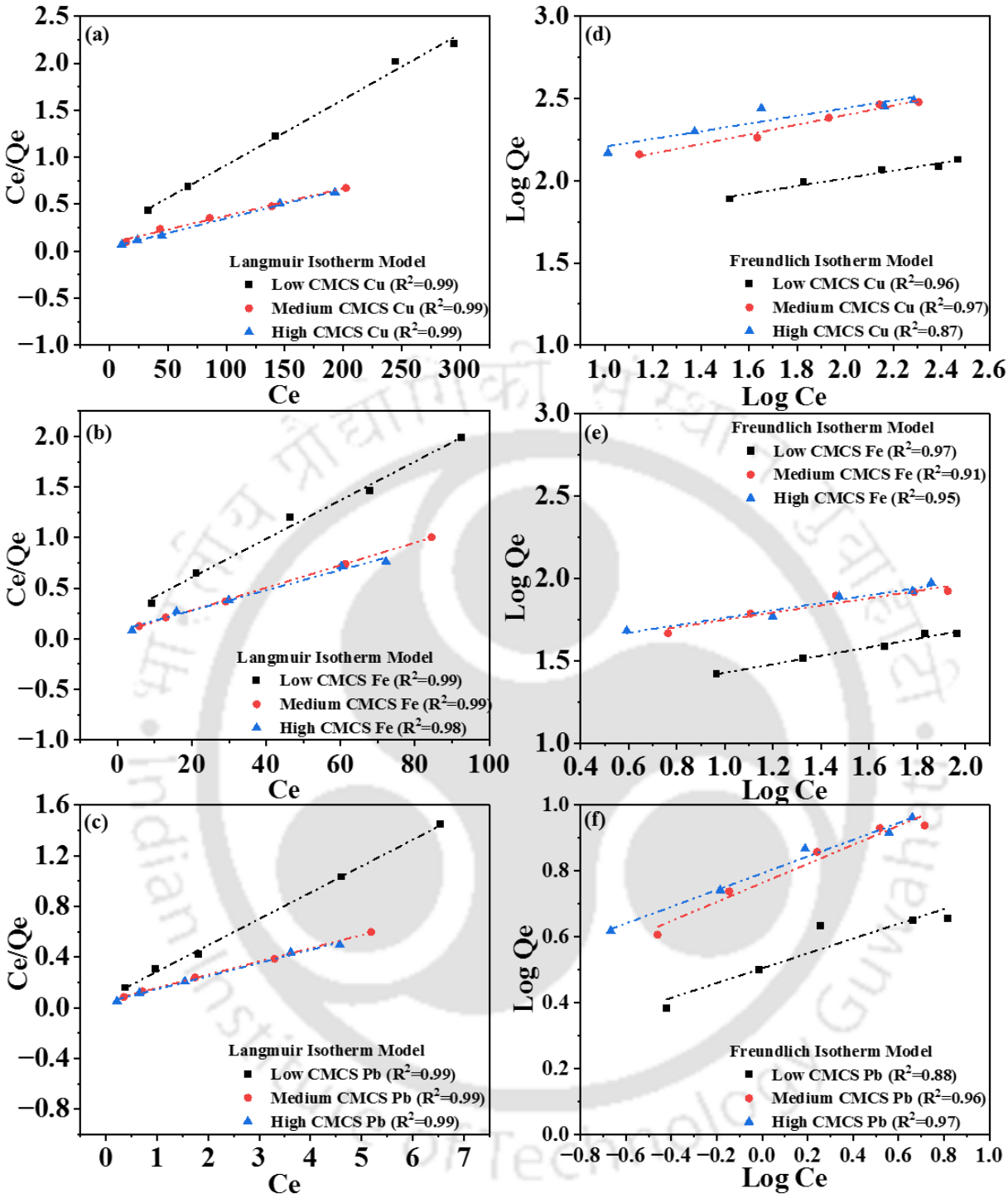

Fig. 6.8. Equilibrium models fitness plots (a-c: Langmuir isotherm model and d-f: Freundlich isotherm model) for CMCS derivatives and Cu dominant adsorbate system.

In order to assess upon the equilibrium characteristics of the resin-based sorption process, the Langmuir isotherm model was used to examine the batch equilibrium sorption dataset. The isotherm postulates monolayer metal sorption onto the sorbent active sites. Relevant findings

have been depicted in (Fig. 6.9a-c). Furthermore, the findings were also evaluated using the Freundlich isotherm model which confirms multilayer metal sorption based on the hypothesis of uniform energy surface heterogeneity. These findings have been depicted in (Fig. 6.9d-f). Since Langmuir isotherm provided the best fit for the data collected monolayer adsorption has been assumed to represent the relevant mechanism. Table 6.2 summarises the equilibrium model fit parametric data for the sorption of Zn, Pb, and Fe.

Table 6.2: Regressed model parameters representing heavy metal adsorption equilibrium data of CMCS derivatives and Zn dominant adsorbate system.

CMCS derivatives	Langmuir parameters				Freundlich parameters		
	Q_o (mg g^{-1})	b (L mg^{-1})	R^2	R_L	K_f	n	R^2
Zn							
Low CMCS	163.93	0.025	0.99	0.06-0.17	36.17	4.06	0.94
Medium CMCS	238.10	0.026	0.99	0.06-0.16	44.29	3.57	0.90
High CMCS	238.10	0.032	0.99	0.05-0.14	53.83	4.00	0.91
Fe							
Low CMCS	108.70	0.038	0.99	0.08-0.20	18.60	3.05	0.95
Medium CMCS	147.06	0.041	0.99	0.07-0.19	24.25	2.92	0.95
High CMCS	151.52	0.042	0.99	0.07-0.18	25.65	2.95	0.97
Pb							
Low CMCS	3.17	1.451	0.99	0.08-0.12	1.77	2.76	0.97
Medium CMCS	4.78	1.747	0.99	0.07-0.10	2.80	2.62	0.95
High CMCS	4.39	2.532	0.99	0.05-0.07	2.91	3.12	0.97

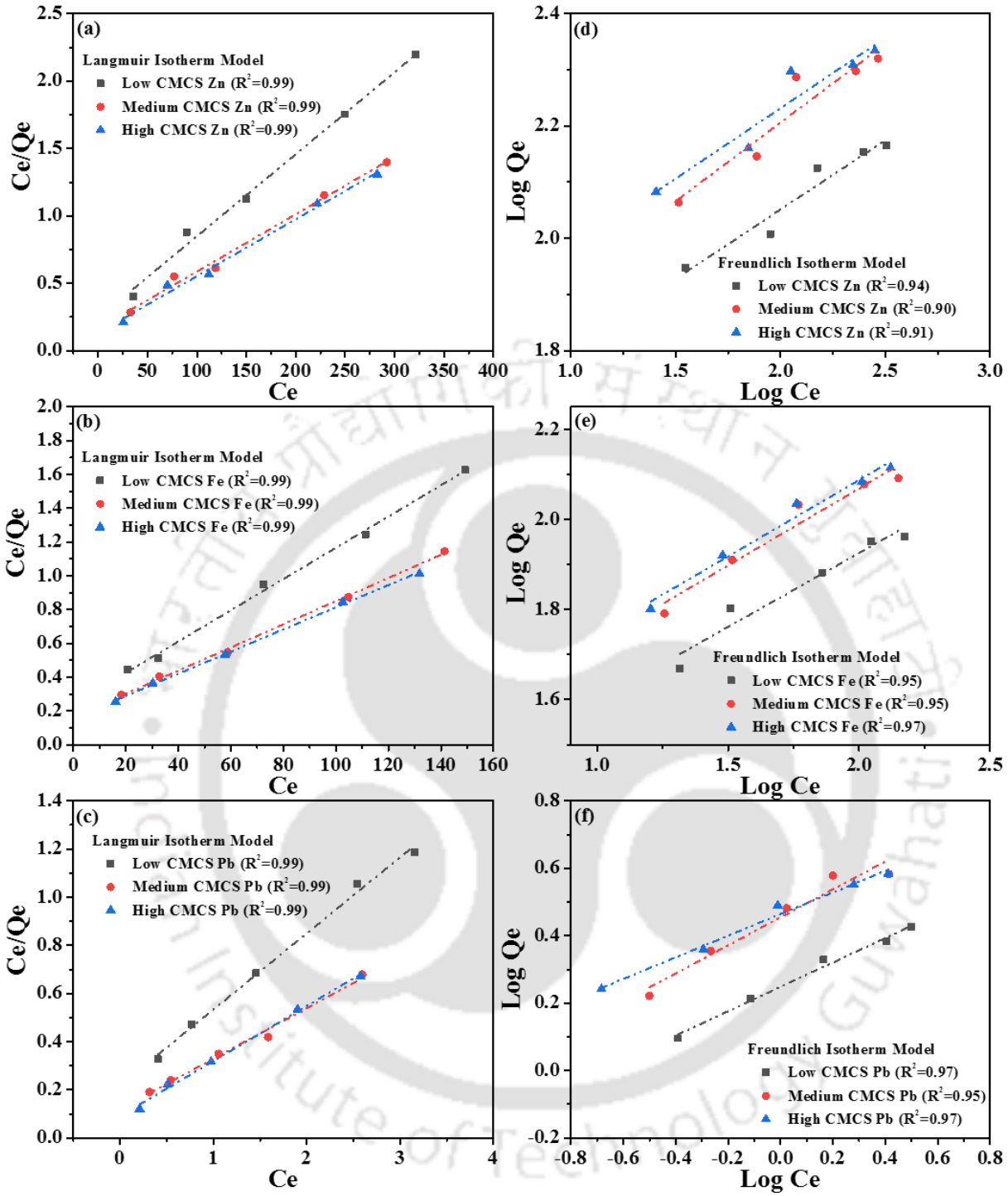

Fig. 6.9. Equilibrium models fitness plots (a-c: Langmuir isotherm model and d-f: Freundlich isotherm model) for CMCS derivatives and Zn dominant adsorbate system.

To assess upon Cu, Pb, and Fe sorption kinetics of CMCS derivative variants, the fitness plots for alternate kinetic models were prepared (Fig. 6.10). Thereby, among all models, the pseudo-second-order model can be concluded to provide the most appropriate fit to characterize the

kinetics of Pb, Cu, and Fe sorption onto CMCS sorbent. Table 6.3 summarizes the values of the kinetic model parameters for Pb, Cu, and Fe heavy metal cases onto CMCS derivatives.

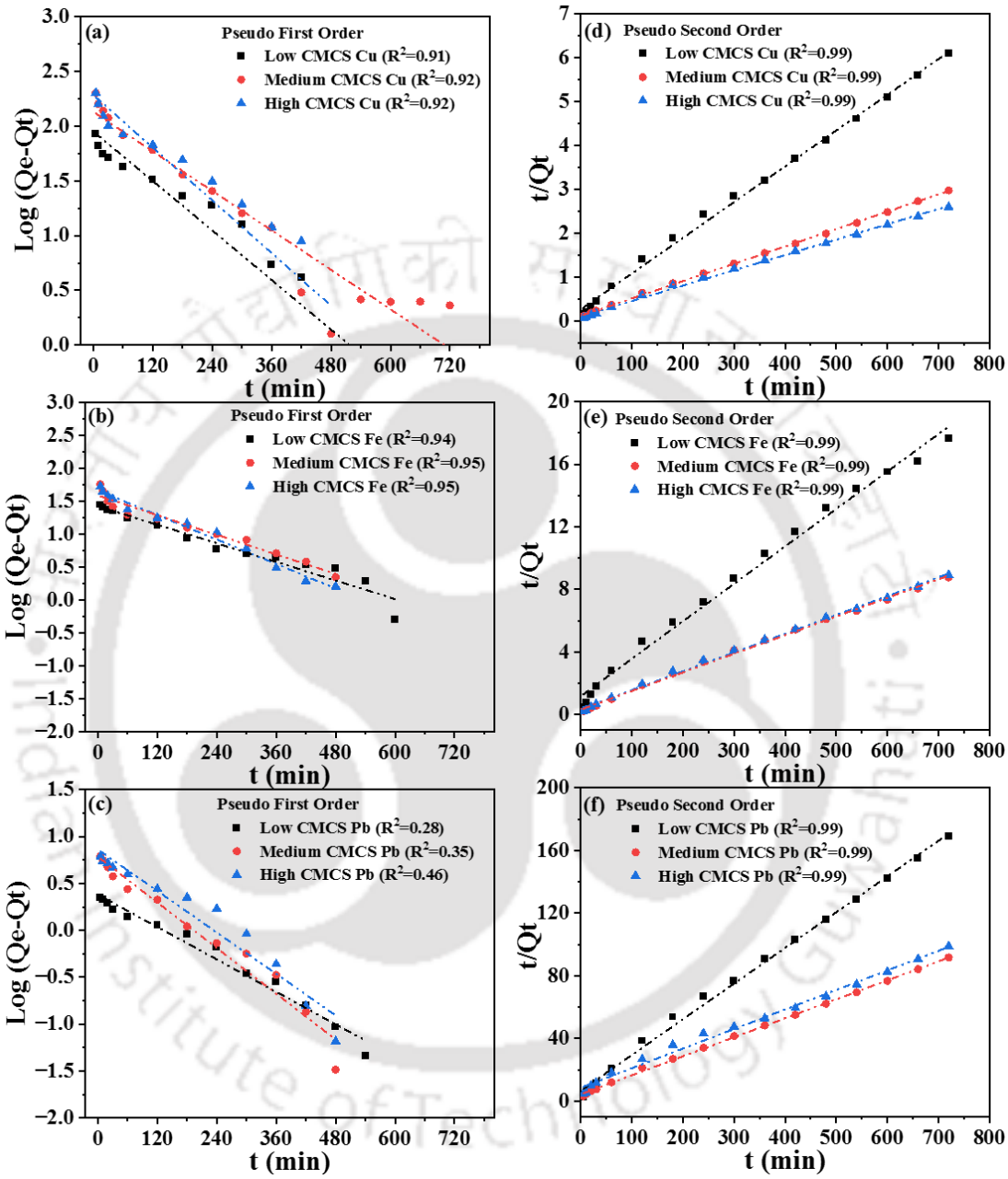

Fig. 6.10. Kinetic models fitness plots (a-c: Pseudo-first-order kinetic model, and d-f: Pseudo-second-order kinetic model) for CMCS derivatives and Cu dominant adsorbate system.

Table 6.3: Regressed model parameters representing heavy metal adsorption kinetic data of CMCS derivatives and Cu dominant adsorbate system.

Experimental capacity (Q_{exp}, mg g^{-1})	CMCS derivatives	Pseudo-first-order model			Pseudo-second-order model		
		Q_e (mg g^{-1})	K_1 (min^{-1})	R^2	Q_e (mg g^{-1})	K_2 (g mg^{-1} min^{-1})	R^2
Cu							
117.76	Low CMCS	73.98	0.007	0.91	121.95	0.00025	0.99
242.10	Medium CMCS	148.76	0.008	0.92	250.00	0.00013	0.99
272.14	High CMCS	165.92	0.008	0.92	285.71	0.00011	0.99
Fe							
40.73	Low CMCS	25.37	0.005	0.94	41.67	0.00049	0.99
81.53	Medium CMCS	38.20	0.006	0.95	84.03	0.00046	0.99
79.81	High CMCS	39.79	0.006	0.95	83.33	0.00040	0.99
Pb							
4.26	Low CMCS	1.36	0.003	0.28	4.39	0.0078	0.99
7.78	Medium CMCS	2.84	0.003	0.35	8.24	0.0034	0.99
7.24	High CMCS	3.87	0.003	0.46	8.01	0.0018	0.99

Table 6.4: Regressed model parameters representing heavy metal adsorption kinetic data of CMCS derivatives and Zn dominant adsorbate system.

Experimental capacity (Q_{exp}, mg g^{-1})	CMCS derivatives	Pseudo-first-order model			Pseudo-second-order model		
		Q_e (mg g^{-1})	K_1 (min^{-1})	R^2	Q_e (mg g^{-1})	K_2 (g mg^{-1} min^{-1})	R^2
Zn							
136.28	Low CMCS	109.55	0.0055	0.88	138.89	0.00013	0.98
195.25	Medium CMCS	98.58	0.0076	0.90	200.00	0.00021	0.99
198.29	High CMCS	53.57	0.0071	0.88	204.08	0.00041	0.99
Fe							
77.50	Low CMCS	45.18	0.0064	0.92	80.65	0.00038	0.99
106.66	Medium CMCS	48.38	0.0067	0.91	111.11	0.00036	0.99
109.36	High CMCS	43.16	0.0068	0.92	113.64	0.00042	0.99
Pb							
2.14	Low CMCS	1.13	0.0030	0.36	2.27	0.00766	0.98
3.06	Medium CMCS	1.04	0.0009	0.05	3.23	0.00849	0.99
3.06	High CMCS	1.00	0.0007	0.04	3.30	0.00768	0.99

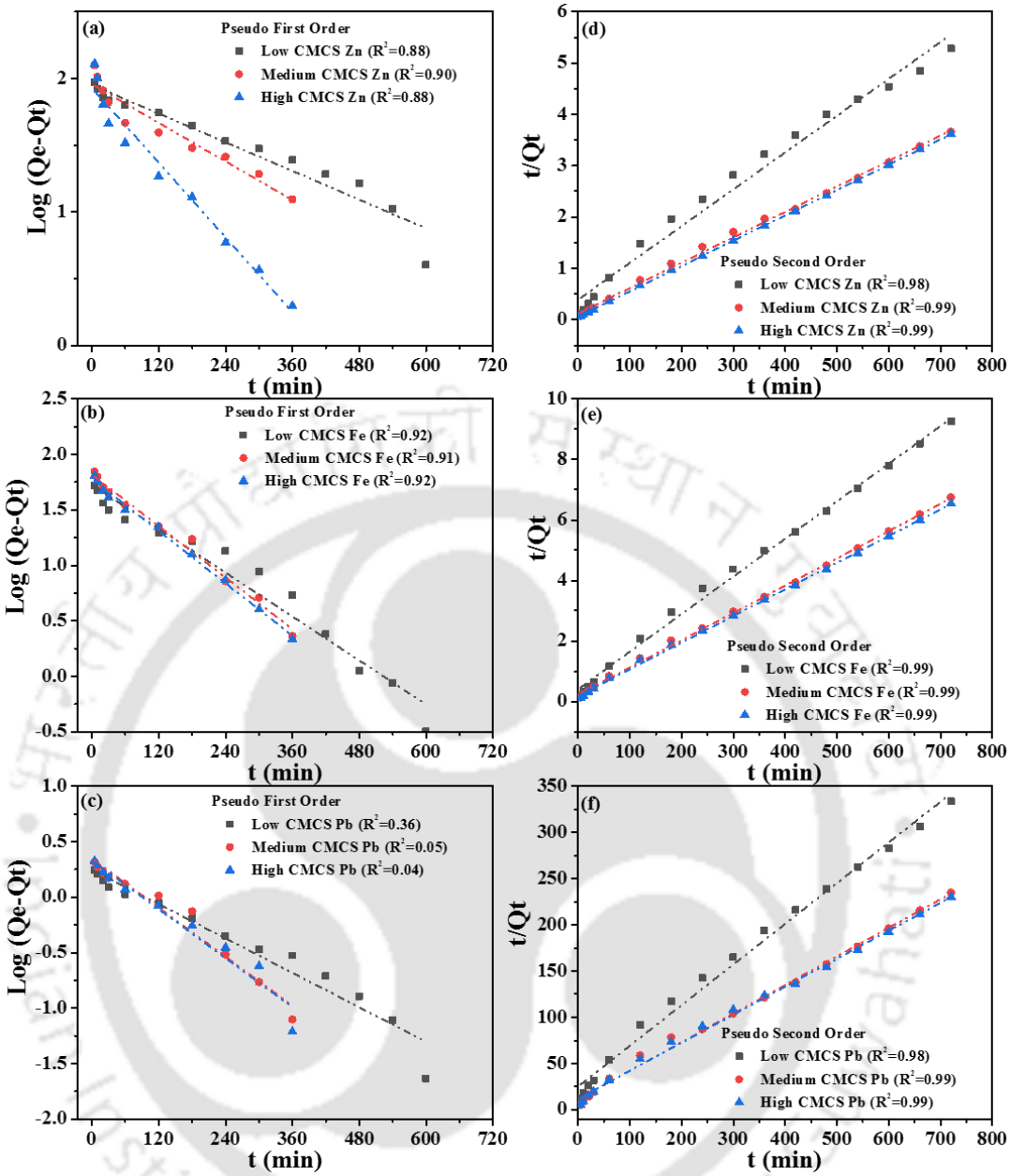

Fig. 6.11. Kinetic models fitness plots (a-c: Pseudo-first-order kinetic model, and d-f: Pseudo-second-order kinetic model) for Cit-CS derivatives and Zn dominant adsorbate system.

In order to determine and assess upon Zn, Pb, and Fe sorption kinetics characters of the CMCS derivative variants fitness plots were prepared for two well-known kinetic models and have been depicted in Fig. 6.11. Among all models, the Pseudo-second-order model was deduced to provide the perfect fit to characterize the kinetics of Pb, Zn, and Fe sorption onto CMCS

sorbent from the Zn dominant adsorbate system. Table 6.4 summarises the kinetic parametric dataset for Pb, Zn, and Fe sorption.

Isotherm models have been targeted to analyze the adsorption of studied heavy metal ions onto the surface of carboxymethyl-chitosan derivative (low CMCS, medium CMCS, high CMCS) and at a constant temperature. Langmuir Isotherm model has been the best-fit isotherm model. It is based on the assumption that adsorption occurs at specific sites on the adsorbent surface, and once a site is occupied by an adsorbate molecule, no further adsorption can take place at that site. Also, the pseudo-second-order model has been inferred to be the best-fit model to represent the kinetics of studied heavy metal ions adsorption from Cu and Zn dominant adsorbate systems and onto carboxymethyl-chitosan derivative (low CMCS, medium CMCS, high CMCS). Thus, the model's basic assumption stated as follows is valid. The rate-limiting step could be the chemisorption involving valency forces through the sharing or exchange of electrons with the prevalent functional groups of the carboxymethyl-chitosan derivative resin. The fitness of the pseudo-second-order model is also justified with the FTIR analysis of metal adsorbed carboxymethyl-chitosan derivative that inferred strong metal ions chemical interaction with the prevalent functional groups of the carboxymethyl-chitosan derivative resin.

6.4 Analytical Characterization

6.4.1 Thermo gravimetric Analysis

Fig. 9 illustrates the TGA curve for medium molecular weight chitosan and medium CMCS derivative. As shown in Fig. 9a, significant weight loss (10.5 %) occurred for chitosan below 150 °C and due to free water loss. However, the weight remained fairly constant upto 250 °C. Thereby, significant weight loss occurred upto 700 °C (66.9 % of total weight loss). In summary, for the medium CMCS resin (Fig. 9b), the total weight loss corresponds to 59.0 % and thereby confirms better thermal stability of the resin in comparison with the chitosan.

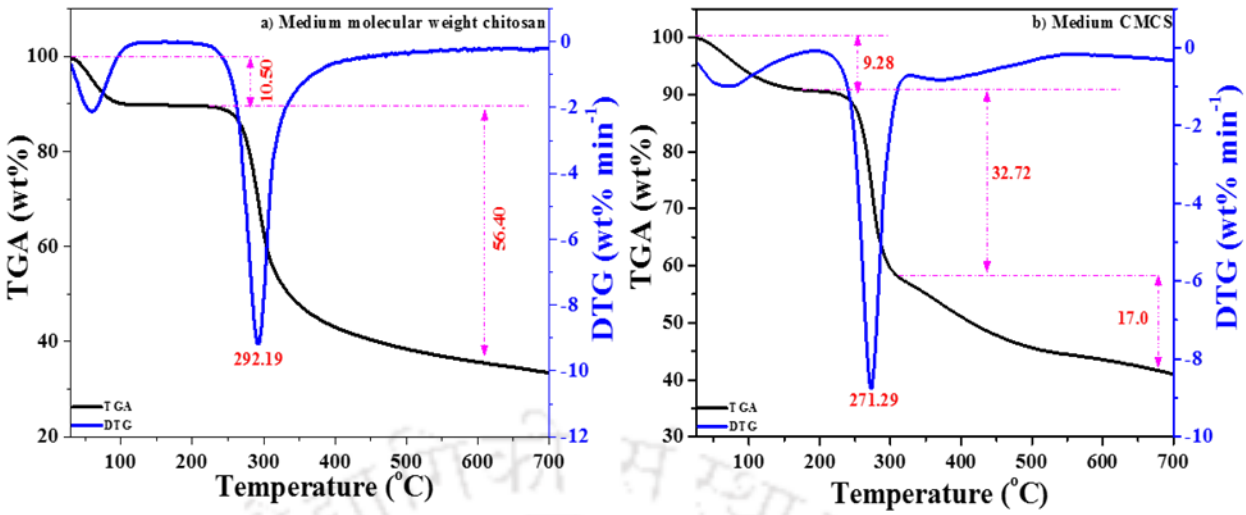

Fig. 6.12. TGA spectra of raw samples of medium molecular weight chitosan and raw medium CMCS derivative resin.

6.4.2 BET Surface Area Analysis

For the raw medium molecular weight chitosan, the BET surface area was 21.45 $m^2 g^{-1}$. For medium CMCS, the BET surface area was 31.43 $m^2 g^{-1}$. Thus, chitosan structural modification with the carboxymethyl groups facilitated pertinent alterations and increment in the surface area of the medium CMCS.

6.4.3 Crystallinity Analysis

Fig. 6.13 illustrates the X-ray diffraction patterns of raw medium molecular weight chitosan, raw medium CMCS derivative, and metal sorbed medium CMCS derivative. Corroborating with the recent literature findings, the XRD results of chitosan with a medium molecular weight (Fig. 6.13a) reveal significant and prominent peaks at 9.11°, 20.16°, and a greater degree of crystallinity. This is attributed to the prevalence of hydroxyl and amino groups. Both groups provided stronger intramolecular and intermolecular hydrogen bonds (Nagireddi et al., 2019). The carboxymethylation resulted in a varied CMCS derivative's XRD pattern (Fig. 6.13b). Thereby, it confirmed upon a reduced crystallinity or greater amorphiety. Also, the same resin structure had even greater amorphiety due to the adsorption of heavy metal ions onto the CMCS derivative surface (Fig. 6.13c).

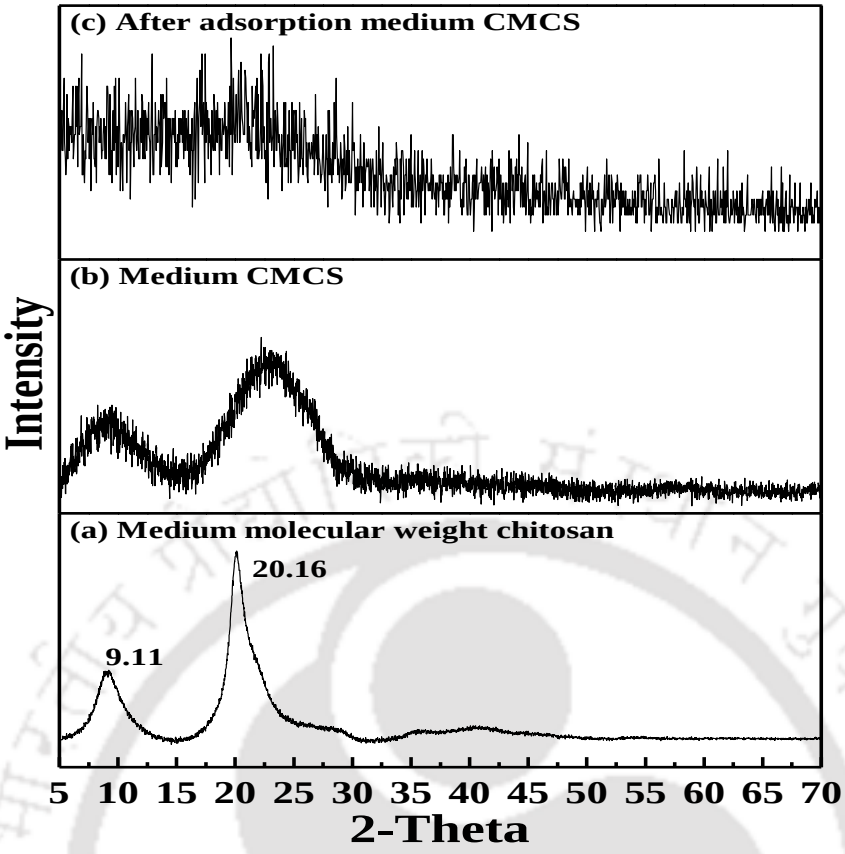

Fig. 6.13. XRD spectra of raw samples of medium molecular weight chitosan and raw medium CMCS derivative resin.

6.4.4 EDX Analysis

The FESEM and EDX spectra of raw and metal-loaded medium CMCS samples have been shown in Fig. 6.14. The EDX trend (Fig. 6.14a) confirmed the presence of C (51.7 %), O (37.1 %), and N (11.2 %) in the raw sample of the medium CMCS derivative. The medium CMCS derivative with heavy metal ions demonstrated the considerable presence of various metals Cu (1.6 %), Fe (0.6 %), and Pb (3.5 %) (Fig. 6.14b) and Zn (1.6 %), Fe (9.1 %), and Pb (1.8 %) on the medium CMCS resin surface (Fig. 6.14c).

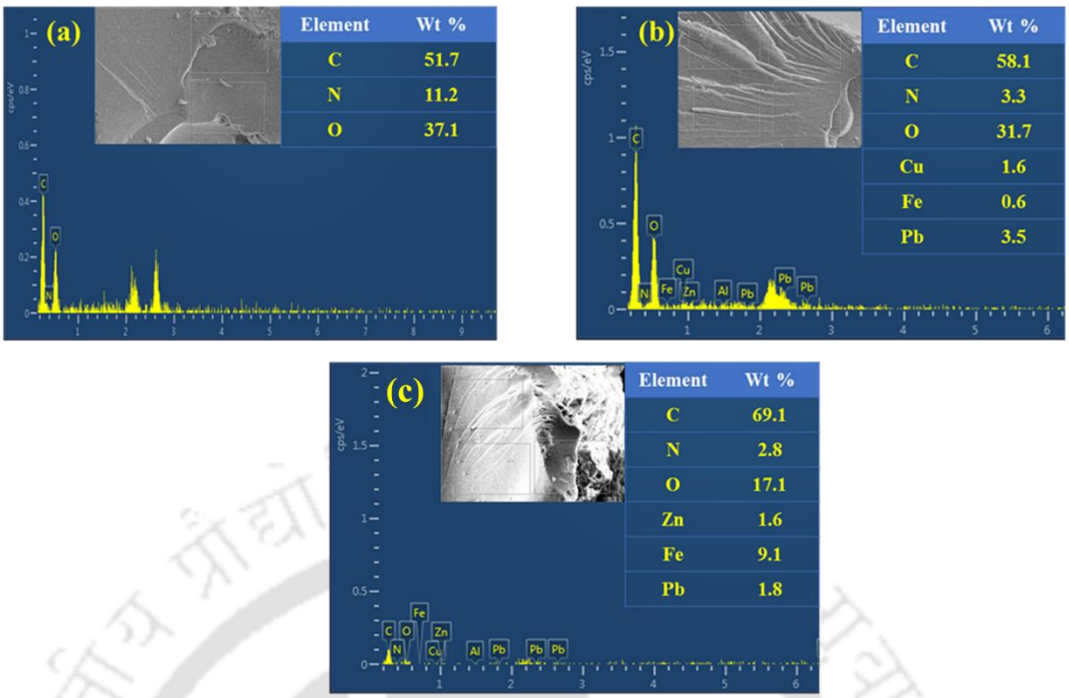

Fig. 6.14. FESEM-EDX spectra of raw and heavy metals loaded medium CMCS derivative resin samples.

6.4.5 FTIR Analysis

The FTIR spectra of medium molecular weight chitosan, and glutaraldehyde crosslinked carboxymethyl grafted chitosan (CMCS) have been shown in Fig. 6.15. In Fig. 6.15a, stretching vibrations of hydroxy (-OH) groups, NH_2 groups, and intermolecular hydrogen bonds have been confirmed at 3420 cm^{-1}. Further, a secondary amine group also exists as confirmed by the peak at 3429 cm^{-1}. Also, the chitosan FTIR spectra affirm upon CH_3 symmetric stretch (2915 cm^{-1}), CH_3 bending vibration (1379 cm^{-1}), and C-N stretching vibration of amide I (1644 cm^{-1}). In addition, the peaks observed at 1154 cm^{-1} and 1072 cm^{-1} refer to C-O-C bending vibration and C-OH stretching vibration. The intrinsic peaks of the carboxy group have been confirmed at the wavenumber of 1738 cm^{-1}. The bands at 1591 cm^{-1} and 1397 cm^{-1} correspond to the carboxy group (which overlaps with N–H bend) and carboxymethyl group, respectively (Fig. 6.15b). Compared with the peaks of chitosan, the peaks of CMC at 1591 cm^{-1} and 1397 cm^{-1}

increased. This affirmed carboxymethylation on both the amino and hydroxyl groups of chitosan (Ge and Luo, 2005). Also, in the crosslinked chitosan, the peak at 1642 cm^{-1} and 1596 cm^{-1} shifted to 1652 cm^{-1} and 1560 cm^{-1} respectively. Thereby, these peak shifts convey effective crosslinking of chitosan with glutaraldehyde (Nagireddi et al., 2017; Suc and Ly, 2013). The band at 1380 cm^{-1} corresponds to the carboxylic group of CMCS. However, after metal adsorption, the peaks weakened and shifted to 1387 cm^{-1} (Fig. 6.15c). This indicates the emergence of new bonds between the carboxyl group and adsorbed heavy metal ions.

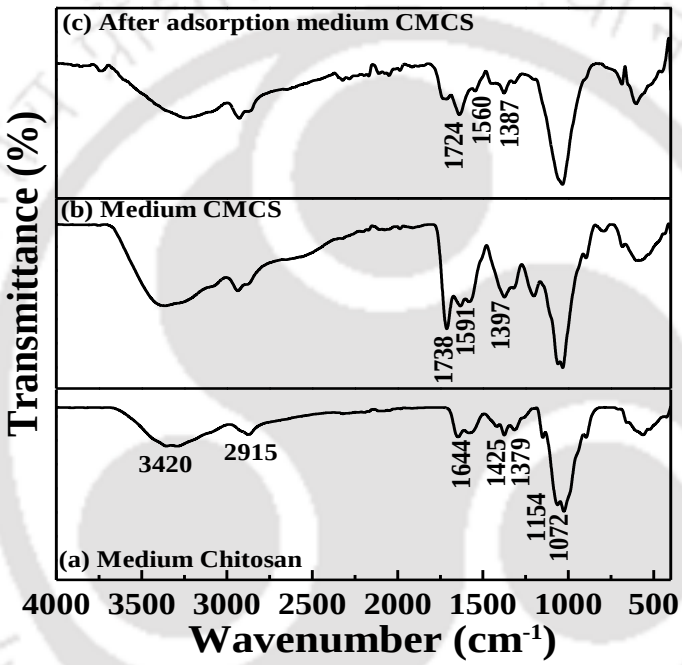

Fig. 6.15. FTIR spectra of raw and heavy metal loaded medium CMCS derivative resin samples.

6.5 Cyclic Multi-Heavy Metal Desorption Characteristics

The reusability and desorption efficiency of CMCS resin were examined to analyze the performance of the resins as a low-cost and effective reversible adsorption technology. Adsorption experiments confirmed that the medium CMCS and high CMCS resins were better in comparison to low CMCS resin. Also, the regenerative ability of medium CMCS resin with

easy-to-use and low cost (such as H_2SO_4, HNO_3, HCl, NaOH, and KOH in the broader range of concentrations (0.1-2M)) as well demonstrated effective desorptive performance.

For the Cu dominant solution and for the 2M HNO_3 eluent, the desorption performances were the best for the simulated wastewater system. Thereby, the Cu desorption performance altered as 72.81-61.52 % for a cycle number alteration from 1-3. Similarly, corresponding desorption performances of Fe varied as 71.45-44.44 % and corresponding Pb desorption performance ranged as 66.49-48.11 %. The order of heavy metal desorption efficiencies was as follows: HNO_3 > H_2SO_4 > HCl. Consequently, both cycle desorption efficiency and overall metal sorption efficacies decreased significantly for the later and consecutive cycles.

Desorption efficacies were comparatively lower for the basic solutions in the concentration range of 0.1-2M. For KOH and NaOH, Cu cycle desorption efficiencies respectively varied as 40.82-24.71 % and 37.91-17.44 % for a cycle number alteration from 1-3. Similarly, the desorption performances of Fe for KOH and NaOH have been respectively obtained as 27.21-17.26 % and 31.13-18.29 % for a cycle number alteration from 1-3. Also, the respective desorption performances of Pb for KOH and NaOH were 41.39-37.88 % and 42.19-39.10 % respectively for a cycle number alteration from 1-3. Consequently, both cycle desorption and overall metal desorption-based performances decreased significantly in consecutive cycles. For the medium CMCS, the adsorption capacity, adsorptive removal (%), and cyclic desorption removal (%) have been illustrated in Fig. 6.16. For Cu, Fe, and Pb, the cyclic desorption % lowered from 72.81-61.52 %, 71.45-44.44 %, and 66.49-48.11 % respectively, for a cycle number alteration from 1 to 3. Corresponding adsorption removal trends were 77.59-59.78 %, 78.08-69.36 %, and 88.65-63.17 %. Hence, cyclic adsorption had a detrimental influence on copper and lead removal but not iron. Thereby, the observation conveyed that while copper exhibited more irreversible chemisorption, lead and iron did not. Furthermore, the corresponding adsorption capacity lowered from 242.72-187.01 mg g^{-1}, 80.49-65.44 mg g^{-1}, and 7.68-5.48 mg g^{-1}, respectively for a cycle number alteration from 1 to 3.

Similarly, for the Zn dominant solution and for the 2 M HNO_3 eluent, the desorption performances were the best for the simulated wastewater system. Thereby, the Zn desorption performance altered as 76.68-64.51 % for an alteration in cyclic number from 1-3. Similarly, corresponding desorption performances of Fe varied as 79.76-61.82 % and corresponding Pb desorption performance ranged as 78.75-53.73 %. The order of heavy metal desorption efficiencies was as follows: HNO_3 > H_2SO_4 > HCl. Consequently, both cycle desorption efficiency and overall metal sorption efficacies decreased significantly for the later and consecutive cycles.

Desorption efficacies were comparatively lower for the basic solutions and in the concentration range of 0.1-2 M. For KOH and NaOH, Zn cycle desorption efficiencies respectively varied as 38.27-28.82 % and 35.57-27.06 % for an alteration in desorption cyclic number from 1-3. Similarly, the desorption performances of Fe for KOH and NaOH have been respectively obtained as 39.85-21.62 % and 37.12-21.10 % for an alteration in desorption cyclic number from 1-3. Also, the respective desorption performances of Pb for KOH and NaOH were 29.60-17.73 % and 31.55-16.82 % respectively for an alteration in desorption cyclic number from 1-3. Consequently, both cycle desorption and overall metal desorption-based performances decreased significantly in consecutive cycles. For the medium CMCS resin, the adsorption capacity, adsorptive removal (%), and cyclic desorption removal (%) have been illustrated in Fig. 6.17. For Zn, Fe, and Pb, the cyclic desorption % lowered from 76.68-64.51 %, 79.76-61.82 %, and 78.75-53.73 % respectively, for a cycle number alteration from 1 to 3. Corresponding adsorption removal trends were 69.99-58.98 %, 70.99-61.40 %, and 81.70-67.17 %. Hence, cyclic adsorption had a detrimental influence on zinc removal but not lead and iron. With this, it can be inferred that while iron and zinc exhibited more irreversible chemisorption, lead did not. Furthermore, the adsorption capacity lowered from 194.86-164.21 mg g^{-1}, 106.28-91.92 mg g^{-1}, and 3.09-2.54 mg g^{-1}, respectively for a cycle number alteration

from 1 to 3. Thus, as expected, the adsorption capacity reduced with an increasing number of adsorption-desorption cycles.

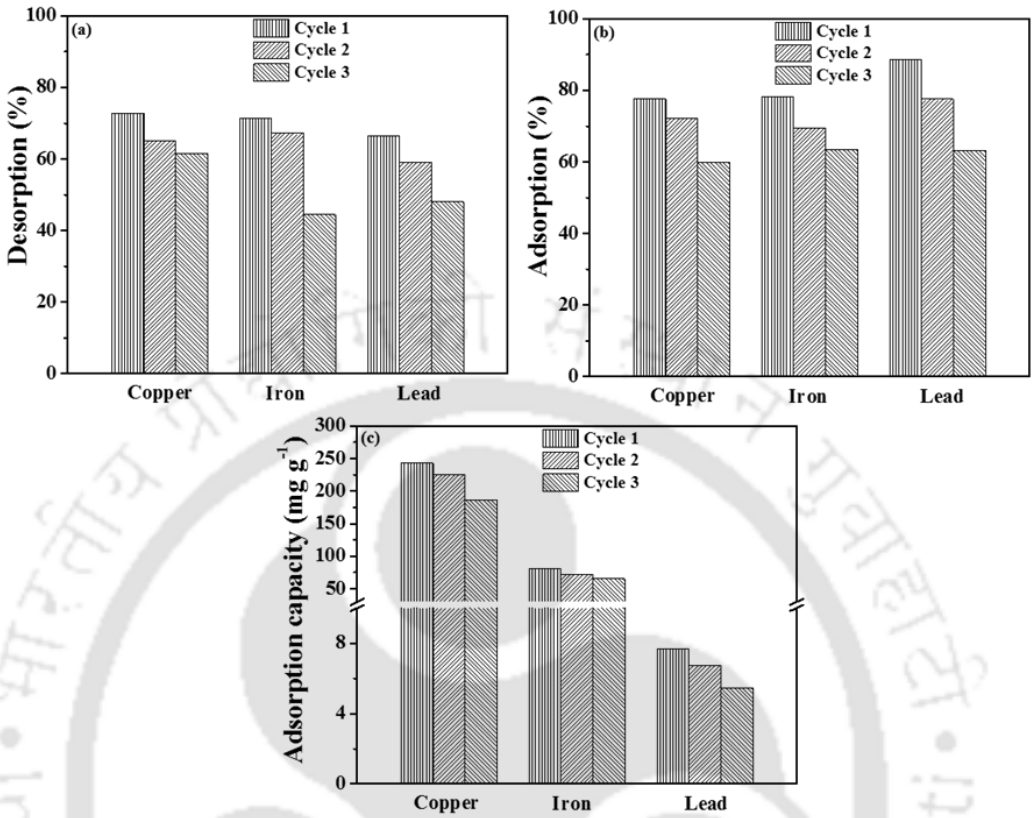

Fig. 6.16. Multi-heavy metal cyclic performance characteristics of medium CMCS derivative resin with Cu dominant adsorbate system (a) desorption % (b) adsorption % and (c) adsorption capacity.

In summary, after 3rd cycle, 61.52, 44.44, and 48.11 % desorption for Cu, Fe, and Pb, respectively were obtained for the Cu dominant solution and 64.51, 61.82, and 53.73 % removal for Zn, Fe, and Pb, respectively were obtained for the Zn dominant solution. These values convey satisfactory performance even in the coexisted cations. Consequently, the results demonstrated that the medium CMCS derivative may perform more successfully in a modified adsorption method that targeted increased removal of Pb and Cu with an appropriate pre-treatment process. Alternately, the functional role of the constituent cations can be investigated. However, theoretical and conceptual cost assessment in terms of resin expenditure per unit mol of total heavy metal elimination provide useful inferences due to relevant insights. This can be

easily addressed in the near future. Relatively lower operating costs and applicability for commercial processes may be apparent for the CMCS due to their ability to renew themselves with excellent desorption performances up to the 3rd adsorption-desorption cycle. Hence, CMCS resin may be considered a trustworthy and recyclable adsorbent for the treatment of effluent systems polluted with mentioned hazardous heavy metals.

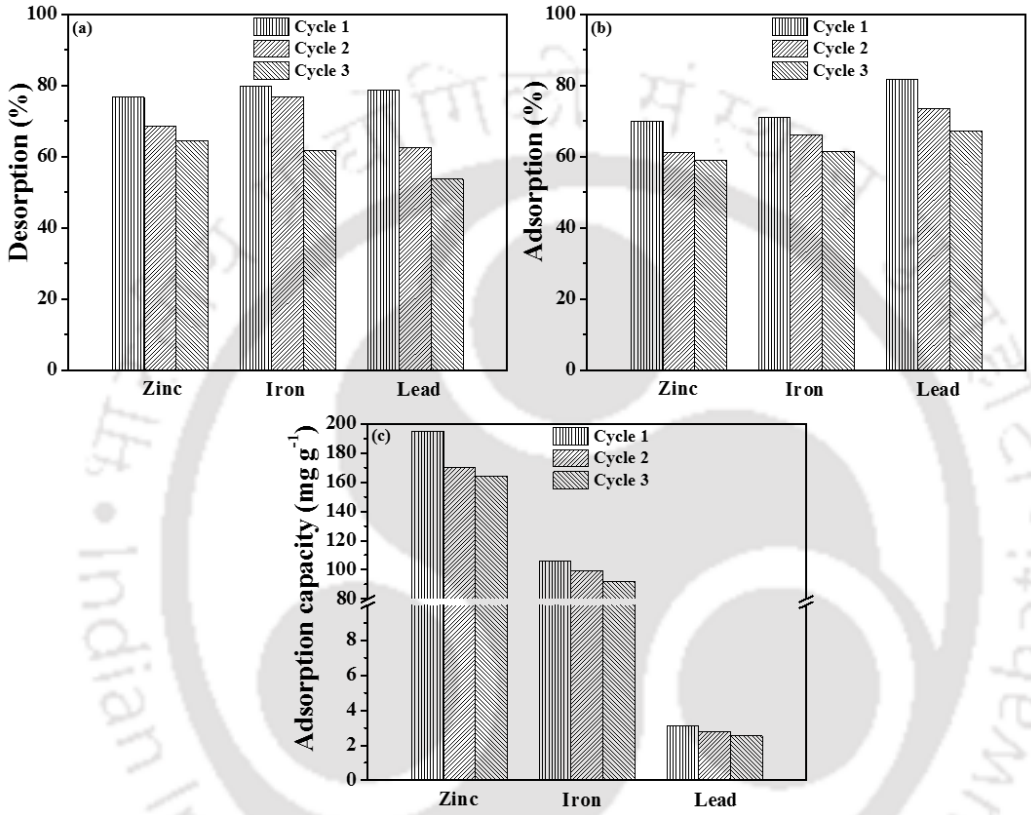

Fig. 6.17. Multi-heavy metal cyclic performance characteristics of medium CMCS derivative resin with Zn dominant adsorbate system (a) desorption % (b) adsorption % and (c) adsorption capacity.

Fig. 6.18 depicts the proposed desorption mechanism of exhausted medium CMCS derivative resin. Eluent solution would provide free H^+ ions for their reaction with exhausted medium CMCS adsorbent sorption sites. Accordingly, the adsorbed multi-heavy metal ions were released from the spent sorbent surface. However, to validate the hypothesis, additional insights are necessary from further characterization such as FTIR, EDX, and XRD analysis of the regenerated adsorbent. Such studies were beyond the scope of the Ph.D. thesis that primarily

aims to screen and scope upon the competence of chitosan derivatives for cyclic desorption-based multi-heavy metal removal from complex adsorbate systems. However, these could be addressed in the near future.

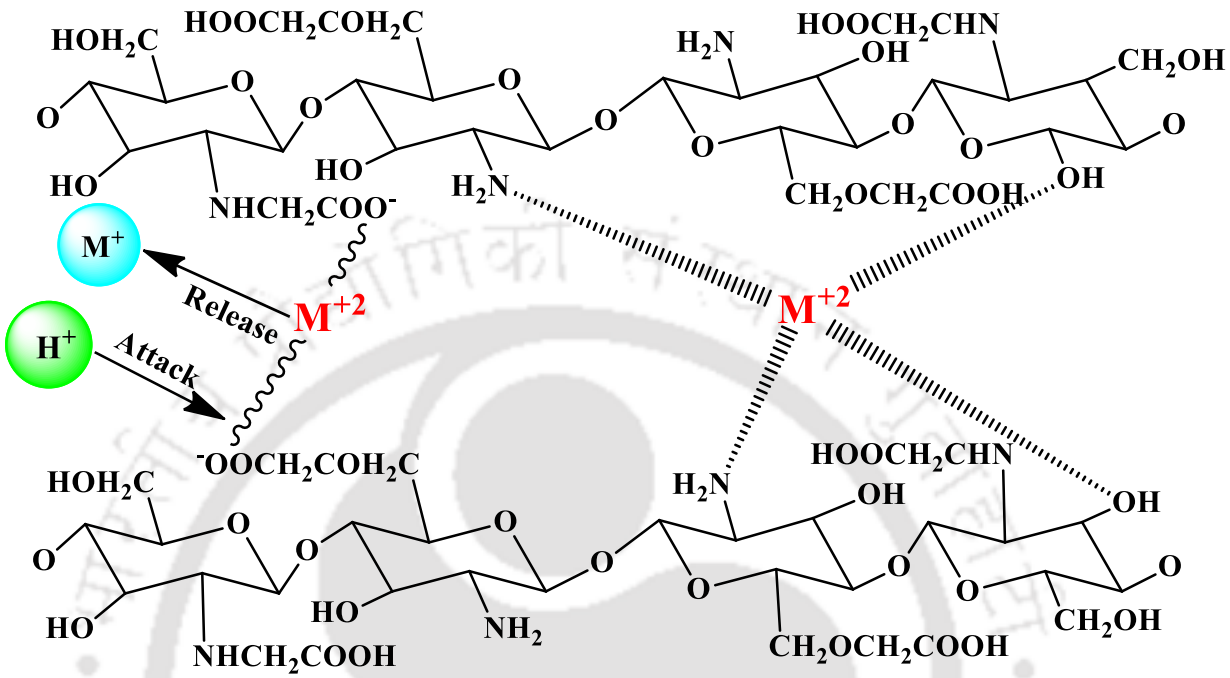

Fig. 6.18. Proposed desorption mechanism of heavy metals loaded medium CMCS resin.

6.6 Literature comparison

The experimental findings with respect to the optimality of adsorption parameters, adsorption and desorption characteristics of low CMCS, medium CMCS, and high CMCS derivatives have been compared with the best available literature for the most relevant adsorbate (multi-heavy metal solution) and adsorbent systems (chitosan-derivatives). A summary of these findings is presented in Table 6.5. For complex industrial wastewater adsorbate systems, the reported data in the Ph.D. thesis is the only relevant data to compare adsorbent performance, as other relevant literature reported data for only aqueous acidic solutions. Based on the data summarized in the table, the following can be inferred:

a) From Zn and Cu removal perspective and for synthetic complex industrial wastewater and among chitosan derivatives, medium CMCS performed promising in comparison

with the glutaraldehyde cross-linked chitosan (adsorption capacity of 238.10 mg g^{-1} for 194.9-584.7 mg L^{-1} initial Zn solution concentration range in comparison to the 72.71 mg g^{-1} for 11.3-92.3 mg L^{-1} initial Zn solution concentration range) (Busuioc et al., 2016). Similarly, the corresponding adsorption capacity of Cu was 344.83 mg g^{-1} for 187.7-563.1 mg L^{-1} initial Cu solution concentration range in comparison to 79.18 mg g^{-1} for 14.6-108.8 mg L^{-1} initial Cu solution concentration range (Busuioc et al., 2016). Hence, the performance of medium CMCS derivatives is comparable with the both adsorption and desorption characteristics of glutaraldehyde cross-linked chitosan resin. The medium CMCS derivative studied in this work performed excellent in terms of heavy metal removal but satisfactory in terms of metal desorption and derivative regeneration after three cycles.

b) From the perspective of the regeneration of the chitosan derivatives after multi-heavy metal desorption from complex synthetic industrial wastewater adsorbate solutions, the medium CMCS derivative can be concluded to have promising performance (72.81, 78.75 and 76.68 compared to 98.4, 96.7 and 98.5 aqueous solution desorption % for Cu, Pb, and Zn, respectively). In addition, the desorption efficiency is significantly better than that of styrene DVB copolymer. Hence, from a heavy metal removal and derivative regeneration perspective and complex adsorbate systems, medium CMCS is the best among PVA/Chitosan beads, EDTA-modified Chi/SiO_2/Fe_3O_4, and PVA/Chitosan foam.

c) All other literature data cannot be compared with the data obtained in this work, as these literature targets heavy metal removal from aqueous solutions with lesser solution complexity.

Table 6.5: Summary of the adsorption and desorption characteristics of alternate CMCS derivatives investigated in this study and prior art.

Adsorbent	Metal Ions	Solution	Dose (g L^{-1})	Contact duration (min)	Conc. range (mg L^{-1})	Adsorption capacity (mg g^{-1})	Removal efficacy (%)	Desorption (%)	Eluents	Ref.
Medium CMCS	Zn Pb Fe	Multi metal solution	1.4	420	194.9 - 584.7 2.65-7.95 104.8 - 314.4	238.10 4.78 147.06	70.13 80.82 71.24	76.68-64.51 78.75-53.73 79.76-61.82 (1-3 cycles)	2.0 M HCl	This study
Medium CMCS	Cu Pb Fe	Multi metal solution	1.2	540	187.7 - 563.1 5.2-15.6 61.9-185.5	344.83 9.59 90.09	77.18 83.24 76.54	72.81-61.52% 66.49-48.11% 71.45-44.44% (1-3 cycles)	2.0 M HNO_3	This study
PVA/Chitosan Beads	Cu Pb Zn Cd	Multi metal solution	2	660 540 660 540	50-500	238.45 166.44 74.18 126.06 (Single solution)	93.90 77.85 10.93 21.31 (Multi-metal solution)	98.4 96.7 98.5 98.5 (Single solution)	0.1M EDTA for Cu 0.1 M HCl for Pb, Zn, Cd	(Li et al., 2011)
GLA/Chitosan	Pb Ni Zn Cu	Multi metal solution	1	420 360 420 360	9.1-90.72 13.4-99.4 11.3-92.3 14.6-108.8	67.17 67.81 72.71 79.18	74.06 73.45 73.16 72.77	-		(Busuioc et al., 2016)
PVA/Chitosan Foam	MG dye Cu	Binary solution	2	360 480	50-800	227.02 111.85	-	97	0.1 M Na_2EDTA	(Li et al., 2012)
EDTA modified Chi/SiO_2/Fe_3O_4	Cu Pb Cd	Mixed solution	1	360 180 360	0.2-5 (mM)	0.699 0.596 0.563	-	75.73	0.01 M Na_2EDTA	(Ren et al., 2013)
Chitosan immobilized Bentonite	Cu Ni Pb	Aqueous binary solution	-	240-360 240-360 240-360	25-200 25-200 25-200	17.09 12.61 20.8	51.41 39.04 80	-	-	(Futalan et al., 2011)

6.7 Summary

Several useful insights can be deduced from the best findings achieved in this work in the field of heavy metal adsorption and desorption characteristics of low CMCS, medium CMCS, and

high CMCS derivatives with synthetic complex industrial adsorbate systems. Firstly, the optimal multi-heavy metal batch adsorption parameters for the medium CMCS derivative in Cu dominant solution were 3.82 pH, 1.2 g L^{-1} dosage, and 540 min contact time. Corresponding adsorption capacity and metal removal % of the resin were 144.69-300.57 mg g^{-1} and 92.50-64.05 % for Cu, 46.70-84.21 mg g^{-1} and 90.61-54.46 % for Fe and 4.04-8.68 mg g^{-1} and 93.33-66.73 % for Pb, respectively for the initial heavy metal ion concentration range of 187.7-563.1 mg L^{-1} for Cu, 61.85-185.55 mg L^{-1} for Fe, and 5.2-15.6 mg L^{-1} for Pb. On the other hand, the optimal heavy metal ion batch adsorption parameters for medium CMCS in Zn dominant solution were 3.64 pH, 1.4 g L^{-1} dosage, and 420 min contact time. Corresponding adsorption capacity and metal removal % of the resin were 115.84-208.98 mg g^{-1} and 83.21-50.04 % for Zn, 61.85-123.56 mg g^{-1} and 82.63-55.02 % for Fe and 1.67-3.82 mg g^{-1} and 88.05-67.34 % for Pb, respectively in the initial heavy metal ion concentration range of 194.9-584.7 mg L^{-1} for Zn, 104.8-314.4 mg L^{-1} for Fe, and 2.65-7.95 mg L^{-1} for Pb. Hence, compared to the Zn dominant solution, the medium CMCS derivative provided higher removal efficiencies with the Cu dominant solution and the medium CMCS resin exhibited higher regeneration characteristics in the Zn dominant solution in comparison with Cu dominant solution. Secondly, after the three cycles, the desorption characteristics were 61.52, 44.44, and 48.11 % for Cu, Fe, and Pb, respectively for the Cu dominant solution and 64.51, 61.82, and 53.73 % for Zn, Fe, and Pb, respectively for the Zn dominant solution. These indicate and confirm satisfactory heavy metal ion removal and resin regeneration.

Further improvement in the heavy metal ion desorption characteristics of medium CMCS can be conveniently targeted through the suitable alteration in functional groups abundance. This can be achieved through stoichiometric and resin synthesis variations. The surface analysis with FTIR, BET, TGA, XRD FESEM-EDX, etc., have been in good agreement with apparent functional interactions between various chemical species.

From the perspective of heavy metal ion removal and resin reusability, compared to the available prior art based on aqueous solution, medium CMCS derivative performed better for complex synthetic industrial wastewater adsorbate systems. With respect to chitosan, all adsorbents exhibited excellent desorption characteristics and thereby confirmed upon the greater role of chelating functional groups in achieving improved resin reusability for multi-heavy metal removal from synthetic industrial wastewater adsorbate systems.

Chapter 7:

Conceptual Resin and Processing Cost Analysis

Chapter 7

Conceptual Resin and Processing Cost Analysis

Based on the unit costs and conceptual sizing and costing procedures, conceptual resin and processing costs were targeted. Accordingly, the findings have been summarized in the chapter. For needful analysis, the best findings data in the previous chapters were chosen. Accordingly, the salient features of the modeling effort have been presented in section 7.1 of the chapter. Thereafter, section 7.2 elucidates on the conceptual resin costs followed by conceptual processing costs in section 7.3. Section 7.4 briefly describes the findings associated to comparative cyclic adsorption-desorption capabilities of synthesized chitosan resins. Thereafter, section 7.5 presents the findings related to the best chitosan-based resin cost for the similar processing cost of the commercial resin (lowest cost). Finally, a summary of the cost analyses has been presented in section 7.6 of the chapter.

7.1 Conceptual Sizing and Costing Methods

Table 7.1 summarizes the unit costs of chemicals (for synthesis), units (adsorbers), electricity, and other entities. The lab scale conceptual fabrication cost was evaluated from the cumulative cost of all costs involved in the synthesis of the chitosan derivative resins (i.e., retail cost of chemicals (as quoted by major suppliers of chemical reagents); manpower cost @ 100 Rs/h for 100 g; electricity cost @ 9 Rs/kWh; miscellaneous equipment cost (20% of total manpower and electricity cost). The industrial scale conceptual fabrication cost of the chitosan derivative resins was evaluated with the assumption that the bulk chemicals cost is about 60% of the retail costs of the chemicals. Further, for the case, all other parameters were considered to be the same as those being considered

for the case of conceptual lab scale fabrication cost. Appendix D elaborates upon the model calculations for the best case (high CSPVA) and for both lab scale and industrial scale conceptual resin cost cases and for the evaluation of conceptual resin cost and processing costs. Notable assumptions in the study refer to

a) 60 % bulk cost of commodities with respect to their respective retail costs.
b) Batch to continuous process scalability efficacy factor of 0.1 i.e., a multiplication factor of 10 to convert process scalability efficacy.

7.2 Conceptual Resin Cost Analysis

7.2.1 CSPVA derivative resin

For the CSPVA resin, an illustrative comparison in the adsorbent synthesis cost (lab scale) of the best-performing chitosan derivative (high CSPVA), commercial resins, and other CSPVA derivatives (low CSPVA and medium CSPVA) has been illustrated in Fig. 7.1a. As conveyed, the lab scale conceptual synthesis costs of the resins were 1141.54, 1187.30, 1298.76, 68.08, and 326.6 INR per 10 g of low CSPVA, medium CSPVA, high CSPVA, Amberlite IR 120H and Lewatit TP 260 resins, respectively. Thus, for such a cost basis of the retail cost, the chitosan-based resins are significantly expensive with respect to commercial Amberlite IR 120H resin. Also, cost variations in the chitosan-based resin have been significant on a molecular weight basis. This is due to the similar synthesis cost of the resins and the very insignificant influence of the chitosan molecular weight on the synthesis cost reduction in this regard. For this case, the best resins are low CSPVA (1141.54 INR per 10 g) and Amberlite IR 120H (68.08 INR per 10 g). Comparatively, Lewatit TP 260 resin was 4.8 times more expensive than the Amberlite IR 120H. Further, Fig. 7.1b illustrated a significant reduction in the resin conceptual synthesis cost for the large-scale synthesis case (40 % retail cost basis) in comparison with the lab-scale synthesis cost. For the scenario, the resin costs

were 632.77, 650.82, 695.41, 27.23, and 130.64 INR per 10 g of low CSPVA, medium CSPVA, high CSPVA, Amberlite IR 120H and Lewatit TP 260 resins, respectively. Thus, the cost of all chitosan PVA resins was similar but higher than the cost of commercial resins. The best chitosan resin for the case has been low CSPVA (632.77 INR per 10 g) which is significantly higher than the value evaluated for the Amberlite IR 120H commercial resin (27.23 INR per 10 g). Thus, chitosan molecular weight alterations did provide dividends in terms of the synthesis cost. Comparatively, Lewatit TP 260 resin was 4.80 times expensive and chitosan PVA resin was 23.24 times comparatively expensive with respect to the Amberlite IR 120H.

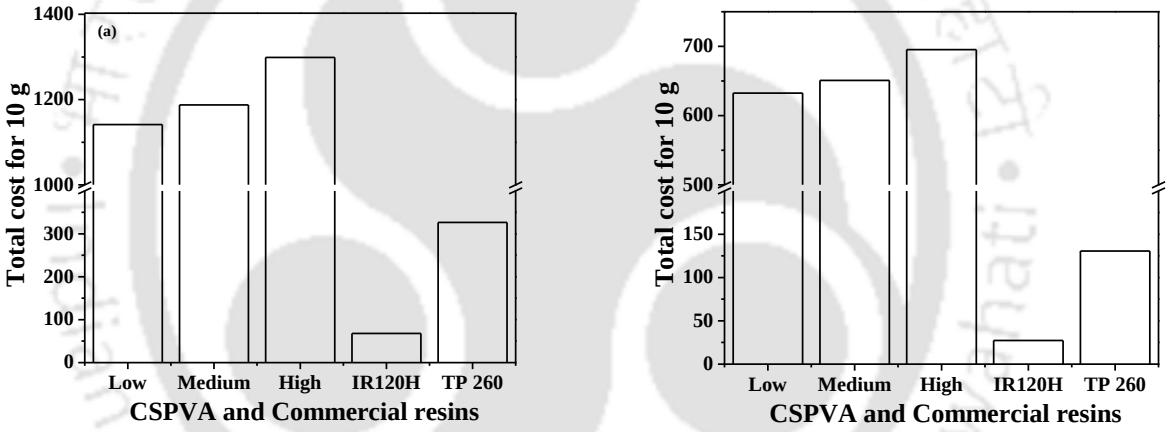

Fig. 7.1. Bar chart depicting the (a) lab scale conceptual fabrication cost and (b) industrial scale conceptual fabrication cost of CSPVA and commercial resins.

7.2.2 Cit-CS derivative resin

For the Cit-CS resin, a comparison in adsorbent synthesis cost (lab scale) of the best-performing chitosan derivative (medium Cit-CS) with the chosen commercial resins and other Cit-CS derivatives (low Cit-CS and high Cit-CS) has been depicted in Fig. 7.2a. The lab scale conceptual synthesis costs of the resins were 1204.05, 1260.21, 1361.27, 68.08, and 326.6 INR per 10 g of

low Cit-CS, medium Cit-CS, high Cit-CS, Amberlite IR 120H, and Lewatit TP 260 resins, respectively. Thus, for such a cost basis of the retail cost, the chitosan-based resins are significantly expensive with respect to commercial Amberlite IR 120H resin. Also, cost variations in the chitosan-based resin have been significant on a molecular weight basis. This is due to the similar synthesis cost of the resins and the very insignificant influence of the chitosan molecular weight on the reduction of the synthesis cost of the chitosan derivatives. Among all, the best resins were low Cit-CS (1204.05 INR per 10 g) and Amberlite IR 120H (68.08 INR per 10 g). Comparatively, Lewatit TP 260 resin is 4.8 times more expensive than the Amberlite IR 120H. Further, Fig. 7.2b illustrated a significant reduction in the resin conceptual synthesis cost for the large-scale synthesis case in comparison with the lab-scale synthesis cost. For the scenario, the resin costs are 627.18, 649.64, 690.07, 27.23, and 130.64 INR per 10 g of low Cit-CS, medium Cit-CS, high Cit-CS, Amberlite IR 120H and Lewatit TP 260 resins, respectively. Thus, the cost of all chitosan citric acid derivative resins was similar but higher than the costs of the commercial resins. The best chitosan resin for the case has been low Cit-CS (627.18 INR per 10 g) which is significantly higher than the Amberlite IR 120H commercial resin (27.23 INR per 10 g). Thus, chitosan molecular weight alterations did provide dividends in terms of the synthesis cost. Comparatively, Lewatit TP 260 resin is 4.8 times more expensive and chitosan citric acid resin is 23.03 times more comparatively expensive with respect to the Amberlite IR 120H commercial resin.

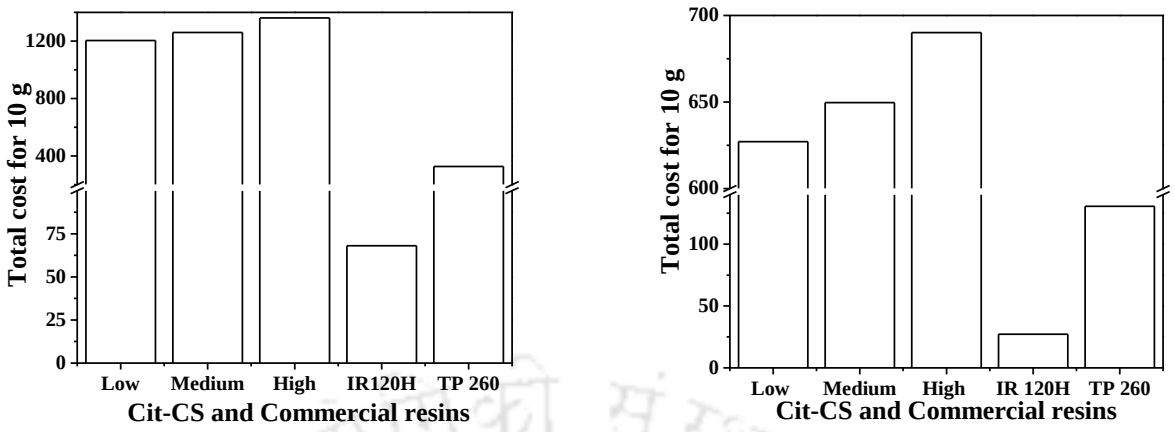

Fig. 7.2. Bar chart depicting the (a) lab scale conceptual fabrication cost and (b) industrial scale conceptual fabrication cost of Cit-CS and commercial resins.

7.2.3 CMCS derivative resin

For the CMCS resin, a comparison in adsorbent synthesis cost (lab scale) of the best-performing chitosan derivative (medium CMCS) with the chosen commercial resins and other CMCS derivatives (low CMCS and high CMCS) has been illustrated in Fig. 7.3a. The lab scale conceptual synthesis costs of the resins were 705.31, 733.4, 817.83, 68.08, and 326.6 INR per 10 g of low CMCS, medium CMCS, high CMCS, Amberlite IR 120H, and Lewatit TP 260 resins, respectively. Thus, for such a cost basis of the retail cost, the chitosan-based resins have been significantly expensive with respect to commercial Amberlite IR 120H resin. Also, cost variations in the chitosan-based resin have been significant on a molecular weight basis. This is due to the similar synthesis cost of the resins and the very insignificant influence of the chitosan molecular weight on the synthesized resin's cost reduction. Among the mentioned resins, the best are low CMCS (705.31 INR per 10 g) and Amberlite IR 120H (68.08 INR per 10 g). Comparatively, Lewatit TP 260 resin was 4.8 times more expensive than the Amberlite IR 120H. Further, Fig. 7.3b illustrated a significant reduction in the resin conceptual synthesis cost for the large-scale synthesis case in

comparison with the lab-scale synthesis cost. For the scenario, the resin costs were 383.77, 395.00, 428.78, 27.23, and 130.64 INR per 10 g of low CMCS, medium CMCS, high CMCS, Amberlite IR 120H, and Lewatit TP 260 resins, respectively. Thus, the cost of all chitosan citric acid resins was similar but higher than the cost of commercial resins. The best chitosan resin for the case has been low CMCS (383.77 INR per 10 g). Incidentally, its cost is significantly higher than that of the Amberlite IR 120H commercial resin (27.23 INR per 10 g). Thus, chitosan molecular weight alterations did provide dividends in terms of the synthesis cost. Comparatively, Lewatit TP 260 resin has been 4.8 times more expensive and chitosan carboxymethyl resin has been 14.09 times more expensive with respect to the best resin (Amberlite IR 120H).

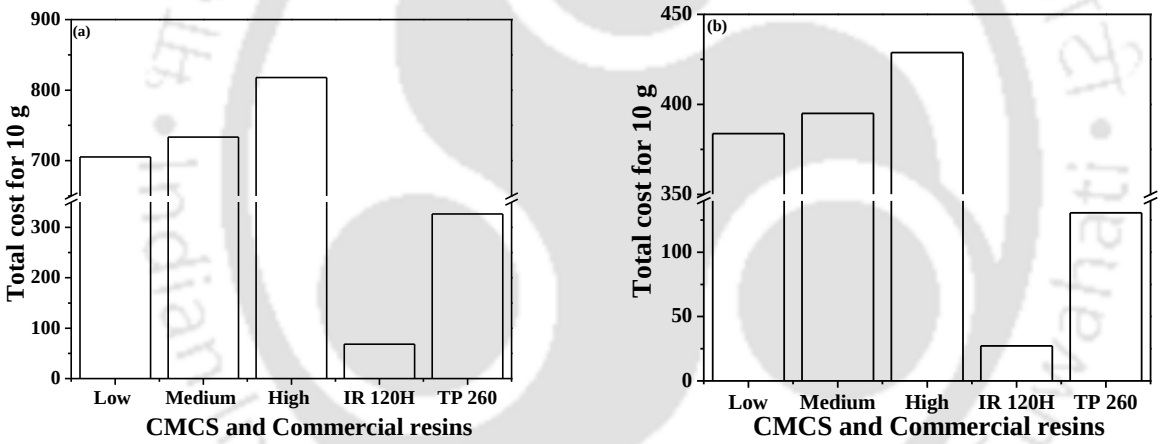

Fig. 7.3. Bar chart depicting the (a) lab scale conceptual fabrication cost and (b) industrial scale conceptual fabrication cost of CMCS and commercial resins.

For the CSPVA resin, a comparison in adsorbent manufacturing cost distribution (lab scale) of the best-performing chitosan derivative (high CSPVA) with the other CSPVA derivatives (low CSPVA and medium CSPVA) has been illustrated in Fig. 7.4. The figure refers to the cost distribution of chitosan, equipment, manpower, electricity, and other chemicals. For low CSPVA, the % contribution of these costs (Fig. 7.4a) are 59.64, 4.28, 14.02, 7.39, and 14.67 % respectively.

Similarly, for medium CSPVA, % contribution of these costs (Fig. 7.4b) are 62.07, 4.12, 13.48, 7.10 and 13.23 % respectively, and for high CSPVA, values are 60.65, 3.76, 12.32, 6.49 and 16.78 % respectively (Fig. 7.4c). Thus in all cases, chitosan cost contributed a very significant cost.

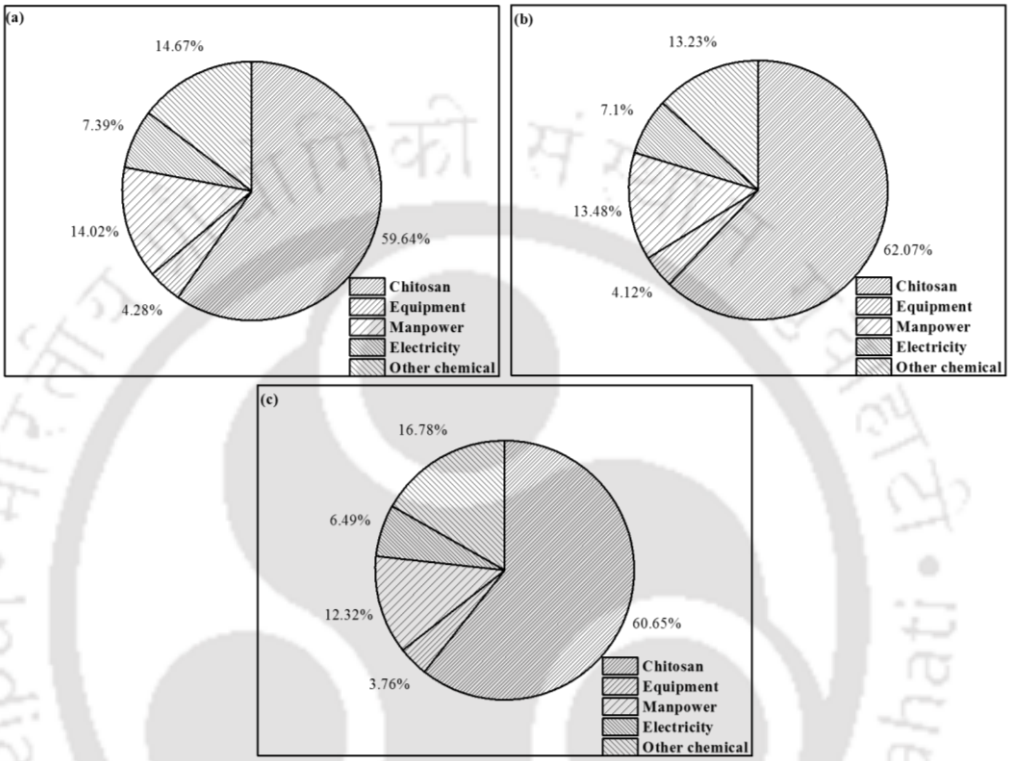

Fig. 7.4. Pie chart depicting the cost contribution of various entities towards the lab scale conceptual resin cost (a) low CSPVA (b) medium CSPVA and (c) high CSPVA resins.

For the Cit-CS resin, a comparison in adsorbent manufacturing cost distribution (lab scale) of the best-performing chitosan derivative (high Cit-CS) with the other Cit-CS derivatives (low Cit-CS and medium Cit-CS) has been illustrated in Fig. 7.5. For low Cit-CS, % contribution of chitosan, equipment, manpower, electricity and other chemicals costs (Fig. 7.5a) were 56.55, 3.36, 13.29, 3.50 and 23.30 % respectively. Similarly, for medium Cit-CS, % contribution of these costs (Fig. 7.5b) were 58.48, 3.21, 12.70, 3.35 and 22.26 % respectively, and for high Cit-CS, values were

obtained as 57.87, 2.97, 11.75, 3.10 and 24.31 % respectively (Fig. 7.5c). Thus in all cases, chitosan cost contributed a very significant cost.

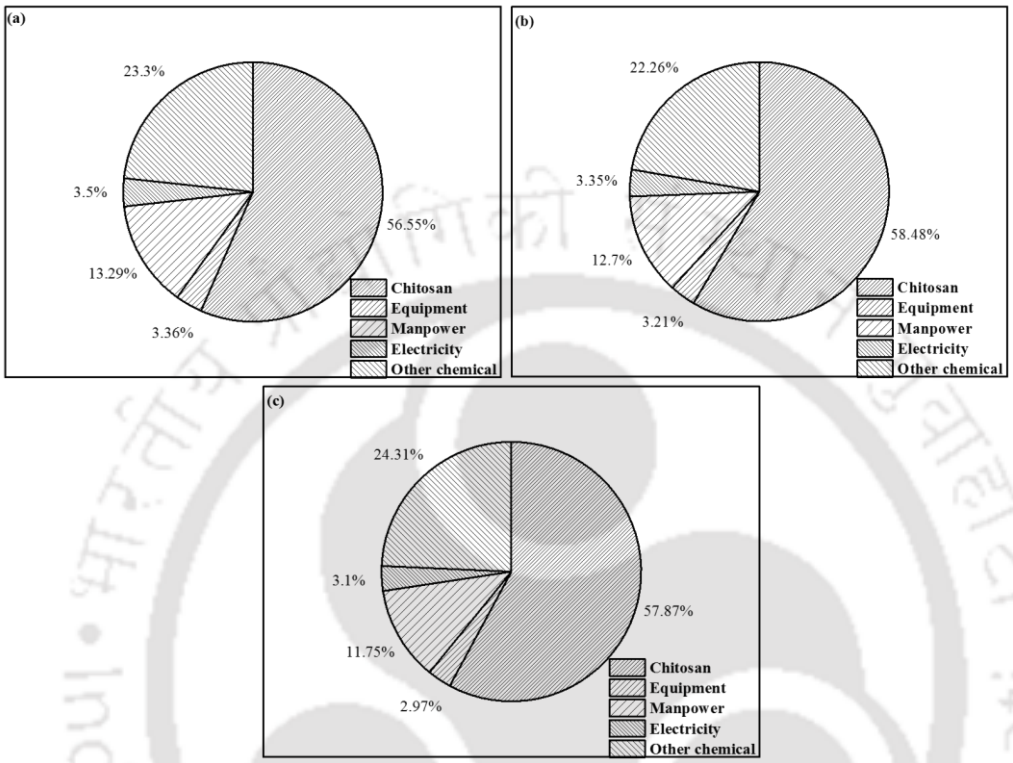

Fig. 7.5. Pie chart depicting the cost contribution of various entities towards the lab scale conceptual resin cost (a) low Cit-CS (b) medium Cit-CS and (c) high Cit-CS resins.

For the CMCS resin, a comparison in adsorbent manufacturing cost distribution (lab scale) of the best-performing chitosan derivative (high CMCS) with the other CMCS derivatives (low CMCS and medium CMCS) has been illustrated in Fig. 7.6. For low CMCS, % contribution of chitosan, equipment, manpower, electricity and other chemicals costs (Fig. 7.6a) were 48.27, 4.00, 14.18, 5.84 and 27.71 % respectively. Similarly, for medium CMCS, % contribution of these costs (Fig. 7.6b) were 50.18, 3.86, 13.66, 5.62 and 26.69 % respectively, and for high CMCS, values were

obtained as 48.16, 3.45, 12.23, 5.03 and 31.13 % respectively (Fig. 7.6c). Thus in all cases, chitosan cost contributed a very significant cost.

For the CSPVA resin, a comparison in adsorbent manufacturing cost distribution (industrial scale) of the best-performing chitosan derivative (high CSPVA) with the other CSPVA derivatives (low CSPVA and medium CSPVA) has been illustrated in Fig. 7.7. Cost distribution consists cost of chitosan, equipment, manpower, electricity, and other chemicals. For low CSPVA, the % contribution of these costs (Fig. 7.7a) were 43.06, 7.72, 25.30, 13.33, and 10.59 % respectively. Similarly, for medium CSPVA, % contribution of these costs (Fig. 7.7b) were 45.30, 7.51, 24.58, 12.95 and 9.65 % respectively, and for high CSPVA, values were obtained as 45.31, 7.03, 23.01, 12.12 and 12.53 % respectively (Fig. 7.7c). Thus in all cases, chitosan cost contributed a very significant cost.

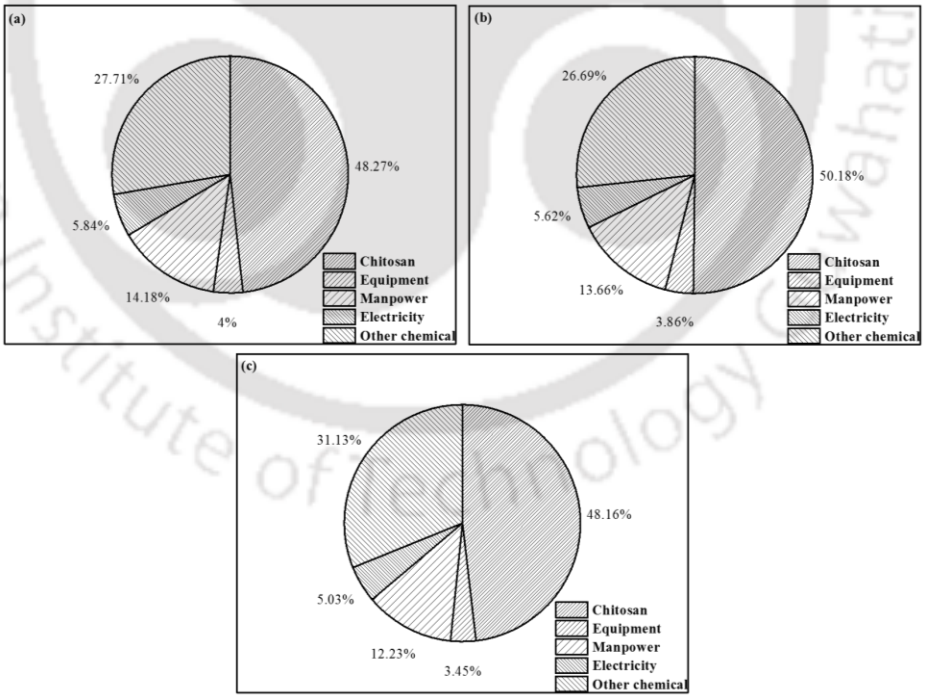

Fig. 7.6. Pie chart depicting the cost contribution of various entities towards the lab scale conceptual resin cost (a) low CMCS (b) medium CMCS and (c) high CMCS resins.

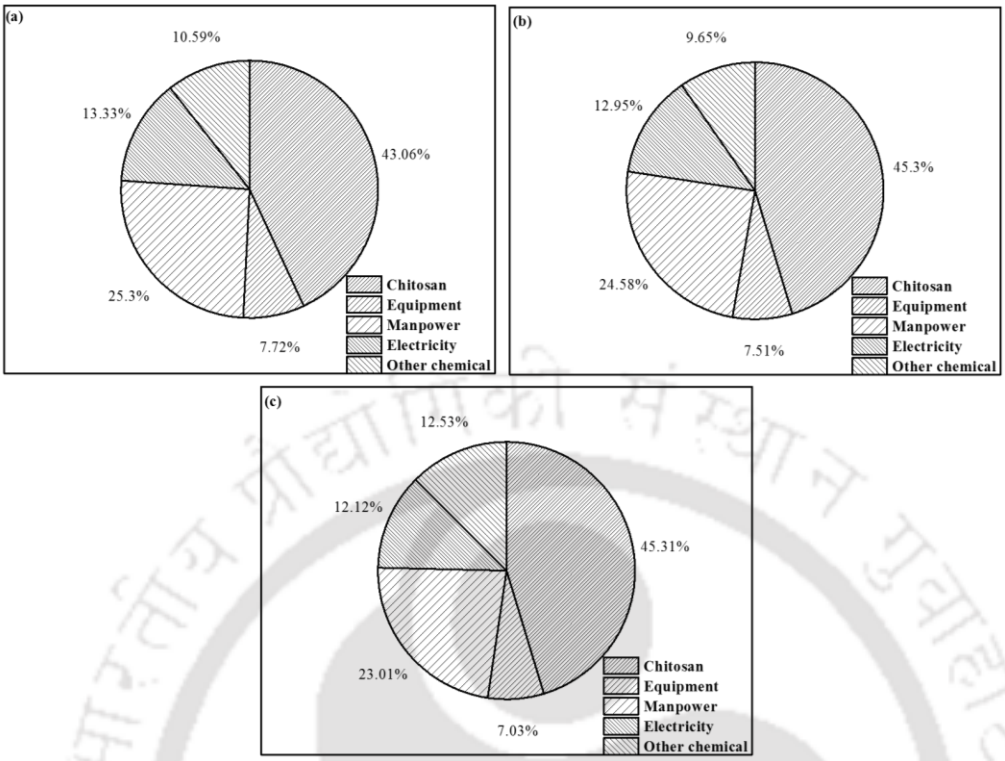

Fig. 7.7. Pie chart depicting the cost contribution of various entities towards the industrial scale conceptual resin cost (a) low CSPVA (b) medium CSPVA and (c) high CSPVA resins.

For the Cit-CS resin, a comparison in adsorbent manufacturing cost distribution (industrial scale) of the best-performing chitosan derivative (high Cit-CS) with the other Cit-CS derivatives (low Cit-CS and medium Cit-CS) has been illustrated in Fig. 7.8. For low Cit-CS, % contribution of chitosan, equipment, manpower, electricity and other chemicals costs (Fig. 7.8a) were 43.43, 6.45, 25.51, 6.72 and 17.89 % respectively. Similarly, for medium Cit-CS, % contribution of these costs (Fig. 7.8b) were 45.38, 6.22, 24.63, 6.49 and 17.28 % respectively, and for high Cit-CS, values were obtained as 45.66, 5.89, 23.19, 6.11 and 19.18 % respectively (Fig. 7.8c). Thus in all cases, chitosan cost contributed a very significant cost.

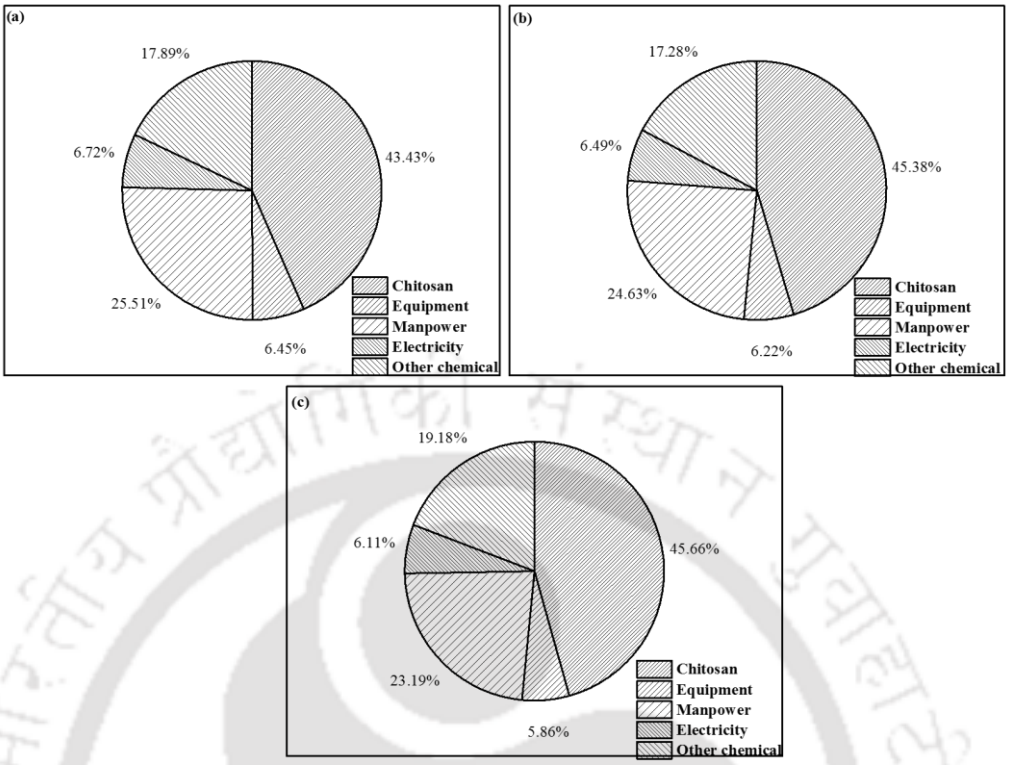

Fig. 7.8. Pie chart depicting the cost contribution of various entities towards the industrial scale conceptual resin cost (a) low Cit-CS (b) medium Cit-CS and (c) high Cit-CS resins.

For the CMCS resin, a comparison in adsorbent manufacturing cost distribution (industrial scale) of the best-performing chitosan derivative (high CMCS) with the other CMCS derivatives (low CMCS and medium CMCS) has been illustrated in Fig. 7.9. For low CMCS, % contribution of chitosan, equipment, manpower, electricity and other chemicals costs (Fig. 7.9a) were 35.48, 7.36, 26.06, 10.73 and 20.37 % respectively. Similarly, for medium CMCS, % contribution of these costs (Fig. 7.9b) were 37.32, 7.15, 25.32, 10.42 and 19.79 % respectively, and for high CMCS, values were obtained as 36.74, 6.59, 23.32, 9.60 and 23.75 % respectively (Fig. 7.9c). Thus in all cases, chitosan cost contributed a very significant cost.

In summary, through a reduction in resin cost from 40 to 10 % of the retail costs, the chitosan resin cost contribution to the overall processing cost was reduced from 428.776-234.25 INR/10 g.

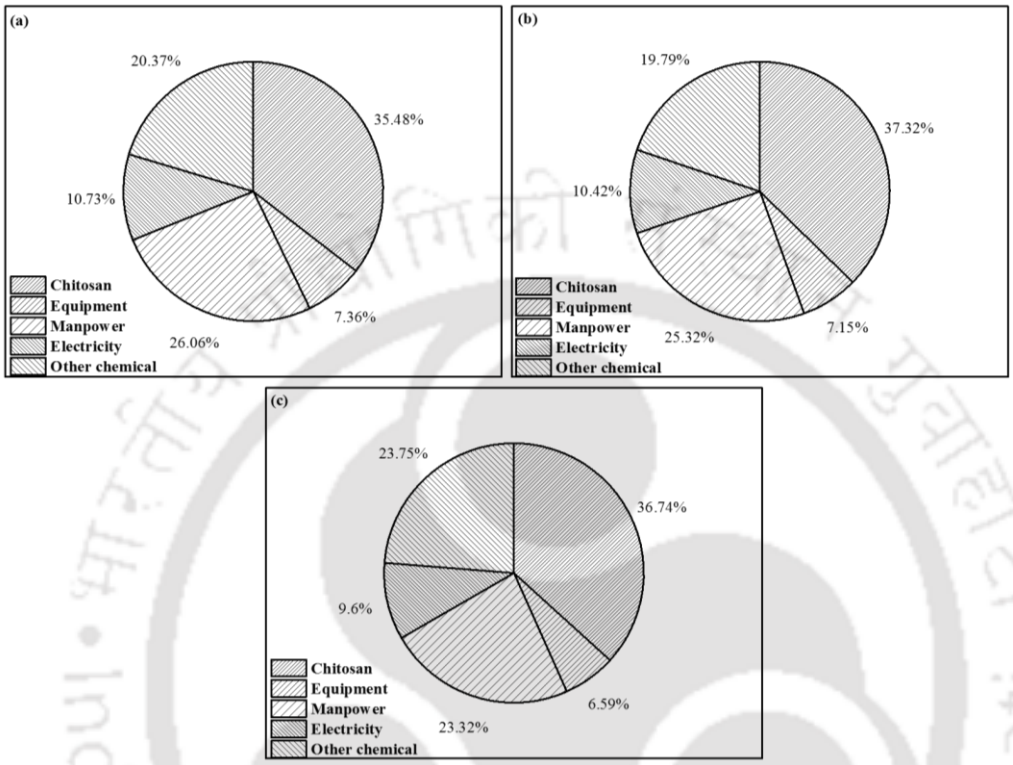

Fig. 7.9. Pie chart depicting the cost contribution of various entities towards the industrial scale conceptual resin cost (a) low CMCS (b) medium CMCS and (c) high CMCS resins.

7.3 Conceptual Processing Cost

For a treatment plant of 3000 m^3 annual plant capacity (flow rate @ 10000 L day^{-1}), the conceptual processing costs per liter of multi-heavy metal-containing industrial wastewater solutions were determined. For this, the adsorption time was assumed to be reduced by 50 % of optimal contact time; the efficiency conversion factor from batch to the continuous process was chosen as 0.1; and the resin cost was chosen as 40 % and 10 % of the costs obtained with retail prices. Table 7.1

summarizes various parameters and their values in the cost calculations. Appendix D elucidates on the sample calculations.

Table 7.1: A summary of process parameters for the evaluation of lab scale conceptual cost-based processing cost of high CSPVA derivative resin.

Requirement	**Quantity**	**Unit / Duration**
Plant Capacity	3000	m^3 yearly
Flow rate	10000	L day^{-1}
Plant Factor	300	days yearly
Adsorption Time	240	min
Reduced Time	2	h
Capacity of Tank	833.3333	L
Final Capacity of Tank	2000	L
No. of Tanks needed	2	
Cost of 2 Tanks	24000	Rs for 5 years
Cost of Tank yearly	4800	Rs yearly
Adsorbent loading	1.6	g L^{-1}
Reduction factor due to bulk order of adsorbent	0.4	
Efficiency Factor due to conversion from batch to continuous process	0.1	
Cost of adsorbent	1298.76	Rs/10 g
Amount of Adsorbent needed Yearly	384	Kg
Cost of adsorbent yearly	19356764	Rs yearly
Cost of Pump Needed 0.5 HP, 370 watt	17600	Rs for 3 years
Cost of Pump Needed 0.5 HP, 370 watt	5866.667	Rs yearly
Electricity	23976	Rs yearly
Manpower	540000	Rs yearly
Total Cost (Manpower + Tank Cost + Pump Cost + Electricity + Adsorbent)	19931407	Rs yearly
Wastewater Processing Cost	**6.643802**	**Rs L^{-1} of wastewater**

After 3rd cycle, the overall desorption capacities of commercial resins were poor in comparison to those achieved for chitosan derivatives in Cu dominant solution. Therefore, higher resin loading and costs are involved for commercial resins to achieve similar desorption removal quantities.

Thereby, a multiplication factor of 2.9 and 3.0 was applied to greater assure equivalent adsorbent weight required for the Amberlite IR 120H and Lewatit TP 260 commercial resins respectively. Consequently, the processing cost for the 40 % resin cost case (Fig. 7.10) were obtained as 6.64, 5.84, 3.01, 1.20, and 3.95 INR per liter of wastewater treated with high CSPVA, medium Cit-CS, medium CMCS, Amberlite IR 120H and Lewatit TP 260 resins, respectively. In dollars, the processing cost for 40 % resin cost case was obtained as 0.081, 0.071, 0.037, 0.015, and 0.048 USD per liter of wastewater treated with high CSPVA, medium Cit-CS, medium CMCS, Amberlite IR 120H and Lewatit TP 260 resins, respectively.

The processing cost for 10 % resin cost (Fig. 7.11) were obtained as 0.59, 0.54, 0.37, 0.25 and 0.43 INR per liter of wastewater treated with high CSPVA, medium Cit-CS, medium CMCS, Amberlite IR 120H and Lewatit TP 260 resins, respectively. For the case, the corresponding processing cost for 10 % resin cost was obtained as 0.0072, 0.0066, 0.0045, 0.0031, and 0.0053 USD per liter of wastewater treated respectively.

Similarly, for the Zn dominant solution, the processing cost for 40 % resin cost case (Fig. 7.12) were obtained as 5.84, 5.84, 3.48, 1.05 and 3.83 INR per liter of wastewater treated with high CSPVA, medium Cit-CS, medium CMCS, Amberlite IR 120H and Lewatit TP 260 resins, respectively. In dollars, the corresponding processing cost for the 40 % resin cost case was obtained as 0.071, 0.071, 0.043, 0.013, and 0.047 USD per liter of wastewater treated respectively.

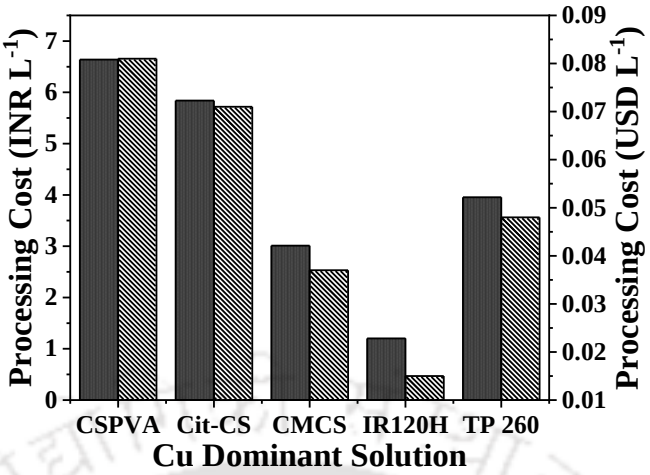

Fig. 7.10. Bar chart depicting the conceptual processing cost of best-performing chitosan derivatives and commercial resins for Cu dominant adsorbate system and industrial scale resin synthesis cost (40% resin cost) case.

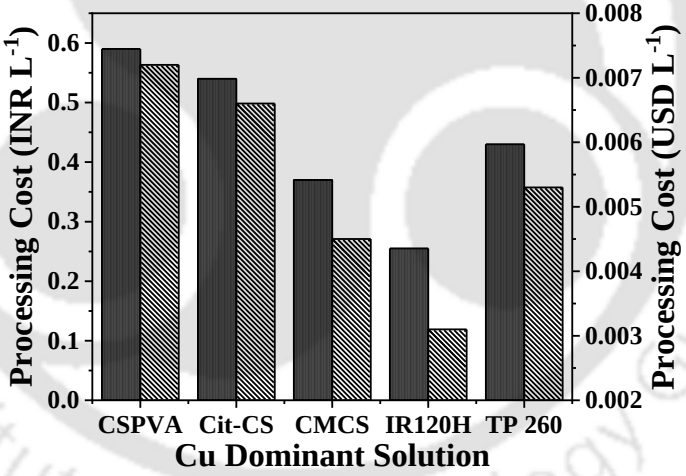

Fig. 7.11. Bar chart depicting the conceptual processing cost of best-performing chitosan derivatives and commercial resins for Cu dominant adsorbate system and industrial scale resin synthesis cost (10% resin cost) case.

The processing cost for 10 % resin cost (Fig. 7.13) was obtained as 0.54, 0.54, 0.40, 0.24, and 0.42 INR per liter of wastewater treated with high CSPVA, medium Cit-CS, medium CMCS, Amberlite

IR 120H and Lewatit TP 260 resins, respectively. The corresponding processing cost for 10 % resin cost were obtained as 0.0066, 0.0066, 0.0049, 0.003, and 0.0051 USD per liter of wastewater treated with high CSPVA, medium Cit-CS, medium CMCS, Amberlite IR 120H, and Lewatit TP 260 resins, respectively. Thus, the best-performing commercial resin-based processing cost was similar to that obtained with CMCS and for a 10 % resin cost case. In other words, the primary bottleneck for large-scale application of chitosan-based resin is its cost. Thus, cheaper extraction methods shall be researched for the production of high-quality chitosan. Academic research in this direction will be largely beneficial for the mentioned noble cause.

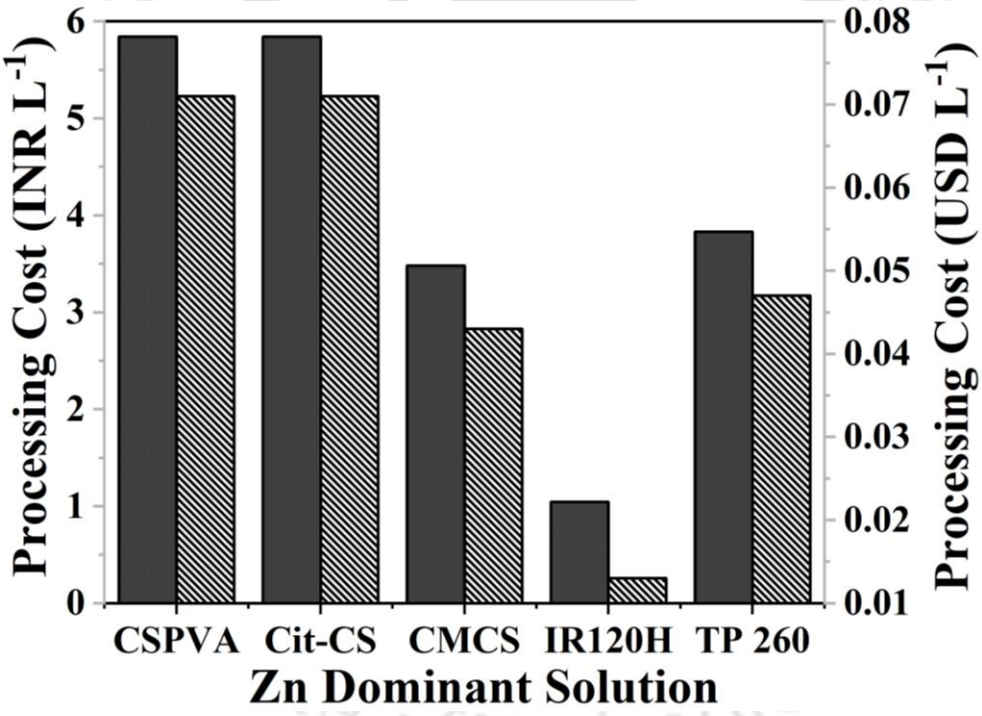

Fig. 7.12. Bar chart depicting the conceptual processing cost of best-performing chitosan derivatives and commercial resins for Zn dominant adsorbate system and industrial scale resin synthesis cost (40% resin cost) case.

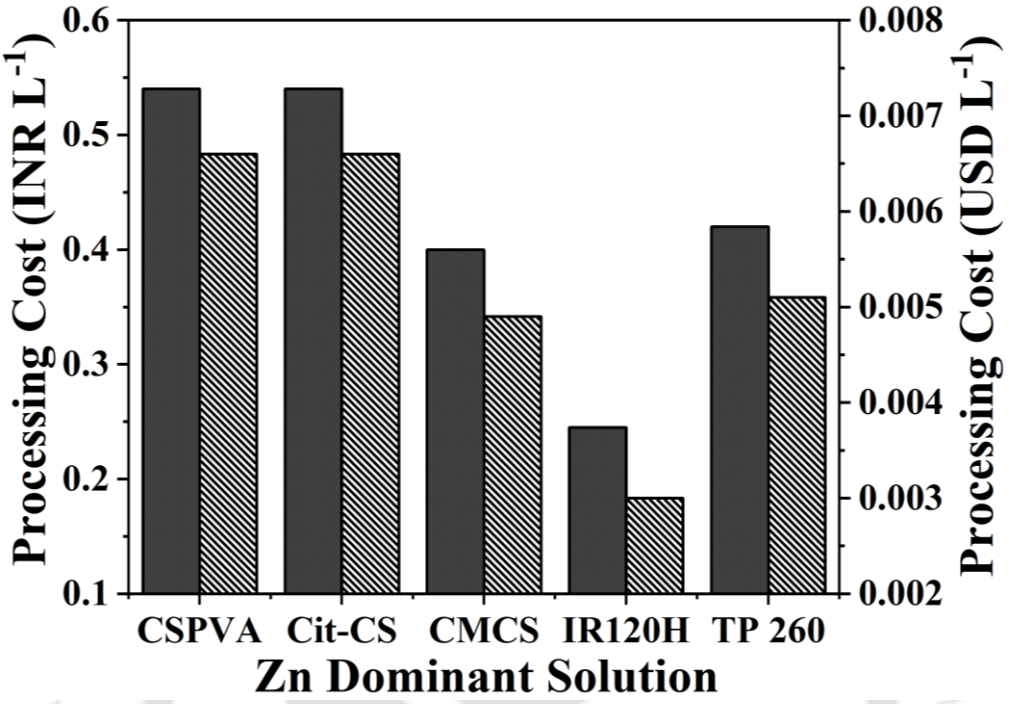

Fig. 7.13. Bar chart depicting the conceptual processing cost of best-performing chitosan derivatives and commercial resins for Zn dominant adsorbate system and industrial scale resin synthesis cost (10% resin cost) case.

7.4 Simulated Comparative Assessment of Cyclic adsorption-desorption Capabilities of synthesized chitosan resins

For the assessment of the desorption efficacies of low CSPVA, and medium CSPVA resins, a desorption pattern similar to that of high CSPVA was considered. After obtaining desorption efficacy values for high CSPVA, a linear proportional rule was applied for the determination of comparatively reduced desorption efficacies of low and medium CSPVA resins. Appendix E presents the model calculations for the determination of desorption efficiencies of low CSPVA and medium CSPVA resins. Similar evaluations are applicable for Cit-CS and CMCS derivative resins.

Fig. 7.14 depicts the cyclic adsorption-desorption characteristics of CSPVA, Cit-CS, and CMCS variant derivatives. The corresponding 3rd cycle desorption efficacies were 44.30, 43.19, and 36.82 % respectively for high CSPVA, medium CSPVA, and low CSPVA and 59.31, 58.9, and 46.51 % respectively for high Cit-CS, medium Cit-CS, and low Cit-CS. Similarly, for high CMCS, medium CMCS, and low CMCS corresponding 3rd cycle desorption efficacies were 72.27, 61.52, and 45.76 % respectively. After the 3rd cycle adsorption-desorption capabilities of low molecular weight chitosan variants (low CSPVA, low Cit-CS, and low CMCS) were very low in comparison to other higher molecular weight chitosan variants. Incidentally, the cost of low molecular-weight chitosan was also lower. Henceforth, the low molecular weight of chitosan for large-scale applications could be beneficial from a cost analysis. Furthermore, considering the desorption capabilities, the processing costs of low, medium, and high CSPVA were obtained as 5.41, 5.42, and 5.75 Rs. L^{-1} respectively and for the 40 % industrial case (Fig. 7.15a). Similarly, processing costs of low, medium, and high Cit-CS were obtained as 4.15, 4.09, and 4.33 Rs. L^{-1} respectively for 40 % of industrial cases (Fig. 7.16a) and were 2.06, 1.98, and 2.02 Rs. L^{-1} respectively for low, medium, and high CMCS cases and for the 40 % industrial case (Fig. 7.17a).

For the 10 % industrial resin cost case, the processing costs of low, medium, and high CSPVA were obtained as 0.39, 0.38, and 0.39 Rs. L^{-1} respectively (Fig. 7.15b). Similarly, processing costs of low, medium, and high Cit-CS were obtained as 0.33, 0.32, and 0.32 Rs. L^{-1} respectively (Fig. 7.16b) and for low, medium, and high CMCS, the values were 0.26, 0.26, and 0.25 Rs. L^{-1} respectively (Fig. 7.17b).

In summary, resin cost increased with the molecular weight of the chitosan due to the higher cost of high molecular weight chitosan and for both 40 % and 10 % industrial cases. However, the processing cost of chitosan derivative resins was reduced initially for low to medium molecular-

weight chitosan resins but enhanced from medium to high molecular-weight chitosan resin cases and for 40 % of industrial cases. The relevant variation was insignificant for 10 % of industrial cases. Henceforth, low molecular weight chitosan has the best utility for the synthesis of chitosan derivatives and is economical for the upgradation of operational scale from 40 (bulk price based on retail costs) to 10 % (bulk price based on process scale-up).

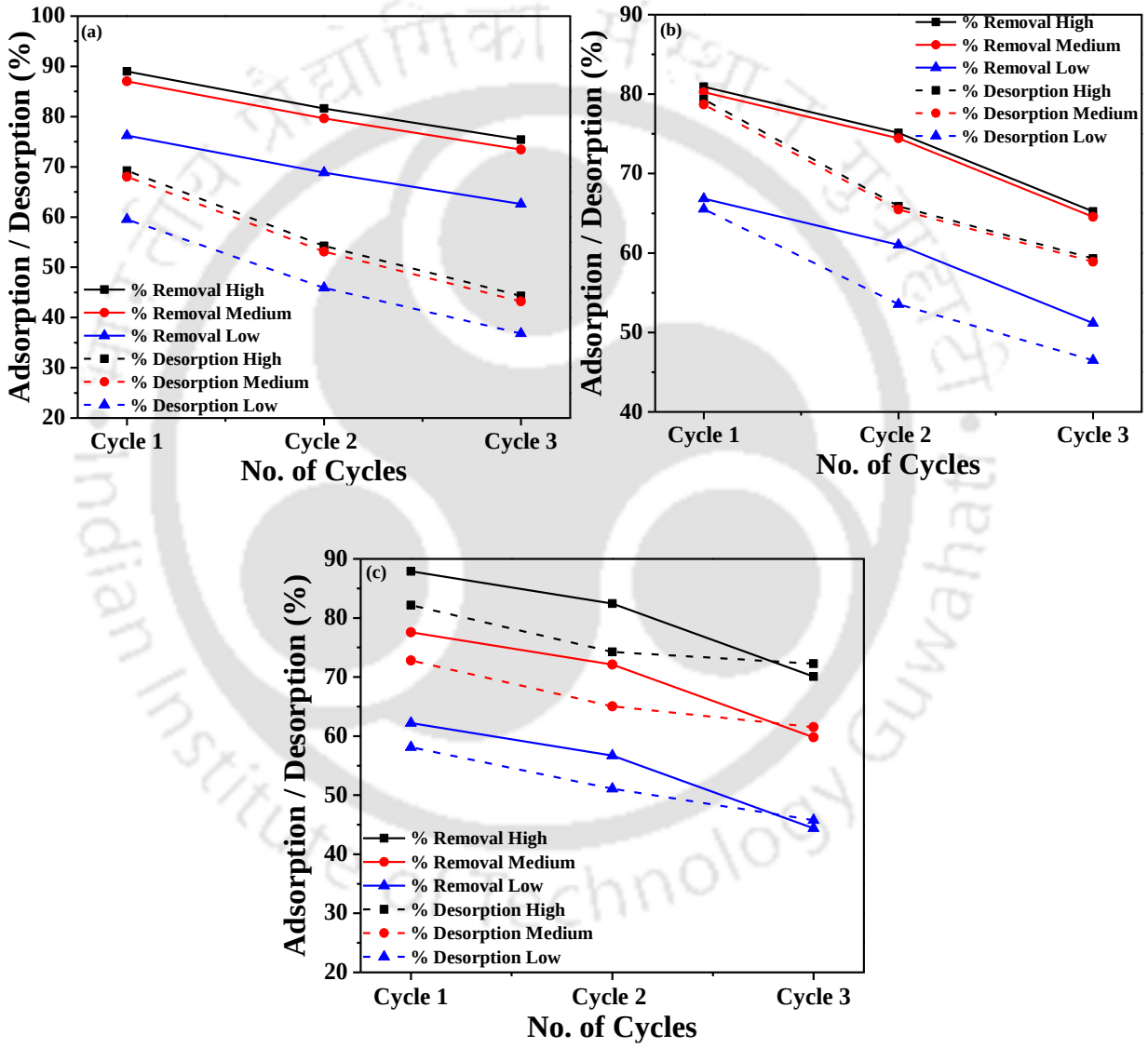

Fig. 7. 14. Comparative cyclic adsorption-desorption capabilities of (a) CSPVA (b) Cit-CS and (c) CMCS resins.

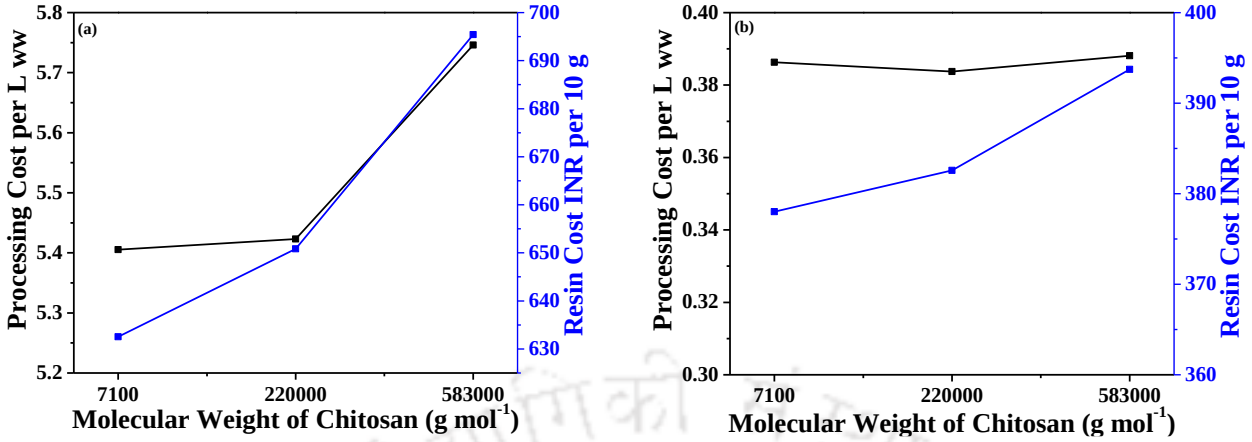

Fig. 7. 15. Resin and processing cost of low, medium, and high CSPVA resins (a) 40 % industrial case and (b) 10 % industrial case.

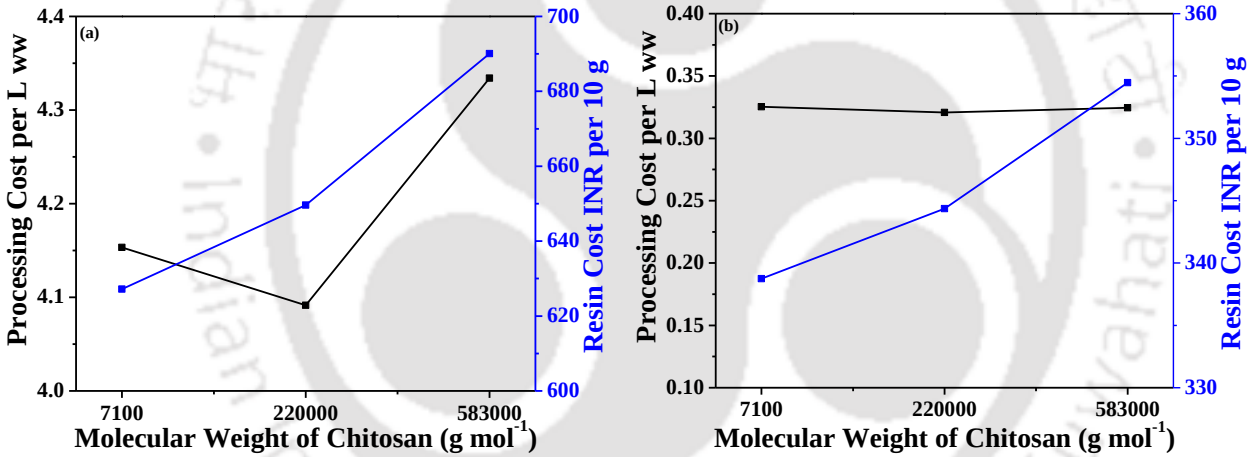

Fig. 7. 16. Resin and processing cost of low, medium, and high Cit-CS resins (a) 40 % industrial case and (b) 10 % industrial case.

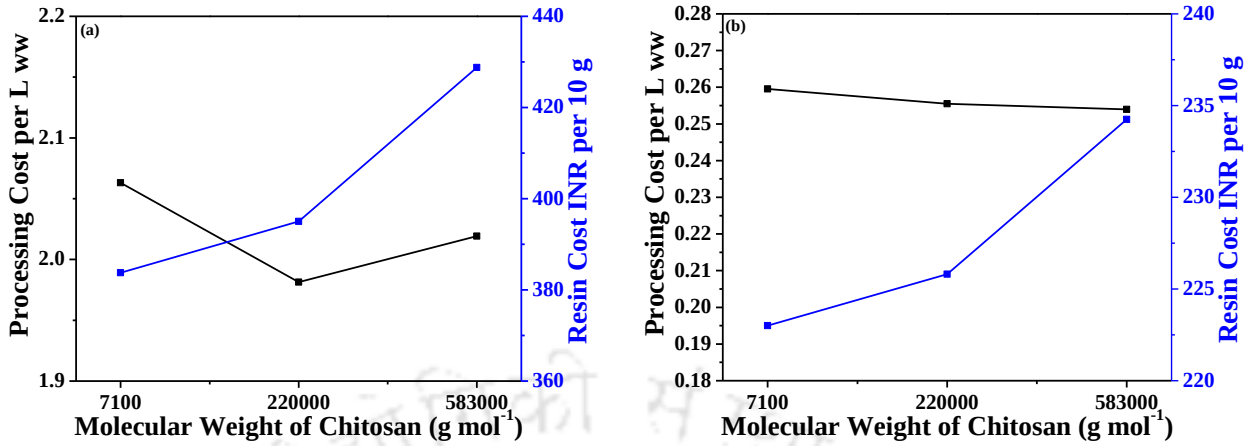

Fig. 7. 17. Resin and processing cost of low, medium, and high CMCS resins (a) 40 % industrial case and (b) 10 % industrial case.

7.5 Targeted Conceptual Costs of Chitosan Resins based on the lowest processing cost of the commercial resin-based adsorption system

Fig. 7.18 depicts the comparative cost assessment for the best-synthesized chitosan derivatives for 40 % of industrial cases (Fig. 7.18a) and 10 % of industrial cases (Fig. 7.18b). To achieve the similar processing cost of Amberlite IR 120H (1.2 Rs. L^{-1}), the CSPVA resin cost (695.41 to 126.26 Rs. per 10 g), Cit-CS resin cost (649.64 to 167.99 Rs. per 10 g), and CMCS resin cost (395.00 to 222.56 Rs. per 10 g) shall be reduced significantly and for the 40 % industrial case. Similarly, for the 10 % industrial case, the CSPVA resin cost (393.73 to 12.93 Rs. per 10 g), Cit-CS resin cost (344.36 to 17.2 Rs. per 10 g), and CMCS resin cost (225.81 to 22.78 Rs. per 10 g) be reduced significantly. This translates into the chitosan cost reduction from (368.52-147.41 INR) for 40 % of cases and (368.52-36.85 INR) for 10 % of cases. Thus, academic research needs such beneficial directives.

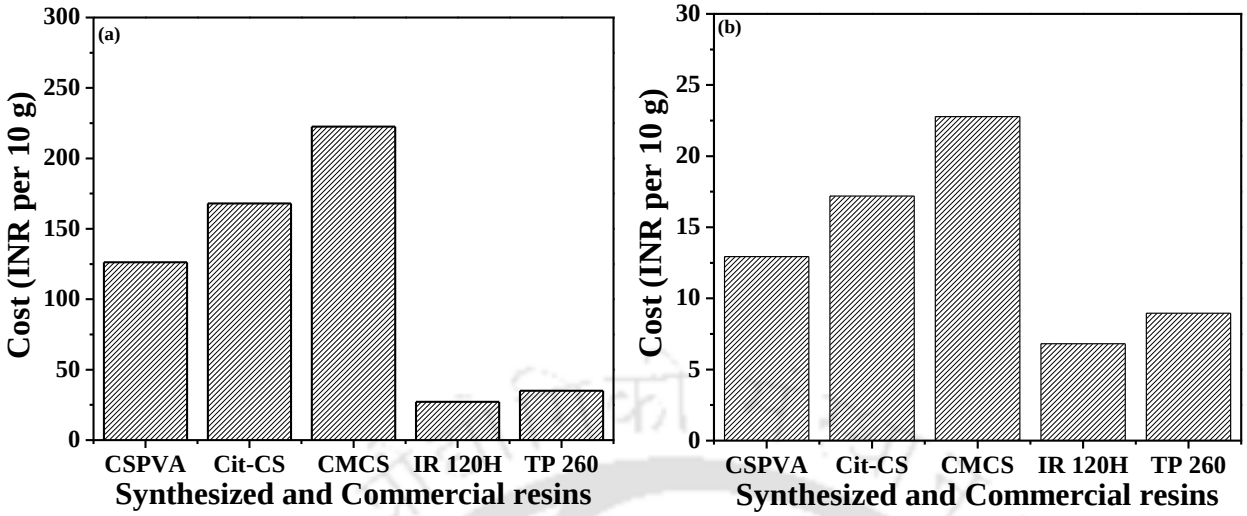

Fig. 7.18. Bar chart depicting the targeted chitosan derivatives cost for the realization of processing cost similar to that of the best case (commercial resin) (a) 40% industrial case and (b) 10% industrial case.

7.6 Summary

Several useful insights can be deduced from the best findings achieved in this work in the field of heavy metal adsorption and desorption characteristics of commercial resin and chitosan derivatives with synthetic complex industrial adsorbate systems. Firstly, chitosan molecular weight alterations did provide dividends in terms of the synthesis cost. Secondly, Lewatit TP 260 resin was 4.8 times more expensive, chitosan PVA resin was 23.24 times, chitosan citric acid resin was 23.03 times and chitosan carboxymethyl resin has been 14.09 times more expensive with respect to the best resin (Amberlite IR 120H). Thirdly, the processing costs for 40 % resin cost case were obtained as 6.64, 5.84, 3.01, 1.20, and 3.95 INR per liter of wastewater treated with high CSPVA, medium Cit-CS, medium CMCS, Amberlite IR 120H, and Lewatit TP 260 resins, respectively for Cu dominant solution. Similarly, for the Zn dominant solution, the processing cost for 40 % resin cost case was obtained as 5.84, 5.84, 3.48, 1.05, and 3.83 INR per liter of wastewater treated with high

CSPVA, medium Cit-CS, medium CMCS, Amberlite IR 120H and Lewatit TP 260 resins, respectively. Fourthly, to achieve a similar processing cost of Amberlite IR 120H (1.2 Rs. L^{-1}), the CSPVA resin cost (695.41 to 126.26 Rs. per 10 g), Cit-CS resin cost (649.64 to 167.99 Rs. per 10 g), and CMCS resin cost (395.00 to 222.56 Rs. per 10 g) shall be reduced significantly for the 40 % industrial case. Table 7.2 depicts the resin cost and processing cost (for 40 % and 10 % industrial cases). The higher cost of chitosan needs to be addressed for the cost-effective performance of chitosan resins in conjunction to the best commercial resin (Amberlite IR 120H).

Table 7.2: A summary of resin and processing costs of commercial resins and chitosan derivatives.

S. No.	Best Resin	40 % Resin cost	40 % processing cost	10 % processing cost
1.	Amberlite IR 120H	27.23	1.2	0.25
2.	Lewatit TP 260	130.64	3.95	0.43
3.	high CSPVA	695.41	6.64	0.59
4.	medium Cit-CS	649.64	5.84	0.54
5.	medium CMCS	395.00	3.01	0.37

Chapter 8:

Conclusions and Scope of Future Work

Chapter 8

Conclusions and Scope of future work

This chapter summarizes important conclusions, possible directions, and scope for future work.

8.1 Conclusions

FTIR, BET, FESEM, EDX, and TGA analyses have been conducted for alternate commercial and chitosan functionalized resins, whose multi-heavy metals adsorption and desorption characteristics have been assessed. Deeper insight into the obtained data and trends indicates the following inferences with respect to the synergy or irrelevance of the results obtained from such characterization studies with respect to obtained trends for studied heavy metal adsorption and desorption characteristics:

- The data from BET surface area analysis is not highly synergistic with the heavy metal adsorption and desorption characteristics. This is due to the fact that chemical and functional group interactions have a stronger role to influence and enhance the measured metal ion adsorption and desorption characteristics.
- The mechanistic understanding with respect to the studied metal ions adsorption process is indicative of the said mechanisms by following a pseudo-second-order model which is in good agreement with the FTIR analysis for commercial resins and chitosan derivative resins. However, the analysis does not account upon the trends obtained for the desorption characteristics. Hence, further research is required to corroborate upon the pertinent trends with additional characterization.

- EDX analysis affirmed the existence of metal ions and oxygen on the adsorbent surface after adsorption and after functional groups-based modification respectively. Such analysis is beneficial to corroborate upon the observed enhancement of metal ions adsorption on the functionalized chitosan.
- FESEM analysis assured morphological insights which are insignificant to elaborate upon trends obtained from metal ions adsorption and desorption studies for both commercial and chitosan functionalized resins.
- The crystallinity of the resins has been indicated by the XRD analysis. Based on the observed trends, chitosan crystallinity decreased after modification with suitable functional groups. Also, the adsorbent surface became amorphous after treatment with the simulated Cu and Zn dominant solutions laden with multi-heavy metal ions.
- TGA analysis indicated that the adsorbents have good thermal stability and up to even higher temperature of 300 ºC.

In summary, multi-heavy metal ions adsorption and desorption characteristics cannot be fully understood from surface characterization analyses. To the best possible extent, these analyses provide a qualitative understanding of the associated resin chemistry information. Adsorbent reusability is very much dependent on its desorption characteristics, which are always influenced with the complex chemistry of the eluents and associated functional interactions. Therefore, studies devoted towards the characterization of materials after several adsorption-desorption cycles shall be addressed in the near future to gain even better understanding of the associated functional group interactions with the mentioned heavy metal ions in the Ph.D. thesis. Such finer analysis with especially FTIR spectral analysis after every adsorption and desorption cycle will be helpful in

quantifying the extent of reversible and irreversible adsorption and desorption. Accordingly, resin reusability can be even better assessed.

Also, among tested adsorbents, synthesized chitosan derivatives provided reasonably better desorption efficiencies after the third cycle of adsorption-desorption in comparison with those obtained for commercial resins. Overall, all adsorbents provided promising heavy metal ions adsorption efficiencies and reasonable desorption efficiencies in comparison with the literature-reported data that involved either aqueous solutions or complex eluents or both.

Based on experimental and modeling studies associated to the removal of multi-heavy metal ions from complex Zn and Cu-based synthetic adsorbate solutions, various conclusions deduced for commercial resins and chitosan derivatives are presented in the following sub-sections for the set objectives.

8.1.1 Cyclic adsorption and desorption based multi-heavy metal removal efficacy of commercial Lewatit TP260 and Amberlite IRA 120H Resins

- The optimal adsorption parameters refer to be adsorbent dose of 1.6 g L^{-1} and 1.4 g L^{-1}, contact time of 420 and 480 min for Amberlite IR 120H commercial resin, respectively from Cu and Zn dominant solutions.
- The optimal adsorption parameters refer to be adsorbent dose of 1.2 g L^{-1}, and a contact time of 300 min for Lewatit TP260 commercial resin from Cu and Zn dominant solutions, respectively.
- For synthetic Cu and Zn dominant complex adsorbate systems and Amberlite IR 120H resin, the removal % and adsorption capacities were obtained as 85.14-48.61 % and 99.88-171.08 mg g^{-1}, 91.53-45.43 % and 35.38-52.68 mg g^{-1} and 92.31-42.24 % and 3.00-4.12 mg g^{-1} for Cu, Fe, and Pb, respectively at an initial heavy metal ions concentration range

of 187.7-563.1 mg L^{-1} for Cu, 61.85-185.55 mg L^{-1} for Fe, and 5.2-15.6 mg L^{-1} for Pb in Cu dominant solution. Similarly, adsorption capacities and removal % were obtained as 91.36-48.46% and 127.19-202.38 mg g^{-1}, 88.97-61.89% and 66.61-139.00 mg g^{-1} and 84.91-38.36% and 1.61-2.18 mg g^{-1} for Zn, Fe and Pb, respectively at an initial heavy metal ions concentration range of 194.9-584.7 mg L^{-1} for Zn, 104.8-314.4 mg L^{-1} for Fe, and 2.65-7.95 mg L^{-1} for Pb in Zn dominant solution.

- For synthetic Cu and Zn dominant complex adsorbate systems and Lewatit TP260 resin, the removal % and adsorption capacities were obtained as 85.14-50.55% and 133.18-237.23 mg g^{-1}, 89.36-45.44% and 46.06-70.26 mg g^{-1} and 82.88-48.65% and 3.59-6.32 mg g^{-1} for Cu, Fe, and Pb, respectively at an initial heavy metal ions concentration range of 187.7-563.1 mg L^{-1} for Cu, 61.85-185.55 mg L^{-1} for Fe, and 5.2-15.6 mg L^{-1} for Pb in Cu dominant solution. Similarly, adsorption capacities and removal % were obtained as 92.45-46.77% and 150.15-227.88 mg g^{-1}, 88.94-58.71% and 77.67-153.83 mg g^{-1} and 73.58-35.72% and 1.63-2.37 mg g^{-1} for Zn, Fe, and Pb, respectively at an initial heavy metal ions concentration range of 194.9-584.7 mg L^{-1} for Zn, 104.8-314.4 mg L^{-1} for Fe, and 2.65-7.95 mg L^{-1} for Pb in Zn dominant solution.
- From a modeling perspective, both derivatives followed Langmuir equilibrium isotherm and pseudo-second-order kinetic models.
- For a variation in the number of cycles from 1-3, Amberlite IR 120H resin exhibited the best desorption efficiencies. The corresponding desorption efficacies were obtained as 51.1-12.00 %, 49.9-13.7 %, and 47.6-20.1 %, respectively for Cu, Fe, and Pb from Cu dominant solution and 49.2-14.3 % Zn, 31.8-23.6 % Fe, and 47.3-14.9 % Pb with 2 M HCl from Zn dominant solution.

- For a variation in the number of cycles from 1-3, Lewatit TP260 resin exhibited the best desorption efficiencies. The corresponding desorption efficacies were obtained as 53.9-12.3 %, 55.00-12.2 %, and 56.5-12.2 %, respectively for Cu, Fe, and Pb from Cu dominant solution and 50.6-14.7 % Zn, 40.31-22.5 % Fe, and 51.96-14.8 % Pb with 2 M NaOH from Zn dominant solution.

8.1.2 Cyclic Adsorption-Desorption based Efficacy of PVA-Chitosan Derivative Resins

- The optimal adsorption parameters were evaluated as the adsorbent dose of 1.6 and 1.4 g L^{-1} and contact time of 240, and 300 min for high CSPVA derivative in Cu and Zn dominant solutions, respectively.
- The adsorption capacities and removal % were obtained as 111.47-230.91 mg g^{-1} and 95.01-65.61 %, 32.14-71.48 mg g^{-1} and 83.14-61.64 % and 3.02-6.27 mg g^{-1} and 92.88-64.27 % for Cu, Fe, and Pb, respectively at an initial heavy metal ions concentration range of 187.7-563.1 mg L^{-1} for Cu, 61.85-185.55 mg L^{-1} for Fe, and 5.2-15.6 mg L^{-1} for Pb in Cu dominant solution. Similarly, adsorption capacities and removal % were obtained as 115.88-203.20 mg g^{-1} and 83.24-48.65 %, 66.74-126.37 mg g^{-1} and 89.15-56.27 % and 1.78-3.42 mg g^{-1} and 94.21-60.29 % for Zn, Fe and Pb, respectively at an initial heavy metal ions concentration range of 194.9-584.7 mg L^{-1} for Zn, 104.8-314.4 mg L^{-1} for Fe, and 2.65-7.95 mg L^{-1} for Pb in Zn dominant solution.
- Among equilibrium models, best fitness models correspond to Langmuir isotherm for low CSPVA, medium CSPVA, and high CSPVA derivatives in Cu and Zn dominant solutions. For all resins, multi-heavy metal adsorption kinetic was represented by a pseudo-second-order model.

- For a variation in the number of cycles from 1-3, high CSPVA derivative exhibited the best desorption efficiencies with 0.1M HCl. The corresponding desorption efficacies were obtained as 69.25-44.3%, 65.83-53.73%, and 57.71-47.37%, respectively for Cu, Fe, and Pb from Cu dominant solution and 60.95-51.89%, 66.71-59.94%, and 60.14-53.70%, respectively for Zn, Fe, and Pb from Zn dominant solution.

8.1.3 Cyclic Adsorption-Desorption based Efficacy of Cit-CS Derivative Resins

- The optimal adsorption parameters were evaluated as the adsorbent dose of 1.4 g L^{-1} and contact time of 420 min for medium Cit-CS derivative in Cu and Zn dominant solutions.
- For a variation in initial metal ions concentration of 187.7-563.1 mg L^{-1} Cu, 61.85-185.55 mg L^{-1} Fe, and 5.2-15.6 mg L^{-1} Pb in Cu dominant solution and 194.9-584.7 mg L^{-1} Zn, 104.8-314.4 mg L^{-1} Fe, and 2.65-7.95 mg L^{-1} Pb in Zn dominant solution, the metal uptakes and removal efficacies varied as 119.50-258.58 mg g^{-1} and 89.12-64.29 %, 37.70-74.31 mg g^{-1} and 85.33-56.06 % and 3.42-7.43 mg g^{-1} and 92.12-66.64 % for Cu, Fe and Pb, respectively in Cu dominant solution. Similarly, adsorption capacities and removal % were obtained as 110.36-205.17 mg g^{-1} and 79.27-49.13 %, 61.85-122.37 mg g^{-1} and 82.63-54.49 % and 1.68-3.41 mg g^{-1} and 88.55-60.13 % for Zn, Fe and Pb, respectively Zn dominant solution.
- Langmuir equilibrium isotherm has been evaluated to be the best-fit model for low Cit-CS, medium Cit-CS, and high Cit-CS derivatives in Cu and Zn dominant solutions. The pseudo-second-order kinetic model has been evaluated to be the best-fit model for all the derivatives.

- For a variation in the number of cycles from 1-3, the medium Cit-CS derivative exhibited the best desorption efficiencies with 2M HCl. The corresponding desorption efficacies were obtained as 78.69-58.9%, 75.31-53.78%, and 69.63-49.40%, respectively for Cu, Pb, and Fe from Cu dominant solution and 75.65-57.76%, 79.14-58.35%, and 68.59-49.83%, respectively for Zn, Pb, and Fe from Zn dominant solution.

8.1.4 Cyclic Multi-heavy Metal Removal Efficacy of CMCS Derivative Resins

- The optimal adsorption parameters were evaluated as adsorbent dose of 1.2 and 1.4 g L^{-1} and contact time of 540, and 420 min for medium CMCS derivative in Cu and Zn dominant solutions, respectively.
- The adsorption capacities and removal % were obtained as 144.69-300.57 mg g^{-1} and 92.50-64.05 %, 46.70-84.21 mg g^{-1} and 90.61-54.46 % and 4.04-8.68 mg g^{-1} and 93.33-66.73 % for Cu, Fe and Pb, respectively at an initial heavy metal ions concentration range of 187.7-563.1 mg L^{-1} for Cu, 61.85-185.55 mg L^{-1} for Fe, and 5.2-15.6 mg L^{-1} for Pb in Cu dominant solution. Similarly, adsorption capacities and removal % were obtained as 115.84-208.98 mg g^{-1} and 83.21-50.04 %, 61.85-123.56 mg g^{-1} and 82.63-55.02 % and 1.67-3.82 mg g^{-1} and 88.05-67.34 % for Zn, Fe and Pb, respectively at an initial heavy metal ions concentration range of 194.9-584.7 mg L^{-1} for Zn, 104.8-314.4 mg L^{-1} for Fe, and 2.65-7.95 mg L^{-1} for Pb in Zn dominant solution.
- Among equilibrium models, best fitness models correspond to Langmuir isotherm for low CMCS, medium CMCS, and high CMCS derivatives in Cu and Zn dominant solutions. Multi-heavy metal adsorption kinetics were represented by a pseudo-second-order model for all resins.

- For a variation in the number of cycles from 1-3, the medium CMCS derivative exhibited the best desorption efficiencies with 2M HNO_3. The corresponding desorption efficacies were obtained as 72.81-61.52 %, 71.45-44.44 %, and 66.49-48.11 %, respectively for Cu, Fe, and Pb from Cu dominant solution and 76.68-64.51 %, 79.76-61.82 %, and 78.75-53.73 %, respectively for Zn, Fe, and Pb from Zn dominant solution.

8.1.5 Conceptual Resin and Processing Cost Analysis of Multi-heavy Metal Removal from Complex Adsorbate Systems

- Chitosan molecular weight alterations did provide dividends in terms of the synthesis cost.
- Lewatit TP 260 resin was 4.8 times more expensive, chitosan PVA resin was 23.24 times, chitosan citric acid resin was 23.03 times and chitosan carboxymethyl resin was 14.09 times more expensive with respect to the best resin (Amberlite IR 120H)
- The processing costs for 40 % resin cost case were obtained as 6.64, 5.84, 3.01, 1.20, and 3.95 INR per liter of wastewater treated with high CSPVA, medium Cit-CS, medium CMCS, Amberlite IR 120H, and Lewatit TP 260 resins, respectively for Cu dominant solution. Similarly, for the Zn dominant solution, the processing cost for 40 % resin cost case was obtained as 5.84, 5.84, 3.48, 1.05, and 3.83 INR per liter of wastewater treated with high CSPVA, medium Cit-CS, medium CMCS, Amberlite IR 120H and Lewatit TP 260 resins, respectively.
- To achieve the similar processing cost of Amberlite IR 120H (1.2 Rs. L^{-1}), the CSPVA resin cost (695.41 to 126.26 Rs. per 10 g), Cit-CS resin cost (649.64 to 167.99 Rs. per 10 g), and CMCS resin cost (395.00 to 222.56 Rs. per 10 g) shall be reduced significantly for

the 40 % industrial case. Table 7.2 depicts the resin cost and processing cost (for 40 % and 10 % industrial cases).

The best results obtained in this work along with the data available in few most competent literatures, the following can be outlined as the most promising conclusions of the Ph.D. thesis:

a) All chitosan derivatives and commercial resins provided promising Cu, Fe, and Pb adsorption capacities for the Cu dominant complex adsorbate system and Zn, Fe, and Pb adsorption capacities for the Zn dominant complex adsorbate system.

b) Compared to prior art data reported in the literature, among commercial resins, Lewatit TP260 resin exhibited the best adsorption capacities of 204.1 mg g^{-1} for Cu and 57.1 mg g^{-1} for Fe from Cu dominant solution and 196.1 mg g^{-1} for Zn and 133.3 mg g^{-1} for Fe from Zn dominant solution. Similarly, among chitosan synthesized derivatives, medium CMCS derivative exhibited the best adsorption capacities of 344.83 mg g^{-1} for Cu and 90.09 mg g^{-1} for Fe from Cu dominant solution, and 237.10 mg g^{-1} for Zn and 147.06 mg g^{-1} for Fe from Zn dominant solution.

c) Among all resins, medium Cit-CS derivative exhibited the best desorption efficiencies (after 3rd cycle) of 58.9 % for Cu, 49.40 % for Pb, and 53.78 % for Fe from Cu dominant solution utilizing 2M HCl and medium CMCS exhibited best desorption efficiencies of 64.51 % for Zn, 53.73 % for Pb and 61.82 % for Fe from Zn dominant solution utilizing 2M HNO_3.

d) Glutaraldehyde crosslinked chitosan derivative CMCS and Cit-CS performed better than the resin prepared without crosslinking of the chitosan (CSPVA derivative) in terms of desorption efficiency and adsorption capacity.

e) Literature findings affirm better adsorption capacity of studied chitosan derivatives and commercial resins in comparison with other derivatives.

f) Compared to glutaraldehyde crosslinked chitosan derivatives namely CMCS and Cit-CS, non-crosslinked chitosan derivatives reported a maximum % removal of 88.78 % for Cu but the desorption % was not promising in comparison with crosslinked chitosan derivatives.

g) Overall, among all considered resins, derivative medium CMCS performed the best followed with commercial resin Lewatit TP 260 in terms of multi-heavy metal removal and resin regeneration.

h) To achieve a similar processing cost of Amberlite IR 120H (1.2 Rs. L^{-1}) for the 10 % industrial case, the CSPVA resin cost (393.73 to 12.93 Rs. per 10 g), Cit-CS resin cost (344.36 to 17.2 Rs. per 10 g), and CMCS resin cost (225.81 to 22.78 Rs. per 10 g) shall be reduced significantly.

8.2 Future Work

The following areas of work have been identified for consideration in the near future to consolidate upon the challenging and exciting research in the field of multi-heavy metal removal and resin regeneration from complex adsorbate systems:

- Adsorbate systems with more complex solution chemistry and real wastewater samples are to be investigated for multi-heavy metal removal and inexpensive resin regeneration schemes.
- Variations to reaction stoichiometry and synthesis procedures are to be examined to enhance the desorption efficiency of all synthesized chitosan derivatives. Further, the utilization of inexpensive reagents and laboratory-extracted chitosan shall be explored to

potentially reduce the cost of chitosan derivatives and foster their cost competence with respect to commercial resin. This will be a very exciting field of research.

- Commercial resins and chitosan-modified derivatives with multiple S/N/O and their combinational function groups shall be investigated for the removal of hazardous multi-heavy metals and dyes from complex adsorbate systems. The role of chelating chemistry for such systems be effectively studied in the context of cyclic desorption and resin regeneration.
- Column studies shall be undertaken to optimize the performance of chitosan derivatives and commercial resins for the continuous adsorption and desorption of multi-heavy metals from complex adsorbate systems.
- The development of super-efficient chelating resins with enhanced multi-heavy metal desorption characteristics shall be explored in terms of chelation and functional group chemistry research.
- Research commercialization and technology transfer of most cost-competitive adsorbents for multi-heavy metal removal and adsorbent regeneration shall be explored for real waste streams and adsorbate systems.

The choice among engineering aspects and considerations for real waste streams and adsorbate systems can vary significantly. It is dependent upon the specific characteristics of the waste stream, the nature of the contaminants, and the intended goals of treatment or adsorption. The following have been outlined for due consideration as relevant engineering aspects for both real and simulated adsorbate systems:

- ❖ A holistic approach shall be adopted that considers the specific characteristics of the system, the desired outcomes, and the broader economic and environmental perspectives.

Thereby, a fruitful collaboration among engineers, environmental scientists, chemists, and regulatory experts is mandatory for the development of effective and sustainable solutions.

- Prior to the implementation of any treatment or remediation strategy, a thorough characterization of the waste stream is essential. Such studies shall be devoted towards the identification of the types and concentrations of contaminants, system pH, temperature, flow capacity, and other relevant parameters. Such characterizations require the implementation of advanced analytical techniques for waste streams possessing greater complexity in terms of solution chemistry.
- Minimization of generated waste at the source shall be targeted through the development and implementation of cleaner production processes and recycling strategies.
- Depending upon the constituent contaminants, pre-treatment processes may become necessary for the elimination or mitigation of certain contaminants. For instance, aluminium has been identified as a key contaminant in the chosen adsorbate system and its mitigation through pre-treatment henceforth becomes a significant option that needs to be explored. Accordingly, the effectiveness of subsequent treatment processes can be ensured.
- The selection of appropriate treatment technologies shall be based on the specific contaminants and characteristics of the waste stream. This could include physical, chemical, biological, or thermal treatment processes or a combination of these. The choice of technology should consider factors such as cost-effectiveness, efficiency, and environmental impact.
- The developed cost-effective technologies shall have compliance with local, regional, and national environmental regulations.

Waste disposal and resource recovery shall be also explored. Accordingly, waste stream recycling, energy recovery, and smart conversion towards value-added byproduct development shall be duly addressed and realized.

Considering the difficulty associated to the removal of heavy metals from resins. Their storage in effectively sealed containers is the best way to dispose of these resins. However, technologies must be developed to translate the adsorbed heavy metals into suitable forms for most dilution-based heavy metal-constituted solid materials. Only then, the heavy metal could be safely disposed of into the environment. Detailed studies involving the leaching characteristics for a prolonged time period (5-10 years) shall be targeted.

The developed adsorbents were based on biodegradable chitosan and other biodegradable materials namely, polyvinyl alcohol, citric acid, and monochloroacetic acid. Few resins utilized a hazardous material (glutaraldehyde) for the resin synthesis. From a spillage perspective, the best resin is the CSPVA, as it does not contain hazardous materials. However, the heavy metal-loaded adsorbents may cause significant hazardous influences upon spillage. Henceforth, it should be handled with greater caution. Similarly, due to being hazardous, both adsorbate systems and adsorbent should be handled with greater caution. Further insights in this regard are beyond the scope of the PhD thesis objectives.

References

References

Abdeen, Z., Mohammad, S. G., & Mahmoud, M. S. (2015). "Adsorption of Mn(II) ion on polyvinyl alcohol/chitosan dry blending from aqueous solution". Environmental Nanotechnology, Monitoring and Management, **3**, 1–9.

Abo-Farha, S. A., Abdel-Aal, A. Y., Ashour, I. A., & Garamon, S. E. (2009). "Removal of some heavy metal cations by synthetic resin purolite C100". Journal of Hazardous Materials, **169(1–3)**, 190–194.

Abreu, F.R. de, Campana-Filho, S.P., (2005). "Preparation and characterization of carboxymethylchitosan". Polímeros: Ciência e Tecnologia, **15**, 79–83.

Aharoni, C., Ungarish, M., (1976). "Kinetics of Activated Chemisorption". Journal of the Chemical Society, Faraday Transactions, **I72**, 400 – 408.

Ahmadi, M., Teymouri, P., Setodeh, A., Mortazavi, M. S., & Asgari, A. (2011). "Adsorption of Pb(II) from aqueous solution onto lewatit FO36 nano resin: Equilibrium and kinetic studies". Environmental Engineering and Management Journal, **10(10)**, 1579–1587.

Ali, E. S., Alsaman, A. S., Harby, K., Askalany, A. A., Diab, M. R., & Ebrahim Yakoot, S. M. (2017). "Recycling brine water of reverse osmosis desalination employing adsorption desalination: A theoretical simulation". Desalination, **408**, 13–24.

Alyüz, B., & Veli, S. (2009). "Kinetics and equilibrium studies for the removal of nickel and zinc from aqueous solutions by ion exchange resins". Journal of Hazardous Materials, **167(1–3)**, 482–488.

Anbazhagan, S., Thiruvengadam, V., & Sukeri, A. (2021). "An Amberlite IRA-400 Cl^- ion-exchange resin modified with: Prosopis juliflora seeds as an efficient Pb^{2+}adsorbent: Adsorption, kinetics, thermodynamics, and computational modeling studies by density functional theory". RSC Advances, **11(8)**, 4478–4488.

Anwar, J., Shafique, U., Waheed-uz-Zaman, Salman, M., Dar, A., & Anwar, S. (2010). "Removal of Pb(II) and Cd(II) from water by adsorption on peels of banana". Bioresource Technology, **101(6)**, 1752–1755.

Atia, A. A., Donia, A. M., & Yousif, A. M. (2008). "Removal of some hazardous heavy metals from aqueous solution using magnetic chelating resin with iminodiacetate functionality". Separation and Purification Technology, **61(3)**, 348–357.

Benavente, M., Moreno, L., & Martinez, J. (2011). "Sorption of heavy metals from gold mining wastewater using chitosan". Journal of the Taiwan Institute of Chemical Engineers, **42(6)**, 976–988.

Boamah, P. O., Huang, Y., Hua, M., Zhang, Q., Wu, J., Onumah, J., & Sam-Amoah, L. K. (2015). "Sorption of heavy metal ions onto carboxylate chitosan derivatives-A mini-review". Ecotoxicology and Environmental Safety, **116**, 113–120.

Busuioc, L. T., Simonescu, C. M., Patescu, R. E., & Onose, C. (2016). "Removal of Lead(II), Nickel(II), Zinc(II) and Copper(II) from Multi-metal Systems by Chitosan-glutaraldehyde Beads". Revista de Chimie - Bucharest, **3**, 1–7.

Cao, Y. R., Liu, Z., Cheng, G. L., Jing, X. B., & Xu, H. (2010). "Exploring single and multi-metal biosorption by immobilized spent Tricholoma lobayense using multi-step response surface methodology". Chemical Engineering Journal, **164(1)**, 183–195.

Cárdenas, G., Orlando, P., & Edelio, T. (2001). "Synthesis and applications of chitosan mercaptanes as heavy metal retention agent". International Journal of Biological Macromolecules, **28(2)**, 167–174.

Chakrabarty, T., Rajesh, A. M., Jasti, A., Thakur, A. K., Singh, A. K., Prakash, S., Kulshrestha, V., & Shahi, V. K. (2011). "Stable ion-exchange membranes for water desalination by electrodialysis". Desalination, **282**, 2–8.

Chen, Y., He, M., Wang, C., & Wei, Y. (2014). "A novel polyvinyltetrazole-grafted resin with high capacity for adsorption of Pb(II), Cu(II) and Cr(III) ions from aqueous solutions". Journal of Materials Chemistry A, **2(27)**, 10444–10453.

Choi, H. Y., Bae, J. H., Hasegawa, Y., An, S., Kim, I. S., Lee, H., & Kim, M. (2020). "Thiol-functionalized cellulose nanofiber membranes for the effective adsorption of heavy metal ions in water". Carbohydrate Polymers, **234**, 115881.

Das, N., Karhika, P., Vimala, R. and Vinodhini. (2008). "Use of natural products as biosorbent of heavy metals o an overview". Natural Product radiance, **7 (2)**, 133 -138.

Demirbas, A., Pehlivan, E., Gode, F., Altun, T., & Arslan, G. (2005). "Adsorption of Cu(II), Zn(II), Ni(II), Pb(II), and Cd(II) from aqueous solution on Amberlite IR-120 synthetic resin". Journal of Colloid and Interface Science, **282(1)**, 20–25.

Dev, V. V., Baburaj, G., Antony, S., Arun, V., & Krishnan, K. A. (2020). "Zwitterion-chitosan bed for the simultaneous immobilization of Zn(II), Cd(II), Pb(II) and Cu(II) from multi-metal aqueous systems". Journal of Cleaner Production, **255**, 120309.

Fato, F. P., Li, D. W., Zhao, L. J., Qiu, K., & Long, Y. T. (2019). "Simultaneous Removal of Multiple Heavy Metal Ions from River Water Using Ultrafine Mesoporous Magnetite Nanoparticles". ACS Omega, **4(4)**, 7543–7549.

Fazeli, M. S., Khosravan, F., Hossini, M., Sathyanarayan, S. and Satish, P.N. (1998). "Enrichment of heavy metals in paddy crops irrigated by paper mill effluents near Narijangud, Mysore District, Karnatka, India". Environmental Geology, **34**, 297 -302.

Freundlich, H. M. "F. (1906). "Over the adsorption in solution". Journal of Physicochemical, **57**, 385-470.

Fu, F., & Wang, Q. (2011). "Removal of heavy metal ions from wastewaters: A review". Journal of Environmental Management, **92(3)**, 407–418.

Futalan, C. M., Kan, C. C., Dalida, M. L., Hsien, K. J., Pascua, C., & Wan, M. W. (2011). "Comparative and competitive adsorption of copper, lead, and nickel using chitosan immobilized on bentonite". Carbohydrate Polymers, **83(2)**, 528–536.

Gherasim, C. V., Křivčík, J., & Mikulášek, P. (2014). "Investigation of batch electrodialysis process for removal of lead ions from aqueous solutions". Chemical Engineering Journal, **256**, 324–334.

Guo, H., Ren, Y., Sun, X., Xu, Y., Li, X., Zhang, T., Kang, J., & Liu, D. (2013). "Removal of Pb^{2+} from aqueous solutions by a high-efficiency resin". Applied Surface Science, **283**, 660–667.

Gupta, A. D., Rawat, K. P., Bhadauria, V., & Singh, H. (2021). "Recent trends in the application of modified starch in the adsorption of heavy metals from water: A review". Carbohydrate Polymers, **269**, 117763.

Hassiba, A. J., El Zowalaty, M. E., Webster, T. J., Abdullah, A. M., Nasrallah, G. K., Khalil, K. A., Luyt, A. S., & Elzatahry, A. A. (2017). "Synthesis, characterization, and antimicrobial properties of novel double layer nanocomposite electrospun fibers for wound dressing applications". International Journal of Nanomedicine, **12**, 2205–2213.

Hossain, M. A., Ngo, H. H., Guo, W. S., Nguyen, T. V., & Vigneswaran, S. (2014). "Performance of cabbage and cauliflower wastes for heavy metals removal". Desalination and Water Treatment, **52(4–6)**, 844–860.

Huacai Ge and Shiying Huang. (2010). "Microwave Preparation and Adsorption Properties of EDTA-Modified Cross-Linked Chitosan". Journal of Applied Polymer Science, **116(5)**, 2658–2667.

Hubicki, Z., Gęca, M., & Kołodynska, D. (2011). "The effect of the presence of metatartaric acid on removal effectiveness of heavy metal ions on chelating ion exchangers". Environmental Technology, **32(8)**, 805–816.

Ivanets, A., Prozorovich, V., Kouznetsova, T., Dontsova, T., Yanushevska, O., Hosseini-Bandegharaei, A., Srivastava, V., Sillanpää, M. (2021). "Effect of Mg2+ ions on competitive metal ions adsorption/desorption on magnesium ferrite: Mechanism, reusability and stability studies. Journal of Hazardous Materials, **411**, 1–9.

Kanai, Y., Oshima, T., & Baba, Y. (2008). "Synthesis of highly porous chitosan microspheres anchored with 1,2-ethylenedisulfide moiety for the recovery of precious metal ions". Industrial and Engineering Chemistry Research, **47(9)**, 3114–3120.

Karim, M.R., Aijaz, M.O., Alharth, N.H., Alharbi, H.F., Al-Mubaddel, F.S., Awual, M.R. (2019). "Composite nanofibers membranes of poly(vinyl alcohol)/chitosan for selective lead(II) and cadmium(II) ions removal from wastewater". Ecotoxicology and Environmental Safety, **169**, 479–486.

Kavitha, E., Kedia, R., Babaria, N., Prabhakar, S., & Rajesh, M. P. (2020). "Optimization of process using carboxymethyl chitosan for the removal of mixed heavy metals from aqueous streams". International Journal of Biological Macromolecules, **149**, 404–416.

Kumar, M., Tripathi, B. P., & Shahi, V. K. (2009). "Crosslinked chitosan/polyvinyl alcohol blend beads for removal and recovery of Cd(II) from wastewater". Journal of Hazardous Materials, **172(2–3)**, 1041–1048.

Kumar, P., Nagireddi, S., Uppaluri, R.V.S., Mohan, L., (2022). "Batch adsorption characteristics of Dowex Marathon MSA commercial resin for Au (III) removal from synthetic electroless plating solutions". Materials Today : Proceedings, **68**, 824-829.

Kumar, R., Kumar, M., Ahmad, R., & Barakat, M. A. (2013). "L-Methionine modified Dowex-50 ion-exchanger of reduced size for the separation and removal of Cu(II) and Ni(II) from aqueous solution". Chemical Engineering Journal, **218**, 32–38.

Langmuir, I., (1919). "The adsorption gases on plane surface of glass, mica and platinum". Journal of the American Chemical Society, **40(9)**, 1361–1403.

Lertlapwasin, R., Bhawawet, N., Imyim, A., & Fuangswasdi, S. (2010). "Ionic liquid extraction of heavy metal ions by 2-aminothiophenol in 1-butyl-3-methylimidazolium hexafluorophosphate and their association constants". Separation and Purification Technology, **72(1)**, 70–76.

LeVan, M. D. (1998). "Adsorption processes and modelling present and future". Fundamentals of Adsorption, F. Meunier (ed.), 19 -29.

Li, X., Li, Y., & Ye, Z. (2011). "Preparation of macroporous bead adsorbents based on poly(vinyl alcohol)/chitosan and their adsorption properties for heavy metals from aqueous solution". Chemical Engineering Journal, **178**, 60–68.

Li, X., Li, Y., Zhang, S., & Ye, Z. (2012). "Preparation and characterization of new foam adsorbents of poly(vinyl alcohol)/chitosan composites and their removal for dye and heavy metal from aqueous solution". Chemical Engineering Journal, **183**, 88–97.

Liang, S., Guo, X., & Tian, Q. (2011). "Adsorption of Pb^{2+} and Zn^{2+} from aqueous solutions by sulfured orange peel". Desalination, **275(1–3)**, 212–216.

Ling, P., Liu, F., Li, L., Jing, X., Yin, B., Chen, K., & Li, A. (2010). "Adsorption of divalent heavy metal ions onto IDA-chelating resins: Simulation of physicochemical structures and elucidation of interaction mechanisms". Talanta, **81(1–2)**, 424–432.

Liu, P., Liu, G. feng, Chen, D. lin, Cheng, S. yi, & Tang, N. (2014). "Adsorption properties of Ag(I), Au(III), Pd(II) and Pt(IV) ions on commercial 717 anion-exchange resin". Bioresource Technology, **160**, 79–88.

Liu, W., Wang, T., Borthwick, A. G. L., Wang, Y., Yin, X., Li, X., & Ni, J. (2013). "Adsorption of Pb^{2+}, Cd^{2+}, Cu^{2+} and Cr^{3+} onto titanate nanotubes: Competition and effect of inorganic ions". Science of the Total Environment, **456–457**, 171–180.

Liu, W., Zhang, J., Jin, Y., Zhao, X., & Cai, Z. (2015). "Adsorption of Pb(II), Cd(II) and Zn(II) by extracellular polymeric substances extracted from aerobic granular sludge: Efficiency of protein". Journal of Environmental Chemical Engineering, **3(2)**, 1223–1232.

Lujanienė, G., Novikau, R., Karalevičiūtė, K., Pakštas, V., Talaikis, M., Levinskaitė, L., Selskienė, A., Selskis, A., Mažeika, J., Jokšas, K., (2024). "Chitosan-minerals-based composites for adsorption of caesium, cobalt and europium". Journal of Hazardous Materials, **462**, 132747.

Lv, S.H., 2016. High-performance superplasticizer based on chitosan. Biopolym. Biotech Admixtures Eco-Efficient Constr. Mater. 131–150.

Ma, B., Qi, J., Wang, X., Ma, M., Miao, S., Li, W., Liu, R., Liu, H., & Qu, J. (2018). "Moderate KMnO4-Fe(II) pre-oxidation for alleviating ultrafiltration membrane fouling by algae during drinking water treatment". Water Research, **142**, 96–104.

Ma, F., Li, Z., Zhao, H., Geng, Y., Zhou, W., Li, Q., & Zhang, L. (2017). "Potential application of graphene oxide membranes for removal of Cs(I) and Sr(II) from high level-liquid waste". Separation and Purification Technology, **188**, 523–529.

Ma, Y., Rajkumar, M., Zhang, C., & Freitas, H. (2016). "Beneficial role of bacterial endophytes in heavy metal phytoremediation". Journal of Environmental Management, **174**, 14–25.

Maarisetty, D., Komandur, J., Sharma, S., Baral, S.S., Mohapatra, P. (2020). "Unravelling the rate controlling step in degradation of phenol on a higher potential photocatalyst". Journal of Environmental Chemical Engineering, **8**, 103938.

Misra, R. K., Jain, S. K., & Khatri, P. K. (2011). "Iminodiacetic acid functionalized cation exchange resin for adsorptive removal of Cr(VI), Cd(II), Ni(II) and Pb(II) from their aqueous solutions". Journal of Hazardous Materials, **185(2–3)**, 1508–1512.

Mnasri-Ghnimi, S., & Frini-Srasra, N. (2019). "Removal of heavy metals from aqueous solutions by adsorption using single and mixed pillared clays". Applied Clay Science, **179**, 105151.

Morcali, M. H., Zeytuncu, B., Baysal, A., Akman, S., & Yucel, O. (2014). "Adsorption of copper and zinc from sulfate media on a commercial sorbent". Journal of Environmental Chemical Engineering, **2(3)**, 1655–1662.

Mozafari, M., Moztarzadeh, Jalali, Alhosseini, N., Asgari, Dodel, Samadikuchaksaraei, & Kargozar. (2012). "Synthesis and characterization of electrospun polyvinyl alcohol nanofibrous scaffolds modified by blending with chitosan for neural tissue engineering". International Journal of Nanomedicine, **7**, 25-34

Nagireddi, S., Katiyar, V., & Uppaluri, R. (2017). "Pd(II) adsorption characteristics of glutaraldehyde cross-linked chitosan copolymer resin". International Journal of Biological Macromolecules, **94**, 72–84.

Nagireddi, S., Golder, A.K., Uppaluri, R. (2019). "Role of EDTA on the Pd(II) adsorption characteristics of chitosan cross-linked 3-amino-1,2,4-triazole-5-thiol derivative from synthetic electroless plating solutions". International Journal of Biological Macromolecules, **127**, 320–329.

Nagireddi, S., Golder, A.K., Uppaluri, R. (2020). "Combinatorial optimality of functional groups, process parameters, and Pd(II) adsorption–desorption characteristics for commercial anion exchange resins-synthetic electroless plating systems". Environmental Science and Pollution Research, **27**, 24614–24626.

Nasernejad, B., Zadeh, T. E., Pour, B. B., Bygi, M. E., & Zamani, A. (2005). "Camparison for biosorption modeling of heavy metals (Cr(III), Cu(II), Zn(II)) adsorption from wastewater by carrot residues". Process Biochemistry, **40(3–4)**, 1319–1322.

Naushad, M., & ALOthman, Z. A. (2015). "Separation of toxic Pb^{2+} metal from aqueous solution using strongly acidic cation-exchange resin: analytical applications for the removal of metal ions from pharmaceutical formulation". Desalination and Water Treatment, **53(8)**, 2158–2166.

Nekouei, R. K., Pahlevani, F., Assefi, M., Maroufi, S., & Sahajwalla, V. (2019). "Selective isolation of heavy metals from spent electronic waste solution by macroporous ion-exchange resins". Journal of Hazardous Materials, **371**, 389–396.

Niu, L., Deng, S., Yu, G., & Huang, J. (2010). "Efficient removal of Cu(II), Pb(II), Cr(VI) and As(V) from aqueous solution using an aminated resin prepared by surface-initiated atom transfer radical polymerization". Chemical Engineering Journal, **165(3)**, 751–757.

Niu, Y., Liu, H., Qu, R., Liang, S., Chen, H., Sun, C., & Cui, Y. (2015). "Preparation and characterization of thiourea-containing silica gel hybrid materials for Hg(II) adsorption". Industrial and Engineering Chemistry Research, **54(5)**, 1656–1664.

Pang, F. M., Kumar, P., Teng, T. T., Mohd Omar, A. K., & Wasewar, K. L. (2011). "Removal of lead, zinc and iron by coagulation-flocculation". Journal of the Taiwan Institute of Chemical Engineers, **42(5)**, 809–815.

Park, J.H., Ok, Y.S., Kim, S.H., Cho, J.S., Heo, J.S., Delaune, R.D., Seo, D.C. (2016). "Competitive adsorption of heavy metals onto sesame straw biochar in aqueous solutions". Chemosphere, **142**, 77–83.

Parmar, M., & Thakur, L. S. (2013). "Heavy metal Cu , Ni and Zn : Toxicity , health hazards and their removal techniques by low cost adsorbents : A short overview" International Journal of Plant, Animal and Environmental Sciences, **3**, 143–157.

Patel, P.K., Pandey, L.M., Uppaluri, R.V.S., (2023). "Adsorptive removal of Zn , Fe , and Pb from Zn dominant simulated industrial wastewater solution using polyvinyl alcohol grafted chitosan variant resins". Chemical Engineering Journal, **459**, 141563.

Pathania, D., Thakur, M., & Mishra, A. K. (2017). "Alginate-Zr(IV) phosphate nanocomposite ion exchanger: Binary separation of heavy metals, photocatalysis and antimicrobial activity". Journal of Alloys and Compounds, **701**, 153–162.

Patrick, G., (2021). O3 Reactions of amines. BIOS Instant Notes Org. Chem. 309–314.

Pavlović, J., Stopić, S., Friedrich, B., & Kamberović, Ž. (2007). "Selective removal of heavy metals from metal-bearing wastewater in a cascade line reactor". Environmental Science and Pollution Research, **14(7)**, 518–522.

Pehlivan, E., & Altun, T. (2006). "The study of various parameters affecting the ion exchange of Cu^{2+}, Zn^{2+}, Ni^{2+}, Cd^{2+}, and Pb^{2+} from aqueous solution on Dowex 50W synthetic resin". Journal of Hazardous Materials, **134(1–3)**, 149–156.

Ren, Y., Abbood, H. A., He, F., Peng, H., & Huang, K. (2013). "Magnetic EDTA-modified chitosan/SiO_2/Fe_3O_4 adsorbent: Preparation, characterization, and application in heavy metal adsorption". Chemical Engineering Journal, **226**, 300–311.

Rengaraj, S., Kim, Y., Joo, C. K., Choi, K., & Yi, J. (2004). "Batch Adsorptive Removal of Copper Ions in Aqueous Solutions by Ion Exchange Resins: 1200H and IRN97H". Korean Journal of Chemical Engineering, **21(1)**, 187–194.

Repo, E., Warchoł, J. K., Bhatnagar, A., & Sillanpää, M. (2011). "Heavy metals adsorption by novel EDTA-modified chitosan-silica hybrid materials". Journal of Colloid and Interface Science, **358(1)**, 261–267.

Singh, S. N. (1994). "Effect of effluents from the sindri factory in the river Damodar". journal of Ecobiology, **6**, 27-32.

Singh, O.P., (2019). Study on Mining Affected Areas and its Impact on Livelihood.

Smolinski, T., Wawszczak, D., Deptula, A., Lada, W., Olczak, T., Rogowski, M., Pyszynska, M., & Chmielewski, A. G. (2017). "Solvent extraction of Cu, Mo, V, and U from leach solutions of copper ore and flotation tailings". Journal of Radioanalytical and Nuclear Chemistry, **314(1)**, 69–75.

Suc, N. Van, Ly, H.T.Y., (2013). "Lead(II) removal from aqueous solution by chitosan flake modified with citric acid via crosslinking with glutaraldehyde". Journal of Chemical Technology & Biotechnology, **88**, 1641–1649.

Sun, S., & Wang, A. (2006a). "Adsorption properties and mechanism of cross-linked carboxymethyl-chitosan resin with Zn(II) as template ion". Reactive and Functional Polymers, **66(8)**, 819–826.

Sun, S., & Wang, A. (2006b). "Adsorption properties of N-succinyl-chitosan and cross-linked N-succinyl-chitosan resin with Pb(II) as template ions". Separation and Purification Technology, **51(3)**, 409–415.

Sun, X. F., Liu, C., Ma, Y., Wang, S. G., Gao, B. Y., & Li, X. M. (2011). "Enhanced Cu(II) and Cr(VI) biosorption capacity on poly(ethylenimine) grafted aerobic granular sludge". Colloids and Surfaces B: Biointerfaces, **82(2)**, 456–462.

Swayampakula, K., Boddu, V.M., Nadavala, S.K., Abburi, K., (2009). "Competitive adsorption of Cu(II), Co(II) and Ni(II) from their binary and tertiary aqueous solutions using chitosan-coated perlite beads as biosorbent". Journal of Hazardous Materials, **170**, 680–689.

Taha, M. H. (2021). "Sorption of U(VI), Mn(II), Cu(II), Zn(II), and Cd(II) from multi-component phosphoric acid solutions using MARATHON C resin". Environmental Science and Pollution Research, **28(10)**, 12475–12489.

The Environment Protection Act, (2002). Standards for Effluent Discharge Regulations.

Trikkaliotis, D.G., Christoforidis, A.K., Mitropoulos, A.C., Kyzas, G.Z., (2020). "Adsorption of copper ions onto chitosan/poly(vinyl alcohol) beads functionalized with poly(ethylene glycol)". Carbohydrate Polymers, **234**, 115890.

Tsai, W. C., De Luna, M. D. G., Bermillo-Arriesgado, H. L. P., Futalan, C. M., Colades, J. I., & Wan, M. W. (2016). "Competitive Fixed-Bed Adsorption of Pb(II), Cu(II), and Ni(II) from Aqueous Solution Using Chitosan-Coated Bentonite". International Journal of Polymer Science, **2016(Ii)**.

Vergili, I., Gönder, Z. B., Kaya, Y., Gürdağ, G., & Çavuş, S. (2017). "Sorption of Pb(II) from battery industry wastewater using a weak acid cation exchange resin". Process Safety and Environmental Protection, **107(Ii)**, 498–507.

Verma, M., Borah, R., Kumar, A., Chae, S.H., Pan, S.Y., Kumar, V., Vlaskin, M.S., Kim, H., (2022a). "Capturing of inorganic and organic pollutants simultaneously from complex wastewater using recyclable magnetically chitosan functionalized with EDTA adsorbent". Process Safety and Environmental Protection, **167**, 56–66.

Verma, M., Kumar, A., Lee, I., Kumar, V., Park, J.H., Kim, H., (2022b). "Simultaneous capturing of mixed contaminants from wastewater using novel one-pot chitosan functionalized with EDTA and graphene oxide adsorbent". Environmental Pollution, **304**, 119130.

Verma, M., Lee, I., Oh, J., Kumar, V., Kim, H., (2022c). "Synthesis of EDTA-functionalized graphene oxide-chitosan nanocomposite for simultaneous removal of inorganic and organic pollutants from complex wastewater". Chemosphere, **287**, 132385.

Wang, G., Shi, G.M., Zhang, S., (2023). "One-step uranium extraction and brine desalination via adsorptive pervaporation by graphene-oxide scaffold membranes". Journal of Hazardous Materials, **457**, 131822.

Wang, J., & Chen, C. (2014). "Chitosan-based biosorbents: Modification and application for biosorption of heavy metals and radionuclides". Bioresource Technology, **160**, 129–141.

Wu, F. C., Tseng, R. L., & Juang, R. S. (2010). "A review and experimental verification of using chitosan and its derivatives as adsorbents for selected heavy metals". Journal of Environmental Management, **91(4)**, 798–806.

Wu, G., Kang, H., Zhang, X., Shao, H., Chu, L., & Ruan, C. (2010). "A critical review on the bio-removal of hazardous heavy metals from contaminated soils: Issues, progress, eco-environmental concerns and opportunities". Journal of Hazardous Materials, **174(1–3)**, 1–8.

Y.S. Ho, G.M., (1999). "Pseudo-second order model for sorption processes". Process Biochemistry, **34**, 451–465.

Yurtsever, M., & Şengil, I. A. (2009). "Biosorption of Pb(II) ions by modified quebracho tannin resin". Journal of Hazardous Materials, **163(1)**, 58–64.

Zawierucha, I., Kozlowska, J., Kozlowski, C., & Trochimczuk, A. (2014). "Sorption of Pb(II), Cd(II) and Zn(II) performed with the use of carboxyphenylresorcinarene-impregnated Amberlite XAD-4 resin". Desalination and Water Treatment, **52(1–3)**, 314–323.

Zhao, X., Li, Z., Tang, W., Gu, X., (2022). "Competitive kinetics of Ni(II)/Co(II) and Cr(VI)/P(V) adsorption and desorption on goethite: A unified thermodynamically based model". Journal of Hazardous Materials, **423**, 127028.

Zhou, L., Liu, J., & Liu, Z. (2009). "Adsorption of platinum(IV) and palladium(II) from aqueous solution by thiourea-modified chitosan microspheres". Journal of Hazardous Materials, **172(1)**, 439–446.

Publications

List of Publications

Published articles in international refereed journals

[1] **Patel, P.K.**, Pandey, L.M., Uppaluri, R.V.S. Adsorptive removal of Zn, Fe, and Pb from Zn dominant simulated industrial wastewater solution using polyvinyl alcohol grafted chitosan variant resins. Chemical Engineering Journal 2023; 459, 141563. https://doi.org/10.1016/j.cej.2023.141563.

[2] **Patel, P.K.**, Pandey, L.M., Uppaluri, R.V.S. Cyclic desorption based efficacy of polyvinyl alcohol-chitosan variant resins for multi heavy-metal removal. International Journal of Biological Macromolecules 2023; 242, 124812. https://doi.org/10.1016/j.ijbiomac.2023.124812.

[3] **Patel, P.K.**, Pandey, L.M., Uppaluri, R.V.S. Synthesized carboxymethyl-chitosan variant composites for cyclic adsorption-desorption based removal of Fe, Pb, and Cu. Chemosphere 2023; 340, 139780. https://doi.org/10.1016/j.chemosphere.2023.139780.

Book Chapters

[1] **Patel, P.K.**, Pandey, L.M., Uppaluri, R.V.S. **Chapter 1-** Multi-metal Adsorption and Cyclic Desorption Characteristics of Zn^{+2} and Cu^{+2} Constituting Multi-component Synthetic Wastewater System Using Commercial Resins, D. Deka, S.K. Majumder, M.K. Purkait (Eds.), Sustainable Environment, Springer Nature Singapore, Singapore, 2023: pp. 3–27. https://doi.org/10.1007/978-981-19-8464-8_1.

Communicated/Under preparation

[1] **Patel, P.K.**, Pandey, L.M., Uppaluri, R.V.S. Cyclic adsorption-desorption based Cu, Fe, and Pb removal with citric acid-chitosan variant derivatives. **(Under Review)**

[2] **Patel, P.K.**, Pandey, L.M., Uppaluri, R.V.S. The role of chitosan-citric acid variant derivatives on Zn, Pb, and Fe cyclic adsorption-desorption removal from Zn dominant adsorbate system. **(Under Review)**

[3] **Patel, P.K.**, Pandey, L.M., Uppaluri, R.V.S. Highly effective removal of multi-heavy metals from simulated industrial effluent through an adsorption process employing carboxymethyl-chitosan composites. **(Revision Submitted)**

[4] **Patel, P.K.,** Pandey, L.M., Uppaluri, R.V.S. Challenges and Opportunities for the Development of Low Cost Multi-Heavy Metal Adsorptive Chelating Resins. **(Under Preparation)**

Conference Presentations (National and International)

[1] **Patel, P.K.**, Nagireddi, S., Uppaluri, R.V.S., Pandey, L.M. Indo-US International Conference on Materials & Sustainable Engineering in Chemical and Allied Industry (MSECAI-2022). 11-12 March, 2022, Chandigarh University, India

[2] **Patel, P.K.**, Pandey, L.M., Uppaluri, R.V.S. North-East Research Conclave towards Sustainable Science and Technology (NERC-2022). 20-22 May, 2022, IIT Guwahati, India

Other Publications

[1] **Patel, P.K.**, Nagireddi, S., Uppaluri, R.V.S., Pandey, L.M. Batch adsorption characteristics of Dowex Marathon MSA commercial resin for Au (III) removal from synthetic electroless plating solutions. Materials Today Proceedings 2022; 68, 824–829. https://doi.org/10.1016/j.matpr.2022.06.258.

[2] Patel, Swati, Jena, Sujata, Said, Prashant, Nayak, Prakash, **Patel, P.K.** Characterization of gluten free composite flour from underutilized buckwheat and sprouted Pahelo dal *(Vigna mungo ssp. viridis)* suitable for bakery products. **(Under Review)**

[3] **Patel, P.K.**, Nagireddi, S., Pandey, L.M., Uppaluri, R.V.S. Adsorptive removal of Au(III) from Simulated Electroless plating solution using Amberlyst A21 Ion Exchange Resin. **(Submitted)**

[4] **Patel, P.K.**, Nagireddi, S., Pandey, L.M., Uppaluri, R.V.S. Kinetic and isothermal investigation of Amberlite IRA958 resin for the removal of Au(III) from complexed electroless plating solution. **(Submitted)**

[5] **Patel, P.K.,** Pandey, L.M., Uppaluri, R.V.S. Challenges and Opportunities for the Development of Low Cost Noble Metal (Au, Pt, and Pd) Adsorptive Chelating Resins. ***(Under Preparation)***

Appendices

Appendix A: Calibration curve for the determination of multi-heavy metal solution concentration

Atomic absorption spectrophotometer (AAS) (Make: M/S Varian BV, Model: Spectra AA 220FS) operated in flame mode at a wavelength of 324.8, 217.0, 213.9 and 248.3 nm was used to determine the absorbance of Cu, Pb, Zn and Fe respectively from complex adsorbate samples before and after adsorption. A calibration curve has been prepared to serve as a supplementary database to determine the concentrations of the fresh and spent adsorbate solutions. Using solution concentrations reported in Table 2.3, 5-20 ppm Pb and Fe solutions, 2-8 ppm Cu solution and 0.5-2 ppm Zn solution have been prepared using dilution approaches of stock solutions. Thereafter, for all standard samples, AAS was used to measure the absorbance. Based on the measured absorbances for various Cu, Pb, Fe and Zn solution concentrations of synthetic wastewater adsorbate systems, Figure A1-A4 illustrates the relevant calibration curve. As shown, the mean absorbance of the samples varied linearly with studied heavy metal ion concentrations.

A calibration curve is required to determine the heavy metal ion solution concentration from measured adsorbate absorbance value. Since it would be possible to obtain different calibration curves for synthetic wastewater adsorbate systems have been prepared.

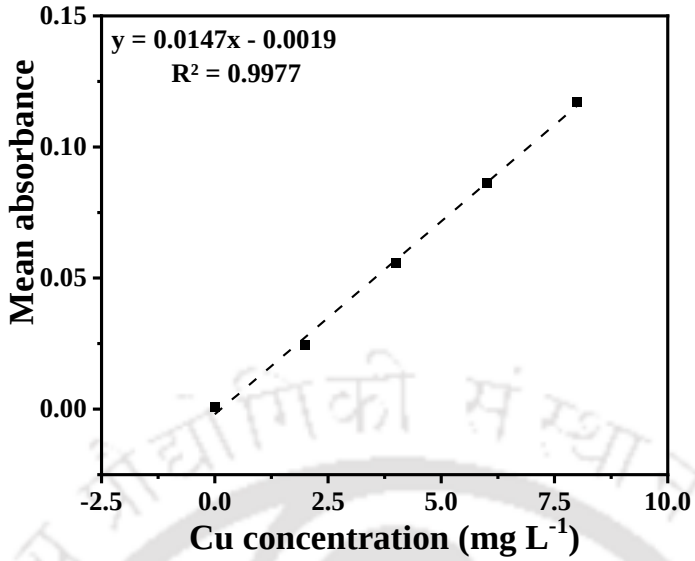

Fig. A1: Calibration curve for the determination of Cu (II) in synthetic wastewater adsorbate systems.

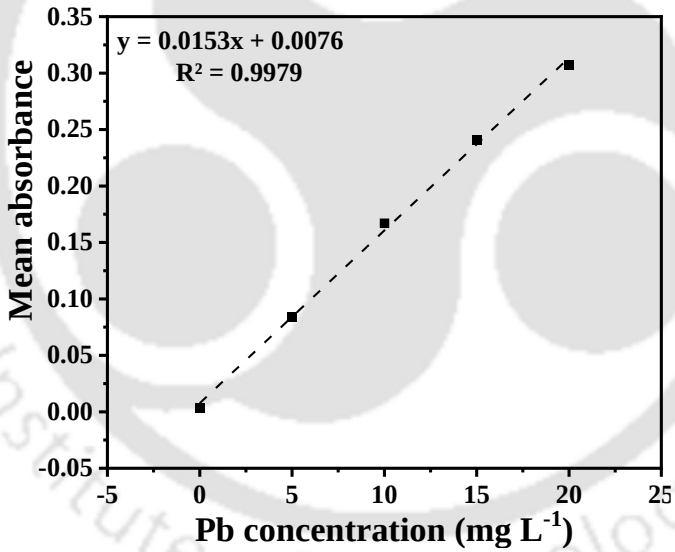

Fig. A2: Calibration curve for the determination of Pb in synthetic wastewater adsorbate systems.

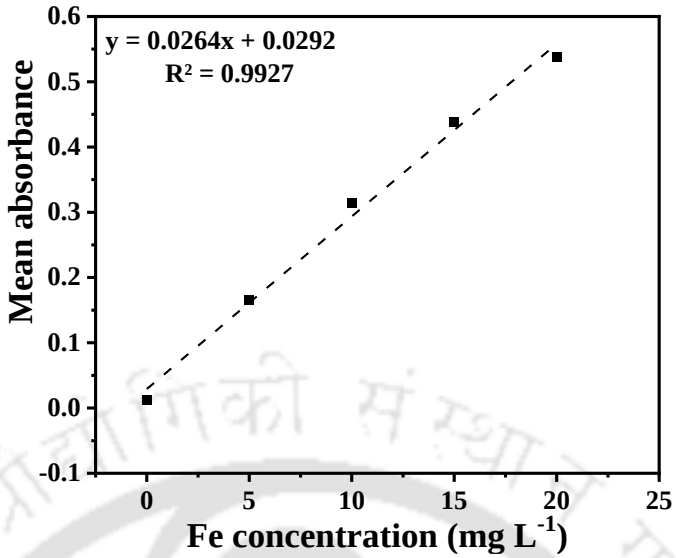

Fig. A3: Calibration curve for the determination of Fe in synthetic wastewater adsorbate systems.

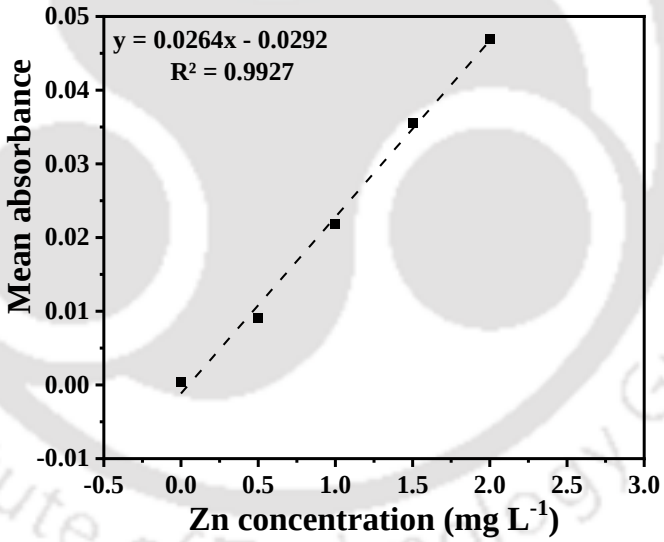

Fig. A4: Calibration curve for the determination of Zn in synthetic wastewater adsorbate systems.

Appendix B: Batch adsorption sample calculations

The following steps summarize the evaluation of heavy metal ion adsorption characteristics of high CSPVA:

a) Adsorption parameters: Adsorbent Dosage: 1.6 g L^{-1} (80 mg); Volume of Cu solution: 50 mL; Contact Time: 240 min; Initial Concentration: 375.4 mg L^{-1}.

b) Final equilibrium Cu solution concentration (C_{eq}): From AAS and calibration curve, C_{eq} = 41.29 mg L^{-1}.

c) Using eq. (**2.1**), % Adsorption = $\frac{(375.4\text{-}41.29)}{375.4} \times 100 = 89.00\ \%$

d) Using eq. (**2.2**), Metal Uptake= $\frac{(375.4-41.29)}{80} \times 50 = 208.82$ mg g^{-1}

e) Langmuir isotherm Parameters:

The determination of Langmuir isotherm parameters requires adsorption equilibrium data. Using the data, for the plot of $\frac{C_{eq}}{Q_{eq}}$ vs C_{eq}, the slope, intercept and regression coefficient (R^2) have been obtained as 0.0041, 0.0481 and 0.999, respectively.

Using slope, q_{max} (monolayer capacity) = $\frac{1}{\text{slope}}$ = 243.90 mg g^{-1}.

Using intercept and q_{max}, b = $\frac{1}{(q_{max} \times \text{intercept})}$ = 0.085.

f) Freundlich isotherm parameters:

For a plot drawn between $\log C_{eq}$ and $\log q_{eq}$, the slope, intercept and regression coefficient have been obtained as 0.2387, 1.8488 and 0.889, respectively.

Using slope, $n = \frac{1}{m} = 4.19$.

Using intercept, $K_f = 10^{1.8488} = 70.58$

g) Psuedo-second order model parameters

For a plot drawn between t vs $\frac{t}{q_t}$, the slope, intercept and regression coefficient have been obtained as, 0.0048, 0.0188 and 0.999, respectively.

Using slope, $Q_e = 1/0.0048 = 208.35$ mg g^{-1}

Using intercept, $k_2 = \frac{1}{(Q_e^2 \times \text{intercept})} = 0.0013$.

Appendix C: Batch desorption sample calculations

The following steps summarize the evaluation of heavy metal ion desorption characteristics of high CSPVA:

a) Adsorption parameters: Adsorbent Dosage: 1.6 g L^{-1} (80 mg); Volume of Cu solution: 50 mL; Contact Time: 240 min; Initial Concentration: 375.4 mg L^{-1}.

Final Cu solution concentration (C_f) = 231.39 mg L^{-1}

Concentration of Cu on adsorbent (A) = C_i-C_f = 144.01 mg L^{-1}

b) Desorption parameters: Adsorbent Dosage: 1.6 g L^{-1} (80 mg); Volume of eluent: 50 mL; Contact Time: 240 min.

$$B = \frac{V_{sol} \times A}{W_{adsorbent}} = \frac{50 \times 144.01}{80} = 90.01$$

$$\text{Desorption, \%} = \frac{(C \times V_{eluent})}{(B \times W_{adsorbent})} \times 100 = \frac{(102.75 \times 50)}{(90.01 \times 80)} \times 100 = 69.25\%$$

Appendix D: Sample calculations to evaluate cost of synthesized chitosan derivatives

The following sections summarize sample calculations associated to the determination of cost of polyvinyl alcohol grafted high molecular weight chitosan derivative (high CSPVA).

A. Lab scale Preparation of high CSPVA

Experimental conditions and chemicals utilized	**Retail cost**	**Estimated cost of various entities in the synthesis**
Polyvinyl Alcohol = 4 g	PVA (1 Kg) = 8850.00	Polyvinyl Alcohol (4 g) = 35.40
High Molecular weight chitosan = 6 g	HMW Chitosan (250 g) = 32821.00	HMW chitosan (6 g) = 787.704
20% Acetic Acid = 120 mL	Acetic Acid (500 mL) = 420.00	Acetic Acid (120 mL) = 100.8
2M NaOH = 500 mL	NaOH (500 g) = 260.00	NaOH (40 g) = 20.8
Ethanol = 300 mL	Ethanol (500 mL) 101.48	Ethanol (300 mL) = 60.89
Temperature = 80°C	Electricity (1kWh) = 9.00	Electricity (46.8375 kWh) =
Time = 12 h + 4h + 5h + 24h = 45h		421.54
Total cost = Total chemical cost + Miscellaneous equipment cost (20% of (manpower + electricity)) + Manpower cost (Rs. 100/h (16 h) for 100 g) + Electricity cost ((46.8375 KWH) for 50 g)		
Total cost for 10 g of high CSPVA = Rs. 1298.761		

B. Industrial scale Preparation of high CSPVA

Experimental conditions and chemicals utilized	**Retail cost**	**Estimated cost of various entities in the synthesis**
Polyvinyl Alcohol = 4 g	PVA (1 Kg) = 8850.00	Polyvinyl Alcohol (4 g) = 35.40
High Molecular weight chitosan = 6 g	HMW Chitosan (250 g) = 32821.00	HMW chitosan (6 g) = 787.704
20% Acetic Acid = 120 mL	Acetic Acid (500 mL) = 420.00	Acetic Acid (120 mL) = 100.8
Temperature = 80°C Time = 12 h + 4h + 5h + 24h = 45h	Electricity (1kWh) = 9.00	Electricity (46.8375 kWh) = 421.54
Total cost = 40 % of (Total chemical cost) + Miscellaneous equipment cost (20% of (manpower + electricity)) + Manpower cost (Rs. 100/h (16 h) for 100 g) + Electricity cost ((46.8375 kWh) for 50 g) Total cost for 10 g of high CSPVA = Rs. 695.41		

C. Industrial scale processing cost of high CSPVA

For a treatment plant of 3000 m^3 annual plant capacity (flow rate @ 10000 L day^{-1}), the conceptual processing costs per liter of multi-heavy metal containing industrial wastewater solutions were determined. For this, the adsorption time was assumed to reduce by 50 % of optimal contact time; the efficiency conversion factor from batch to the continuous process was chosen as 0.1; and the resin cost was chosen as 40 % and 10 % of the costs obtained with retail prices. For 40 % case and medium CMCS resin sample calculations are as follows:

Plant capacity = 3000 m^3 yearly

Flow rate = 10000 L day^{-1}

Plant Factor = 300 days yearly

Adsorption Time = 540 min (considered from contact time optimization)

Reduced Time = 4.5 h (50 % reduction due to continuous adsorption process)

Capacity of Tank = (flow rate × reduced time)/h in one day = (10000×4.5)/24 = 1875 L

Final Capacity of Tank = 2000 L (with overhead clearance)

No. of Tanks needed = 2 (one for adsorption and one for desorption)

Cost of 2 tanks = 24000 Rs.

Life of tanks = 5 years

Cost of tank yearly = 24000/5 = 4800 Rs.

Adsorbent loading = 1.2 g L^{-1} (considered from adsorbent loading optimization)

Reduction factor = 0.4 (considered due to reduction in cost for bulk orders)

Efficiency factor = 0.1 (considered efficiency factor due to conversion from batch to continuous process)

Cost of adsorbent = 395.00 Rs./10 g (for 40 % lab scale resin cost)

Amount of Adsorbent needed Yearly = (3000×1.2×0.4×0.1×2×1.18) = 339.84 Kg

Cost of adsorbent yearly = (339.84×395×0.4×1000)/10 = 5369518.76 Rs./year

Cost of 2 pumps (0.5 HP, 370 watt) = 8800×2 = 17600 Rs.

Life of pump = 3 years

Cost of 2 pumps (0.5 HP, 370 watt) = 17600/3 = 5866.67 Rs. yearly

Electricity cost = 9.5 Rs./kWh

Electricity = 23976 Rs. yearly

Manpower = 540000 Rs. yearly

Total Cost (Manpower + Tank Cost + Pump Cost + Electricity + Adsorbent) = 5944161.43 Rs. yearly

Wastewater Processing Cost = 5944161.43/(3000×1000) = 1.981 Rs./L of ww

Similar calculations were carried out for all the chitosan derivatives utilized in the PhD. Thesis.

Appendix E: Sample calculations to evaluate desorption efficiency of low, medium, and high molecular weight chitosan derivative resins

The following sections summarize sample calculations associated to the determination of desorption performance of polyvinyl alcohol grafted low molecular weight chitosan derivative (low CSPVA) and polyvinyl alcohol grafted medium molecular weight chitosan derivative (medium CSPVA).

A. Percent Removal Calculations

% Removal in 1st Cycle (high CSPVA) = 89.01 % (obtained from desorption experiments)

% Removal in 2nd Cycle (high CSPVA) = 81.62 % (obtained from desorption experiments)

% Removal in 3rd Cycle (high CSPVA) = 75.39 % (obtained from desorption experiments)

Difference in % removal of 1st cycle and 2nd cycle = 89.01-81.62 % = 7.39 %

Difference in % removal of 2nd cycle and 3rd cycle = 81.62-75.39 % = 6.23 %

Using similar difference in % removal of low CSPVA derivative,

% Removal in 1st Cycle (low CSPVA) = 76.22 % (obtained from adsorption experiments)

% Removal in 2nd Cycle (low CSPVA) = 76.22-7.39 % = 68.83 %

% Removal in 3rd Cycle (low CSPVA) = 68.83-6.23 % = 62.60 %

Using similar difference in % removal of medium CSPVA derivative,

% Removal in 1st Cycle (medium CSPVA) = 87.04 % (obtained from adsorption experiments)

% Removal in 2nd Cycle (medium CSPVA) = 87.04-7.39 % = 79.65 %

% Removal in 3rd Cycle (medium CSPVA) = 79.65-6.23 % = 73.42 %

B. Percent Desorption Calculations

% Desorption in 1st Cycle (high CSPVA) = 69.25 % (obtained from desorption experiments)

% Desorption in 2nd Cycle (high CSPVA) = 54.27 % (obtained from desorption experiments)

% Desorption in 3rd Cycle (high CSPVA) = 44.30 % (obtained from desorption experiments)

Change in % removal to % desorption of 1st cycle = 89.01/69.25 = 1.28

Change in % removal to % desorption of 2nd cycle = 81.62/54.27 = 1.50

Change in % removal to % desorption of 3rd cycle = 75.39/44.30 = 1.70

Using similar change in % removal to % desorption of low CSPVA derivative,

% Desorption in 1st Cycle (low CSPVA) = 76.22/1.28 = 59.55 %

% Desorption in 2nd Cycle (low CSPVA) = 68.83/1.50 = 45.89 %

% Desorption in 3rd Cycle (low CSPVA) = 62.60/1.70 = 36.82 %

Using similar change in % removal to % desorption of medium CSPVA derivative,

% Desorption in 1st Cycle (medium CSPVA) = 87.04/1.28 = 68.00 %

% Desorption in 2nd Cycle (medium CSPVA) = 79.65/1.50 = 53.10 %

% Desorption in 3rd Cycle (medium CSPVA) = 73.42/1.70 = 43.19 %

Similar calculations were followed for the Cit-CS and CMCS derivative resins.

Appendix F: Sample calculations for cyclic desorption efficiency and overall adsorption capacity

Sample calculations for the evaluation of desorption efficiency of the high CSPVA resin and Cu dominant solution system and for each cycle. For the case, the adsorption-desorption process parameters were 1.6 g L^{-1} dosage, 50 mL solution volume and 0.1 M KOH eluent

First adsorption-desorption cycle:

Initial concentration of Pb in solution before adsorption = 10.4 mg L^{-1}

Concentration of Pb in solution after adsorption =1.81 mg L^{-1}

Adsorption capacity of adsorbent = $((10.4) - (1.81)) \times (50/80)$ = 5.37 mg g^{-1}

Amount of Pb on adsorbent = $((10.4) - (1.81)) \times (50/1000)$ = 0.43 mg

Final concentration of Pb in solution after 1st cycle desorption = 1.74 mg L^{-1}

Amount of Pb in solution = $(1.74) \times (50/1000)$ = 0.09 mg

Amount of Pb on adsorbent surface = $(0.43) - (0.09)$ = 0.34 mg

Desorption % of 1st cycle = $(0.09/0.43) \times (100)$ = 20.93 %

Second adsorption-desorption cycle:

Initial concentration of Pb in solution before adsorption =10.4 mg L^{-1}

Concentration of Pb in solution after adsorption =2.31 mg L^{-1}

Adsorption capacity of adsorbent = $((10.4) - (2.31)) \times (50/80)$ = 5.06 mg g^{-1}

Amount of Pb on adsorbent = $((10.4) - (2.31)) \times (50/1000)$ = 0.40 mg

Total amount of Pb on adsorbent = $(0.40) + (0.34)$ = 0.74 mg

Final concentration of Pb in solution after 2nd cycle desorption = 2.1 mg L^{-1}

Amount of Pb in solution = $(2.1) \times (50/1000)$ = 0.11 mg

Rest amount of Pb on adsorbent = $(0.75) - (0.11)$ = 0.63 mg

Desorption % of 2nd cycle = $(0.11/0.75) \times (100)$ = 14.86 %

Third adsorption-desorption cycle:

Initial concentration of Pb in solution before adsorption =10.4 mg L^{-1}

Concentration of Pb in solution after adsorption =3.33 mg L^{-1}

Adsorption capacity of adsorbent = 4.42 mg g^{-1}

Amount of Pb on adsorbent = $((10.4) - (3.33)) \times (50/1000)$ = 0.35 mg

Total amount of Pb on adsorbent = $(0.35) + (0.64)$ = 1.00 mg

Final concentration of Pb in solution after 3rd cycle desorption = 1.7 mg L^{-1}

Amount of Pb in solution = $(1.7) \times (50/1000)$ = 0.085 mg

Rest amount of Pb on adsorbent = $(1.00) - (0.085)$ = 0.9 mg

Desorption % = $(0.09/1.00) \times (100)$ = 9 %

Appendix G: Evaluation of Error functions of equilibrium and kinetic models for CSPVA, Cit-CS, and CMCS derivative resins

Tables G1-G12 summarize error functions namely, Chi-square, Root mean square deviation, Residual sum of squares, and ANOVA analysis of CSPVA (Tables G1-G4), Cit-CS (Tables G5-G8), and CMCS derivative resins (Tables G9-G12) and for Cu and Zn dominant simulated adsorbate systems. For each resin, three experimental trails were carried out for alterations in time and concentration and thereby relevant models have been evaluated for their fitness using mentioned error functions. These error functions were evaluated based on the average values of the mentioned experimental trails. The fitness evaluated models refer to Langmuir isotherm, Freundlich isotherm, Pseudo first order kinetic model and Pseudo second order kinetic model. For all cases, higher F-values and lower p-values have been obtained and these conveyed the significance of the evaluated parameters for the batch adsorption characteristics of multi heavy metals for chosen combinations of resins and adsorbate systems. For all cases, highest F-value was obtained for Langmuir isotherm model and Pseudo second order kinetic model. Henceforth, it is apparent that among all studied models, Langmuir isotherm model and Pseudo second order kinetic model were the best fit models for all investigated chitosan derivative resins. Other error functions also affirmed the best relevance of Langmuir isotherm model and Pseudo second order kinetic model. In summary, the error functions affirm confidence with respect to the appropriately fit models that represent multi heavy metal ion adsorption characteristics of the mentioned resins and for the chosen adsorbate systems.

Table G1: A summary of alternate error functions data of Langmuir and Freundlich isotherm model parameters for CSPVA resin and Cu dominant adsorbate system.

Molecular weight	R^2	Chi-square Test	RMSE	RSS	ANOVA	
					F-Value	p-Value
Langmuir Isotherm Model						
Cu						
Low	0.98	0.00107	0.0337	0.0032	1381.63	<0.0001
Medium	0.99	0.00009	0.0097	0.0003	8768.11	<0.0001
High	0.99	0.00019	0.0137	0.0006	4024.75	<0.0001
Fe						
Low	0.98	0.00041	0.0012	0.0012	3877.24	<0.0001
Medium	0.98	0.00014	0.0004	0.0004	5643.53	<0.0001
High	0.99	0.00017	0.0132	0.0001	2962.18	<0.0001
Pb						
Low	0.98	0.00010	0.0102	0.0003	469.86	0.00021
Medium	0.99	0.00006	0.0077	0.0002	712.48	0.00011
High	0.98	0.00004	0.0067	0.0001	656.37	0.00013
Freundlich Isotherm Model						
Cu						
Low	0.93	0.00119	0.0345	0.0036	45.61	0.00663
Medium	0.90	0.00158	0.0397	0.0047	41.04	0.00771
High	0.88	0.00272	0.0521	0.0082	24.20	0.01609
Fe						
Low	0.95	0.00042	0.0206	0.0012	113.36	0.00177
Medium	0.94	0.00058	0.0241	0.0017	117.83	0.00167
High	0.94	0.00058	0.0241	0.0017	132.78	0.00140
Pb						
Low	0.91	0.00199	0.0446	0.0059	30.39	0.01175
Medium	0.90	0.00196	0.0443	0.0058	30.32	0.01179
High	0.93	0.00172	0.0414	0.0051	40.75	0.00778

Table G2: A summary of alternate error functions data of Langmuir and Freundlich isotherm model parameters for CSPVA resin and Zn dominant adsorbate system.

Molecular weight	R^2	Chi-square Test	RMSE	RSS	ANOVA	
					F-Value	p-Value
Langmuir Isotherm Model						
Zn						
Low	0.98	0.00953	0.0976	0.0286	151.31	0.00116
Medium	0.99	0.00622	0.0788	0.0186	213.86	0.00069
High	0.98	0.00637	0.0798	0.0191	154.81	0.00112
Fe						
Low	0.99	0.00071	0.0267	0.0021	1248.40	<0.0001
Medium	0.99	0.00092	0.0303	0.0027	854.03	<0.0001
High	0.99	0.00070	0.0265	0.0021	942.51	<0.0001
Pb						
Low	0.99	0.00047	0.0218	0.0014	1059.55	<0.0001
Medium	0.99	0.00025	0.0160	0.0008	1626.01	<0.0001
High	0.99	0.00039	0.0197	0.0011	1143.99	<0.0001
Freundlich Isotherm Model						
Zn						
Low	0.93	0.00072	0.0268	0.0021	43.73	0.00704
Medium	0.95	0.00048	0.0219	0.0014	68.30	0.00371
High	0.96	0.00051	0.0226	0.0015	73.43	0.00334
Fe						
Low	0.95	0.00069	0.0263	0.0020	59.53	0.00452
Medium	0.94	0.00088	0.0297	0.0026	47.13	0.00633
High	0.92	0.00130	0.0360	0.0039	34.71	0.00976
Pb						
Low	0.97	0.00044	0.0210	0.0013	127.94	0.00148
Medium	0.91	0.00019	0.0140	0.0006	308.10	0.00040
High	0.97	0.00045	0.0214	0.0013	126.49	0.00151

Table G3: A summary of alternate error functions data of Pseudo first order and Pseudo second order kinetic model parameters for CSPVA resin and Cu dominant adsorbate system.

Molecular weight	R^2	Chi-square Test	RMSE	RSS	ANOVA	
					F-Value	p-Value
Pseudo First Order Kinetic Model						
Cu						
Low	0.88	0.00476	0.0689	0.0332	166.46	<0.0001
Medium	0.81	0.02713	0.1647	0.2170	129.07	<0.0001
High	0.74	0.02759	0.1661	0.1379	33.72	0.00214
Fe						
Low	0.87	0.00339	0.0582	0.0237	375.54	<0.0001
Medium	0.45	0.07230	0.2688	0.5783	78.32	<0.0001
High	0.40	0.05226	0.2286	0.2612	57.84	0.00062
Pb						
Low	0.44	0.00365	0.0603	0.0255	183.36	<0.0001
Medium	0.015	0.01139	0.1067	0.0911	449.80	<0.0001
High	0.063	0.01024	0.1012	0.0512	52.93	0.00077
Pseudo Second Order Kinetic Model						
Cu						
Low	0.99	0.00449	0.0670	0.0628	6118.84	<0.0001
Medium	0.99	0.00004	0.0062	0.0005	554115.36	<0.0001
High	0.99	0.00003	0.0062	0.0005	545176.04	<0.0001
Fe						
Low	0.98	0.05808	0.2409	0.8130	5723.41	<0.0001
Medium	0.99	0.00212	0.0460	0.0297	146670.47	<0.0001
High	0.99	0.00052	0.0227	0.0072	555861.37	<0.0001
Pb						
Low	0.98	13.69	3.7000	191.67	2205.22	<0.0001
Medium	0.99	0.30	0.5478	4.20	102832.59	<0.0001
High	0.99	0.43	0.6557	6.02	66403.26	<0.0001

Table G4: A summary of alternate error functions data of Pseudo first order and Pseudo second order kinetic model parameters for CSPVA resin and Zn dominant adsorbate system.

Molecular weight	R^2	Chi-square Test	RMSE	RSS	ANOVA	
					F-Value	p-Value
Pseudo First Order Kinetic Model						
Zn						
Low	0.94	0.07728	0.2779	0.5409	61.28	0.0001047
Medium	0.88	0.00227	0.0476	0.0158	360.27	<0.0001
High	0.76	0.07821	0.2891	0.5508	60.27	0.0001145
Fe						
Low	0.94	0.01507	0.1227	0.1356	152.65	<0.0001
Medium	0.88	0.00225	0.0474	0.0157	578.30	<0.0001
High	0.87	0.01710	0.1307	0.1196	90.34	<0.0001
Pb						
Low	0.24	0.00253	0.0502	0.0227	413.72	<0.0001
Medium	0.06	0.01464	0.1209	0.1024	112.15	<0.0001
High	0.05	0.12667	0.3559	0.8866	23.40	0.00188
Pseudo Second Order Kinetic Model						
Zn						
Low	0.99	0.00117	0.0341	0.0163	29584.40	<0.0001
Medium	0.99	0.00736	0.0858	0.1030	5593.68	<0.0001
High	0.99	0.00117	0.0341	0.0163	29584.40	<0.0001
Fe						
Low	0.99	0.02274	0.1507	0.3183	3919.35	<0.0001
Medium	0.99	0.00780	0.0883	0.1091	10086.57	<0.0001
High	0.99	0.01253	0.1119	0.1753	5734.36	<0.0001
Pb						
Low	0.98	133.534	11.55	1869.47	778.11	<0.0001
Medium	0.99	42.7935	6.541	599.10	2309.82	<0.0001
High	0.99	29.4924	5.43	412.89	2786.80	<0.0001

Table G5: A summary of alternate error functions data of Langmuir and Freundlich isotherm model parameters for Cit-CS resin and Cu dominant adsorbate system.

Molecular weight	R^2	Chi-square Test	RMSE	RSS	ANOVA	
					F-Value	p-Value
Langmuir Isotherm Model						
Cu						
Low	0.99	0.00195	0.04415	0.00585	484.87	0.000205
Medium	0.99	0.000468	0.02163	0.0014	477.82	0.000209
High	0.99	0.000224	0.01497	0.000672	1096.43	<0.0001
Fe						
Low	0.98	0.00742	0.08613	0.02226	178.890	0.0009035
Medium	0.99	0.0005573	0.02361	0.00167	866.993	<0.0001
High	0.99	0.0003238	0.018	0.0009715	1592.428	<0.0001
Pb						
Low	0.99	0.0006989	0.02644	0.0021	1074.96	<0.0001
Medium	0.99	0.0002812	0.01677	0.0008437	886.529	<0.0001
High	0.99	0.0000765	0.00875	0.0002296	3590.975	<0.0001
Freundlich Isotherm Model						
Cu						
Low	0.95	0.000953	0.03087	0.00286	62.213	0.00425
Medium	0.96	0.000937	0.03061	0.00281	85.441	0.00268
High	0.97	0.0007366	0.02714	0.00221	104.437	0.002
Fe						
Low	0.95	0.000670	0.02589	0.00201	67.295	0.00379
Medium	0.96	0.000832	0.02885	0.0025	73.168	0.00336
High	0.97	0.0002137	0.01462	0.0006411	263.245	0.000509
Pb						
Low	0.83	0.0021	0.04584	0.0063	29.1086	0.01248
Medium	0.90	0.0046	0.06782	0.0138	15.4632	0.02928
High	0.95	0.0011	0.03314	0.00329	65.14008	0.00397

Table G6: A summary of alternate error functions data of Langmuir and Freundlich isotherm model parameters for Cit-CS resin and Zn dominant adsorbate system.

Molecular weight	R^2	Chi-square Test	RMSE	RSS	ANOVA	
					F-Value	p-Value
Langmuir Isotherm Model						
Zn						
Low	0.98	0.01193	0.10924	0.0358	157.819	0.00109
Medium	0.99	0.00105	0.03241	0.00315	696.903	0.000119
High	0.99	0.00153	0.0391	0.00459	546.783	0.000171
Fe						
Low	0.99	0.0009967	0.03157	0.00299	644.003	0.000134
Medium	0.99	0.000469	0.02166	0.00141	1105.102	<0.0001
High	0.99	0.0001267	0.01126	0.00380	3909.0567	<0.0001
Pb						
Low	0.99	0.000932	0.03053	0.0028	389.638	0.000284
Medium	0.99	0.000384	0.0196	0.00115	991.125	<0.0001
High	0.99	0.000543	0.0233	0.00163	598.076	0.00015
Freundlich Isotherm Model						
Zn						
Low	0.93	0.000699	0.02644	0.0021	45.212	0.00671
Medium	0.98	0.0001806	0.01344	0.000542	288.936	0.0004435
High	0.97	0.00027156	0.01648	0.000815	164.0014	<0.0001
Fe						
Low	0.94	0.0008011	0.0283	0.0024	70.1534	0.00357
Medium	0.91	0.0013	0.03602	0.00389	46.865	0.00638
High	0.93	0.000958	0.03095	0.00287	63.630	0.00411
Pb						
Low	0.97	0.000476	0.02182	0.00143	142.0552	0.00127
Medium	0.88	0.00211	0.04596	0.00634	31.1151	0.01137
High	0.96	0.0006372	0.02504	0.00188	105.216	0.00198

Table G7: A summary of alternate error functions data of Pseudo first order and Pseudo second order kinetic model parameters for Cit-CS resin and Cu dominant adsorbate system.

Molecular weight	R^2	Chi-square Test	RMSE	RSS	ANOVA	
					F-Value	p-Value
Pseudo First Order Kinetic Model						
Cu						
Low	0.95	0.00702	0.08377	0.06315	289.82	<0.0001
Medium	0.92	0.00334	0.0578	0.02673	628.01	<0.0001
High	0.93	0.00324	0.05691	0.02591	603.767	<0.0001
Fe						
Low	0.89	0.01179	0.10858	0.10611	322.478	<0.0001
Medium	0.87	0.01116	0.10562	0.08925	178.936	<0.0001
High	0.91	0.01365	0.11684	0.10922	172.8497	<0.0001
Pb						
Low	0.18	0.01108	0.10527	0.09974	221.354	<0.0001
Medium	0.35	0.01116	0.10562	0.08925	178.936	<0.0001
High	0.40	0.01419	0.11912	0.11353	144.970	<0.0001
Pseudo Second Order Kinetic Model						
Cu						
Low	0.99	0.00647	0.08044	0.09059	6875.29	<0.0001
Medium	0.99	0.001	0.03163	0.014	18636.42	<0.0001
High	0.99	0.00238	0.04881	0.03336	7599.623	<0.0001
Fe						
Low	0.99	0.07345	0.27102	1.02834	6897.998	<0.0001
Medium	0.99	0.00949	0.09742	0.1329	21063.611	<0.0001
High	0.99	0.01738	0.13182	0.2433	11279.757	<0.0001
Pb						
Low	0.99	11.3898	3.375	159.46	3743.498	<0.0001
Medium	0.99	1.28542	1.134	17.996	14545.371	<0.0001
High	0.99	4.4064	2.099	61.6902	4234.8261	<0.0001

Table G8: A summary of alternate error functions data of Pseudo first order and Pseudo second order kinetic model parameters for Cit-CS resin and Zn dominant adsorbate system.

Molecular weight	R^2	Chi-square Test	RMSE	RSS	ANOVA	
					F-Value	p-Value
Pseudo First Order Kinetic Model						
Zn						
Low	0.92	0.01014	0.1007	0.09127	126.864	<0.0001
Medium	0.89	0.00149	0.03866	0.01196	390.894	<0.0001
High	0.91	0.00187	0.04321	0.01493	1500.5089	<0.0001
Fe						
Low	0.94	0.01752	0.13235	0.15765	125.983	<0.0001
Medium	0.91	0.00359	0.05996	0.02876	637.856	<0.0001
High	0.91	0.00157	0.03966	0.01258	1506.058	<0.0001
Pb						
Low	0.15	0.0014	0.0374	0.0126	788.249	<0.0001
Medium	0.07	0.00837	0.0915	0.064	246.817	<0.0001
High	0.09	0.00302	0.05493	0.024	504.628	<0.0001
Pseudo Second Order Kinetic Model						
Zn						
Low	0.99	0.03608	0.18996	0.50517	1446.831	<0.0001
Medium	0.99	0.01272	0.11276	0.17802	2211.1501	<0.0001
High	0.99	0.000709	0.02663	0.00993	39964.37	<0.0001
Fe						
Low	0.99	0.04002	0.20004	0.56021	3058.074	<0.0001
Medium	0.99	0.01133	0.10643	0.15858	6677.425	<0.0001
High	0.99	0.00465	0.0682	0.06511	15717.48	<0.0001
Pb						
Low	0.98	87.349	9.346	1222.88	1566.262	<0.0001
Medium	0.99	33.138	5.757	463.927	2730.445	<0.0001
High	0.99	24.506	4.950	343.080	3524.498	<0.0001

Table G9: A summary of alternate error functions data of Langmuir and Freundlich isotherm model parameters for CMCS resin and Cu dominant adsorbate system.

Molecular weight	R^2	Chi-square Test	RMSE	RSS	ANOVA	
					F-Value	p-Value
Langmuir Isotherm Model						
Cu						
Low	0.99	0.00464	0.06809	0.01391	528.43	0.000180
Medium	0.99	0.0006709	0.0259	0.00201	289.513	0.000442
High	0.99	0.000271	0.01647	0.000813	937.541	<0.0001
Fe						
Low	0.99	0.00479	0.06923	0.01438	348.986	0.0003348
Medium	0.99	0.0000935	0.00967	0.000280	5906.668	<0.0001
High	0.99	0.0017	0.04117	0.00509	200.028	0.000766
Pb						
Low	0.99	0.00064	0.02536	0.00193	1848.352	<0.0001
Medium	0.99	0.0000597	0.00773	0.000179	2908.495	<0.0001
High	0.99	0.000350	0.01871	0.00105	437.665	0.000239
Freundlich Isotherm Model						
Cu						
Low	0.96	0.0004016	0.0200	0.0012	85.683	0.00267
Medium	0.97	0.0005577	0.02362	0.00167	129.6597	0.00145
High	0.87	0.00303	0.05509	0.0091	20.5815	0.02005
Fe						
Low	0.97	0.000284	0.0169	0.000853	154.67	0.00112
Medium	0.91	0.0013	0.0361	0.00391	32.2418	0.00995
High	0.95	0.000885	0.0298	0.00266	61.19445	0.00435
Pb						
Low	0.88	0.00226	0.04754	0.00678	22.545	0.01772
Medium	0.96	0.000915	0.03026	0.00275	83.959	0.00275
High	0.97	0.000373	0.0193	0.00112	208.277	0.000722

Table G10: A summary of alternate error functions data of Langmuir and Freundlich isotherm model parameters for CMCS resin and Zn dominant adsorbate system.

Molecular weight	R^2	Chi-square Test	RMSE	RSS	ANOVA	
					F-Value	p-Value
Langmuir Isotherm Model						
Zn						
Low	0.99	0.00431	0.0657	0.0129	465.07	0.000218
Medium	0.99	0.00242	0.04921	0.0073	346.60	0.000338
High	0.99	0.00212	0.04605	0.0064	383.201	0.000291
Fe						
Low	0.99	0.00108	0.0329	0.00324	915.9897	<0.0001
Medium	0.99	0.000287	0.01695	0.000862	1712.974	<0.0001
High	0.99	0.000166	0.0128	0.000494	2483.769	<0.0001
Pb						
Low	0.99	0.000836	0.0289	0.00251	647.921	0.000433
Medium	0.99	0.000486	0.02206	0.00146	300.163	0.000419
High	0.99	0.000244	0.01561	0.000731	835.99	<0.0001
Freundlich Isotherm Model						
Zn						
Low	0.94	0.000706	0.02657	0.00212	50.278	0.00577
Medium	0.90	0.00159	0.0399	0.00477	28.693	0.01273
High	0.91	0.00137	0.03699	0.0041	32.044	0.01092
Fe						
Low	0.95	0.000984	0.0314	0.000295	56.8297	0.00484
Medium	0.95	0.00107	0.0327	0.00322	58.019	0.0047
High	0.97	0.000460	0.0215	0.00138	142.395	0.00127
Pb						
Low	0.97	0.000258	0.016	0.000775	276.142	0.000474
Medium	0.95	0.00154	0.039	0.00461	59.459	0.00453
High	0.97	0.000373	0.0193	0.00112	216.118	0.000683

Table G11: A summary of alternate error functions data of Pseudo first order and Pseudo second order kinetic model parameters for CMCS resin and Cu dominant adsorbate system.

Molecular weight	R^2	Chi-square Test	RMSE	RSS	ANOVA	
					F-Value	p-Value
Pseudo First Order Kinetic Model						
Cu						
Low	0.91	0.03144	0.17731	0.377	262.302	<0.0001
Medium	0.92	0.05569	0.236	0.7797	151.713	<0.0001
High	0.92	0.08503	0.2916	0.8503	61.224	<0.0001
Fe						
Low	0.94	0.01518	0.123	0.182	211.408	<0.0001
Medium	0.95	0.0086	0.093	0.086	232.58	<0.0001
High	0.95	0.0048	0.069	0.048	653.42	<0.0001
Pb						
Low	0.28	0.00727	0.0852	0.0799	502.668	<0.0001
Medium	0.35	0.02044	0.1429	0.2044	260.365	<0.0001
High	0.46	0.02546	0.1596	0.2546	172.638	<0.0001
Pseudo Second Order Kinetic Model						
Cu						
Low	0.99	0.01364	0.1168	0.191	4551.066	<0.0001
Medium	0.99	0.000548	0.02342	0.00768	26625.715	<0.0001
High	0.99	0.00181	0.04249	0.0253	6349.318	<0.0001
Fe						
Low	0.99	0.294	0.542	4.117	1823.895	<0.0001
Medium	0.99	0.023	0.152	0.32	5715.741	<0.0001
High	0.99	0.0219	0.148	0.308	6142.10	<0.0001
Pb						
Low	0.99	11.569	3.4013	161.968	4196.484	<0.0001
Medium	0.99	0.85062	0.922	11.909	16160.1028	<0.0001
High	0.99	8.118	2.849	113.652	1795.94	<0.0001

Table G12: A summary of alternate error functions data of Pseudo first order and Pseudo second order kinetic model parameters for CMCS resin and Zn dominant adsorbate system.

Molecular weight	R^2	Chi-square Test	RMSE	RSS	ANOVA	
					F-Value	p-Value
Pseudo First Order Kinetic Model						
Zn						
Low	0.88	0.01001	0.100	0.1202	185.369	<0.0001
Medium	0.90	0.00833	0.0913	0.0666	107.3295	<0.0001
High	0.88	0.01342	0.1158	0.1073	249.26	<0.0001
Fe						
Low	0.92	0.01978	0.14066	0.237	317.99	<0.0001
Medium	0.91	0.0036	0.05998	0.029	637.496	<0.0001
High	0.92	0.00157	0.0396	0.013	1509.62	<0.0001
Pb						
Low	0.36	0.0151	0.123	0.1816	255.586	<0.0001
Medium	0.05	0.0088	0.0938	0.070	236.909	<0.0001
High	0.04	0.0115	0.107	0.0917	181.656	<0.0001
Pseudo Second Order Kinetic Model						
Zn						
Low	0.98	0.058	0.2415	0.8163	824.902	<0.0001
Medium	0.99	0.0039	0.0622	0.0542	5921.45	<0.0001
High	0.99	0.000126	0.0112	0.00176	181278.74	<0.0001
Fe						
Low	0.99	0.03695	0.192	0.517	3905.09	<0.0001
Medium	0.99	0.00618	0.079	0.087	12292.51	<0.0001
High	0.99	0.00443	0.0666	0.0044	16348.192	<0.0001
Pb						
Low	0.98	99.6899	4.657	1395.658	1813.751	<0.0001
Medium	0.99	27.561	5.2499	385.853	3244.96	<0.0001
High	0.99	21.684	9.984	303.569	3956.259	<0.0001